THE UNIVERSITY
OF MICHIGAN
MAR 16 1959
ENGINEERING
LIBRARY

JOURNAL OF FLUID MECHANICS

VOLUME 5 PART 2

FEBRUARY 1959

PUBLISHED BY

CAMBRIDGE UNIVERSITY PRESS

BENTLEY HOUSE, 200 EUSTON ROAD, LONDON, N.W.1

AMERICAN BRANCH: 32 EAST 57TH STREET, NEW YORK 22, N.Y.

Price 30*s.* (*U.S.A.* $5.00)

The JOURNAL OF FLUID MECHANICS exists for the publication of theoretical and experimental investigations of all aspects of the mechanics of fluids, and is issued in four parts per volume.

EDITOR

DR G. K. BATCHELOR

Cavendish Laboratory, University of Cambridge, Cambridge, England

ASSISTANT EDITORS

DR T. B. BENJAMIN, DR I. PROUDMAN, DR P. G. SAFFMAN

Cavendish Laboratory, University of Cambridge, Cambridge, England

ASSOCIATE EDITORS

PROF. G. F. CARRIER

Pierce Hall, Harvard University, Cambridge 38, *Massachusetts, U.S.A.*

DR W. C. GRIFFITH

Research and Development Laboratory, Missile Systems Division, Lockheed Aircraft Corporation, Palo Alto, California, U.S.A.

PROF. M. J. LIGHTHILL

Department of Mathematics, The University, Manchester, England

PROF. R. R. LONG

School of Engineering, The Johns Hopkins University, Baltimore 18, *Maryland, U.S.A.*

Authors wishing to have papers published in the JOURNAL should communicate them to any one of the persons named above, choosing one in their own country where possible.

Authors are urged to ensure that their papers are written clearly and attractively, in order that their work will be readily accessible to readers.

Manuscripts should be typed in double spacing on one side of the paper only, with references listed at the end in alphabetical order of authors. Drawings should be done on a large scale in Indian ink on tracing cloth or drawing paper, the lettering being shown clearly in pencil for reproduction by the printer; the list of captions should be typed at the end of the manuscript. Proofs of papers from overseas will usually be despatched to authors by airmail. There is no charge for publication. Authors are entitled to receive 50 offprints of a paper in the JOURNAL free of charge, and additional offprints can be purchased if ordered in advance.

SUBSCRIPTIONS

The subscription price for a volume of four parts is £5. 10*s*. net, post free, payable in advance; separate parts 30*s*. net, plus postage. Subscriptions may be sent to any bookseller, or to the Cambridge University Press, Bentley House, 200 Euston Road, London, N.W.1.

Subscribers in the United States should send their orders to the Cambridge University Press, American Branch, 32 East 57th Street, New York 22. The subscription price per volume is $18.50, post free, payable in advance; separate parts $5.00, plus postage.

The scattering of gravity waves by turbulence

By O. M. PHILLIPS

Department of Mechanical Engineering, The Johns Hopkins University, Baltimore

(Received 17 June 1958)

A theory is developed to describe the properties of waves on the free surface of a liquid in turbulent motion. The distinction between the interacting wave and turbulent motions is achieved by separating the velocity field uniquely into a surface-induced contribution characteristic of the wave motion and a vorticity-induced contribution associated with the turbulence. The theory is applied to the scattering of gravity waves passing over the surface of deep water which has a turbulent motion of sufficiently low mean square vorticity. Expressions are derived for the directional distribution of the scattered wave (equation 4.19) and for the logarithmic decrement resulting from the scattering (4.20). It is shown that, under typical conditions in open sea, the attenuation from scattering will be greater than that from direct viscous dissipation for wavelengths greater than about 3 m.

1. Introduction

The problem of wave motion on the surface of a turbulent fluid has several different aspects. One of these is concerned with the propagation of an incident gravity wave through a region of turbulent fluid (water) and with the attenuation of the wave that results from the interation between the turbulence and wave motion. This aspect may well be of interest in oceanography, since there is little doubt that the motion in the upper layers of the open ocean is usually turbulent, although the turbulent velocity fluctuations are likely to be much smaller than those generally found in the atmosphere. In studies of propagation of surface waves over great distances across the ocean, it is probable that the scattering of waves by oceanic turbulence may have a significant effect. For example,† if waves originating in one storm have to pass through another storm (where presumably the turbulent intensity is high) to reach an observer, one effect of scattering is to increase the average path length taken by wave energy in passing from source to observer, and so to distribute and delay their arrival. Such a delay has been observed by Darbyshire (1952), and the most natural explanation seems to be in terms of this scattering process.

A second aspect of the interaction between surface waves and turbulence in the water is concerned with the generation of waves on the surface of the liquid, and with the derivation of relations between the properties of the surface displacements and the structure of the turbulence that induces them. An associated

† I am indebted to the referee for pointing out this example.

problem concerns the rate at which energy is transferred from the turbulence to the waves and is carried away by the wave motion from, say, a localized region of turbulence. It might be anticipated from visual observations of the water surface below, say, the spillway of a dam, that the transfer of energy from turbulence to propagating waves is relatively slow, so that the process would be relatively insignificant in most oceanographical contexts, although it may be important in other situations. This second aspect of the problem will be discussed in a succeeding paper.

Let us return to consideration of the problem of present interest, namely, the attenuation of an incident wave moving across the surface of a deep turbulent liquid, where the intensity of the turbulence is sufficiently small that the process of wave generation is unimportant. One can see physically that there are two possible types of interaction, each of which will result in an attenuation of the incident wave. The first can be called an 'eddy viscosity interaction' in which energy is transferred from the wave motion to the turbulence. The passage of the wave results in straining the elements of fluid near the surface in a manner which is almost, but not quite, periodic in time. The mean strain per cycle of the incident wave is of second order, namely $(a/\lambda)^2$, where a is the amplitude and λ the wavelength of the incident wave. The wave motion therefore provides a mechanism for stretching the vortex lines that operates in addition to the stretching inherent in the turbulence itself, and so tends to increase $\overline{\omega^2}$, the mean square vorticity associated with the turbulence, until a balance is reached with the diffusive action of viscosity. Two comments are pertinent to this eddy viscosity type of interaction. The first is that the energy of the waves is transferred to turbulence having a length scale smaller than the wavelength of the incident wave and so, from the point of view of the turbulence, provides a source of energy at fairly large wave numbers (though not as large as those associated with the dissipation range). In the second place, the additional straining process is, for a given level of $\overline{\omega^2}$ in the water, of second order in a/λ and so it might be expected to be most important for a given wavelength when the amplitude a of the incident wave is large and less important when a is small, as in ocean swell.

Another process which might be expected to influence the propagation of surface waves can be described as a scattering phenomenon. The presence of random velocity fluctuations in the water of a length scale comparable with the wavelength of the waves will result in the convective distortion of the wave fronts, and so in the establishment of a scattered wave field. It is clear that the amplitude of the scattered wave system will be proportional to the amplitude of the incident wave, as in other scattering problems (see, for example, the discussion by Batchelor (1957), which contains a bibliography of significant earlier work in these fields) so that the incident wave suffers a true logarithmic decrement. This scattering effect is clearly of lower order in (a/λ), and the attenuation time will be independent of wave amplitude. Furthermore, since the incident wave will be supposed to have a very small slope, only terms of lowest order in a/λ will be retained in the analysis, so that only the scattering phenomenon would be expected to be described. This makes it possible to neglect the effect of the waves on the turbulence, so that the turbulent field can be regarded as

prescribed by other considerations, such as the existence of mean velocity gradients set up by ocean currents.

One of the fundamental differences between the scattering of gravity waves and most other scattering problems that have been considered is that gravity waves in deep water are dispersive: the phase velocity is a function of wavelength. This suggests that from the outset, the analysis might be developed most conveniently in terms of the Fourier components of both the incident wave field and the vorticity fluctuations characteristic of the turbulence. This plan is adopted in the later sections of this paper.

2. Specification of the problem

The first difficulty with which we are faced in discussing the wave motion on the surface of a turbulent liquid is that we can define neither a velocity potential nor a stream function, since the turbulence is essentially rotational and three-dimensional, and consequently we are denied many of the simple and powerful methods developed in the past for the theory of water waves. This difficulty is overcome to some extent by expressing the Navier–Stokes equations for the motion of the water, namely,

$$\frac{\partial \mathbf{u}}{\partial t} + \mathbf{u}.\nabla\mathbf{u} = -\nabla(p/\rho - gz) + \nu\nabla^2\mathbf{u} \tag{2.1}$$

in the equivalent form

$$\frac{\partial \mathbf{u}}{\partial t} - \mathbf{u}\times\boldsymbol{\omega} = -\nabla(p/\rho - gz + \tfrac{1}{2}u^2) - \nu\nabla\times\boldsymbol{\omega}, \tag{2.2}$$

where $\boldsymbol{\omega} = \nabla\times\mathbf{u}$ is the vorticity at the point $\mathbf{x}$ and the z co-ordinate axis is taken vertically downwards. In regions where the motion is irrotational, that is $\boldsymbol{\omega} = 0$, equation (2.2) reduces to the Bernoulli equation, and the combination

$$(p/\rho - gz + \tfrac{1}{2}u^2)$$

forms an acceleration potential for the motion. In the turbulent regions $\boldsymbol{\omega} \neq 0$, and the two additional terms of (2.2) describe the effects of viscous damping and of the interactions between the waves and the turbulence and the turbulence with itself.

This immediately raises a second difficulty which concerns the separation of the motion into components associated with the waves and the turbulence respectively, since it is the interaction between these two components that we wish to study. As far as the vorticity field is concerned there is little problem, since in a fluid of small viscosity it is almost entirely associated with the turbulence. But for a velocity field that does not vanish at infinity in all directions, there is no simple unambiguous separation into rotational and irrotational parts, and we are obliged to seek an alternative representation. In the present problem, it is convenient to perform the separation in the following manner.

Since

$$\boldsymbol{\omega} = \nabla\times\mathbf{u},$$

and the liquid can be assumed to be incompressible, so that $\nabla . \mathbf{u} = 0$, it follows that

$$\nabla^2 \mathbf{u} = -\nabla \times \boldsymbol{\omega}. \tag{2.3}$$

The solution of (2.3) for the velocity components $\mathbf{u}$ can be expressed as

$$\mathbf{u}(\mathbf{x}) = \frac{1}{4\pi} \int_V \nabla \times \boldsymbol{\omega}(\mathbf{y}) \frac{d\mathbf{y}}{|\mathbf{x}-\mathbf{y}|} - \frac{1}{4\pi} \int_S \{|\mathbf{x}-\mathbf{y}|^{-1} d\mathbf{S} . \nabla \mathbf{u}(\mathbf{y}) - \mathbf{u}(\mathbf{y}) \nabla |\mathbf{x}-\mathbf{y}|^{-1} . d\mathbf{S}\}, \tag{2.4}$$

where the first integral is taken over the domain occupied by the fluid and the second over the surface bounding this domain. Several comments concerning this representation are worthy of attention. The first is that it clearly provides a unique separation of the velocity field into components associated with a given vorticity field and with a given velocity distribution over the boundaries of the domain. In the present problem, this corresponds to contributions to the velocity field from the turbulence and from the wave motion of the surface. Secondly, the separation is *not* one into rotational and irrotational parts of the velocity field, but into parts $\mathbf{u}_1$ and $\mathbf{u}_2$ which satisfy the equations $\nabla^2 \mathbf{u}_1 = -\nabla \times \boldsymbol{\omega}$ and $\nabla^2 \mathbf{u}_2 = 0$.

The distinction may be illustrated clearly in some simple examples. The velocity field associated with a localized region of vorticity in an unconfined fluid at rest at infinity is given entirely by the first (or vorticity) integral of (2.4) even outside the vortical region where the motion is irrotational. Again, if our control surface is taken in the interior of a fluid in uniform shearing motion, then the flow inside the surface is described wholly by the second (or surface) integral, since the vorticity is uniform and $\nabla \times \boldsymbol{\omega} = 0$. This second example also illustrates one restriction on the usefulness of this representation (though not, of course, on its validity). If the control surface is chosen arbitrarily in the fluid, then the motion over these surfaces will depend in general on the vorticity distribution, so that the two parts in this representation are kinematically related, and little is achieved by it. However, if the control surfaces are chosen to coincide with physical boundaries of the flow, the surface motion can be prescribed and the vorticity distribution is related to it only through the dynamical interaction. The two contributions to the velocity field represented by the terms on the right of (2.4) can conveniently be called the vortex-induced and surface-induced contributions to the velocity field.

The simplest scattering problem, analogous to the 'single scattering' of sound or radio waves, occurs when a surface wave traverses a region where the mean square vorticity fluctuations are sufficiently small that in the interaction term $\mathbf{u} \times \boldsymbol{\omega}$ of equation (2.2), the velocity $\mathbf{u}$ near the surface is determined predominantly by the surface-induced contribution from the incident wave. It appears later that the influence of the turbulence on the wave motion decreases very rapidly with increasing depth, so that we need only be concerned with the restrictions imposed by this condition when applied to the motion near the surface. The mean square value of the first integral is

$$\frac{1}{16\pi^2} \iint \overline{\nabla \times \boldsymbol{\omega}(\mathbf{y}) . \nabla \times \boldsymbol{\omega}(\mathbf{z})} \frac{d\mathbf{y}\, d\mathbf{z}}{yz},$$

where the origin is chosen at $\mathbf{x} = 0$, and if the length scale of the inhomogeneities in the vorticity field is much greater than the integral length scales of the vorticity covariances, it can be shown that this expression is of order

$$\frac{\overline{\omega^2}}{l_\omega^2} L_\omega^4,$$

where l_ω and L_ω are differential and integral length scales of the vorticity fluctuations. The root mean square magnitude of the first integral in (2.4) is then of order $(\overline{\omega^2})^{\frac{1}{2}} L_\omega^2 / l_\omega$. Near the surface, the second integral is of order αn, where α represents the height of the incident waves and n their frequency, which for gravity waves of wavelength λ is of order $(g/\lambda)^{\frac{1}{2}}$. A necessary condition, therefore, for the validity of a first-order scattering theory is that

$$u_t = \frac{(\overline{\omega^2})^{\frac{1}{2}} L_\omega^2}{l_\omega} \ll \frac{\alpha g^{\frac{1}{2}}}{\lambda^{\frac{1}{2}}},$$

where u_t represents the root-mean-square turbulent velocity fluctuations.

This restriction relates the Froude number of the turbulence to length scales of the turbulence and of the waves, since it can be expressed as

$$\left(\frac{L_\omega}{\lambda}\right)^{\frac{1}{2}} F^{\frac{1}{2}} \ll \frac{\alpha}{\lambda}, \tag{2.5}$$

where $F = \mathbf{u}_t^2 / g L_\omega$. Since, in a linearized wave theory α/λ itself must be small, of order 1/10 or less, we require that $F^{\frac{1}{2}}(L_\omega/\lambda)^{\frac{1}{2}}$ be even smaller. An alternative expression of (2.5), using the condition $\alpha/\lambda \ll 1$, is that

$$u_t \ll (g\lambda)^{\frac{1}{2}} = c(\kappa), \tag{2.6}$$

the phase velocity of the incident waves, where the triple inequality sign can be interpreted to mean 'is less by a factor of probably one hundred than'.

3. The wave propagation equation

The process of taking the divergence of (2.2) yields

$$\nabla^2(p/\rho - gz + \tfrac{1}{2}u^2) = \nabla . \mathbf{u} \times \boldsymbol{\omega}. \tag{3.1}$$

This equation provides the starting-point of the derivation of an inhomogeneous wave equation that describes the propagation of surface waves on deep turbulent water. There are three main steps in the analysis:

(*a*) Consider $(p/\rho - gz + \frac{1}{2}u^2) = f$, say, as our basic dependent variable and solve (3.1) formally for f in terms of its normal gradient $\partial f/\partial z$ at the equilibrium level $z = 0$, and of the distribution of $\nabla . \mathbf{u} \times \boldsymbol{\omega}$.

(*b*) Express $\partial f/\partial z$ at $z = 0$ in terms of the surface acceleration and the vorticity distribution by means of the vertical component of the momentum equation (2.1). These two steps give the function f throughout the fluid in terms of the surface acceleration and the vorticity distribution.

(*c*) The function f at the plane $z = 0$ is also expressed in terms of the surface displacement, using the boundary condition of constant pressure. This leads to the required equation between the surface displacement, surface acceleration and the vorticity distribution.

It will be supposed that the motion in the water is statistically homogeneous in planes parallel to the undisturbed surface $z = 0$, both on the grounds of analytical convenience and in the belief that this will represent a good approximation to the oceanographical situation. The motion can then be described by stationary random functions of the position variables x and y parallel to this plane (z being taken vertically downwards) and we can define Fourier–Stieltjes transforms $d\phi(\boldsymbol{\kappa}, z, t)$ and $d\chi(\boldsymbol{\kappa}, z, t)$ of the functions occurring in equation (3.1):

$$p/\rho - gz + \tfrac{1}{2}u^2 = \int d\phi(\boldsymbol{\kappa}, z, t)\, e^{i\boldsymbol{\kappa}.\mathbf{x}}, \tag{3.2}$$

$$\nabla . \mathbf{u} \times \boldsymbol{\omega} = \int d\chi(\boldsymbol{\kappa}, z, t)\, e^{i\boldsymbol{\kappa}.\mathbf{x}}, \tag{3.3}$$

where $\boldsymbol{\kappa} = (\kappa_1, \kappa_2)$ represents a two-dimensional horizontal wave-number so that $\boldsymbol{\kappa}.\mathbf{x} = \kappa_1 x + \kappa_2 y$, and the integrals are taken over all values of $\boldsymbol{\kappa}$. The analysis below is divided into three sections corresponding to the three main steps that have already been described.

(*a*) *Formal solution of equation* (3.1)

The relation between the Fourier–Stieltjes transforms $d\phi(\boldsymbol{\kappa}, z, t)$ and $d\chi(\boldsymbol{\kappa}, z, t)$ equivalent to (3.1) is

$$\left(\frac{\partial^2}{\partial z^2} - \kappa^2\right) d\phi(\boldsymbol{\kappa}, z) = d\chi(\boldsymbol{\kappa}, z), \tag{3.4}$$

where $\kappa^2 = \kappa_1^2 + \kappa_2^2$ and the time dependence is implicit. The boundary conditions to be imposed on (3.1) are that $\partial f/\partial z$ at the equilibrium level $z = 0$ is supposed to be given (it will be related to the surface acceleration in step (*b*)), and that both f and $\nabla . \mathbf{u} \times \boldsymbol{\omega}$ remain finite as $z \to \infty$, since the turbulent energy is presumed to be finite at very great depths. The corresponding conditions on the functions $d\phi$ and $d\chi$ in equation (3.4) are

$$\left.\begin{aligned} &\frac{\partial}{\partial z} d\phi(\boldsymbol{\kappa}, z, t) = d\Phi(\boldsymbol{\kappa}, t), \quad \text{say,} \quad \text{at } z = 0, \\ &d\phi(\boldsymbol{\kappa}, z, t), \quad d\chi(\boldsymbol{\kappa}, z, t) \quad \text{finite,} \quad \text{as } z \to \infty. \end{aligned}\right\} \tag{3.5}$$

The solution to (3.4) can be expressed as

$$d\phi(\boldsymbol{\kappa}, z, t) = \frac{1}{2\kappa} \int_0^z d\chi(\eta) \{e^{-\kappa(z-\eta)} - e^{\kappa(z-\eta)}\} d\eta + d\alpha\, e^{\kappa z} + d\beta\, e^{-\kappa z}, \tag{3.6}$$

where $\kappa = |\boldsymbol{\kappa}|$, η is a variable of integration in the vertical direction, and the dependance of $d\chi$ upon $\boldsymbol{\kappa}$ and time t is regarded as implicit. The functions $d\alpha(\boldsymbol{\kappa}, t)$ and $d\beta(\boldsymbol{\kappa}, t)$ are to be determined from the conditions (3.5). As $z \to \infty$, we find from (3.6) that

$$d\phi(z) \to e^{\kappa z}\left\{d\alpha - \frac{1}{2\kappa}\int_0^\infty d\chi(\eta)\, e^{-\kappa\eta}\, d\eta\right\} + \frac{1}{2\kappa}\int_0^z d\chi(\eta)\, e^{-\kappa(z-\eta)}\, d\eta,$$

so that in order to satisfy the condition of boundedness of $d\phi(z)$ as $z \to \infty$, it is necessary that

$$d\alpha(\boldsymbol{\kappa}, t) = \frac{1}{2\kappa}\int_0^\infty d\chi(\boldsymbol{\kappa}, \eta, t)\, e^{-\kappa\eta}\, d\eta. \tag{3.7}$$

Note that if the vorticity fluctuations extend to only a finite depth, then in fact $d\phi(\boldsymbol{\kappa}, z, t) \to 0$ as $z \to \infty$; and the fluid is at rest at very great depths.

Using the relation (3.7), the solution (3.6) can now be expressed as

$$d\phi(\boldsymbol{\kappa},z,t) = \frac{1}{2\kappa}\int_0^z d\chi(\eta)\,e^{-\kappa(z-\eta)}\,d\eta + \frac{1}{2\kappa}\int_z^\infty d\chi(\eta)\,e^{\kappa(z-\eta)}\,d\eta + d\beta\,e^{-\kappa z},$$

so that $$\left[\frac{\partial}{\partial z}\,d\phi(\boldsymbol{\kappa},z,t)\right]_{z=0} = \frac{1}{2}\int_0^\infty d\chi(\eta)\,e^{-\kappa\eta}\,d\eta - \kappa\,d\beta = d\Phi(\boldsymbol{\kappa},t), \quad \text{say},$$

the boundary function in which we desire to express our solution. Thus

$$d\beta(\boldsymbol{\kappa},t) = \frac{1}{2\kappa}\int_0^\infty d\chi(\boldsymbol{\kappa},\eta,t)\,e^{-\kappa\eta}\,d\eta - \frac{1}{\kappa}d\Phi(\boldsymbol{\kappa},t), \tag{3.8}$$

and the solution (3.6) finally becomes

$$d\phi(\boldsymbol{\kappa},z,t) = \frac{1}{2\kappa}\int_0^z d\chi(\eta)\,\{e^{-\kappa(z-\eta)} - e^{\kappa(z-\eta)}\}\,d\eta + \frac{1}{\kappa}\cosh\kappa z\int_0^\infty d\chi(\eta)\,e^{-\kappa\eta}\,d\eta - \frac{e^{-\kappa z}}{\kappa}\,d\Phi(\boldsymbol{\kappa},t). \tag{3.9}$$

(*b*) *Relation between* $d\Phi$ *and the surface acceleration*

This next step is achieved by considering the vertical component of the vector equation (2.2) at the surface. If the suffix z is taken to denote downwards vertical components, then

$$\frac{\partial}{\partial z}(p/\rho - gz + \tfrac{1}{2}u^2) = (\mathbf{u}\times\boldsymbol{\omega} - \nu\nabla\times\boldsymbol{\omega})_z - \frac{\partial u_z}{\partial t}, \tag{3.10}$$

or if $\xi(x,y,t)$ represents the surface displacement measured upwards,

$$\frac{\partial}{\partial z}(p/\rho - gz + \tfrac{1}{2}u^2) = (\mathbf{u}\times\boldsymbol{\omega} - \nu\nabla\times\boldsymbol{\omega})_z + \frac{\partial^2\xi}{\partial t^2}, \tag{3.11}$$

if the surface slope is small.

To express this equation in terms of its Fourier components, we must now introduce the further Fourier–Stieltjes transforms

$$\left.\begin{aligned}\mathbf{u}\times\boldsymbol{\omega} &= \int d\boldsymbol{\Gamma}(\boldsymbol{\kappa},z,t)\,e^{i\boldsymbol{\kappa}.\mathbf{x}},\\ (\nabla\times\boldsymbol{\omega})_z &= \int d\Delta(\boldsymbol{\kappa},z,t)\,e^{i\boldsymbol{\kappa}.\mathbf{x}},\end{aligned}\right\} \tag{3.12}$$

and for the surface displacement

$$\xi(x,y,t) = \int dA(\boldsymbol{\kappa},t)\,e^{i\boldsymbol{\kappa}.\mathbf{x}}. \tag{3.13}$$

It is clear that $d\boldsymbol{\Gamma}$ is simply related to the function defined by (3.3), for from the first of (3.12),

$$\nabla.\,\mathbf{u}\times\boldsymbol{\omega} = \int\left(i\boldsymbol{\kappa}.d\boldsymbol{\Gamma} + \frac{\partial}{\partial z}d\boldsymbol{\Gamma}_z\right)e^{i\boldsymbol{\kappa}.\mathbf{x}} = \int d\chi\,e^{i\boldsymbol{\kappa}.\mathbf{x}},$$

so that $$d\chi(\boldsymbol{\kappa},z,t) = i\boldsymbol{\kappa}.d\boldsymbol{\Gamma}(\boldsymbol{\kappa},z,t) + \frac{\partial}{\partial z}d\Gamma_z(\boldsymbol{\kappa},z,t). \tag{3.14}$$

Equation (3.11) can therefore be expressed as a relation between these Fourier–Stieltjes transforms:

$$\left[\frac{\partial}{\partial z}d\phi\right]_{z=0} = [d\Gamma_z - \nu\, d\Delta]_{z=0} + \frac{\partial^2}{\partial t^2}dA$$
$$= d\Phi,$$

from (3.5), where again the dependence of the various functions on $\boldsymbol{\kappa}, t$ and, where relevant, z, is understood. Equation (3.9) therefore becomes

$$d\phi(\boldsymbol{\kappa}, z, t) = \frac{1}{2\kappa}\int_0^z d\chi(\eta)\{e^{-\kappa(z-\eta)} - e^{\kappa(z-\eta)}\}\,d\eta + \kappa^{-1}\cosh\kappa z \int_0^\infty d\chi(\eta)\, e^{-\kappa\eta}\,d\eta$$
$$-\kappa^{-1}e^{-\kappa z}\left\{d\Gamma_z(\boldsymbol{\kappa}, t) - \nu\, d\Delta(\boldsymbol{\kappa}, t) + \frac{\partial^2}{\partial t^2}dA(\boldsymbol{\kappa}, t)\right\}, \quad (3.15)$$

where the quantities $d\Gamma_z$ and $d\Delta$ are taken at $z = 0$.

This equation provides a relation (admittedly rather a complicated one) between the Fourier–Stieltjes components of the function $f = p/\rho - gz + \frac{1}{2}u^2$ and those involving the vorticity distribution and the surface accelerations. It is subject only to the restriction that the surface gradients are small; no approximations have yet been made concerning the relative magnitudes of velocities associated with the waves and the turbulence. It is therefore applicable equally to the problem of scattering of gravity waves by turbulence of low intensity and to the problem of wave *generation* when the turbulent intensity is greater. The further consideration of this latter problem is postponed to a later paper; from this point in the present paper attention will be confined to the scattering problem in which the turbulent intensity is sufficiently small that the condition (2.5) is satisfied.

(c) *Derivation of the inhomogeneous wave equation*

The boundary condition at the free surface $z = -\xi$ is that the pressure is constant and can be taken as zero. Under the condition (2.5), the velocity near the surface is predominantly a result of the surface-induced contributions, so that $\frac{1}{2}u^2$ is of order $\alpha^2 n^2$, where α is the height of the incident wave and n is its frequency. For gravity waves in deep water, n^2 is of order g/λ, where λ is the wavelength, so that $\frac{1}{2}u^2$ is of order $g\alpha^2/\lambda$. To the first order in the wave slope α/λ, therefore,

$$[p/\rho - gz + \tfrac{1}{2}u^2]_{z=0} \simeq [p/\rho - gz + \tfrac{1}{2}u^2]_{z=-\xi}$$
$$\simeq g\xi.$$

The free surface boundary condition, together with (2.6) requiring α/λ to be small, therefore leads to the relation

$$g\, dA(\boldsymbol{\kappa}, t) = [d\phi(\boldsymbol{\kappa}, z, t)]_{z=0} \quad (3.16)$$

between the Fourier–Stieltjes transforms defined by (3.2) and (3.13). This, together with (3.15), provides an equation for the propagation of the components $dA(\boldsymbol{\kappa}, t)$ of the surface displacement

$$\left(\frac{\partial^2}{\partial t^2} + g\kappa\right)dA(\boldsymbol{\kappa}, t) = \int_0^\infty d\chi(\eta)\, e^{-\kappa\eta}\,d\eta - d\Gamma_z(\boldsymbol{\kappa}, t) - \nu\, d\Delta(\boldsymbol{\kappa}, t). \quad (3.17)$$

The relation (3.14) can be used to express $d\chi(\eta)$ in terms of $d\mathbf{\Gamma}(\eta)$, and on substitution into (3.17) and integration by parts, we find that

$$\left\{\frac{\partial^2}{\partial t^2}+\left(\frac{g}{\kappa}\right)\kappa^2\right\}dA(\boldsymbol{\kappa},t)=\int_0^\infty(\kappa\,d\Gamma_z+i\boldsymbol{\kappa}.d\mathbf{\Gamma})\,e^{-\kappa\eta}\,d\eta-\nu\,d\Delta(\boldsymbol{\kappa},t), \tag{3.18}$$

where, yet again, the variation of $d\mathbf{\Gamma}$ with $\boldsymbol{\kappa}$, η and time t is to be understood and $d\Delta$ is taken at $z=0$.

The left-hand side of this equation is recognizable as the Fourier transform of a wave equation in which the phase velocity of the waves is $(g/\kappa)^{\frac{1}{2}}$. The right-hand side represents the influence of the inhomogeneities introduced by the turbulence, together with the viscous damping term. It will be noticed that, in view of the exponential factor in the integral, the vorticity fluctuations at depths greater than about a wavelength have little influence upon the propagation of surface waves, verifying the statement made in anticipation in §2. The viscous dissipation term is probably negligible for all but very short waves. In the absence of turbulent scattering, an expression given by Lamb (1932, p. 624) indicates that a water wave of wavelength 20 m travels a distance of 8400 km before its amplitude is reduced by a factor e^{-1}. It is therefore likely (an *a posteriori* justification can be made from the results of the next section) that unless the mean square turbulent vorticity fluctuations in the ocean are exceedingly minute, the effect of viscous dissipation in waves of moderate wavelength will be small compared to the effects of turbulent scattering, and the term $\nu\,d\Delta$ in (3.18) can be neglected.

4. The scattered wave system

Suppose that, at an initial instant, a wave of amplitude α and wavelength $2\pi/k$ is travelling along the surface of the water in the direction of the positive x-axis. If the fluctuations in vorticity in the water are sufficiently small, the motion is, to a first approximation, that of an irrotational surface wave in which the surface displacement is

$$\alpha e^{-i(kx-nt)},$$

and the surface-induced components of the velocity field are

$$\left.\begin{aligned} u_1 &= \alpha n\, e^{-i(kx-nt)}e^{-kz},\\ u_2 &= 0,\\ u_3 &= -i\alpha n\, e^{-i(kx-nt)}e^{-kz},\end{aligned}\right\} \tag{4.1}$$

where the suffices 1, 2 and 3 indicate velocity components in the x, y and z directions respectively, and the wave frequency $n=(gk)^{\frac{1}{2}}$.

The next approximation, which describes the scattered wave field is obtained by substituting from (4.1) into the interaction term of the inhomogeneous equation (3.18). To do this, we make use of the theorem which states that if $f(\boldsymbol{\kappa})$ is the Fourier transform of $F(\mathbf{x})$, then the Fourier transform of $F(\mathbf{x})\,e^{-ikx}$ is

$$\begin{aligned}\int F(\mathbf{x})\,e^{-ikx}\,e^{i\boldsymbol{\kappa}.\mathbf{x}}\,d\mathbf{x} &= \int F(\mathbf{x})\,e^{i(\kappa_1-k)x+i\kappa_2 y}\,d\mathbf{x}\\ &= f(\mathbf{K}),\end{aligned} \tag{4.2}$$

where the new wave-number vector $\mathbf{K} = (\kappa_1 - k, \kappa_2)$. Now $d\Gamma_1$ is the Fourier–Stieltjes transform of $(u_2\omega_3 - u_3\omega_2)$ or of $-u_3\omega_2$ approximately, since from (4.1), to the first approximation, the surface-induced contribution to u_2 from the incident wave vanishes. Therefore, if the vorticity fluctuations are represented by

$$\boldsymbol{\omega}(\mathbf{x}, t) = \int d\boldsymbol{\Omega}(\boldsymbol{\kappa}, z, t)\, e^{i\boldsymbol{\kappa}.\mathbf{x}}, \tag{4.3}$$

where $\boldsymbol{\kappa} = (\kappa_1, \kappa_2)$, we have from (4.1) and (4.2) that

$$d\Gamma_1 = i\alpha n\, e^{int} e^{-kz} d\Omega_2(\mathbf{K}).$$

Similarly,

$$d\Gamma_2 = -i\alpha n\, e^{int} e^{-kz}\{d\Omega_1(\mathbf{K}) + i\, d\Omega_3(\mathbf{K})\},$$

$$d\Gamma_3 = -i\alpha n\, e^{int} e^{-kz} d\Omega_2(\mathbf{K}),$$

so that from equation (3.18),

$$\left(\frac{\partial^2}{\partial t^2} + g\kappa\right) dA(\boldsymbol{\kappa}, t) = \alpha n\, e^{int} d\psi(\mathbf{K}, \boldsymbol{\kappa}, t), \tag{4.4}$$

say, where

$$d\psi(\mathbf{K}, \boldsymbol{\kappa}, t) = \int_0^\infty \{\kappa_2 d\Omega_1(\mathbf{K}) - (\kappa_1 + i\kappa) d\Omega_2(\mathbf{K}) + i\kappa_2 d\Omega_3(\mathbf{K})\}\, e^{-(\kappa + ik)\eta}\, d\eta, \tag{4.5}$$

the dependence of $d\Omega_i(\mathbf{K})$ upon η and time t being understood.

Equation (4.4) specifies the rate of growth of the wavelets of wave-number $\boldsymbol{\kappa}$ set up by the passage of the wave of wave-number k through the turbulent fluid, where the subsequent scattering of these wavelets themselves is neglected. This process is analogous to that of 'single scattering' of sound or radio waves in a medium in which the wave velocity varies irregularly from one point to another. In the case of gravity waves on the surface of a liquid, however, the phase and group velocities are determined not by the local surface conditions but by the motion throughout a whole layer of fluid near the surface, and this fact is reflected by the integral expression as given by (4.5) that appears on the right-hand side of the scattering equation (4.4).

We will suppose that at the initial instant $t = 0$ the amplitude of the scattered wave system is zero, and we will investigate the growth of the scattered components during subsequent times. The initial conditions relevant to (4.4) are then that

$$dA(\boldsymbol{\kappa}, t) = \frac{\partial}{\partial t} dA(\boldsymbol{\kappa}, t) = 0 \quad \text{at} \quad t = 0,$$

so that the solution can be expressed as

$$\begin{aligned} dA(\boldsymbol{\kappa}, t) &= \frac{n}{2in'} \int_0^t \alpha\, d\psi(\mathbf{K}, \boldsymbol{\kappa}, \tau)\, e^{in\tau}\{e^{in'(t-\tau)} - e^{-in'(t-\tau)}\}\, d\tau \\ &= \frac{n}{2in'} \int_0^t \alpha\, d\psi(\mathbf{K}, \boldsymbol{\kappa}, \tau)\, \{e^{in't} e^{i(n-n')\tau} - e^{-in't} e^{i(n+n')\tau}\}\, d\tau, \end{aligned} \tag{4.6}$$

where $n = (gk)^{\frac{1}{2}}$ and $n' = (g\kappa)^{\frac{1}{2}}$. The variation with time of $d\psi(t)$ is determined by the variation of the vorticity fluctuations with time, and in many problems of interest, particularly in oceanographical contexts, this is very much slower than the time variations characteristic of the waves. It is possible to neglect the

temporal variation of the vorticity if the time taken for the wave to propagate through a distance equal to the length scale L_ω of the vorticity fluctuations is small compared with the time scale of these fluctuations, that is, if

$$\frac{L_\omega}{(g\lambda)^{\frac{1}{2}}} \ll (\overline{\omega^2})^{\frac{1}{2}},$$

where λ is the wavelength. This condition can be restated in terms of the Froude number of the turbulence as follows:

$$\left(\frac{L_\omega}{\lambda}\right)^{\frac{1}{2}} F^{\frac{1}{2}} \ll \frac{L_\omega}{l_\omega},$$

where F is the Froude number and l_ω the differential length scale defined at the end of § 2. In general the integral scale L_ω would be expected to be rather larger than the differential scale l_ω so that this condition is much less restrictive than (2.5) and should hold automatically when (2.5) is satisfied.

The amplitude α of the incident wave also is contained within the time integral of (4.6). Its variation with time occurs as a result of the loss of energy to the scattered components, but since the vorticity level in the water has already been presumed small, it can be anticipated that this variation is also likely to be slow. For times less than the time scale γ^{-1} of the attenuation of the incident wave due to scattering, therefore, equation (4.6) simplifies to

$$\begin{aligned} dA(\boldsymbol{\kappa}, t) &\doteq \frac{\alpha n}{2in'} d\psi(\mathbf{K}, \boldsymbol{\kappa}, 0) \int_0^t \{e^{in't} e^{i(n-n')\tau} - e^{-in't} e^{i(n+n')\tau}\} d\tau, \\ &= \frac{-\alpha n}{2n'} d\psi(\mathbf{K}, \boldsymbol{\kappa}) \left\{ \frac{e^{int} - e^{in't}}{n - n'} - \frac{e^{int} - e^{-in't}}{n + n'} \right\}. \end{aligned} \tag{4.7}$$

where α and $d\psi$ represent the appropriate quantities at the initial instant $t = 0$. This equation can be expressed as

$$dA(\boldsymbol{\kappa}, t) = \frac{-\alpha n}{2n'} d\psi(\mathbf{K}, \boldsymbol{\kappa}) t \left\{ \frac{e^{i\sigma} - e^{i\sigma'}}{\sigma - \sigma'} - \frac{e^{i\sigma} - e^{-i\sigma'}}{\sigma + \sigma'} \right\},$$

where $\sigma = nt = (gk)^{\frac{1}{2}} t$ and $\sigma' = n't = (g\kappa)^{\frac{1}{2}} t$. The spectrum of the scattered waves is

$$\begin{aligned} \Phi(\boldsymbol{\kappa}, t) &= \frac{\overline{dA(\boldsymbol{\kappa}, t)\, dA^*(\boldsymbol{\kappa}, t)}}{d\kappa_1 d\kappa_2} \\ &= \frac{\alpha^2 n^2}{4n'^2} \Psi(\mathbf{K}, k) t^2 \Gamma(\kappa, k, t), \end{aligned} \tag{4.8}$$

where $\Psi(\mathbf{K}, k) \equiv \Psi(\mathbf{K}, \boldsymbol{\kappa})$ is the spectral function corresponding to the Fourier–Stieltjes components $d\psi(\mathbf{K}, \boldsymbol{\kappa}) \equiv d\psi(\mathbf{K}, k)$:

$$\Psi(\mathbf{K}, k) = \frac{d\psi(\mathbf{K}, k)\, d\psi^*(\mathbf{K}, k)}{d\kappa_1 d\kappa_2}, \tag{4.9}$$

and the function Γ is given by

$$\begin{aligned} \Gamma(\kappa, k, t) &= \left\{ \frac{e^{i\sigma} - e^{i\sigma'}}{\sigma - \sigma'} - \frac{e^{i\sigma} - e^{-i\sigma'}}{\sigma + \sigma'} \right\} \left\{ \frac{e^{-i\sigma} - e^{-i\sigma'}}{\sigma - \sigma'} - \frac{e^{-i\sigma} - e^{i\sigma'}}{\sigma + \sigma'} \right\} \\ &= \frac{2}{(\sigma - \sigma')^2} \{1 - \cos(\sigma - \sigma')\} - \frac{2}{\sigma^2 - \sigma'^2} \{1 + \cos 2\sigma' \\ &\qquad - \cos(\sigma + \sigma') - \cos(\sigma - \sigma')\} + \frac{2}{(\sigma + \sigma')^2} \{1 - \cos(\sigma + \sigma')\}. \end{aligned} \tag{4.10}$$

The wave-number k is specified by the incident wave field, and when Γ is regarded as a function of σ', it is evident by inspection that Γ has a maximum when $\sigma = \sigma'$ or $k = \kappa$, when the (scalar) wave-numbers of the incident and scattered waves are equal. Near this maximum, if $\sigma = \sigma' + \epsilon$,

$$\Gamma(\kappa, k, t) \doteq \frac{2(1-\cos\epsilon)}{\epsilon^2}, \tag{4.11}$$

neglecting terms of order ϵ/σ. If we consider only the wave components scattered in a given direction θ, the direction of the vector $\boldsymbol{\kappa}$, it follows from (4.8) that the spectral density is greatest near $\kappa = k$, and from (4.10) that the 'band width' $\delta\kappa$ of the spectrum of the scattered components is given by

$$\epsilon = [g(k+\delta\kappa)]^{\frac{1}{2}}\, t - [gk]^{\frac{1}{2}}\, t = \pi.$$

or

$$\frac{\delta\kappa}{k} = \frac{2\pi}{t}\,(gk)^{-\frac{1}{2}} = \frac{2\pi}{nt}. \tag{4.12}$$

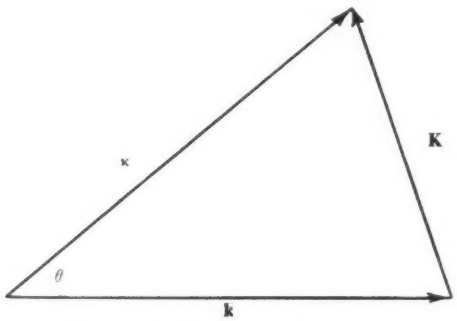

FIGURE 1. The scattering vector.

If the elapsed time t is much greater than the periodic time of the incident waves, this 'band width' of the scattered waves is narrow, and decreases in inverse proportion to t, so that the spectrum of the scattered waves at a given scattering angle θ becomes more and more concentrated about the wave-number $\kappa = k$, the wave-number of the incident waves.

It follows from equation (4.8) in the light of these considerations that the scattered waves of wave-number $\boldsymbol{\kappa} = (\kappa_1, \kappa_2)$ in the direction θ with respect to the direction of the incident waves result from the components of the vorticity field of wave-number $\mathbf{K} = (\kappa_1 - k, \kappa_2)$, where $k = \kappa = (\kappa_1^2 + \kappa_2^2)^{\frac{1}{2}}$. The same vector $\mathbf{K}$ is important in other scattering problems, where it is usually called the 'scattering vector', and the same name can conveniently be used in the present context. It is clear from figure 1 that, since $\kappa = k$, the vector $\mathbf{K}$ is perpendicular to the line bisecting the directions of the incident and scattered waves, and is of magnitude

$$K = 2\kappa \sin\tfrac{1}{2}\theta = 2k \sin\tfrac{1}{2}\theta. \tag{4.13}$$

The appearance of the scattering vector might be expected on geometrical grounds (as shown, for example, by Batchelor 1957) by considering two scattering points P and P', as shown in figure 2, separated by a distance $l = 2\pi/K$.

For reinforcement of the scattered waves, the path APB must equal one wavelength of the incident wave, or $2\pi/k$. Thus $(\pi/k)/(2\pi/K) = \sin\frac{1}{2}\theta$, leading immediately to (4.13).

The mean square amplitude of the waves scattered per unit angle in the direction θ is found from (4.8) by integration over wave-numbers κ in this direction. When the elapsed time t is much greater than the period of the incident waves, the approximation (4.11) can be used, and

$$\Phi(\theta, t) \doteq \frac{\alpha^2}{4} \Psi(\mathbf{K})\, t^2 \int_0^\infty \frac{2 - 2\cos\epsilon}{\epsilon^2} \kappa\, d\kappa, \tag{4.14}$$

since over the small range of values of κ corresponding to $-\frac{1}{2}\pi < \epsilon < \frac{1}{2}\pi$, $n' \doteq n$ and the variation of the vector K and so of the function $\Psi(K)$ is small. Now,

$$d\epsilon = \tfrac{1}{2} g^{\frac{1}{2}} \kappa^{-\frac{1}{2}} t\, d\kappa \doteq \tfrac{1}{2} g^{\frac{1}{2}} k^{-\frac{1}{2}} t\, d\kappa$$

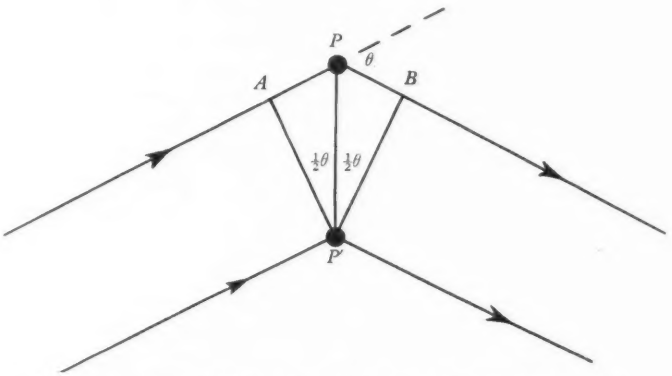

FIGURE 2. A geometrical interpretation of the scattering vector.

near $\kappa = k$, so that (4.14) can be expressed as

$$\begin{aligned} \Phi(\theta, t) &\doteq \frac{\alpha^2 k^2}{2(gk)^{\frac{1}{2}}} \Psi(\mathbf{K})\, t \int_{-\infty}^{\infty} \frac{1 - \cos\epsilon}{\epsilon^2}\, d\epsilon \\ &= \frac{\pi \alpha^2 k^2}{(gk)^{\frac{1}{2}}} \Psi(\mathbf{K})\, t. \end{aligned} \tag{4.15}$$

The directional distribution of the scattered waves is described conveniently by the ratio of the mean energy flux developed in the scattered waves per unit length of wave front per unit angle in the direction θ per unit time to the energy flux in the incident wave per unit length of wave front. This ratio is given by

$$\begin{aligned} s(\theta, k) &= \frac{1}{\alpha^2} \frac{\partial}{\partial t} \Phi(\theta, t), \\ &= \frac{\pi k^2}{(gk)^{\frac{1}{2}}} \Psi(\mathbf{K}), \end{aligned} \tag{4.16}$$

which has dimensions (time)$^{-1}$. The fraction of the energy of the incident wave lost by scattering per unit time, or the logarithmic decrement of attenuation due to scattering is

$$\gamma(k) = \int_{-\pi}^{\pi} s(\theta, k)\, d\theta,$$

$$= \frac{\pi k^2}{(gk)^{\frac{1}{2}}} \int_{-\pi}^{\pi} \Psi(\mathbf{K})\, d\theta, \tag{4.17}$$

where the scattering vector $\mathbf{K}$ has magnitude $2k \sin \frac{1}{2}\theta$ and direction $\frac{1}{2}(\pi + \theta)$.

If further progress beyond expressions such as (4.16) and (4.17) is to be made, some information is necessary concerning the form of the function $\Psi(\mathbf{K})$. It can be seen readily from (4.5) and (4.9) that $\Psi(\mathbf{K})$ has the same dimensions as the two-dimensional vorticity spectrum of the turbulence, and since the Reynolds number of the turbulence encountered in the ocean is extremely large, it is to be expected that $\Psi(\mathbf{K})$ is directly proportional to this vorticity spectrum. The length scales associated with the vorticity spectrum in oceanic turbulence cover a very wide range, perhaps from several hundred metres down to a microscale, or scale of the smallest eddies, of order 1 cm, which certainly includes the wavelengths of incident waves in which we are likely to be most interested. This fact precludes the use of the limiting approximations found useful in considering the scattering of acoustical or radio waves (see Batchelor 1957) which suppose that the length scale of the scatterers is either much greater or much less than the wavelength of the incident waves.

The observation that $\Psi(\mathbf{K})$ is proportional to the two-dimensional vorticity spectrum suggests that use might be made of the predictions of the local similarity theory, but this cannot be done without some caution. We are interested in the form of the vorticity spectrum near the free surface, measured in a plane parallel to the surface. It is well known experimentally, and indeed it is only to be expected on *a priori* grounds that near a *rigid* surface with large mean velocity gradients, the theory of local similarity is inapplicable in a description of the flow. However, a *free* surface imposes fewer constraints on the motion in the immediate neighbourhood; the mean shear now vanishes and the fluid is free to move parallel to the surface. The conditions are much closer to those which the local similarity theory seeks to describe, and the function $\Psi(\mathbf{K})$ to which it might be applied seems to be almost the most appropriate that could be found, since it represents an integral throughout a layer near the surface and should not therefore be crucially dependent upon the conditions immediately at the interface.

With these reservations in mind, then, we will make use of this theory to determine the functional form of $\Psi(\mathbf{K})$. Except when θ is very small (cf. 4.13), the values of K corresponding to waves of moderate length fall in the 'inertial subrange' of the spectrum of the turbulence, so that $\Psi(\mathbf{K})$ should be determined by $\mathbf{K}$ and ϵ, the rate of energy dissipation in the turbulence, and not by any of the other parameters describing the turbulence. On dimensional grounds, therefore,

$$\Psi(\mathbf{K}) = B\epsilon^{\frac{2}{3}} K^{-\frac{3}{3}}, \tag{4.18}$$

where B is an absolute constant. The directional distribution $s(\theta, k)$ of the scattered waves is found by substitution of (4.18) and (4.13) into (4.17):

$$s(\theta, k) = 2^{-\frac{3}{3}} B\pi g^{-\frac{1}{2}} \epsilon^{\frac{2}{3}} k^{\frac{5}{3}} (\sin \tfrac{1}{2}\theta)^{-\frac{3}{3}}. \tag{4.19}$$

Near $\theta = 0$, in the forward direction, this expression becomes invalid, since the wave-numqers $K \doteqdot k\theta$ then correspond to length scales in the scattering vorticity field of the same order as the horizontal scale L of the energy-containing components of the turbulence. Indeed, when $\theta = 0$, it can be shown that $s(\theta, k) = 0$, and there is no energy scattered in the direction of the incident wave. This follows from some expressions that we have already derived, for when $\theta = 0$, $K = 0$ and (4.9) and (4.5) can be used to show that $\Gamma(0) = 0$, which, in virtue of (4.16) implies that $s(\theta, k) = 0$ when $\theta = 0$. The directional distribution function of the scattered waves is thus of the form shown in figure 3, where the dotted line indicates the continuation of (4.19) near $\theta = 0$. The maximum value of $s(\theta, k)$ occurs at a value of θ of approximately λ/L, where λ is the wavelength of the incident waves.

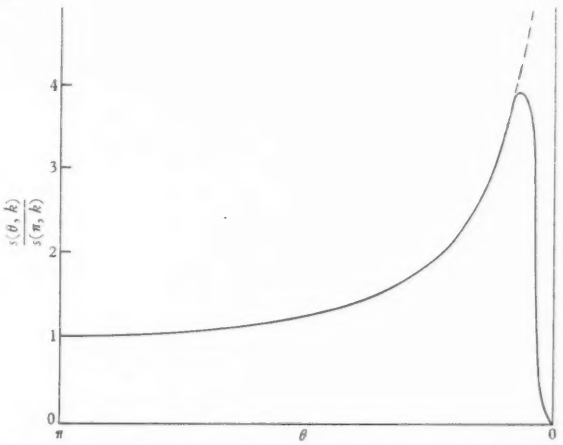

FIGURE 3. The directional distribution of scattered waves in the ocean.

An approximate expression for the logarithmic decrement $\gamma(k)$, valid when λ/L is sufficiently small, is obtained by integration of (4.19) from $\theta = 0$ to 2π and neglecting the decrease of $s(\theta, k)$ to zero when $\theta = 0$. This yields

$$\begin{aligned}\gamma(k) &\doteqdot 2^{-\frac{2}{3}} B\pi g^{-\frac{1}{2}} \epsilon^{\frac{2}{3}} k^{\frac{5}{6}} . 2 \int_0^{\pi} (\sin \tfrac{1}{2}\theta)^{-\frac{2}{3}} \, d\theta \\ &= 2^{\frac{1}{3}} B\pi \left\{ \frac{\Gamma(\frac{1}{6})\,\Gamma(\frac{1}{2})}{\Gamma(\frac{2}{3})} \right\} g^{-\frac{1}{2}} \epsilon^{\frac{2}{3}} k^{\frac{5}{6}} \\ &\doteqdot 29 B g^{-\frac{1}{2}} \epsilon^{\frac{2}{3}} k^{\frac{5}{6}}. \end{aligned} \tag{4.20}$$

It is interesting to compare this result with that derived by Stokes (and discussed by Lamb 1932, §§348, 349) for the logarithmic decrement resulting from viscous dissipation, namely

$$\gamma_v(k) = 2\nu k^2.$$

The attenuation resulting from scattering will predominate if

$$29 B g^{-\frac{1}{2}} \epsilon^{\frac{2}{3}} k^{\frac{5}{6}} > 2\nu k^2,$$

i.e.

$$k < \left\{ \frac{15 B \epsilon^{\frac{2}{3}}}{\nu g^{\frac{1}{2}}} \right\}^{\frac{6}{7}}. \tag{4.21}$$

The rate of turbulent energy dissipation in the open ocean may be estimated from some fairly rough diffusion measurements described by Stommel (1949) and a typical value for ϵ in the open ocean appears to be of order $10^{-5}\,\mathrm{cm\,sec^{-3}}$. The gravitational acceleration g is approximately $10^3\,\mathrm{cm\,sec^{-2}}$ and the kinematic viscosity ν for water is approximately $1{\cdot}5\times10^{-2}\,\mathrm{cm^2\,sec^{-1}}$. With these values, and if B is of order unity, it follows from (4.21) that attenuation resulting from scattering predominates for wave-numbers less than about $2\times10^{-2}\,\mathrm{cm^{-1}}$; or for wavelengths greater than about 3 m. In tidal waters where the turbulence may be more intense than it is in the open ocean, the attenuation resulting from scattering may be important for even shorter wavelengths.

It is doubtful whether oceanographical wave measurements are yet sufficiently precise to make meaningful observations on the attenuation of surface waves. The results of this paper, however, suggest that when this is done, the cause of the attenuation of the longer components of the wave field may lie not in the dissipative action of viscosity but in the scattering action of the oceanic turbulence.

This work was supported by the Office of Naval Research under Contract Nonr 38 (248).

REFERENCES

Batchelor, G. K. 1957 Article in *Symposium on Naval Hydrodynamics*, 1956. Publication 515, National Academy of Sciences—National Research Council, Washington.

Darbyshire, J. 1952 *Proc. Roy. Soc.* A, **215**, 299.

Lamb, H. 1932 *Hydrodynamics*, 6th ed. Cambridge University Press.

Stommel, H. 1949 *J. Mar. Res.* **8**, 199.

The slow motion of two or more spheres through a viscous fluid

By G. J. KYNCH
Department of Mathematics, The Manchester College of Science and Technology

(Received 5 July 1958)

Expressions are derived for the velocity of two spheres, moving slowly under external forces through a viscous fluid, as a function of their separation and radii. They compare favourably with the available experimental data. A discussion of the interactions of three particles and some general comments on the settling of a swarm of spheres are also included.

1. Introduction

Despite the long time which has elapsed since Stokes's law was proved for the slow motion of a rigid sphere through a viscous fluid, there has been no connected account of the slow motion of two spheres. In this paper an attempt is made to remedy this omission for the very good reason that experiments are now being made (e.g. Hall 1956) of sufficient accuracy to justify a comparison with theory.

It should also be borne in mind that the results of these calculations are used as the basis for theories of sedimentation of collections of particles and of the flow of suspensions. A satisfactory account should, therefore, be of such a type that it can readily be developed to discuss the motion of many particles. The first calculation to be made (Smoluchowski 1911) was of this type and was used to estimate the motion of a cloud of particles. Smoluchowski calculated the first terms in an expansion in powers of the ratio of the particle radius to the distance between centres, and his results are valid only for small values of this parameter. Later Burgers (1942) extended this calculation to one higher order with the same purpose in mind, using arguments based to a large extent on physical intuition. In the meantime Stimson & Jeffery (1926) gave a complete solution of the problem of two spheres falling one behind the other, where there is axial symmetry, but their method uses the symmetry and cannot be extended to handle more than two particles.

The method described below is essentially an extension of that of Smoluchowski and Burgers. In the next three sections we discuss the solutions of the fluid equations that are needed for the solution of the two-body problem and comparison with experiment. It is not assumed that the spheres are equal, but §4 is mostly concerned with theoretical predictions for equal spheres, and the measurements which are needed to verify them. The method is easily extended to describe the motion of more than two particles and two later sections describe briefly some special results for three or more particles.

The essential features of the motion of two particles are predicted in the paper by Smoluchowski. Equal spheres falling under gravity fall together with a constant separation, but they only fall vertically when the line of centres is either horizontal or vertical; otherwise they tend to slide downwards along the line of the centres. The experimental results of Hall agree qualitatively with these calculations for large separations of the particles, the discrepancies being due almost certainly to experimental error. Hall also compares his results with the predictions of Stimson & Jeffery (1926). A complete theory, neglecting inertia terms, is obtained by combining the solution of Stimson & Jeffery with another, still to be obtained, of the problem where the line joining the spheres is perpendicular to the direction of motion.

A reader who is more interested in the qualitative results of this work need not examine too closely the next two sections which contain the mathematical analysis, although these sections define the notation used subsequently.

2. Solutions of the Navier–Stokes equations

The hydrodynamic equations for an incompressible viscous fluid, neglecting inertia terms, are

$$\nabla^2 u_\alpha = 2\partial p/\partial x_\alpha - (F_\alpha/\mu), \quad \sum_\alpha (\partial u_\alpha/\partial x_\alpha) = 0, \tag{2.1}$$

where $2\mu p$ is the mean pressure, μ is the coefficient of viscosity, $x_\alpha = (x, y, z)$ are Cartesian co-ordinates and u_α, F_α the Cartesian components of the velocity and body forces, respectively. If the body forces are zero, it is easily deduced that $\nabla^2 p = 0$, and the solutions can be written in the form $u_\alpha = v_\alpha + x_\alpha p$, where $\nabla^2 v_\alpha = 0$ (Kynch 1954). This result was used to derive the results stated below.

It is not difficult to find solutions of these equations such that two of the velocity components are zero and the third component varies in an arbitrary manner on the surface of the sphere $r = a$. If the non-zero component is $u_\beta = f$ at $r = a$, where f is a homogeneous function of the co-ordinates of degree m, which satisfies Laplace's equation, then the fluid motion is

$$u_\alpha = f\delta_{\alpha\beta} + \frac{r^2 - a^2}{2(1-m)} \frac{\partial^2 f}{\partial x_\alpha \partial x_\beta}, \tag{2.2}$$

$$p = -\frac{2m-1}{2(m-1)} \frac{\partial f}{\partial x_\beta}. \tag{2.3}$$

For example, when $m = -(n+1)$, the function f can be any of the nth derivatives of $(1/r)$. If m is positive or zero the solutions are regular at the origin, and if m is negative they have a singularity at the origin.

To derive solutions corresponding to more general boundary conditions at $r = a$, we note that any function can be expanded on a sphere in terms of surface harmonics. In particular, if ϕ is any function defined on the surface, then

$$\phi = A\left(\frac{1}{r}\right) + A_\alpha \frac{\partial}{\partial x_\alpha}\left(\frac{1}{r}\right) + A_{\alpha\beta} \frac{\partial^2}{\partial x_\alpha \partial x_\beta}\left(\frac{1}{r}\right) + \ldots \quad (\text{on } r = a), \tag{2.4}$$

where $A, A_\alpha, A_{\alpha\beta}, \ldots$ are constants. In this equation the usual summation convention has been adopted, repeated suffices $\alpha, \beta, \ldots$ being summed over their three

values. To facilitate the manipulation of these expressions, a further convention is adopted where a group of n suffices $(\alpha_1, \alpha_2, \alpha_3, \ldots, \alpha_n)$ is denoted by a single roman letter (n), and a repeated suffix (n) is summed over all values of the group of n suffices and usually over all values of $n = 0, 1, 2, 3, \ldots$ as well. Thus equation (2.4) becomes

$$\begin{aligned}\phi &= A(1/r) + A_\alpha (1/r)_\alpha + A_{\alpha\beta}(1/r)_{\alpha\beta} + \ldots \\ &= \Sigma A_n (1/r)_n \quad \text{on} \quad (r = a),\end{aligned}$$

i.e.
$$\phi = \Sigma A_n (1/a)_n. \tag{2.5}$$

Let the velocity components u_β have values, on a sphere A of radius a, expanded in the form,

$$u_\beta = \sum_m A_{\beta m} (1/a)_m \quad \text{on } A. \tag{2.6}$$

Let us also assume that the velocity tends to zero at infinity. Then by writing $f = (1/r)_m$ in the particular solutions (2.2), we derive the solution

$$u_\alpha = \sum_{\beta, m} A_{\beta m} S^\alpha_{\beta m}(A), \quad \text{where} \quad S^\alpha_{\beta m} = \left(\frac{1}{r}\right)_m \delta_{\alpha\beta} + \frac{r^2 - a^2}{2(m+2)} \left(\frac{1}{r}\right)_{\alpha\beta m},$$

$$p = -\sum_{\beta, m} A_{\beta m} \frac{2m+3}{2(m+2)} \left(\frac{1}{r}\right)_{\beta m}. \tag{2.7}*$$

The irrotational motion of a non-viscous fluid due to a moving body is usually described in terms of a suitable distribution of sources, dipoles and so on, whose velocity potentials are known. The solutions S can be regarded as those which arise from a generalization of this idea for viscous fluids. The radius a appears because we are specially interested in the motion of spherical particles, but it is simply an arbitrary parameter. The method used by Burgers (1942), which he attributes to Oseen (1927), seems to be based on these solutions when $a = 0$. The following interpretation of the pressure term is also due to Oseen. According to equation (2.1) any body force corresponds to a certain distribution of pressure and any term in the pressure can be regarded as the potential body force. Thus the motion (2.7) can be interpreted as the motion due to a distribution of body forces with a potential proportional to the pressure. If this motion is due to a moving body, the external force required to keep the body in motion through the viscous fluid is equivalent to a distribution of body forces throughout the fluid.

The expansion in terms of sources, dipoles and so on is not believed to be strongly convergent, and the use of a general notation which implies that a number of terms in the expansion are to be used, may, therefore, seem unnecessary. In fact, the solutions used here involving the radius of the sphere not only make it easier to satisfy the boundary conditions, but also seem to lead to expressions which converge quite rapidly unless $(r - a) \ll a$.

To illustrate the use of these results, let us consider two simple problems. The Stokes problem is that of a rigid sphere of radius a and velocity components V^A_α,

* In precisely the same way we can derive a solution with the same variation on the surface of the sphere but regular inside it, using the solutions $r^{2n+1}(1/r)_n$ of Laplace's equation. These solutions are homogeneous of degree n in the co-ordinates.

but no angular velocity, moving through a fluid otherwise at rest. If there is no slipping the solution is

$$u_\alpha^0 = \sum_\beta a V_\beta^A S_{\beta 0}^\alpha(A). \tag{2.8}$$

To maintain the motion of the sphere it is necessary that there should be an external force with components,

$$F_\alpha^A = 6\pi\mu a V_\alpha^A, \tag{2.9}$$

It is often convenient to refer, not to the external force on a particle but the Stokes velocity, or the velocity derived from the force by this equation.

It can be shown, using the solutions (2.2) or in some other way, that in a general motion the force resisting the motion of a spherical particle is zero unless the fluid velocity contains the term $S_{\beta 0}^\alpha(A)$, i.e. a certain type of singularity in A, and that the external force necessary to balance the resistance is proportional to the coefficient of the term, in fact that

$$F_\alpha = 6\pi\mu A_{\alpha 0}. \tag{2.10}$$

The second problem is that of a sphere rotating with angular velocity $\boldsymbol{\omega}$. Since the surface velocity is $\boldsymbol{\omega} \wedge \mathbf{a}$, the boundary conditions are

$$\bar{A}_{xy} = \tfrac{1}{2}(A_{x,y} + A_{y,x}) = 0, \quad \hat{A}_{xy} = \tfrac{1}{2}(A_{x,y} - A_{y,x}) = -\omega_z a^3 \tag{2.11}$$

with similar equations for other pairs of suffixes. The solution is the elementary solution ($p = x, y, z$)

$$u_\alpha = \sum_{\beta,p} A_{\beta p}(1/r)_p \delta_{\alpha\beta} = (\boldsymbol{\omega} \wedge \mathbf{r})_\alpha / r^3. \tag{2.12}$$

A calculation of the forces on the particle shows that this motion is only maintained by an external couple with components

$$G_x = -8\pi\mu\hat{A}_{yz}, \text{ etc.} \tag{2.13}$$

Considerations similar to those for forces show that, in any general motion, the fluid only exerts a couple on the sphere when the constants $\hat{A}_{\alpha\beta}$ are not zero, and that the external couple applied to the sphere is given by the last equation.

In the next section of this paper it is necessary to expand in the neighbourhood of A the solutions $S_{\beta m}^\alpha(B)$, with a singularity at the centre B of a sphere of radius b.* These can be expressed in various ways using the formulae and the notation given in this paper and in Kynch (1956). If the position of the origin A relative to B is given by the vector $\mathbf{R} = \overrightarrow{BA}$, then

$$S_{\beta,m}^\alpha(B) = \sum_n \left\{ \left(\frac{1}{R}\right)_{mn} \delta_{\alpha\beta} + \frac{d_n^2}{2(m+2)} \left(\frac{1}{R}\right)_{\beta m \alpha n} + \frac{1}{m+2} R_\epsilon \left(\frac{1}{R}\right)_{\beta m \alpha (n-\epsilon)} \right\} \frac{(-)^n}{n!!} r^{2n+1} \left(\frac{1}{r}\right)_n,$$

$$d_n^2 = R^2 - b^2 - (2m+3)\, r^2/(2n+3). \tag{2.14}$$

* It is in expansions of this type that it is better to use derivatives of (14) rather than associated Legendre polynomials. Such expansions have been used by Kirkwood in connexion with the transport and electrical properties of gases. The technique of using these expansions is not included here as it would involve explanations as long as those normally devoted to an account of the properties of expansions in terms of Legendre polynomials.

Derivatives of $(1/R)$ are calculated with respect to the co-ordinates of A, and we have used the notation

$$n!! = n!1.3.5\ldots(2n-1) = 2n!/2^n.$$

Values on the surface of a sphere of radius a about A are immediately obtained by putting $r = a$ in this equation. In the expression so obtained the term in $n = 1$, where we replace n by the single suffix p, deserves special mention. The coefficient of $(1/r)_p \equiv (1/a)_p$ has two suffices α and p, and we separate it into that part which does not change sign when these two are interchanged and that part which does change sign. These two are referred to as the symmetrical and anti-symmetrical parts of the coefficient, respectively, and we distinguish the latter by the use of square brackets and reserve round brackets for the symmetric part and the other coefficients. Thus, on $r = a$, we write

$$S^{\alpha}_{\beta m}(A) = (BA)^{\alpha 0}_{\beta m}(1/a) + \{(BA)^{\alpha p}_{\beta m} + [BA]^{\alpha p}_{\beta m}\}(1/a)_p + \sum_{n>1}(BA)^{\alpha n}_{\beta m}(1/a)_n. \quad (2.15)$$

3. The two-particle problem

The fluid motion due to two spheres A and B, when the distance R between their centres is large, is the sum of the motions due to each, i.e. a combination of two solutions already obtained in equation (2.10)

$$u_\alpha = A_{\beta 0}S^{\alpha}_{\beta 0}(A) + B_{\beta 0}S^{\alpha}_{\beta 0}(B). \quad (3.1)$$

The forces acting on the spheres are

$$F^A_\alpha = 6\pi\mu A_{\alpha 0}, \quad F^B_\alpha = 6\pi\mu B_{\alpha 0}. \quad (3.2)$$

In the limit of infinite separation, the velocities of the spheres are

$$U^A_\alpha = A_{\alpha 0}/a, \quad U^B_\alpha = B_{\alpha 0}/b. \quad (3.3)$$

Equation (3.1) is used as an approximation by both Smoluchowski (1911) and Burgers (1942). Smoluchowski assumes that the velocities of the particles are given and uses the equation to obtain an approximate expression for the applied forces. Using the expansion (2.19) for the second term of the equation (3.1) and equating the velocity of A to that term in the fluid velocity which does not vary over its surface, we find that, to this approximation,

$$aU^A_\alpha = A_{\alpha 0} + \sum_\beta B_{\beta 0}(BA)^{\alpha 0}_{\beta 0}. \quad (3.4a)$$

Similarly

$$bU^B_\alpha = B_{\alpha 0} + \sum_\beta A_{\beta 0}(AB)^{\alpha 0}_{\beta 0}. \quad (3.4b)$$

Smoluchowski solves these equations for the constants $A_{\alpha 0}$, $B_{\alpha 0}$, to a first approximation and derives the formulae

$$A_{\alpha 0} = aU^A_\alpha - bU^B_\beta(BA)^{\alpha 0}_{\beta 0}, \quad (3.5)$$
$$B_{\alpha 0} = bU^B_\alpha - aU^A_\beta(AB)^{\alpha 0}_{\beta 0}.$$

The forces are determined by equations (3.2).

Burgers (1942) assumes that the forces are known, and calculates the particle velocities. Thus $A_{\alpha 0}$, $B_{\alpha 0}$ are known and the velocities are given directly by

equations (3.4). It is clear that this result is more accurate than the other. Inserting the values of the brackets and replacing forces by Stokes velocities (cf. 2.10), we deduce the formula,

$$U_\alpha^A = V_\alpha^A + (b/4R)\, V_\beta^B \{3(\delta_{\alpha\beta} + n_\alpha n_\beta) - (3n_\alpha n_\beta - \delta_{\alpha\beta})(a^2+b^2)/R^2\}. \tag{3.6}$$

$\mathbf{R} = \overrightarrow{BA}$, and n_α are the direction cosines of the directed line BA. Since the components of the Stokes velocity $\mathbf{V}^B$ along the line of centres are $V_R^B = V_\beta^B n_\beta$, the term $(V_\beta^B n_\beta) n_\alpha$ represents a velocity of magnitude V_R^B along that line. In vector form

$$\mathbf{U}^A = \mathbf{V}^A + \left(\frac{3b}{4R}\right)\mathbf{V}^B\left(1 + \frac{a^2+b^2}{3R^2}\right) + \left(\frac{3b}{4R}\right)(\mathbf{V}^B.\mathbf{n})\,\mathbf{n}\left(1 - \frac{a^2+b^2}{R^2}\right). \tag{3.7}$$

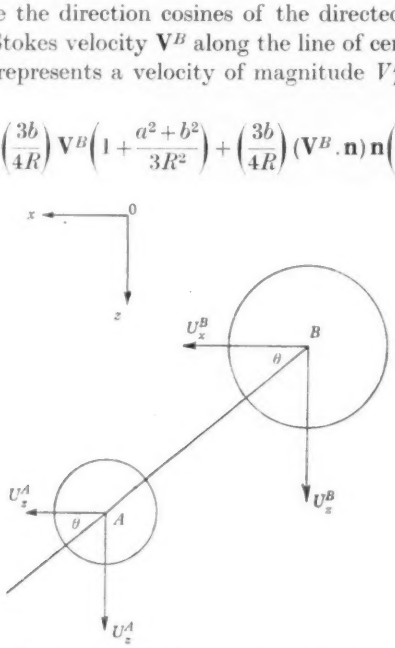

FIGURE 1. Co-ordinates and velocity components for two falling spheres.

When the particles fall under gravity, the last term is absent when the line of centres is horizontal: otherwise it represents a velocity *downwards* along the line of centres. The same is true for B, so that the particles not only fall with an increased velocity but move sideways in the same sense, as if it were easier to move along the line of centres than across it. This effect was first pointed out by Smoluchowski. If the line of centres is inclined at an angle to the horizontal (figure 1) the horizontal and vertical velocities are

$$\left.\begin{aligned} U_z^A &= V^A + \frac{3b}{4R}\, V^B\left[\left(1 + \frac{a^2+b^2}{3R^2}\right) + \sin^2\theta\left(1 - \frac{a^2+b^2}{R^2}\right)\right], \\ U_x^A &= \left(\frac{3b}{4R}\right) V^B \sin\theta\cos\theta\left(1 - \frac{a^2+b^2}{R^2}\right). \end{aligned}\right\} \tag{3.8}$$

These expressions are not symmetric in the radii, so that the smaller of two unequal particles with the same Stokes velocities moves faster than the larger.

Burgers, by an argument based on equivalent body forces, deduces the first of further corrections which are needed to satisfy the boundary conditions. The

nature of these corrections is found by expanding the approximation (3.1) on the surface of B,

$$u_\alpha^0 = B_{\alpha 0} + A_{\beta 0}\{(AB)_{\beta 0}^{\alpha 0}(1/b) + [AB]_{\beta 0}^{\alpha p}(1/b)_p + (AB)_{\beta 0}^{\alpha p}(1/b)_p + (AB)_{\beta 0}^{\alpha pq}(1/b)_{pq} + \ldots\}. \quad (3.9)$$

As in the previous section, the symbols p and q are used to denote single indices, with three values. The fluid does not slip over B if B is given a translation corresponding to the first two terms, an angular velocity corresponding to the third term involving $[AB]_{\beta 0}^{\alpha p}$, and if in addition extra terms are added to the fluid velocity to cancel the remaining terms in the expansion. The most important of these is the fourth term, $A_{\beta 0}(AB)_{\beta 0}^{\alpha p}(1/b)_p$, which is cancelled on the surface of B by the correction

$$u_\alpha = -A_{\beta 0}(AB)_{\beta 0}^{\gamma p} S_{\gamma p}^\alpha(B). \quad (3.10)$$

Adding a similar term for the correction on the surface of A we obtain

$$u_\alpha^1 = A_{\beta 0} S_{\beta 0}^\alpha(A) - A_{\beta 0}(AB)_{\beta 0}^{\gamma p} S_{\gamma p}^\alpha(B) + B_{\beta 0} S_{\beta 0}^\alpha(B) - B_{\beta 0}(BA)_{\beta 0}^{\gamma p} S_{\gamma p}^\alpha(A). \quad (3.11)$$

Picking out terms which are constant on A, as before, we obtain for the velocity of A

$$aU_\alpha^A = A_{\alpha 0} + B_{\beta 0}(BA)_{\beta 0}^{\alpha 0} - A_{\beta 0}(AB)_{\beta 0}^{\gamma p}(BA)_{\gamma p}^{\alpha 0}. \quad (3.12)$$

The third term which is the correction term can be evaluated using the expressions

$$\left.\begin{aligned}(AB)_{\beta 0}^{\gamma p} &= (3a^3/4R^2)\, n_\beta(\delta_{\gamma p} - 3n_\gamma n_p) - (a^3/12)(3b^2+5a^2)(1/R)_{\beta\gamma p},\\ \tfrac{1}{2}(BA)_{\gamma p}^{\alpha 0} + \tfrac{1}{2}(BA)_{p\gamma}^{\alpha 0} &= (a/2R^2)\, n_\alpha(\delta_{p\gamma} - 5n_p n_\gamma)(a/18)(3b^2+5a^2)(1/R)_{\alpha\gamma p}.\end{aligned}\right\} \quad (3.13)$$

Summing over γ and p, we find that the main part of the correction is

$$\Delta U_\alpha^A = -(15ab^3/R^4)(V_\beta^A n_\beta)\, n_\alpha. \quad (3.14)$$

This correction somewhat reduces the speed of A downwards along the line of centres given by equation (3.9). It is the correction given by Burgers (1942).

It is now clear that it is possible to use our equations to derive systematically all the necessary corrections to any order. The fluid velocity must have the form

$$u_\alpha = u_\alpha(A) + u_\alpha(B), \quad p = p(A) + p(B), \quad (3.15)$$

where $u_\alpha(A) = \sum_{\gamma, m} A_{\gamma m} S_{\gamma m}^\alpha(A)$ and $u_\alpha(B) = \sum_{\gamma, m} B_{\gamma m} S_{\gamma m}^\alpha(B)$.

According to equations (2.10) and (2.13) of the previous section, the constants $A_{\alpha 0}$, $B_{\alpha 0}$ are proportional to the external forces and the antisymmetrical parts $\hat{A}_{\alpha p}$, $\hat{B}_{\alpha p}$ ($p = 1$) to the external couples on the particles A and B. The latter are zero in the absence of body couples and hence the coefficients $A_{\alpha p}$, $B_{\alpha p}$ are symmetrical in the two suffices.

The remaining coefficients are determined by the boundary conditions. For example, on the surface of A

$$u_\alpha = U_\alpha^A - \mathscr{A}_{\alpha\gamma p}\omega_\gamma^A a^3(1/a)_p,$$

where U^A and ω^A are the translational velocity and angular velocity of A, and $\mathscr{A}_{\alpha\gamma p}$ is the alternating tensor. Expanding the expressions in equation (3.15) on

the surface of A with the end of the previous section we obtain equations which are satisfied if*

$$A_{\alpha 0}+\Sigma B_{\gamma m}(BA)^{\alpha 0}_{\gamma m}=aU^A_\alpha, \tag{3.16}$$

$$\bar{A}_{\alpha p}+\Sigma B_{\gamma m}[BA]^{\alpha p}_{\gamma m}=\mathscr{A}_{\alpha\gamma p}\omega^A_\gamma a^3, \tag{3.17}$$

$$\bar{A}_{\alpha p}+\Sigma B_{\gamma m}(BA)^{\alpha p}_{\gamma m}=0, \tag{3.18}$$

$$A_{\alpha n}+\Sigma B_{\gamma m}(BA)^{\alpha n}_{\gamma m}=0 \quad (n>1). \tag{3.19}$$

The bracket notation is explained at the end of § 2.

When the external forces are known, the unknown constants $A_{\alpha n}$ are obtained by solving equations (3.18) and (3.19) and the corresponding set of equations for the particle B. The velocity and angular velocity of the particles are then derived from equations (3.16) and (3.17).

These equations were solved by successive approximations, no more satisfactory method having been found, for the velocities of the spheres in terms of the forces acting upon them.† Since the expressions $(BA)^{\alpha n}_{\gamma m}$ are proportional to various powers of the ratio of the particle radii to the distances between centres the expansion is approximately but not strictly in powers of this ratio. No attempt was made to collect all the terms of a given power, as it was quite clear that better convergence is obtained by retaining the grouping corresponding to the brackets (BA).

The translation velocity of A is such that

$$aU^A_\alpha = A_{\alpha 0}+B_{\beta 0}(BA)^{\alpha 0}_{\beta 0}-A_{\beta 0}(AB)^{\gamma m}_{\beta 0}(BA)^{\alpha 0}_{\gamma m}+\ldots \quad (m>0) \tag{3.20}$$

and its angular velocity

$$\mathscr{A}_{\alpha\gamma p}\omega^A_\gamma a^3 = B_{\beta 0}[BA]^{\alpha p}_{\beta 0}-A_{\beta 0}(AB)^{\gamma m}_{\beta 0}[BA]^{\alpha p}_{\gamma m}+\ldots \quad (m>0). \tag{3.21}$$

The third term in equation (3.20) could be easily evaluated exactly, so that this was done, but only a few terms of the next term were obtained. The final result is written as

$$U^A_\alpha = V^A_\beta(K\delta_{\alpha\beta}+Ln_\alpha n_\beta)+bV^B_\beta(M\delta_{\alpha\beta}+Nn_\alpha n_\beta), \tag{3.22}$$

where

$$\left.\begin{aligned}
K &= 1+17ab^5/16+\sum_{m>0}(ab^{2m+1}/48)\{54b^4-6a^2b^2(4m^2+6m-1)\\
&\qquad +a^4(m+1)^2(2m+1)(2m+3)\},\\
L &= (15ab^3/4)+15ab^5/16-15a^3b^5/2+\sum_{m>0}(ab^{2m+1}/48)\\
&\qquad \times\{54b^4-18a^2b^2(4m^2+18m+9)\\
&\qquad +a^4(m+1)(m+3)(2m+1)(2m+3)\},\\
M &= \tfrac{1}{4}(3+a^2+b^2)+a^3b^3\{f_{11}+(a^2+b^2)f_{12}\},\\
N &= \tfrac{3}{4}(1-a^2-b^2)+a^3b^3\{g_{11}+(a^2+b^2)g_{12}\}.\\
8f_{11} &= -(3b^2+5a^2)(3a^2+5b^2),\\
8(g_{11}+f_{11}) &= 150-420(a^2+b^2)+6(63a^4+63b^4+130a^2b^2),\\
4f_{12} &= (5a^2+3b^2)\{5-\tfrac{1}{4}(39a^2+77b^2)+\tfrac{15}{28}(5a^2+7b^2)(7b^2+3a^2)\},\\
4(g_{12}+f_{12}) &= 195-3(185a^2+249b^2)+3(173\tfrac{4}{7}a^4+482a^2b^2+301b^4)\\
&\qquad -(15/7)(5a^2+3b^2)(3a^2+7b^2)(7b^2+5a^2).
\end{aligned}\right\} \tag{3.23}$$

* This is a particular solution. Other solutions lead to the same results

† The solution for the forces in terms of the velocities is not only less useful but much more slowly convergent.

The distance between centres is chosen as the unit length so that $R = 1$ and a, b now measure the radii as fractions of R.

Because some of the coefficients of the higher powers of a and b are rather large, it seemed worth while to obtain an approximate solution containing contributions from all the terms in equation (3.20). Such a solution can be obtained by assuming that the constants $A^{\alpha n} = 0$, for all $n > 1$; the various sums simplify and can be evaluated.

The answer obtained in this way yields the values

$$\left.\begin{aligned} K &= 1-(3ab^3/4)\,Q(b^2+\tfrac{5}{3}a^2), \quad (1/Q) = 1-\tfrac{1}{4}a^3b^3(5-8a^2-8b^2)^2,\\ L &= -(15ab^3/4)\,P(1-a^2-\tfrac{3}{5}b^2), \quad (1/p) = 1-a^3b^3(5-6a^2-6b^2)^2,\\ M &= \tfrac{1}{4}(3+a^2+b^2)+(3a^3b^3/8)\,Q(b^2+\tfrac{3}{5}a^2)\,(b^2+\tfrac{5}{3}a^2)\,(5-8a^2-8b^2),\\ N &= \tfrac{3}{4}(1-a^2-b^2)+(3a^3b^3/8)\,[10P(1-a^2-\tfrac{3}{5}b^2)\,(1-b^2-\tfrac{3}{5}a^2)\,(5-6a^2-6b^2)\\ &\qquad -Q(b^2+\tfrac{3}{5}a^2)\,(b^2+\tfrac{5}{3}a^2)\,(5-8a^2-8b^2)]. \end{aligned}\right\} \tag{3.24}$$

The approximation $P = Q = 1$, yields terms which have already been included in the earlier expressions (3.22) and (3.23) so that the corrections due to higher order terms are proportional to $(P-1)$ and $(Q-1)$. These corrections are small unless one sphere is very much larger than the other. It seems likely, therefore, although it is not certain, that higher-order terms in the expansion (3.20) are not appreciable unless one sphere is much larger than the other, and that the series expansion is useful even up to the point where the two spheres are almost in contact.

4. Discussion for two particles

The analysis of the fall of two particles can be discussed without reference to the work of the previous two sections and the results of the discussion compared with the available experimental results. With the aid of the calculations of those two sections we can evaluate the constants and compare directly these results with our theory.

The theoretical calculations of Smoluchowski and Burgers should agree satisfactorily with experimental results on the fall of two equal spheres when the distance between centres is more than three times their diameter. For smaller distances between centres the only theory available is that of Stimson & Jeffery, for spheres falling behind one another with equal velocities. In this section we consider some general implications of our calculations and extend the comparison with experiment not only for equal spheres but for unequal spheres, as far as that is possible at present.

From the linearity of the hydrodynamic equations we conclude that the particle velocities can be derived from the vector equations,

$$\left.\begin{aligned} U^A_\alpha &= V^A_\beta(K\delta_{\alpha\beta}+Ln_\alpha n_\beta)+bV^B_\beta(M\delta_{\alpha\beta}+Nn_\alpha n_\beta),\\ U^B_\alpha &= V^B_\beta(K'\delta_{\alpha\beta}+L'n_\alpha n_\beta)+aV^A_\beta(M'\delta_{\alpha\beta}+N'n_\alpha n_\beta), \end{aligned}\right\} \tag{4.1}$$

where the velocity coefficients K, K', ..., N' denote functions only of the radii and the distance between centres, approximate values of which are given in the

previous section. In the limit of infinite separation K and K' tend to unity and the other constants tend to zero.

If the velocities are resolved along and perpendicular to the line of centres, these equations become

$$\left.\begin{aligned} U_p^A &= (K+L)\,V_p^A + b(M+N)\,V_p^B, \\ U_n^A &= K V_n^A + bM V_n^B, \end{aligned}\right\} \tag{4.2}$$

together with two similar equations for the velocity of B. Thus the velocity coefficients can be obtained by solving first the problem where both particles are acted on by forces along the line of centres, and then by solving a second problem where the forces are perpendicular to the line of centres. The first of these two problems has been solved in the most important case of equal velocities by Stimson & Jeffery, but a solution of the second has not yet been obtained. The values given below for these coefficients are determined from our series expansion.

Experiments are usually conducted with particles falling under gravity in a vertical plane (figure 1). If the line of centres is inclined at an angle θ to the horizontal, the horizontal and vertical velocities are

$$\left.\begin{aligned} U_z^A &= V^A(K+L\sin^2\theta) + bV^B(M+N\sin^2\theta), \\ U_x^A &= (V^A L + bV^B N)\sin\theta\cos\theta, \\ U_z^B &= B^B(K'+L'\sin^2\theta) + aV^A(M'+N'\sin^2\theta), \\ U_x^B &= (aV^A N' + L'V^B)\sin\theta\cos\theta. \end{aligned}\right\} \tag{4.3}$$

Equal particles with the same Stokes velocities V have the same velocity components

$$\left.\begin{aligned} (U_z/V) &= (K+aM) + (L+aN)\sin^2\theta, \\ (U_x/V) &= (L+aN)\sin\theta\cos\theta. \end{aligned}\right\} \tag{4.4}$$

Hall (1956), having taken great care to manufacture almost identical particles, has verified that the velocity and the inclination θ of the line of centres are constant during the motion of equal particles. The above equations suggest further conditions on the velocity which are independent of the values of the constants. First, the vertical velocity, for a given distance between centres, should be a linear function of $\sin^2\theta$. Secondly, the particles move away from the vertical with a velocity proportional to $(L+aN)$ which is the slope of the graph of the horizontal velocity. The greatest transverse velocity is $\frac{1}{2}(L+aN)$ when $\theta = 45°$, or one half of the difference between the vertical velocities of fall for $\theta = 0$ and $\theta = 90°$.

The only experimental data on pairs of spheres available at the moment is that of Hall (1956) and, owing to the large variation of the viscosity of the liquid with temperatures and the possibility that circulation of the liquid was not entirely prevented, his values may not be accurate enough to judge the theory.

Figure 2 shows, for one pair of spheres,* the speed of fall plotted against $\sin^2\theta$ for various values of the ratio $2a = d/R$ of particle diameter to the distance

* These are the particles labelled by Hall P3. The other experimental data given here relate to the same pair. Curves drawn for a second pair of particles are very similar and differ from the theory in the same way.

between centres. This diagram does not confirm a linear relation but the experimental errors are such that a relationship of this kind is not denied.

Assuming that it exists, the sum $m = (L+aN)$ equals the slope of the line, for each value of (d/R). Slopes calculated by two methods are given in table 1. The first is calculated by a least squares method, taking

$$10m_1 = \{8(U_{90}-U_0)+4(U_{60}-U_{30})\}/V_\infty.$$

The second is calculated by the simple formula

$$m_2 = (U_{90}-U_0)/V_\infty.$$

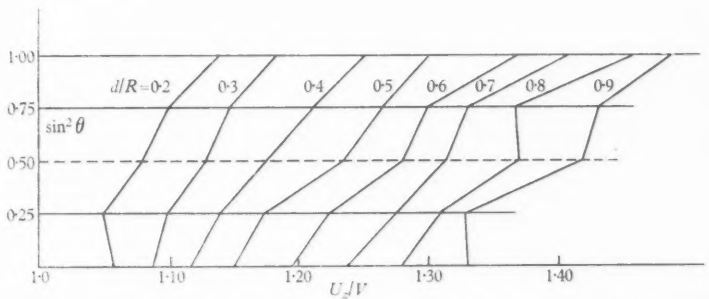

FIGURE 2. Speed of fall of equal spheres for various ratios of diameter to distance between centres (experimental).

Finally, the table includes the values of a third quantity determined by the experimental data. The measurements include the angle ϵ between the direction of fall and the vertical. According to equations (4.4), when ϵ is small

$$\tan\epsilon = \frac{U_x}{U_z} = \frac{(L+aN)\sin\theta\cos\theta}{(K+aM)+(L+aN)\sin^2\theta}$$

$$= (L+aN)\sin\theta\cos\theta/(K+aM), \quad \text{approx.}$$

Now $(K+aM) = (Uz)_0/V$, where $(U_z)_0$ is the vertical velocity when $\theta = 0$. Thus, applying the equation for $\tan\epsilon$ when $\theta = 45°$, we deduce that

$$m_3 = 2\frac{(U_z)_0}{V_\infty}\tan\epsilon = (L+aN).$$

These three quantities agree as well as can be expected and, in particular, they all vary in the same way with the distance between centres.

Figure 3 shows the same data in a different form, the velocity of fall being plotted against (d/R) for various directions of the line of centres for the pair of particles. These curves have kinks which may be due to experimental error (although it is curious that they appear in the same places for all θ) and it is noteworthy that they are continuous up to the value of $d/R = 1$, which corresponds to contact between the spheres.

Only two theoretical curves, for $\theta = 0$ and $\theta = 90$, are drawn for comparison, the others being very similar, and it is clear that agreement with experiment is not

very good. This may well be due to a deficiency in the theory, but it may again be due to experimental error. Thus, in the case of large separation, where the theory is unlikely to be in error, the experimental values are some 20 % less than the theoretical values.

d/R	m_1	m_2 (experimental)	m_3	$m = L + aN$ (theoretical)
0·2	0·065	0·056	0·071	0·073
0·3	0·10	0·098	0·098	0·105
0·4	0·14	0·136	0·131	0·133
0·5	0·16	0·153	0·150	0·152
0·6	0·17	0·173	0·161	0·163
0·7	0·16	0·170	0·161	0·165
0·8	0·16	0·166	0·154	0·161
0·9	0·17	0·158	0·149	0·154
1·0	0·16	0·152	0·138	0·155

TABLE 1. Comparison of theoretical and experimental values of the slopes of the lines shown in figure 2, for various values of (d/R).

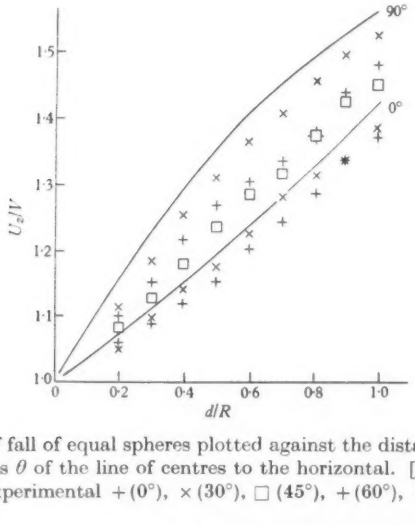

FIGURE 3. Velocity of fall of equal spheres plotted against the distances between centres, for various inclinations θ of the line of centres to the horizontal. [Theoretical – full lines for $\theta = 0$ and 90°: Experimental + (0°), × (30°), □ (45°), + (60°), × (90°)].

The theoretical curves were derived from the expressions given in the previous section written in the form,

$$1024K = 1024 - 17d^6 - 5d^8 - (69/16)\,d^{10} - (31/8)\,d^{12},$$

$$1024L = -240d^4 + 105d^6 + 47d^8 + (233/16)\,d^{10} - (33/16)\,d^{12},$$

$$1024aM = 384d + 64d^3 + 6d^{11} - (113/10)\,d^{13} + (225/28)\,d^{15},$$

$$1024aN = 384d - 192d^3 + 150d^7 - 15d^9 - (471/2)\,d^{11} + (176\tfrac{9}{35})\,d^{13} - (40\tfrac{5}{28})\,d^{15},$$

which yield the values of the velocity constants as a function of $d\,(R = 1)$ given in table 2.

d	K	L	aM	aN
0·0	1·0	0·0	0·0	0·0
0·1	1·000	−0·000	0·038	0·037
0·2	1·000	−0·000	0·076	0·074
0·3	1·000	−0·002	0·114	0·107
0·4	1·000	−0·006	0·154	0·138
0·5	1·000	−0·013	0·195	0·165
0·6	0·999	−0·025	0·239	0·188
0·7	0·998	−0·041	0·284	0·207
0·8	0·994	−0·060	0·332	0·221
0·9	0·986	−0·075	0·384	0·229
1·0	0·965	−0·073	0·440	0·228

TABLE 2. Theoretical values of K, L, aM and aN of equations for values of (d/R) between 0 and 1.

5. Three-particle interactions

In this section we consider the interactions between particles when three or more are falling through a liquid. In addition to the interactions between pairs of particles, previously considered, there are now some that involve three distinct particles, namely, the effect of one particle on another in the presence of a third, and even more complicated interactions. Although these interactions arise in higher order approximation than the two-body interactions, it will appear that they are not always negligible. They can be very numerous and they may be important for certain configurations of the particles. Thus the main correction to the fluid motion around B due to a particle C distant S from it is proportional to (V^C/S^2) (cf. equation 3.10). As this is a dipole correction, it gives to a third particle A a velocity of order V^C/R^2S^2, where $R = AB$. In some circumstances, therefore, this term is quite important. In this section it is not our intention to evaluate these interactions to high order, or to discuss the general sedimentation problem, but rather to examine a few of the interactions in detail. Until methods of calculating the particle motions are discovered, which are more satisfactory than those used so far, there is little point in calculating these complicated terms to very high accuracy.

The general formulae are easily obtained by extending equations (3.15) to (3.20) so that they apply to more than two particles. The general formula for the velocity of any particle A is

$$aU_\alpha^A = aV_\alpha^A + bV_\beta^B(BA)_{\beta 0}^{\alpha 0} - \sum_{C \neq B} cV_\beta^C \sum_{B \neq A} (CB)_{\beta 0}^{\gamma m}(BA)_{\gamma m}^{\alpha 0} + \ldots \quad (m > 0). \quad (5.1)$$

In this equation the sum over B includes all particles other than A; and the sum over C includes all particles other than B, including $C = A$, so that this expression reduces to that already given in equation (3.24) when there are only two particles. The second term is the vector sum over all particles of the main term in their two-body intersection with A. This is the term which is normally considered in an aggregate of particles. On account of its long range it is responsible for the shielding effect (Kynch 1954) and tends to make all the particles move together, but the details of the effects of this term have still to be worked out. Except for

special arrangements it is difficult to deduce the motion of just three particles, even when this two-body interaction is the only one included. One special arrangement is that where one particle A is in a vertical plane midway between the others. If the three particles have the same Stokes velocity, the two particles separate to allow A to pass between them and then close up behind it. This motion is stable with respect to small displacements of A on either side of the vertical plane.

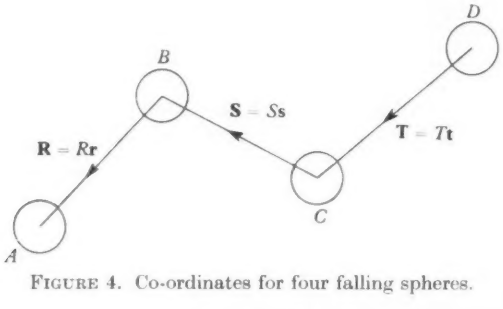

FIGURE 4. Co-ordinates for four falling spheres.

The third term contains three-body interactions, those which involve three distinct particles (CBA) and that due to the reaction of (ABA) of A on itself due to the presence of B. Interactions involving four distinct particles appear first in the next term of the series. The main term in the velocity of A due to C in the presence of B, using a notation shown in figure 4, is

$$(CBA) \quad U_\alpha^A = (c/a)\, V_\beta^C (CB)_{\beta 0}^{\gamma p} (BA)_{\gamma p}^{\alpha 0} \quad (p = 1). \tag{5.2}$$

Since this expression is symmetrical in α and p, and the principal terms of $\frac{1}{2}(BA)_{\gamma p}^{\alpha 0} + \frac{1}{2}(BA)_{p\gamma}^{\alpha 0}$ are proportional to BA_α, it follows that the principal terms lead to a correction directed along the line BA. They give

$$(CBA) \quad U_\alpha^A = (15cb^3/8R^2S^2)\,(3\cos^2\theta - 1)\,(V_\beta^C s_\beta)\, r_\alpha. \tag{5.3}$$

Its dependence on the relative positions of the particles is not too complicated. Let us assume the $\mathbf{V}^c$ is directed vertically downwards. The correction is directed along the line AB and, when C is below B, it is from A towards B as long as $3\cos^2\theta > 1$, i.e. the line AB lies within a cone with BC as axis and semi-vertical angle $\alpha = \cos^{-1}(\frac{1}{3})$. If C is above B the sense is reversed. Hence, for certain orientations the velocity (CBA) increases the main term (BA), whereas for other orientations it tends to cancel it. The change of sign when the direction of CB is reversed means that the three body terms tend to cancel under certain circumstances. For example, when a set of particles falls downwards in a line, these terms tend to cancel for particles in the middle, to increase the speed of those at the top and to decrease the speed of those at the bottom, i.e. to keep the particles together. (They are, of course, usually rather less in magnitude than the two-body interactions which tend to separate the particles.)

The reaction of A on itself due to the presence of B is obtained by making $C = A$ and $\theta = 180°$. It is, as given in equation (3.14),

$$(ABA) \quad U_\alpha^A = -(15ab^3/4R^4)\,(V_\beta^A r_\beta)\, r_\alpha. \tag{5.4}$$

The correction of next importance comes from the remaining parts of (5.2) and the next term in (5.1) with $m = 2$

$$\begin{aligned}(CBA)\quad \mathbf{U}^A = {} & \{3cb^3(3b+5a^2)\}(\mathbf{V}.\mathbf{s})\{(1-5\cos^2\theta)\mathbf{r}+2\cos\theta\mathbf{s}\}\\ & +\{3cb^3(3b^2+5c^2)\}\{(\mathbf{V}.\mathbf{s})(1-5\cos^2\theta)\mathbf{r}+2(\mathbf{V}.\mathbf{r})\cos\theta\mathbf{r}\}\\ & -(cb^5/64R^3S^3)[\mathbf{V}(117\cos^2\theta-49)-(\mathbf{V}.\mathbf{r})54\cos\theta\mathbf{s}\\ & +(\mathbf{V}.\mathbf{s})(1575\cos^3\theta-729\cos\theta)\mathbf{r}\\ & -\{(\mathbf{V}.\mathbf{s})\mathbf{s}+(\mathbf{V}.\mathbf{r})\mathbf{r}\}(315\cos^2\theta-93)].\end{aligned} \tag{5.5}$$

This expression reduces, when $C = A$, to the expression given in equation (3.27)

$$(ABA)\quad \mathbf{U}^A = (15a^3b^3/2R^6)(\mathbf{V}.\mathbf{r})\mathbf{r}-(ab^5/16R^6)\{17\mathbf{V}+15(\mathbf{V}.\mathbf{r})\mathbf{r}\}. \tag{5.6}$$

If the position of C is changed so that the direction of $\mathbf{s}$ (or $\overrightarrow{CB}$) is reversed, the terms in the first two lines of (5.5) change sign but those after do not. Let us compare with (5.6) the correction when C is diametrically opposite to A, though the same distance from B as A, so that, when $a = c$,

$$\mathbf{U}^A = -(15a^3b^3/2R^6)(\mathbf{V}.\mathbf{r})\mathbf{r}-(ab^5/16R^6)\{17\mathbf{V}+159(\mathbf{V}.\mathbf{r})\mathbf{r}\}. \tag{5.7}$$

Comparing (5.6) and (5.7) we see that the coefficients of the third line are sufficiently large to produce an appreciable and complicated variation with the configuration of the particles. This is not unexpected since, as shown in the previous paragraph, there is a considerable variation in the two-body correction with orientation which must be reflected in these more complicated corrections.

Without comment, we give the first four-body correction, which is directed along the line BA

$$\begin{aligned}(DCBA)\quad dV_\beta^D(DC)_{\beta\delta}^{\delta q}(CB)_{\delta q}^{\chi p}(BA)_{\gamma p}^{\alpha 0} = {} & \frac{75ab^3c^3d}{16R^2S^3T^2}(\mathbf{V}^D.\mathbf{t})\,r_\alpha\\ & \times[1-3(\mathbf{r}.\mathbf{s})^2+3(\mathbf{t}.\mathbf{s})^2\{5(\mathbf{r}.\mathbf{s})^2-1\}-6(\mathbf{r}.\mathbf{s})(\mathbf{s}.\mathbf{t})(\mathbf{t}.\mathbf{r})].\end{aligned} \tag{5.8}$$

6. Comments on sedimentation

This section contains some general remarks on the calculation of sedimentation velocities with small concentrations of particles, which follow naturally from the results of the previous sections. In §5 a few comments were made about the role of the two-body interaction in an assembly of particles; here we are concerned with the higher order corrections.

A finite assembly of identical particles falling freely under gravity through a viscous medium cannot do so in the form of a regular lattice array. Differences between the motion of particles near the edge and those near the centre of the assembly produce perturbations which spread inwards from the boundary and spoil the regularity. On the other hand, the shielding effect mentioned earlier tends to prevent differences in velocity between particles, and it could happen that there is short-range order amongst the particles even when long-range order is absent. If there is short-range order this must be allowed for in any calculation of high-order interactions. If it is absent the mean corrections can be calculated by taking an average for a random distribution of particles.*

With this in mind, let us now examine the various terms of equation (5.1), assuming first that particles near a given particle A form a regular array over

* We neglect the effect of aggregation and other complicating factors, such as wall effects.

distances for which the corrections are appreciable. It can be shown that many terms vanish independently of the form of the array. To prove this we note that all the terms start in the same way,

$$\sum_{C \neq B} cV_\beta^C (CB)_{\beta 0}^{\gamma m} \ldots.$$

Now $(CB)_{\beta 0}^{\gamma m} = (-)^m (BC)_{\beta 0}^{\gamma m}$, which changes sign when m is odd (though not when m is even) if the position of C is changed so that BC is reversed in direction. But, in a lattice array, all the particle C can be taken in pairs on opposite sides of B; hence all those terms are zero where m is odd. For lattices the first relevant value of m is 2. The corrections given in the previous section in equation (5.4) can be ignored and only the third line of equation (5.5), which comes from $m = 2$, need be considered, and this is of order d^6, where d is the ratio of particle diameter to distance between centres. Summing over all particles leads to a term in the velocity or order (concentration)^2.

This argument does not apply when there is no order. To prove this we consider the three-body terms only, although the same method can be applied to the other terms, where it takes a much more complicated form. The three-body interactions are either of the type (CBA) or (ABA),

$$\sum_{C \neq A, B} cV_\beta^C (CB)_{\beta 0}^{\gamma m} (BA)_{\gamma m}^{\alpha 0} + \sum_{B \neq A} aV_\beta^A (AB)_{\beta 0}^{\gamma m} (BA)_{\gamma m}^{\alpha 0}.$$

In the absence of correlations, for given positions of A and B, we now average over all positions of C. Neglecting the finite size of the particle, the first term is zero for all $m > 0$, owing to the angular variation of $(CB)_{\beta 0}^{\gamma m}$. Owing to the finite size of the particles, however, C is excluded from a region near the particle A of radius $2a$. The average value of $(CB)_{\beta 0}^{\gamma m}$ when C is in this region is approximately $(AB)_{\beta 0}^{\gamma m}$ and the probability of its being there is $8c$, where c is the volume concentration of particles. Thus the correction becomes approximately

$$(1 - 8c) \sum_m aV_\beta^A (AB)_{\beta 0}^{\gamma m} (BA)_{\gamma m}^{\alpha 0}.$$

The first term of this sum with $m = p = 1$, namely $aV_\beta (AB)_{\beta 0}^{\gamma p} (BA)_{\gamma p}^{\alpha 0}$, already given in equation (3.12), was, in fact, used by Burgers in his calculation of the sedimentation velocity (1942). It has been criticized (Hawksley 1950) on the grounds that it gives a correction which is too small. The arguments given here suggest precisely the opposite: that it overestimates the correction when there is a random distribution of particles and is much too large when there is partial order. Assuming that the basis of these calculations is correct we must attribute the error to neglect of higher order correctives which have large coefficients.

REFERENCES

Burgers, J. M. 1942 *Proc. K. Ned. Akad. Wet.* **43**, 307, 425, 625.

Hall, E. W. 1956 Ph.D. Thesis (Birmingham).

Hawksley, P. G. W. 1950 Inst. Phys. Conf. on Some Aspects of Fluid Flow.

Kynch, G. J. 1954 *Brit. J. Appl. Phys.* **3** (supplement), 5.

Kynch, G. J. 1956 *Proc. Roy. Soc.* A, **237**, 90.

Oseen, W. 1927 *Hydrodynamik*. Leipzig: Akademische Verlagsges.

Smoluchowski, M. A. 1911 *Bull. Acad. Sci., Cracow*, **1***a*, 28.

Stimson, M. & Jeffery, G. B. 1926 *Proc. Roy. Soc.* A, **111**, 110.

Temperature fluctuations over a heated horizontal surface

By A. A. TOWNSEND
Emmanuel College, Cambridge

(Received 21 July 1958)

The previous work of Thomas (1956) on the turbulent convection over a single, heated, horizontal surface has been extended using improved methods of analysis of the temperature fluctuations, and it has been possible to measure the distributions of mean temperature, the mean squares of the temperature fluctuation, the temperature gradient and the rate-of-change of temperature, and the statistical distributions of these quantities. These measurements were made for three different values of the convective heat flux, and the results are consistent with the dimensional consequences of assuming that the convection near the surface is independent of the distant boundaries and determined by the heat flux and the viscosity and conductivity of the fluid.

The most striking feature of the observations is that the fluctuations of temperature, temperature gradient, and rate-of-change of temperature, all show periods of activity, characterized by large fluctuations, alternating with periods of quiescence with comparatively small ones. Both the proportion and frequency of occurrence of the active periods decrease with increasing distance from the surface and they probably occur when rising columns of hot air pass through the point of observation. The quiescent periods occur when the point of observation lies outside the columns, and analysis of the statistical distributions of the various fluctuations shows that, during these periods, they are nearly independent of height. It is concluded that the quiescent fluctuations are typical of the turbulent convection far from the surface while the active fluctuations are the manifestation of the convective processes arising near the rigid boundary. These processes may be described as the detachment of columns of hot air from the edge of the conduction layer and the erosion of these rising columns by contact with the surrounding air which is in vigorous turbulent motion. Since the variations of the intensities with height is dominated by the contributions of the active periods, it is not surprising that no agreement is found with the predictions of the similarity theory which assumes the convection to be independent of the conduction layer at a sufficient distance from it. The Malkus theory of turbulence, which emphasizes dependence on the conduction layer, is in qualitative agreement with this inferred mechanism of the convection and is in quantitative agreement with the observed distribution of mean temperature. A brief discussion is given of the effect of a horizontal shearing motion on the convection and of the relation of these measurements to measurements of the temperature distribution in the earth's boundary layer with upward flux of total heat.

1. Introduction

Although the convective motion over a heated, horizontal surface is a simple form of turbulence with desirable properties of homogeneity and symmetry, there have been very few investigations of the fluctuations in velocity and temperature that underlie the gross phenomenon of heat transport. Malkus (1954*a*) was able to estimate turbulent velocities by observing the motion of suspended particles and Thomas (Thomas & Townsend, 1957) measured intensities and autocorrelation functions of the temperature fluctuations, but the experimental material is very meagre by comparison with our knowledge of the turbulent motion in shear flow and it was considered useful to continue and extend the earlier measurements of Thomas. Another, less general, reason for this investigation was a desire to test as fully as possible the predictions of a novel theory of turbulence proposed by Malkus (1954*b*, 1956), which seeks to relate the transport properties of the fully turbulent flows to the neutrally stable disturbances of the corresponding laminar flows and which, without introducing disposable constants, has succeeded in predicting the mean velocity distribution for turbulent flow in a two-dimensional channel with reasonable accuracy. Although the absence of arbitrary constants makes the theory attractive, its basic assumptions are neither immediately convincing nor open to direct experimental verification and the possibility of deriving similar results using established principles of similarity is an obstacle to its acceptance. However, applied to convection between parallel horizontal planes, the Malkus theory predicts a distribution of mean temperature quite different from that predicted by arguments of similarity and that the convection is everywhere dependent on the viscosity and conductivity of the fluid. Both the massive evidence that turbulent transport processes become independent of viscosity and conductivity for large Reynolds numbers of flow and the details of the theory suggest that, if this happens, it is because the whole convection depends on processes occurring close to the surface where thermal conductivity dominates the heat transfer and viscous stresses the turbulent motion. So the Malkus theory may be tested in two ways, by comparison of the observed and predicted variations of mean temperature with height and by looking for evidence of an intimate connexion between local temperature and processes occurring near the surface. On the other hand, the similarity theory, which successfully describes many aspects of turbulent flow in channels, rules out dependence on processes occurring in the conduction layer and predicts definite functional forms for the variations of mean temperature, mean square temperature fluctuations, and a number of other quantities.

The experiments to be described form a detailed study of the temperature fluctuations in a practical system of natural convection that approximates to the ideal one considered in the theory. The particular characteristics of the fluctuations that were measured are simply those that could be measured conveniently without excessive complication of equipment or observational difficulty.

2. Notation

The ideal system, to which the experimental arrangement is an approximation, is convection over a single, infinite, horizontal surface in a perfect gas without other boundaries, and the motion and temperature field may be described using a system of rectangular co-ordinates in which the Oz axis is vertical and the origin is in the surface. The convection should be statistically homogeneous with respect to variation of the horizontal co-ordinates. The following notation will be used:

u, v, w	are the velocity components parallel to Ox, Oy and Oz respectively,
$q^2 =$	$u^2+v^2+w^2$,
P, p	are the mean pressure and the pressure fluctuation from the mean,
T, θ	are the mean absolute temperature and the temperature fluctuation from the mean,
ν	is the kinematic viscosity,
k	is the thermal conductivity,
κ	is the thermometric conductivity,
ρ	is the fluid density,
H	is the constant upward flux of total heat,
$Q = \dfrac{H}{\rho c_p T}$	is a constant flux of buoyancy,
$z_0 = \left(\dfrac{\kappa^3}{gQ}\right)^{\frac{1}{4}}$	is a scale of length,
$u_0 = (\kappa g Q)^{\frac{1}{4}}$	is a scale of velocity,
$\theta_0 = \left(\dfrac{Q^3}{\kappa g}\right)^{\frac{1}{4}}$	is a scale of logarithmic temperature,
T_1	is the absolute temperature at the surface,
T_a	is the ambient or reference temperature, measured at a point 40 cm. above the surface,
N	is the frequency with which the instantaneous temperature passes through its mean value from below,
$S(x)$	is the probability that the instantaneous value of a fluctuating quantity shall exceed x,
$P(x) = -\dfrac{dS(x)}{dx}$	is the probability density function for the quantity.

It may be shown that z_0, u_0 and θ_0 are scales whose variation is sufficient to describe the change in the convection with different heat transfers, provided that the motion and temperature field close to the surface are unaffected by the distant boundaries and by the mechanism of removal of heat from the system and that fluids of only one Prandtl number are used. Measurements of heat transfer (e.g. Malkus, 1954*a*) and of mean temperature near the heated surface show that the variation of mean temperature is concentrated in a shallow surface layer and is effectively independent of the other boundaries. This might suggest that the detailed structure of this surface layer is also determined by the heat flux

and the fluid properties, and then the only change produced by a change in heat flux is the alteration in the characteristic scales. How far this is true is a question that the present work may help to answer.

3. Experimental arrangements

The practical convection system is an open-topped box, with bottom a horizontal and uniformly heated plate, 30 cm × 40 cm whose construction has been described before (Thomas & Townsend 1957). The sides of the box are of hardboard 56 cm high, and are intended to ensure that convective transport of heat is as far as possible by turbulent transport and as little as possible by steady streaming motions. The boundary conditions of this system are defined by the surface temperature and the room temperature if we ignore unwanted but

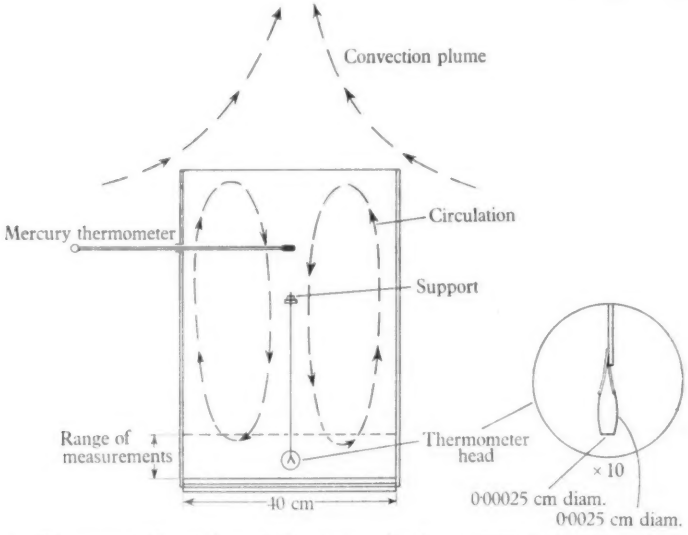

FIGURE 1. Diagrammatic section of the convection box. (The dashed lines indicate the form of the steady circulation inferred from the horizontal distribution of mean temperature.)

unavoidable disturbances from air-currents in the room, while the ideal system is defined by surface temperature and by the temperature at infinity. For the purpose of relating experimental measurements to the ideal system, it is better to use as 'temperature at infinity' the temperature at the base of the convection plume rising from the open top of the box rather than the room temperature. In these experiments, the temperature at a point 40 cm above the surface (16 cm below the open top) was measured with a mercury-in-glass thermometer and used as a reference temperature and as an approximation to the effective 'temperature at infinity'. During the course of a run it was not unusual for the room temperature and the reference temperature to change by one or two degrees and it was necessary to correct the observed mean temperatures for this drift. This was done by assuming that all temperatures in the system changed by the same amount and

subtracting from any observed temperature the excess of room temperature over 20·0 °C. In all the experiments the room temperature lay between 17° and 23 °C.

With this arrangement the most likely causes of deviations from ideal behaviour are the presence and finite height of the side-walls of the box. The simple presence of side-walls may make itself felt in two ways, by restrictions on horizontal movement of the fluid and by steady circulations of large scale induced by unequal temperature gradients near the walls and in the centre of the box. It is not very likely that horizontal motion could be seriously restricted in the layer of depth 8 cm in which all measurements were made, but there is some evidence of a weak

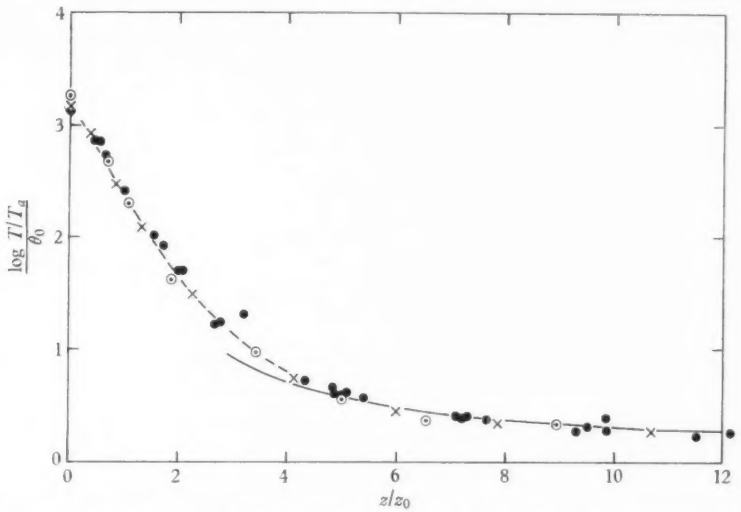

FIGURE 2. Distribution of mean temperature for z/z_0 less than 12. (●, heat flux A; ×, heat flux B; ⊙, heat flux C.)

circulation with cold air descending near the centre of the box and warm air rising near the edges (figure 1). Whether this circulation is due to the side-walls, or whether it is an eddy induced by the convection plume from the open top, is difficult to determine but it is believed to be of too low an intensity to be of much significance for the flow as a whole. It may be pointed out that the measurements of Thomas showed good agreement between the heat flux computed from the heat loss over the whole plate and the heat flux computed from the local temperature gradient near the middle of the plate, a result that is unlikely if the circulatory motion carries with it appreciable heat. The finite height of the side-walls might lead to two types of disturbance, transient disturbances by uncontrolled draughts in the room and a steady disturbance induced by the convection plume. The relative importance of these will depend on the absolute strength of the convection plume.

All the results of the measurements are presented in the non-dimensional form appropriate to the ideal system, with units the non-dimensional scales of length, velocity and logarithmic temperature that may be constructed from the buoyancy

flux Q, the gravitational acceleration and the thermometric conductivity. Logarithms of the absolute temperature are used instead of ordinary temperature, a procedure which is known to lead to better correlation between convection experiments with widely different temperature loadings and which has some theoretical justification (Thomas & Townsend 1957). A general inspection of figures 2–10, which show the variation with height of a variety of mean values

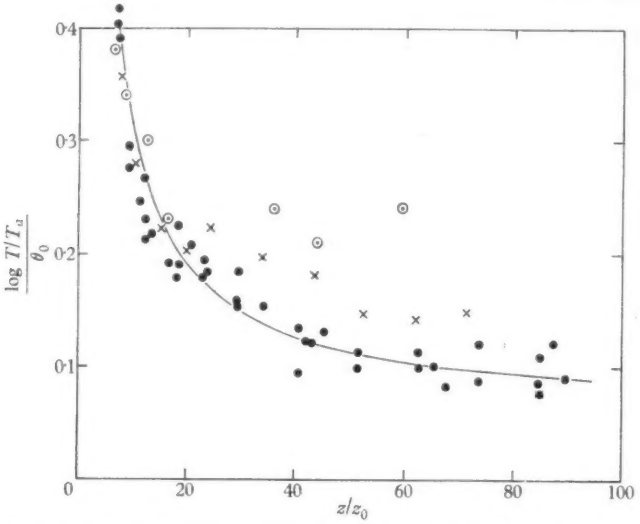

FIGURE 3. Distribution of mean temperature for z/z_0 greater than 8. (●, heat flux A; ×, heat flux B; ⊙, heat flux C.)

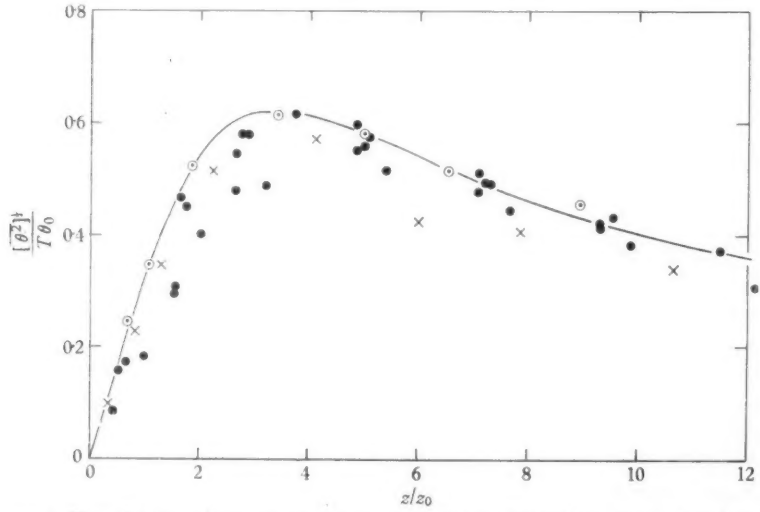

FIGURE 4. Distribution of root-mean-square temperature fluctuation for z/z_0 less than 12. (●, heat flux A; ×, heat flux B; ⊙, heat flux C.)

connected with the temperature field for three different values of the heat flux, shows that the results of dimensional analysis of the ideal system are valid for the experimental system except within the conduction layer and at considerable distances from the surface. The discrepancies within the conduction layer (z/z_0

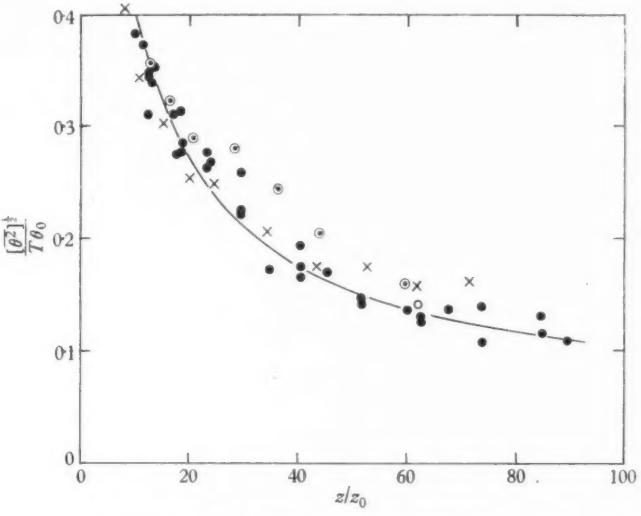

FIGURE 5. Distribution of root-mean-square temperature fluctuation for z/z_0 greater than 8. (●, heat flux A; ×, heat flux B; ⊙, heat flux C.)

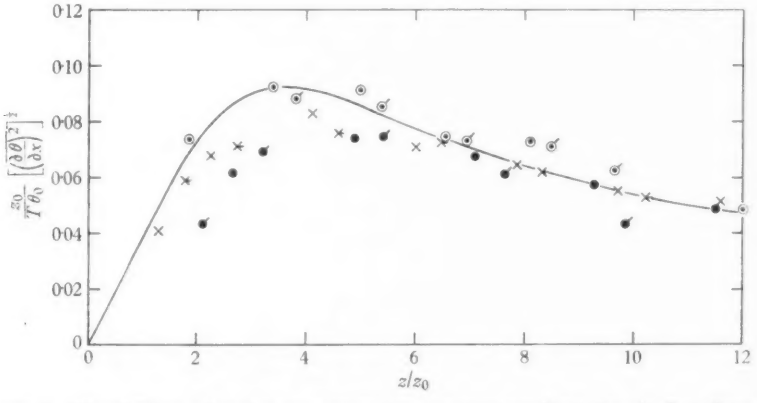

FIGURE 6. Distribution of root-mean-square temperature gradient for z/z_0 less than 12. (●, heat flux A; ×, heat flux B; ⊙, heat flux C.)

less than three) are caused by the variation with temperature of thermometric conductivity and kinematic viscosity (the variations are most clearly distinguishable in the measurements of temperature fluctuations and temperature gradients in figures 4 and 6), which the dimensional analysis assumes to have the same values in all parts of the flow, an approximation nearly valid outside the

conduction layer but not inside it for these surface temperatures. The discrepancies that become noticeable for large values of z/z_0 are probably due to deviations from ideal behaviour induced by the open top, in particular by air-currents in the room. Consistently with this conclusion, the measurements for

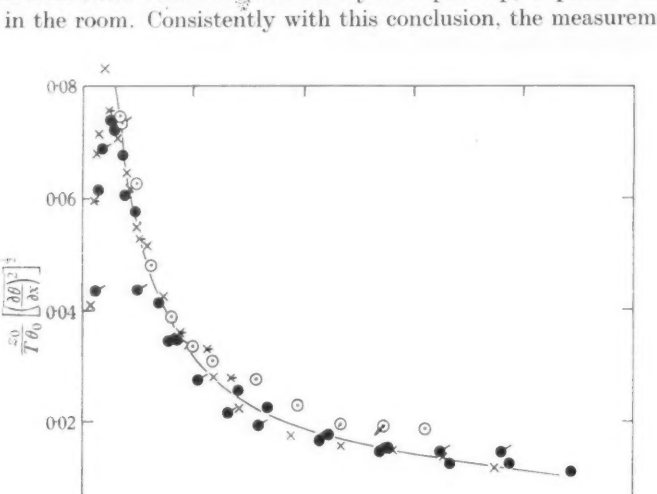

FIGURE 7. Distribution of root-mean-square temperature gradient for z/z_0 greater than 8. (●, heat flux A; ×, heat flux B; ⊙, heat flux C.)

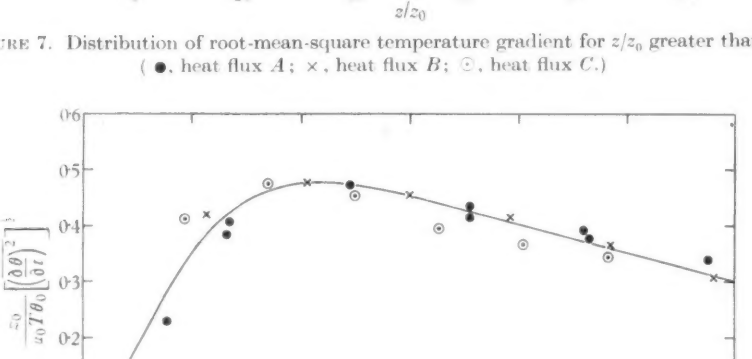

FIGURE 8. Distribution of root-mean-square rate of change of temperature for z/z_0 less than 12. (●, heat flux A; ×, heat flux B; ⊙, heat flux C.)

the smaller heat fluxes and the weaker convection plumes deviate from the measurements for the largest heat flux at heights that increase as the heat flux increases. For the lowest heat flux, deviations begin at $z/z_0 = 20$ (the exact value depends on the quantity measured) but for the intermediate flux deviations begin at $z/z_0 = 40$. Below these values no systematic departures from dimensional

similarity are to be found, and it is reasonable to suppose that the observations for the largest heat flux represent the ideal system sufficiently well for z/z_0 less than sixty. Within the conduction layer, the ideal behaviour is best represented by observations at the lowest heat flux and the curves have been drawn with this in mind.

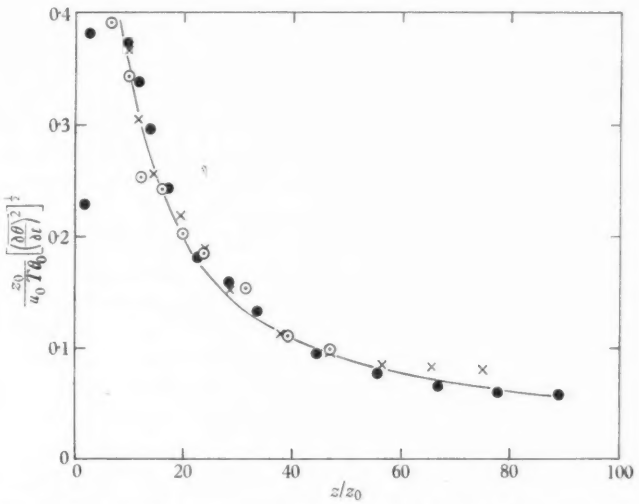

FIGURE 9. Distribution of root-mean-square rate of change of temperature for z/z_0 greater than 8. (●, heat flux A; ×, heat flux B; ⊙, heat flux C.)

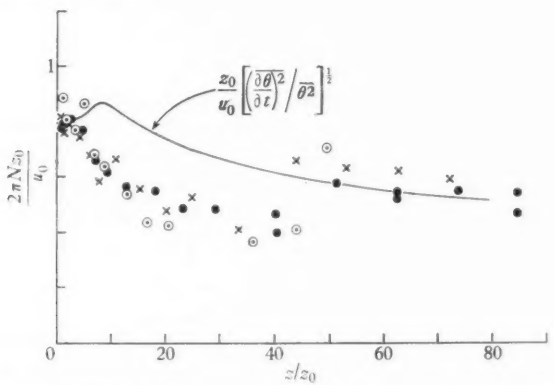

FIGURE 10. Distribution of mean frequency of zero temperature fluctuation. (Full line represents theoretical values if θ and $\partial\theta/\partial t$ are statistically independent and normally distributed.)

4. Use of a resistance thermometer to measure temperature fluctuations

The measurement of temperature in a turbulent motion with small or zero mean velocity presents the special problem of interference with the motion by the thermometer element and its supports. In the earlier work, the thermometer

element was supported by parallel wires stretched horizontally across the convection box, an arrangement convenient for measurements between parallel planes. In this series of measurements, the flow is open from the top and the element is carried by a vertical length of hypodermic tubing, 1 mm in diameter and 15 cm long, itself supported by a brass tube 3 mm in diameter and 15 cm long. The whole is carried by a bridge whose height above the surface can be adjusted by micrometer screws. The sensitive element is a short length (1–2 mm) of platinum wire, of diameter 2·5 μ, etched from Wollaston wire and supported by pieces of unetched wire of diameter 25 μ and length about 5 mm (figure 1). In still air the time constant of such a wire is about 0·5 msec, and there is no doubt that the resistance of the element responds to temperature fluctuations more rapidly than the electrical circuit can respond to the changes in resistance. The wire current was sufficiently low to avoid appreciable ohmic heating.

The question is, how closely does the temperature measured by this arrangement resemble the temperature in the absence of the thermometer element and its support? Differences could arise in two ways, from the influence of the thermometer on the whole motion and from inability of the thermometer to measure temperature accurately, especially if there is appreciable conduction of heat along the supports or if the approach of fluid from certain directions is impeded by the supports. The effect of the thermometer assembly on the whole motion is difficult to assess, and the reasons for considering it to be negligible are that these measurements of mean temperature agree well with earlier measurements using the horizontal support and that measurements with a variety of thermometer heads are internally consistent. For similar reasons, heat conduction by the supports and support interference are believed to cause errors less than the statistical uncertainty of the measurements. Radiative exchange of heat with the surroundings has a negligible effect on the equilibrium temperature of wires of diameter 2·5 μ.

In order to obtain useful approximations to the mean values, it was necessary to take averages over periods of 10 min, and this was conveniently done by converting the electrical output of the resistance thermometer into pulses whose repetition rate was a linear function of the wire resistance. The electrical circuits used to do this and to make the other measurements are described in another paper (Townsend 1959).

5. Measurement of defining parameters

The ideal convection flow considered in the theory may be specified either by the flux of total heat or by the temperatures at the heated surface and at infinity. The definition of 'temperature at infinity' in the experimental arrangement has been discussed already, and the reference temperature is considered to be a good approximation to it. The surface temperature was measured in two ways, by thermocouples embedded in the dural plate and by extrapolation of the measurements of mean temperature to the position of the surface. This position can be established with considerable accuracy from measurements of the root-mean-square of the temperature fluctuation, a quantity that is proportional to distance from the surface within the conduction layer (figure 4).

The convective flux of total heat may be measured directly by subtracting from the total heat loss of the surface the computed loss by radiation, but the earlier work showed that these values were in good agreement with values computed from the observed gradient of mean temperature near the surface using the relation

$$H = -k\left[\frac{\partial T}{\partial z}\right]_{z=0}, \tag{5.1}$$

and that there was little to choose between the apparent accuracy of each set of values. In view of the uncertainty in the radiative heat loss, it was decided to use the second method which has the advantage of measuring all the parameters with one basic instrument, the platinum wire resistance thermometer.

Run	T_1 (°C)	T_a (°C)	$H \times 10^2$ (W. cm^{-2})	$\log \frac{T_1}{T_a}$	Q (cm sec^{-1})	θ_0	z_0 (cm.)	u_0 (cm sec^{-1})	$\theta_0^{-1} \log \frac{T_1}{T_a}$
B*	93·8	27·0	5·60	0·2011	0·157	0·0658	0·0887	2·39	3·06
C*	86·6	27·0	4·95	0·1817	0·139	0·0600	0·0914	2·32	3·03
F 2†	94·0	27·7	5·26	0·1995	0·148	0·0628	0·0903	2·36	3·18
F 5	91·0	27·0	5·15	0·1932	0·145	0·0618	0·0905	2·34	3·13
F 1†	63·1	23·9	2·78	0·1240	$0·078_4$	0·0392	0·1044	2·00	3·16
F 4	60·3	23·9	2·54	0·1154	$0·071_4$	0·0365	0·107	1·95	3·16
F 3	42·8	22·2	1·85	0·0674	0·0334	0·0207	0·128	1·61	3·26

* These runs were made with light cardboard walls of height 35 cm.

† These runs were made with side-walls of height 28 cm.

Note. All measurements have been corrected for deviations of room temperature from 20 °C.

TABLE 1

Heat flux	θ_0	z_0 (cm)	u_0 (cm sec^{-1})	$T_1 - 20$ (°C)	Q (cm sec^{-1})
A	0·0618	0·0905	2·34	71·0	0·145
B	0·0365	0·107	1·95	43·1	0·0714
C	0·0207	0·128	1·61	22·8	0·0334

TABLE 2

Table 1 shows the results of these measurements for seven distinct runs with various surface temperatures and experimental arrangements, together with the computed values of the buoyancy flux Q, of the characteristic scales of logarithmic temperature, length and velocity, and of the heat transfer coefficient, $\log T_1/T_a\,(kg/Q^3)^{\frac{1}{4}}$. It will be noticed that the measured values of the heat transfer coefficient have a mean value of $3·14 \pm 0·03$ and a standard deviation of 2·3 %, and that no correlation with heat flux or wall height is visible. This result is further confirmation of the hypothesis that the convective heat loss is determined by the motion and structure of a thin surface layer, too thin to be affected by external influences peculiar to the particular experimental arrangement.

The runs, F 3, F 4, F 5, were made with standard values of the electrical power input to the plate assembly, and the values of the scales computed from these runs

were used in the reduction of later measurements with the same power inputs and, presumably, the same heat fluxes. In some of the later runs temperature measurements were made in the conduction layer and the assumed values of the convective heat loss were confirmed. For convenience, the characteristic scales for the three standard heat fluxes, which will be distinguished by the letters, A, B, C, are collected in table 2.

6. Mean temperatures and intensities of temperature fluctuations

Although the measurement of mean temperature was not the first object of the work, a large number of measurements were produced in the course of measuring mean squares of the temperature fluctuation and some of these are shown in figures 2 and 3. Within the limitations already mentioned, the consistency of measurements for different heat fluxes is good and the experimental points lie around a common curve that is consistent with the earlier measurements although the range of z/z_0 is much greater. The scatter of the observations is such that they might be represented for z/z_0 greater than ten by a power law,

$$\theta_0^{-1} \log \frac{T}{T_a} = A\left(\frac{z}{z_0}\right)^{-n} + B, \tag{6.1}$$

with almost any value of n between 0·3 and 1·5. If we select $n = 1$, corresponding to the Malkus theory, the best representation is

$$\theta_0^{-1} \log \frac{T}{T_a} = 2{\cdot}6\left(\frac{z}{z_0}\right)^{-1} + 0{\cdot}06 \tag{6.2}$$

for z/z_0 greater than 8, although an extreme possibility is

$$\theta_0^{-1} \log \frac{T}{T_a} = 2{\cdot}0\left(\frac{z}{z_0}\right)^{-1} + 0{\cdot}07 \tag{6.3}$$

for z/z_0 greater than 10. The additive constant in each of these expressions corresponds with an effective ambient temperature (or 'temperature at infinity') somewhat above the reference temperature. If we select $n = \frac{1}{3}$, as predicted by the similarity theory, the best representation is

$$\theta_0^{-1} \log \frac{T}{T_a} = 0{\cdot}95\left(\frac{z}{z_0}\right)^{-\frac{1}{3}} - 0{\cdot}12 \tag{6.4}$$

for z/z_0 greater than 8. Representation of the results by (6.4) is decidedly less satisfactory than representation by (6.2), and the multiplicative constant is very different from the one inferred from the measurements of Swinbank (Priestley 1954, 1955, 1956) which indicate that

$$\theta_0^{-1} \log \frac{T}{T_a} = 3{\cdot}5\left(\frac{z}{z_0}\right)^{-\frac{1}{3}} + \text{constant}. \tag{6.5}$$

It is only expected that the variation of mean temperature should be described by a power law if nearly all the heat flux is carried by turbulent movements, i.e. if $\overline{\theta w} \gg -\kappa(\partial T/\partial z)$. The ratio of the two sides of this inequality is easily computed using any of the possible representations, and the condition is strongly satisfied for z/z_0 greater than 8 ($-\kappa[\partial T/\partial z]/\overline{\theta w} = 0{\cdot}04$ for $z/z_0 = 8$).

Mean squares of the temperature fluctuations were measured at the same time, with the results shown in figures 4 and 5. For z/z_0 less than 1·5, the root-mean-square of the fluctuation is nearly proportional to z/z_0, although the constant of proportionality depends on the temperature loading, $\log T_1/T_a$. For the lowest heat flux C, which corresponds most nearly with the condition of very small temperature loading assumed in the basic theory,

$$\frac{(\overline{\theta^2})^{\frac{1}{2}}}{T\theta_0} = 0{\cdot}35\frac{z}{z_0} \quad (z/z_0 < 1{\cdot}5). \tag{6.6}$$

The fluctuation intensity rises to a maximum value near $z/z_0 = 3$ and then decreases in a manner adequately described by

$$\frac{(\overline{\theta^2})^{\frac{1}{2}}}{T\theta_0} = 1{\cdot}60\left(\frac{z}{z_0}\right)^{-0{\cdot}6} \tag{6.7}$$

for z/z_0 greater than 6.* It is not possible to represent the measurements by the power-law predicted by the similarity theory

$$\frac{(\overline{\theta^2})^{\frac{1}{2}}}{T\theta_0} \propto \left(\frac{z}{z_0}\right)^{-\frac{1}{3}}. \tag{6.8}$$

The points in figures 4 and 5 include observations with single and with double thermometer elements, and the close agreement shows that increased size and complexity of the thermometer has little effect on the measured fluctuations. It is therefore reasonable to believe that the resistance thermometer detects temperature fluctuations resembling closely those that would occur in the absence of the thermometer.

7. Gradients and rates-of-change of temperature

Temperature gradients were measured with a thermometer head with two sensitive elements, each about 1·5 mm long and held parallel to each other with a horizontal separation of 0·212 cm. If the elements are connected in adjacent arms of the Wheatstone bridge, the output of the bridge is a linear function of the resistance ratio and, if the lead resistance is negligible and the temperature fluctuations small compared with the absolute temperature, of the temperature difference. The mean square of the temperature difference is determined in the usual way and the mean square gradient is computed by dividing by the square of the separation. The extent to which the finite difference resembles the local gradient was investigated in a second series of measurements in which the separation of the elements was 0·461 cm. Since, for small separations,

$$\overline{\left(\frac{\theta(x)-\theta(x+r)}{r}\right)^2} = \overline{\left(\frac{\partial\theta}{\partial x}\right)^2} - \frac{r^2}{12}\overline{\left(\frac{\partial^2\theta}{\partial x^2}\right)^2}, \tag{7.1}$$

* No significance attaches to the exact value of the exponent which has been rounded off to the nearest 0·05. These and following power-laws (equations 7.3–4) merely represent in a compact form the experimental measurements over the range of observation and may have no validity outside this range.

a comparison of the two series of measurements enables the possible error to be determined. It was found to be rather less than the scatter of the observations and has been neglected. Figures 6 and 7 show the root-mean-squares of the temperature gradients obtained in this way. The variation with height is generally similar to that of the root-mean-square temperature fluctuation, although the effects of temperature loading at small values of z/z_0 are rather larger. For the lowest heat flux,

$$\frac{z_0}{T\theta_0}\left[\overline{\left(\frac{\partial\theta}{\partial x}\right)^2}\right]^{\frac{1}{2}} = 0{\cdot}4\frac{z}{z_0} \tag{7.2}$$

for z/z_0 less than 1·5, while for the largest values of z/z_0 a good representation is

$$\frac{z_0}{T\theta_0}\left[\overline{\left(\frac{\partial\theta}{\partial x}\right)^2}\right]^{\frac{1}{2}} = 0{\cdot}30\left(\frac{z}{z_0}\right)^{-0{\cdot}75} \quad (z/z_0 > 6). \tag{7.3}$$

The similarity theory predicts an exponent of $-\frac{2}{3}$.

Intensities of the time-rate of change of temperature were measured using an electrical differentiating circuit with the results shown in figures 8 and 9. For z/z_0 greater than 6, the measurements are described by

$$\frac{z_0}{u_0\theta_0 T}\left[\overline{\left(\frac{\partial\theta}{\partial t}\right)^2}\right]^{\frac{1}{2}} = 2{\cdot}48\left(\frac{z}{z_0}\right)^{-0{\cdot}85}. \tag{7.4}$$

The similarity theory predicts an exponent of $-\frac{1}{3}$.

A convenient method of obtaining information about the time-rate of change of a fluctuating quantity is to measure the frequency with which it passes through a particular value, usually the mean value (see, for example, Liepmann 1952). It may be shown (Rice 1944, 1945) that the frequency N with which the temperature fluctuation passes through its mean value from below is

$$N = \int_0^\infty P(0 \mid \dot{\theta})\,\dot{\theta}\,d\dot{\theta}, \tag{7.5}$$

where $P(\theta \mid \dot{\theta})$ is the joint probability distribution function for the temperature θ and the time derivative of the temperature $\dot{\theta}$. If the temperature fluctuation and its rate of change are statistically independent,

$$N = \tfrac{1}{2}P(0)\,\overline{|\dot{\theta}|} \tag{7.6}$$

and, if both are normally distributed,

$$N = \frac{1}{2\pi}[\overline{\dot{\theta}^2}/\overline{\theta^2}]^{\frac{1}{2}}. \tag{7.7}$$

Measurements of this rate have been made and are compared with direct measurements of $[\overline{\dot{\theta}^2}/\overline{\theta^2}]^{\frac{1}{2}}$ in figure 10. Good agreement is found only at large and at small values of z/z_0, and it is inferred that substantial deviations from a normal distribution may exist.

8. Statistical distributions of temperature

Comparison of figures 3 and 5 will show that the root-mean-square temperature fluctuation is very roughly equal to the difference between the mean and reference temperatures for all values of z/z_0 greater than five, so it is not surprising that measurements of the statistical distribution of instantaneous temperature show that 'cold' air occurs with significant frequency in all parts of the flow outside

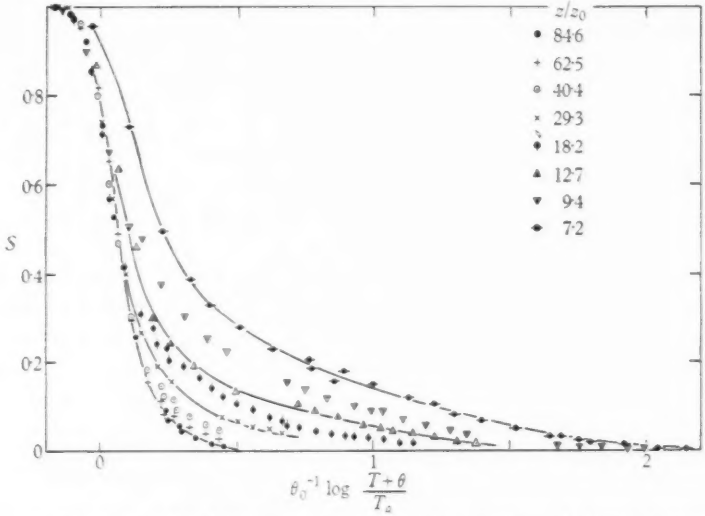

FIGURE 11. Statistical distributions of instantaneous temperature for large values of z/z_0.

the conduction layer. The way in which this happens is more surprising. The most obvious feature of figure 11, which shows the probabilities of occurrence of temperatures greater than set values, is that the low temperature parts of the curves are nearly identical in shape, particularly for the larger values of z/z_0. This behaviour suggests that $S(x)$, the probability that the temperature should exceed x, is of the form,

$$S(x) = (1-\gamma)\,S_1(x) + \gamma S_2(x), \tag{8.1}$$

where S_1 is independent of height and γ is a duration factor which decreases with increase in distance from the surface.* The interpretation of (8.1) is that the temperature at a point may vary in two distinct ways, either with small fluctuations and a low mean temperature or with large fluctuations and a high mean temperature. More definite evidence of the existence of two modes of fluctuation is to be found in measurements of the statistical distributions of temperature gradients and rates of change, but it is also strongly suggested by visual observations of the behaviour of the measuring equipment. Comparatively infrequent 'active' periods during which the temperature oscillates wildly between wide limits alternate with extended periods of quiescence during which the tempera-

* See figure 23, in which $S(1-\gamma)^{-1}$ is plotted as a function of temperature.

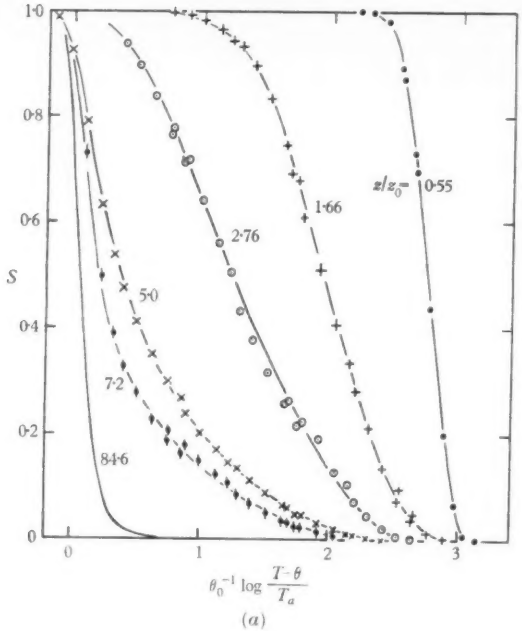

(*a*)

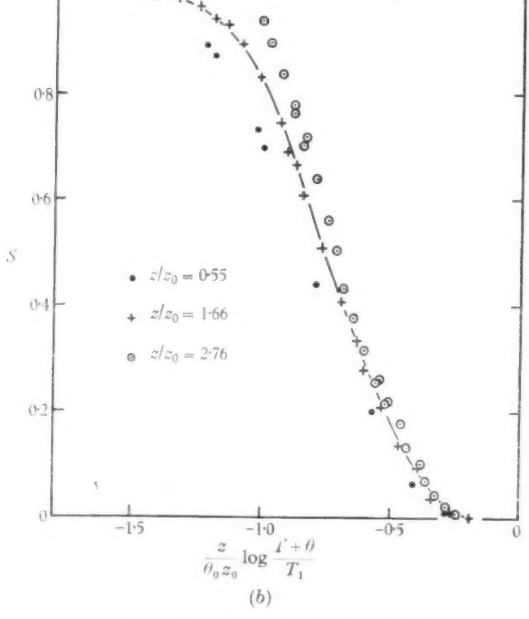

(*b*)

FIGURE 12. Statistical distributions of instantaneous (*a* and *b*) temperature for small values of z/z_0.

ture is low and varies very little. The relative duration and frequency of the active periods decreases with increasing height.

Within and near the conduction layer, it is not possible to distinguish two components of the fluctuation, and, for z/z_0 less than 2, the integrated probability function is nearly of the form

$$S(T+\theta) = S_{uc}\left(\frac{z}{z_0}\theta_0^{-1}\log\frac{T+\theta}{T_1}\right), \tag{8.2}$$

as expected in a region dominated by the effects of conduction. Figure 12 shows distributions of temperature fluctuations in and near the conduction layer plotted against $\theta_0^{-1}\log[(T+\theta)/T_a]$ and $(z/z_0)\theta_0^{-1}\log[(T+\theta)/T_1]$. It may be noticed (i) that, for $z/z_0 = 2{\cdot}76$, $\theta_0^{-1}\log[(T+\theta)/T_a]$ is observed to assume all values between $-0{\cdot}1$ and $+2{\cdot}64$, which is 80 % of the total range of temperature, and (ii) that the statistical similarity of temperature fluctuations within the conduction layer expressed by equation (8.2) is most persistent for the higher temperatures, i.e. the smaller temperature gradients.

9. Statistical distributions of the space and time derivatives of the temperature fluctuation

The statistical distributions of temperature gradient and rate of change of temperature suggest strongly the existence of two modes of fluctuation. Figures 13 and 14, which show on a Gaussian probability plot the distributions of temperature gradient, $\partial\theta/\partial x$, for $z/z_0 = 7{\cdot}1$ and $22{\cdot}6$, are naturally interpreted as composite distributions. The behaviour at large deviations will be determined by the

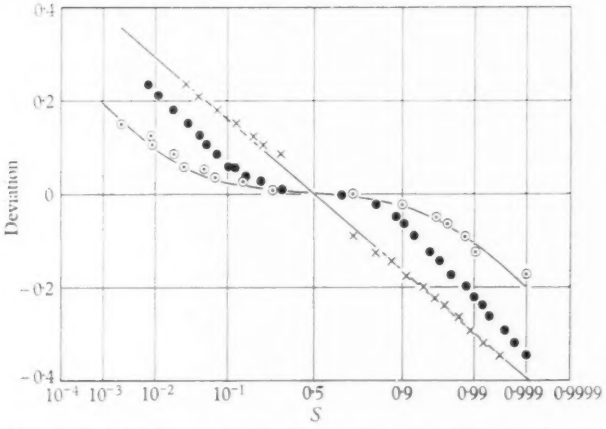

FIGURE 13. Statistical distribution of temperature gradient, $\partial\theta/\partial x$, at $z/z_0 = 7{\cdot}1$ on a Gaussian probability plot. (●, original measurements; ×, $S/\gamma \rightarrow S_1$ (normally distributed); ⊙, $(S-\gamma S_1)/(1-\gamma)$ the residual component.)

component of larger variance and it is found to be Gaussian within the experimental uncertainty. Assuming this component to be normally distributed, it is possible to determine its variance and its relative duration from the measurements at large deviations and to obtain the other residual component by subtracting the

inferred intense component from the measured probabilities. The steps in the analysis are indicated on the diagrams and the results of the process, which has been applied to all the measured distributions of $\partial\theta/\partial x$, are summarized in figures 15 to 17. These show the variation with height of the relative duration and intensity of the intense ('active') component and of the distribution of the residual component.

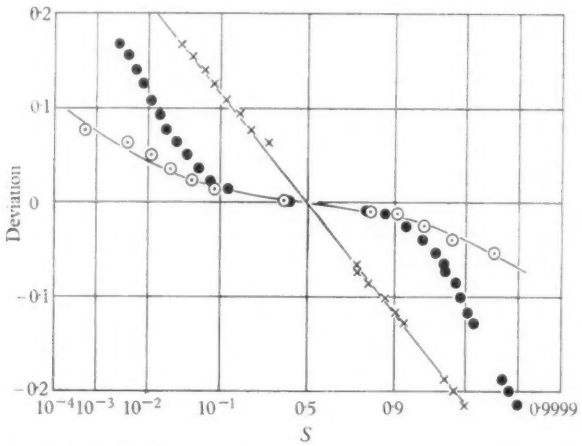

FIGURE 14. Statistical distribution of temperature gradient, $\partial\theta/\partial x$, at $z/z_0 = 22{\cdot}6$ on a Gaussian probability plot. (●, original measurements; ×, $S/\gamma \rightarrow S_1$ (normally distributed); ⊙, $(S-\gamma S_1)/(1-\gamma)$ the residual component.)

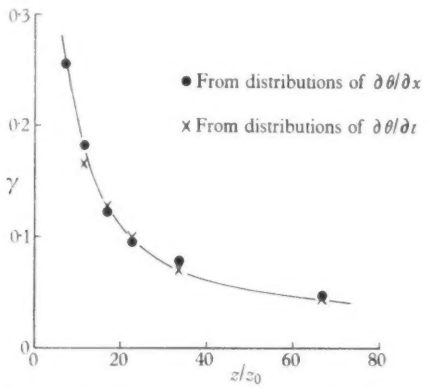

FIGURE 15. Variation with z/z_0 of the relative duration, γ, of periods of activity.

It is not possible to analyse the distributions of $\partial\theta/\partial t$ in the same way, as these distribution functions do not behave normally at large deviations, approaching zero or unity less rapidly than a normal distribution (figure 18). If the local Reynolds and Péclet numbers of the turbulent motion are large, the time rate of change of temperature is almost entirely due to convection of temperature gradients by the fluid velocities past the point of observation. In an appendix it is shown that the convection of a normally distributed field of temperature gradient

by a normally distributed and uncorrelated field of velocity leads to rates of change of temperature with a distribution function of the form

$$P_c(x) = \tfrac{1}{2}|x|\, H_1^{(1)}(i\,|x|), \tag{9.1}$$

where $H_1^{(1)}(ix)$ is the Bessel function of imaginary argument tabulated by Jahnke & Emde (1933). For large positive values of x,

$$P_c(x) \sim \sqrt{\frac{x}{2\pi}}\, e^{-x}\left(1+\frac{3}{8x}-\frac{15}{128x^2}+\ldots\right). \tag{9.2}$$

The measurements are of the integrated distribution function, corresponding with

$$S_c(x) \sim \sqrt{\frac{x}{2\pi}}\, e^{-x}\left(1+\frac{7}{8x}-\frac{71}{128x^2}+\ldots\right). \tag{9.3}$$

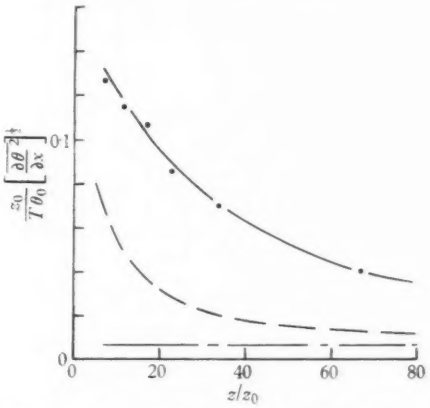

FIGURE 16. Variation with z/z_0 of the root-mean-square of the active component of $\partial\theta/\partial x$. (The dashed line indicates the directly observed values of $[(\partial\theta/\partial x)^2]^{\frac{1}{2}}$ given in figure 7, and the horizontal line the intensity of the quiescent component.)

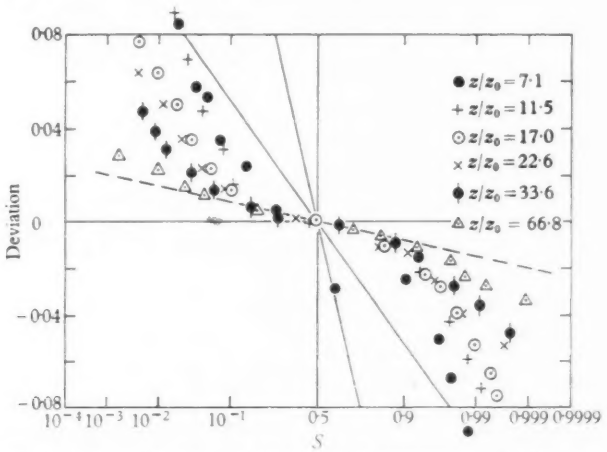

FIGURE 17. Statistical distributions of the residual components of $\partial\theta/\partial x$, i.e. what is left after subtracting the active component and renormalizing.

and the observations of the distributions of $\partial\theta/\partial t$ for large deviations are in much better accord with this type of asymptotic behaviour than the behaviour of a normal distribution.

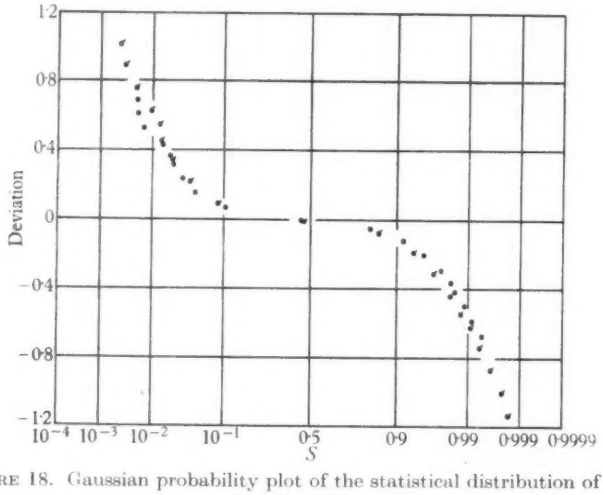

FIGURE 18. Gaussian probability plot of the statistical distribution of $\partial\theta/\partial t$ for $z/z_0 = 22{\cdot}6$.

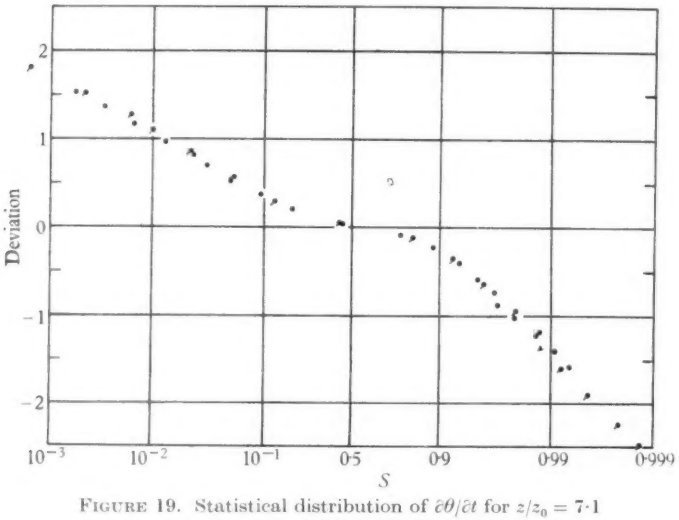

FIGURE 19. Statistical distribution of $\partial\theta/\partial t$ for $z/z_0 = 7{\cdot}1$ on a 'convection' probability plot.

The measured distributions of $\partial\theta/\partial t$ have been analysed into two components, the more intense one being distributed according to the 'convection' distribution (9.1) and having an intensity and relative duration determined by the observed probabilities of large deviations. In figures 19 and 20, two measured distributions have been plotted using the analogue of the Gaussian probability

plot (i.e. one on which a distribution of the form (9.1) appears as a straight line), and the results of the analysis are shown in figures 15, 21 and 22 and in table 3. At the smaller values of z/z_0, the distributions of $\partial\theta/\partial t$ become asymmetrical and,

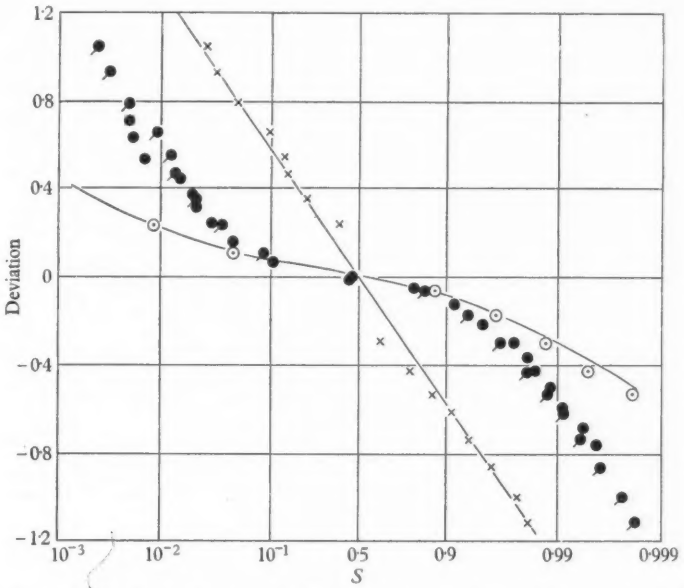

FIGURE 20. Statistical distribution of $\partial\theta/\partial t$ for $z/z_0 = 22{\cdot}6$ on a 'convection' probability plot. (●, original measurements; ×, $S/\gamma \rightarrow S_1$ (normally distributed); ⊙, $(S-\gamma S_1)/(1-\gamma)$ the residual component).

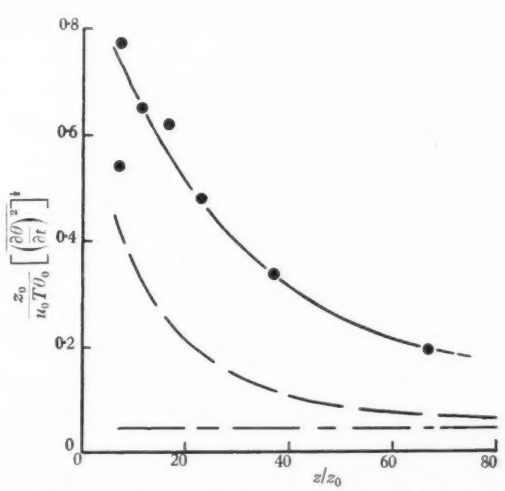

FIGURE 21. Variation with z/z_0 of the root-mean-square of the active component of $\partial\theta/\partial t$. (The dashed line indicates the directly observed values of $[\overline{(\partial\theta/\partial t)^2}]^{\frac{1}{2}}$ given in figure 9, and the horizontal line the intensity of the quiescent component.)

although they preserve the same asymptotic behaviour for both large positive and large negative deviations, it is not possible to analyse the distribution for $z/z_0 = 7{\cdot}1$ and barely possible for $z/z_0 = 11{\cdot}5$. The sense of the asymmetry is that large negative values of $\partial\theta/\partial t$ are more probable than large positive ones.

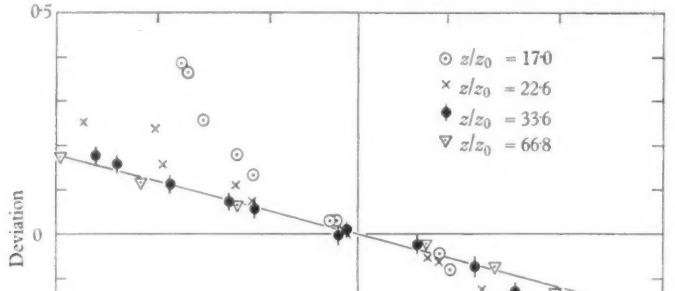

FIGURE 22. Statistical distributions of the residual components of $\partial\theta/\partial t$, i.e. what is left after subtracting the active component and renormalizing).

Quantity		7·1	11·5	17·0	22·6	33·6	66·8
$\overline{\partial\theta/\partial x}$	$\gamma =$	0·255	0·182	0·121	0·096	0·078	0·047
	Variance	0·127	0·115	0·107	0·086	0·070	$0{\cdot}040_5$
$\overline{\partial\theta/\partial t}$	$\gamma =$	—	0·165	0·128	0·099	0·072	0·046
	Variance	—	0·65	0·621	0·483	0·368	0·197

TABLE 3. Properties of the active components of $\partial\theta/\partial x$ and $\partial\theta/\partial t$.

A comparison of the two sets of distributions shows that: (i) The duration factors inferred from the distributions of $\partial\theta/\partial x$ and $\partial\theta/\partial t$ are consistent and decrease rapidly with increase of height. It is very likely that the 'active' components of $\partial\theta/\partial x$ and $\partial\theta/\partial t$ are consequences of the same 'active' periods.

(ii) The intensities of the active components also decrease rapidly with distance from the surface (figures 16, 21).

(iii) The distribution of the residual components is independent of height except for extreme values of the deviation with low probability of occurrence (figures 17, 22). The departures from normal and 'convection' distributions are least for the greatest heights and may be due to transition zones between the active and quiescent regions in the flow. The variances corresponding to the invariant parts of the residual components are respectively 0·0064 for $\partial\theta/\partial x$ and 0·045 for $\partial\theta/\partial t$, both in the appropriate non-dimensional units.

10. Comparison with theoretical predictions and with measurements in the atmosphere

Before discussing possible structures of the convection that would be consistent with the observations, it is convenient to consider the extent to which the several theories are confirmed by experiment. The primitive theory is that there exists a surface layer within which the temperature structure is uniquely determined by the heat flux, the gravitational acceleration and the molecular conductivity and viscosity. If this is true, measurements for all heat transfers should coincide if expressed in terms of the appropriate scales of temperature, length and velocity. This prediction is well confirmed by these and the previous measurements, except within the conduction layer and at considerable distances from the surface.* Deviations at considerable distances are believed to be caused by external air-currents and diminish as the intensity of the convection increases, while the deviations within the conduction layer are caused by the variation with temperature of thermometric conductivity and kinematic viscosity. A rough argument to establish the magnitude of the last effect is as follows. Within the conduction layer, eddying motions do not develop and the motion is in a critical state of stability. Just outside the layer, the fluid velocities are of order u_0 and the temperature differences across the layer are of order $T_1\theta_0$, so that the stability criterion is of the form

$$fn\left[\frac{u_0 z_c}{\nu_c}, \quad \frac{g\theta_0 z_c^3}{\nu_c \kappa_c}\right] = 1, \tag{10.1}$$

where z_c is the layer thickness, and ν_c, k_c are mean values of the kinematic viscosity and thermometric conductivity in the layer. If u_0 and θ_0 are both set by the convection in the cooler fluid outside the layer, it is likely that the layer thickness varies at some rate intermediate between proportionality to ν_c ($u_0 z_c/\nu_c$ = constant) and proportionality to the $\frac{2}{3}$-power of ν_c ($g\theta_0 z_c^3(\nu_c\kappa_c)^{-1}$ = constant). Altering the horizontal scales of figures 4 and 6 in either of these ways removes the greater part of the variation with temperature loading.

The measurements of mean temperature and, much more definitely, the measurements of temperature fluctuations are not reconcilable with the similarity theory of convection and there can be little doubt that the theory does not apply to convection in the laboratory. It remains to account for the opposite conclusion drawn from measurements in the atmosphere, and here recent work by Webb (1958) has made it clear that wind-shear had an effect on the earlier measurements of Swinbank (Priestley 1954, 1955, 1956). Webb's measurements show that three regions may be distinguished in the earth's boundary layer with upward transfer of heat: (*a*) near the ground, a region of forced convection with temperature gradient inversely proportional to height; (*b*) farther up, a region of apparently free convection with temperature gradient varying as the $-\frac{4}{3}$-power of height and independent of wind-shear; and (*c*) an upper region of imperceptible temperature gradient. The boundaries between these regions may be expressed by critical

* It is unlikely that the fluctuations during periods of quiescence are unaffected by the distant boundaries, but their contribution to the total intensities is too small to falsify the prediction (see § 11).

values of the local Richardson number. The earlier measurements did not extend above the intermediate region but the existence of a third region shows that, although the temperature gradient may be independent of wind-shear in the intermediate region, this is only true for a limited range of wind-shear and a sufficient reduction in wind-shear will lead to transition to another type of convection, presumably similar to the convection over a flat surface without wind.

The imposition of a horizontal shearing motion on homogeneous natural convection may have several effects, but two obvious ones are a transfer of energy from the mean flow to the turbulent motion and a restriction on the freedom of vertical movement of the fluid. The first tends to increase turbulent velocities while the second restricts the vertical scale of the convective movements, and it is not obvious whether the presence of a shearing motion will increase or decrease the temperature gradient for a given heat flux. Webb's measurements show that the first effect of a moderate wind-shear is to increase the temperature gradient but that a condition is reached in which further increase of wind-shear is at first without effect on the temperature gradient and then decreases it as the contribution to the turbulent energy by working against Reynolds stresses becomes dominant. Our hypothesis is that this is caused by an initial decrease in vertical scale of the convective motion which is later offset by the increase in turbulent intensity arising from the transfer of energy from the mean flow.

Experimental support of this hypothesis could only be obtained from detailed measurements of the flow, but it is interesting that the present measurements indicate length scales much larger (relative to height above the surface) than occur in forced convection through a boundary layer. The destruction of temperature fluctuations by conductivity depends on a 'cascade' process of intensification of temperature gradients by the turbulent motion that, like the closely analogous process of turbulent energy dissipation proceeds at a rate independent of the viscosity and conductivity of the fluid if the Reynolds number of the motion is large. The rate of destruction of $\frac{1}{2}\overline{\theta^2}$ is then

$$3\kappa\overline{\left(\frac{\partial\theta}{\partial x}\right)^2} = c'\frac{u_s}{l_s}\overline{\theta^2}, \tag{10.2}$$

where u_s, l_s are scales of velocity and length characteristic of the turbulent motion. This relation is analogous to the established form for the energy dissipation,

$$\epsilon = -\nu\overline{u_i\nabla^2 u_i} = cu_s^3/l_s. \tag{10.3}$$

Measurements by Kistler, O'Brien & Corrsin (1956) of the decay of temperature fluctuations suggest that

$$3\kappa\overline{\left(\frac{\partial\theta}{\partial x}\right)^2} = \tfrac{1}{3}c'\frac{(\overline{w^2})^{\frac{1}{2}}}{L}\overline{\theta^2}, \tag{10.4}$$

where $c' \doteqdot 0{\cdot}8$ and L is the integral scale of the turbulent motion. Making use of the measurements of $\overline{\theta^2}$ and $\overline{\left(\frac{\partial\theta}{\partial x}\right)^2}$ as expressed by equations (6.7) and (7.3), it follows that

$$\frac{L}{z} = 2{\cdot}0c'\left(\frac{z}{z_0}\right)^{-0{\cdot}1}\frac{(\overline{w^2})^{\frac{1}{2}}(\overline{\theta^2})^{\frac{1}{2}}}{\theta\overline{w}}, \tag{10.5}$$

and that $L/z \doteqdot 2$ for the larger values of z/z_0. In forced convection through a turbulent boundary layer, $L/z \doteqdot 0{\cdot}4$, relatively much smaller. Obviously, the presence of the shearing motion exercises a powerful restriction on the scale of the motion.

The measurements support the Malkus theory of turbulence in that the observed distribution of mean temperature well outside the conduction layer is described by

$$\theta_0^{-1} \log \frac{T}{T_a} = 2{\cdot}6 \left(\frac{z}{z_0}\right)^{-1} + 0{\cdot}06 \qquad (10.6)$$

within the experimental error. It is interesting that the multiplicative constant, 2·6, based on these more extensive measurements is nearer to the theoretical value,* 2·0, than that based on the earlier measurements over a more limited range of z/z_0, and that the magnitude of the additive constant, 0·06, might have been inferred from a study of the distributions of temperature fluctuations (see § 11).

11. Physical description of the flow

Possibly the most striking feature of the observations is the existence of two modes of temperature fluctuation, but no hint of it is to be found in either theory of the convection and it must be a part of the physical mechanism of the convection that underlies the generalizations of the theory. If the temperature at a fixed point has two distinct modes of fluctuations, the space occupied by the fluid at any instant must be divided by comparatively well-defined bounding surfaces into corresponding regions of 'activity' and 'quiescence', and the properties of the modes are also those of the regions. Within the active regions temperature fluctuations are large and the mean temperature is high, while within the quiescent regions the fluctuations are much smaller and the mean temperature only slightly above the reference temperature. The proportion of the active mode in a period of observation decreases fairly rapidly with increase of height and the average time interval between successive periods of activity increases. As the fluctuations are, very nearly, statistically homogeneous over horizontal planes, these observations mean that both the number and the total area of the sections of active regions by a horizontal plane decrease as the height of the plane increases and this suggests that the source of active regions may be warm, buoyant air-currents rising from the conduction layer.

If rising currents of this sort exist, they must be very different from the convection plumes that rise from localized heat sources in still air because in this arrangement all the air is in vigorous turbulent motion. This could be inferred by observing that, far from the surface, active regions are too few to transport much of the heat flux and that the major part is necessarily carried by turbulent

* This 'theoretical' value would probably not be obtained from a strict application of the theory, as it depends on an analysis in which the orthogonal functions used to represent the fields of velocity and temperature satisfy some but not all of the boundary conditions (Malkus 1954*b*). It is likely that use of the correct orthogonal functions would lead to a somewhat larger multiplicative constant. A similar effect would arise from a subsequent modification of the theory (Malkus & Veronis 1958).

movements in the quiescent regions, but it is also possible to estimate the mean square of the turbulent velocity in each kind of region from the measured distributions of $\partial\theta/\partial x$ and $\partial\theta/\partial t$. If the Reynolds and Péclet numbers of a turbulent motion are large and if the fluctuations of velocity and temperature gradient are statistically independent, it may be shown that (see the Appendix)

$$\overline{\left(\frac{\partial\theta}{\partial t}\right)^2} = \overline{q^2}\overline{\left(\frac{\partial\theta}{\partial x}\right)^2}. \tag{11.1}$$

The first condition is satisfied for large enough values of z/z_0 but the second is not satisfied if the mean values extend over the whole time of observation without distinction between active and quiescent periods. Within regions of one kind, the distributions of $\partial\theta/\partial x$ and $\partial\theta/\partial t$ have, very nearly, the forms expected if both conditions were satisfied and if the distributions of velocity and temperature gradient were normal. Assuming this, the mean square of the turbulent velocity in each kind of region can be estimated, with fair accuracy for the active regions but with considerable uncertainty for the quiescent regions, by using the results of the analysis of the statistical distributions (table 3). In the active regions, the root-mean-square of the velocity is about $5{\cdot}5u_0$, almost independent of height but with a tendency to decrease slowly as z/z_0 increases. For the quiescent regions, variances computed from the central part of the observed distributions give a root-mean-square velocity of $7u_0$, but the uncertainty is considerable and this value may be too small. In any event, the turbulent velocities are somewhat greater in the 'quiescent' periods than they are in the 'active' periods.

It appears probable that active regions are formed by more or less localized emission of heat from the conduction layer, most likely in the neighbourhood of points or lines of flow 'separation' where the horizontal velocity just outside the conduction layer happens to be small or zero. The hot air rising from such a place will mix rapidly with the surrounding turbulent air, but in these circumstances the distinction between air that has received heat from the heat source and air that has not remains fairly sharp as is shown by observations of the spread of heat through a turbulent boundary layer (Batchelor 1954; Johnson 1955). The presence and persistence of 'up-draught sites' has been described by Malkus (1954*a*) who observed the motion of suspended particles in acetone and water, and these may be identified with the hypothetical heat sources.* The persistence of the sources is confirmed in these experiments by the comparatively long duration of the active periods (of order 10 sec compared with a scale time $(z_0/u_0$ of about 0·5 sec), and a possible explanation is that, once a site is established, it attracts to itself air heated by passage through the conduction layer which adds to the strength and stability of the up-draught.

The distribution of mean temperature is determined by the extent to which these up-draughts penetrate the cool 'quiescent' air, which is dependent on the initial cross-section and strength of the up-draught, both closely related to the thickness of the conduction layer. It is probably in this way that the scale length

* The existence of similar up-draughts in the atmosphere with light winds and uniform surface heating is well recognized, but they are often identified with convection plumes from isolated sources of heat.

z_0 enters into the temperature distribution far from the conduction layer and that the viscosity and conductivity of the fluid can affect the convection at those large values of z/z_0, for which their direct effects are negligible. Natural convection of this type will occur over a rough horizontal surface and in the outer part of a horizontal boundary layer of sufficient thickness, and then viscosity and conductivity are not expected to have any direct influence on the convection. If this view of the way in which molecular transfer influences the convection over a smooth plane is correct, the distribution of mean temperature will be described by the same equation (10.6) but with a value of the scale length related to the scale of the surface roughness or, for the boundary layer, to the horizontal scale of the temperature fluctuations at the level where natural convection becomes dominant.* In these circumstances, the convection depends on the quantities z_0, g and Q, and the scales of velocity and logarithmic temperature are

$$\left.\begin{aligned} u_0 &= (gQz_0)^{\frac{1}{3}}, \\ \theta_0 &= Q^{\frac{2}{3}}(gz_0)^{-\frac{1}{3}}. \end{aligned}\right\} \tag{11.2}$$

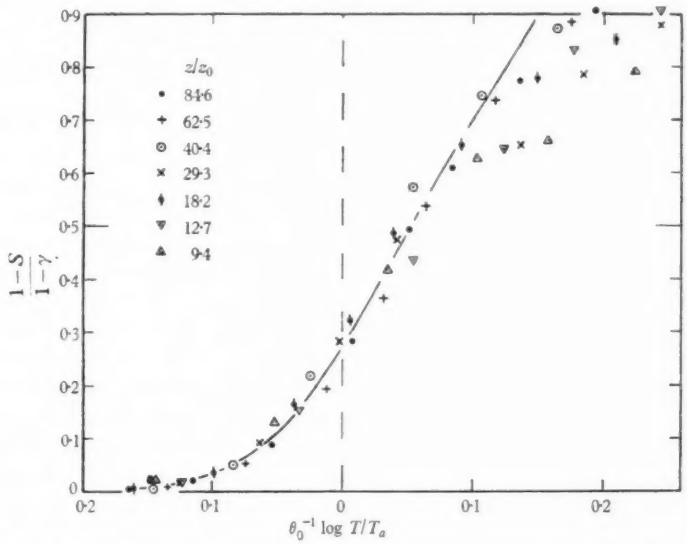

FIGURE 23. Statistical distributions of instantaneous temperature, plotted as $(1-S)/(1-\gamma)$ to show invariance of quiescent components.

Although the hot 'active' regions are certainly characteristic of the surface layer and would be expected to appear whatever the dimensions of the complete convection box, it is most unlikely that the temperature and velocity structure of the cool 'quiescent' regions is independent of these dimensions. It has been pointed out that the contributions of the 'quiescent' regions to the distributions of temperature and temperature gradient are nearly independent of height

* A very deep boundary layer with a constant Reynolds stress, τ_0, and a constant upward flux of total heat has a characteristic length $\tau_0^{\frac{1}{2}}(gQ)^{-1}$ (Ellison 1957) and the appropriate value of the scale length z_0 will be a multiple of this.

(allowing for the variation of duration factor), and this indicates that the temperature structure in these regions is characteristic of the whole flow and not just of the surface layer. The evidence for this statement is contained in figures 17 and 22, and in figure 23 which shows the statistical distributions of instantaneous temperature at various heights (previously given in figure 11) replotted in terms of this hypothesis using the duration factors inferred from analysis of the distributions of $\partial\theta/\partial x$ and $\partial\theta/\partial t$. The identity of form, particularly at the lower temperatures, and the apparent asymptotic approach to a universal form suggest strongly an essential homogeneity of temperature fluctuations in the quiescent regions. If the fluctuations in the quiescent regions are characteristic of the whole flow, it will not be possible to retain strict dimensional similarity but the contribution of these regions to the measured quantities is so small that a lack of dimensional similarity would be impossible to detect in these experiments.

It may be noticed that the medians of all the distributions in figure 23 lies very close to $\theta_0^{-1}\log(T+\theta)/T_a = 0{\cdot}055$, and, since there is no indication that the asymptotic statistical distribution of temperature is strongly asymmetric, the mean value at great heights must also lie near 0·055. This observation provides a meaning for the additive constant, 0·06, in the equation (10.6) which describes the variation of mean temperature as the mean temperature of the air far from the surface layer.

Although it is difficult to compare the measurements of velocity fluctuations in turbulent flows of constant density with these measurements of temperature fluctuations, there is little doubt that the turbulent motion over a heated horizontal surface differs in kind from the turbulent motion in a boundary layer. At first sight, this lack of resemblance is very surprising and its confirmation is probably the most convincing argument in favour of the theory of turbulence proposed by Malkus which, with the same set of assumptions, produces all the accepted results for wall turbulence (Malkus 1956) and makes predictions for thermal turbulence that are consistent with experiment. In the theory, the differences appear to arise from a difference in nature of the corresponding problems of laminar stability but a direct reason for the inapplicability of similarity considerations to thermal turbulence can be found by considering the balance of turbulent kinetic energy that would occur if the similarity theory were valid. To the usual approximation, the equation for the kinetic energy is

$$\frac{\partial}{\partial z}\left(\frac{1}{\rho}\overline{pw}+\tfrac{1}{2}\overline{q^2w}\right) = \frac{g}{T}\overline{\theta w}-\epsilon, \tag{11.3}$$

where ϵ is the local rate of conversion of kinetic energy to heat. The similarity theory predicts that

$$(\overline{w^2})^{\frac{1}{2}} = a(gQz)^{\frac{1}{3}}, \quad \frac{1}{\rho}\overline{pw}+\tfrac{1}{2}\overline{q^2w} = -\beta(\overline{w^2})^{\frac{3}{2}}, \quad \epsilon = \frac{(\overline{w^2})^{\frac{3}{2}}}{L_\epsilon}, \tag{11.4}$$

where L_ϵ is proportional to z and is nearly the integral scale of the turbulent motion. Substitution of these relations in the energy equation leads to an expression for a,

$$a = \left(\frac{z}{L_\epsilon}-\beta\right)^{-\frac{1}{3}}. \tag{11.5}$$

This quantity determines the general level of turbulent intensity and is essentially positive, while β, which describes the transport of energy from one part of the flow to another is positive if energy transport takes place down intensity gradients. Measurements in constant density flows with gradients of turbulent intensity show that z/L_ϵ and β are very similar in magnitude (e.g. Townsend 1951), and it is at least possible that β is greater than z/L_ϵ in which event equation (11.5) has no meaning except that transport of turbulent energy from one part of the flow to another prevents the establishment of a motion described by equations (11.4). If transfer of turbulent energy dominates the balance of kinetic energy, it is unlikely that similarity considerations, based on the notion that the surface layer is independent of both the conduction layer and the outer flow, are ever applicable. This kind of difficulty does not arise in the treatment of wall turbulence in which the gradient of turbulence intensity and the net energy flux are both negligible.

A further point of difference has already been mentioned, the presence of shearing motion tending to restrict the effective scale of turbulent movements which is greater in natural convection without shear.

12. Production and destruction of temperature fluctuations

A direct consequence of the heat equation and of the symmetry of the flow is that

$$\frac{\partial}{\partial t}(\tfrac{1}{2}\overline{\theta^2}) + \left[QT + \kappa\frac{\partial T}{\partial z}\right]\frac{\partial T}{\partial z} + \frac{\partial}{\partial z}(\tfrac{1}{2}\overline{\theta^2 w}) = \kappa\frac{\partial^2}{\partial z^2}(\tfrac{1}{2}\overline{\theta^2}) - \kappa\left[2\overline{\left(\frac{\partial\theta}{\partial x}\right)^2} + \overline{\left(\frac{\partial\theta}{\partial z}\right)^2}\right]. \tag{12.1}$$

The first term, the time rate of change of $\frac{1}{2}\overline{\theta^2}$, is zero for steady convection but has been included to make clear the meaning of the equation as the balance between the production, transport and destruction of temperature fluctuations. The remaining terms represent production of temperature fluctuations by interaction between the turbulent motion and the gradient of mean temperature, the net effect of convection of temperature fluctuations by turbulent movements, the net effect of molecular diffusion of temperature fluctuations, and the destruction of fluctuations by conduction.

Well outside the conduction layer, it is likely that

$$\overline{\left(\frac{\partial\theta}{\partial x}\right)^2} = \overline{\left(\frac{\partial\theta}{\partial z}\right)^2}, \tag{12.2}$$

and then all the terms of equation (12.1) may be calculated from the results of this work, excepting the one describing turbulent convection which may be obtained by difference. For the region $z/z_0 > 10$ then, equation (12.1) may be written in the non-dimensional form

$$-2{\cdot}6\left(\frac{z}{z_0}\right)^{-2} + \frac{z_0}{u_0\theta_0^2 T^2}\frac{\partial}{\partial z}(\tfrac{1}{2}\overline{\theta^2 w}) = -0{\cdot}27\left(\frac{z}{z_0}\right)^{-1{\cdot}5}, \tag{12.3}$$

where use has been made of equations (6.2) and (7.3) to represent the observed variations of mean temperature and mean square temperature gradient, and two

terms, $\kappa\left(\frac{\partial T}{\partial z}\right)^2$ and $\kappa\frac{\partial^2}{\partial z^2}(\tfrac{1}{2}\overline{\theta^2})$, are negligible and have been omitted. The integral of this equation is

$$2{\cdot}6\left(\frac{z}{z_0}\right)^{-1}+\frac{\overline{\theta^2 w}}{2u_0\theta_0^2T^2}=0{\cdot}54\left(\frac{z}{z_0}\right)^{-0{\cdot}5}+a_0, \tag{12.4}$$

where a_0 is a constant of integration. If the power-laws used to describe the variations of mean temperature and mean square temperature gradient were valid for all large values of z/z_0, the constant would necessarily be zero, but the double structure of the convection and the identification of the quiescent regions with the flow 'at infinity' make it extremely unlikely that simple power laws will be valid except as approximations within the range of observation. In principle, the constant could be calculated by integrating equation (12.1) from the surface to a point in the range of validity of equation (12.4), but the accuracy of this procedure would be very low since most of the production and destruction of fluctuations takes place in the layer z/z_0 less than five, and small inaccuracies in the estimation of, say, rate of destruction would lead to an uncertainty in a_0 large compared with terms in equation (12.4).

The main conclusion from this analysis is that the production of fluctuations tends to exceed the destruction over most of the fully turbulent region, and it follows that convection of temperature fluctuations by turbulent movements is of importance.

Appendix: The relation between rate of change of temperature and temperature gradient in turbulent flow

In flows of nearly constant density, the temperature fluctuation satisfies the equation

$$\frac{D\theta}{Dt}=\frac{\partial\theta}{\partial t}+\mathbf{u}.\nabla\theta=\kappa\nabla^2\theta. \tag{1}$$

If the Reynolds number of the turbulent motion is large, the substantial rate of change of temperature, $D\theta/Dt$, is usually small compared with either $\partial\theta/\partial t$ or $\mathbf{u}.\nabla\theta$ and the rate of change of temperature at a point fixed in space is related to the local velocity and temperature gradient by

$$\frac{\partial\theta}{\partial t}+\mathbf{u}.\nabla\theta=0. \tag{2}$$

The justification for this approximation is that the greater part of the temperature gradient is derived from Fourier components of the temperature field with wave-numbers near $(\epsilon/\nu^3)^{\frac{1}{4}}$ (ϵ is the rate of viscous dissipation of turbulent energy),* and so the time rate of change of temperature by molecular conduction is of order $\kappa(\epsilon/\nu^3)^{\frac{1}{2}}\theta_d$, where θ_d is the 'amplitude' of the Fourier components which contribute to the temperature gradient. This rate should be compared with the rate of change due to convection of the temperature field past the point of observation

* This discussion is only valid for fluids for which the Prandtl number, ν/κ, is near one. For a detailed account of the spectrum of the temperature fluctuations, see Batchelor (1959).

which is of order $u_0\theta_d(\epsilon/\nu^3)^{\frac{1}{4}}$, where u_0 is the root-mean-square of the turbulent velocity. It follows that the order of magnitude of $\mathbf{u}.\nabla\theta$ is greater than that of $D\theta/Dt = \kappa\nabla^2\theta$ in the ratio $u_0\kappa^{-1}(\epsilon/\nu^3)^{-\frac{1}{4}}$. It is well known that $\epsilon = u_0^3/L_\epsilon$, where L_ϵ is nearly equal to the integral scale of the turbulent motion, and so the ratio is nearly $(u_0 L_\epsilon/\nu)^{\frac{1}{4}}$ which is large if the Reynolds number of the motion is large.

Using this approximation, we may derive the relation between the probability distribution functions of $\mathbf{u}$, of $\nabla\theta$ and of $\partial\theta/\partial t$. Consistently with the assumption of large Reynolds number, we assume that the turbulent velocity and the temperature gradient are statistically independent and that the temperature gradients are isotropically distributed.* Then the distribution function for $\partial\theta/\partial t$ is

$$P_1\left(\frac{\partial\theta}{\partial t}\right) = \int_0^\infty P_2(u)\, P_3\left(-\frac{\dot\theta}{u}\right)\frac{du}{u}, \tag{3}$$

where $P_2(u)\,du$ is the probability that the turbulent velocity should lie between u and $u+du$, and $P_3(\theta_x)$ is the probability that the component of the temperature gradient in a particular direction (actually in the direction of $\mathbf{u}$) should have the value θ_x. It is a simple consequence of equation (3) that the product of the nth-order moments of the distributions of $|\mathbf{u}|$ and θ_x equals the nth-order moment of the distribution of $\partial\theta/\partial t$. In particular, the second moments are related by

$$\overline{\left(\frac{\partial\theta}{\partial t}\right)^2} = \overline{|\mathbf{u}|^2}\,\overline{\left(\frac{\partial\theta}{\partial r}\right)^2} = \overline{q^2}\,\overline{\left(\frac{\partial\theta}{\partial x}\right)^2}, \tag{4}$$

a result obtainable directly from equation (2).

The product rule which relates the moments of the three distributions implies that one at least of $\mathbf{u}$, $\nabla\theta$ and $\partial\theta/\partial t$ is not normally distributed, and the distribution of $\partial\theta/\partial t$ is the most likely to depart from normality. It is interesting to compute the distribution function for $\partial\theta/\partial t$, assuming that $\mathbf{u}$ and $\nabla\theta$ are normally distributed. In real flows, it is unlikely that these last two quantities have exactly normal distributions but the experimental evidence suggests that the departures from normality may not be large. We set

$$P_2(u) = \left(\frac{2}{\pi}\right)^{\frac{1}{2}} u^2 e^{-\frac{1}{2}u^2}, \quad P_3(\theta_x) = \left(\frac{1}{2\pi}\right)^{\frac{1}{2}} e^{-\frac{1}{2}\theta_x^2}, \tag{5}$$

corresponding to normal distributions with variances $\sqrt{3}$ and 1 respectively. Then,

$$\begin{aligned} P_\epsilon(\dot\theta) &= \frac{1}{\pi}\int_0^\infty u \exp\left[-\frac{1}{2}\left(u^2+\frac{\dot\theta^2}{u^2}\right)\right] du \\ &= \frac{\dot\theta}{2\pi}\int_0^\infty \exp\left[-\tfrac{1}{2}\dot\theta(\lambda+\lambda^{-1})\right] d\lambda = -\tfrac{1}{2}\dot\theta H_1^{(1)}(i\dot\theta), \end{aligned} \tag{6}$$

* Statistical independence of turbulent velocity and temperature gradient requires that, if there exist regions or periods of unusually large velocity fluctuations, these are not associated either with unusually large or small fluctuations of temperature gradient. If they are, it may still be possible to use this analysis by confining attention to regions in which turbulent velocity and temperature gradient have a spatially uniform distribution of fluctuations.

in the notation used by Jahnke & Emde (1933) for the Bessel functions of imaginary argument. The probability distribution function specified by equation (6) is very different from a normal distribution as can be seen in figure 24.

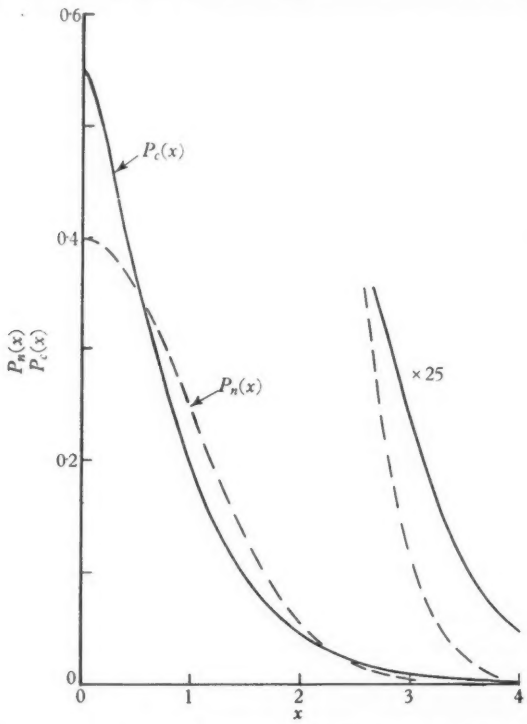

FIGURE 24. Comparison of normal Gaussian and 'convection' probability distribution functions of unit variance.

For large values of $\dot{\theta}$,

$$P_c(\dot{\theta}) = \left(\frac{\dot{\theta}}{2\pi}\right)^{\frac{1}{2}} e^{-\dot{\theta}}\left[1 + \frac{3}{8\dot{\theta}} - \frac{15}{128\dot{\theta}^2} + \ldots\right], \tag{7}$$

in contrast to the normal distribution function

$$P_n(x) = \left(\frac{1}{2\pi}\right)^{\frac{1}{2}} e^{-\frac{1}{2}x^2}. \tag{8}$$

The experimental measurements are of the probabilities that $\partial\theta/\partial t$ and $\partial\theta/\partial x$ shall exceed set values, i.e.

$$S_1(\dot{\theta}) = \int_{\dot{\theta}}^{\infty} P_1(x)\,dx \quad \text{and} \quad S_3(\theta_x) = \int_{\theta_x}^{\infty} P_3(x)\,dx,$$

and comparison should be made with the integral of the distribution function defined by equation (6),

$$S_c(\dot{\theta}) = -\int_{\dot{\theta}}^{\infty} \frac{x}{2} H_1^{(1)}(ix)\,dx. \tag{9}$$

Values of $S_c(x)$ have been calculated, in part by numerical integration and in part using the asymptotic series,

$$S_c(x) = \left(\frac{x}{2\pi}\right)^{\frac{1}{2}} e^{-x}\left[1+\frac{7}{8x}-\frac{71}{128x^2}+\frac{765}{1024x^3}-\ldots\right] \tag{10}$$

with the results shown in table 4. For convenience, distributions similar to those defined by the functions $P_c(x)$ and $S_c(x)$ may be called 'convection' distributions. The most obvious difference from normal distributions is the relatively greater probability of occurrence of very large deviations.

x	$P_c(x)$	$S_c(x)$	x	$P_c(x)$	$S_c(x)$
0	0·3183	0·5000	2·5	—	0·0666
0·2	0·3040	0·4378	3·0	0·0384	0·0427
0·4	0·2782	0·3796	3·5	—	0·0274
0·6	0·2488	0·3269	4·0	0·0159	0·0174
0·8	0·2194	0·2800	4·5	—	0·0110
1·0	0·1916	0·2390	5·0	—	0·00695
1·2	0·1660	0·2032	5·5	—	0·00437
1·4	0·1430	0·1723	6·0	—	0·00274
1·6	0·1226	0·1457	6·5	—	0·00169
1·8	0·1046	0·1230	7·0	—	0·00102
2·0	0·0890	0·1036			

TABLE 4. 'Convection' distribution functions

REFERENCES

BATCHELOR, G. K. 1954 *Quart. J. Roy. Met. Soc.* **80**, 339.

BATCHELOR, G. K. 1959 *J. Fluid Mech.* **5**, 113.

ELLISON, T. H. 1957 *J. Fluid Mech.* **2**, 456.

JAHNKE, E. & EMDE, F. 1933 *Tables of Functions.* Teubner: Leipzig and Berlin.

JOHNSON, D. S. 1955 *Johns Hopkins Univ., Rep.* no. OSR TN 55–289.

KISTLER, A. L., O'BRIEN, V. & CORRSIN, S. 1956 *J. Aero. Sci.* **23**, 96.

LIEPMANN, H. W. 1952 *Z. angew. Math. Phys.* **3**, 321.

MALKUS, W. V. R. 1954*a* *Proc. Roy. Soc.* A, **225**, 185.

MALKUS, W. V. R. 1954*b* *Proc. Roy. Soc.* A, **225**, 196.

MALKUS, W. V. R. 1956 *J. Fluid Mech.* **2**, 521.

MALKUS, W. V. R. & VERONIS, G. 1958 *J. Fluid Mech.* **4**, 225.

PRIESTLEY, C. H. B. 1954 *Austr. J. Phys.* **7**, 176.

PRIESTLEY, C. H. B. 1955 *Quart. J. Roy. Met Soc.* **81**, 139.

PRIESTLEY, C. H. B. 1956 *Proc. Roy. Soc.* A, **238**, 287.

RICE, S. O. 1944 *Bell. Tech. J.* **23**, 282.

RICE, S. O. 1945 *Bell. Tech. J.* **24**, 46.

THOMAS, D. B. 1956 Ph.D. dissertation: University of Cambridge.

THOMAS, D. B. & TOWNSEND, A. A. 1957 *J. Fluid Mech.* **2**, 473.

TOWNSEND, A. A. 1951 *Proc. Camb. Phil. Soc.* **47**, 375.

TOWNSEND, A. A. 1959 *J. Fluid Mech.* (to be published).

WEBB, E. K. 1958 *Quart. J. Roy. Met. Soc.* **84**, 118.

The hypersonic viscous effect on a flat plate with finite leading edge

By ANDREW G. HAMMITT
Princeton University, Princeton, New Jersey

(Received 6 June 1958)

A method has been developed for calculating the viscous effects of the hypersonic flow on the fore part of various bodies. This method takes into account the finite leading-edge thickness of the body and the detached shock wave. The calculated pressure distributions agree with all experimental results for both air and helium over a wide range of Mach numbers and Reynolds numbers. The calculation predicts skin frictions of the order of twice those predicted by ordinary boundary-layer theory.

1. Introduction

The flow about the leading edge of a flat plate at hypersonic speeds has been considered in several theoretical and experimental studies. The first mention of the problem in the literature is by Becker (1950). In some experiments made in the N.A.C.A. hypersonic tunnel at Langley Field, it was observed that the pressure on the forward surface of a wedge-shaped airfoil was not constant as predicted by classical inviscid flow theory, and was above the indicated value near the leading edge. It was suggested that the growth of the boundary layer on the surface created an effectively curved surface, and rough calculations showed that this mechanism seemed to account for the observed results.

Following this initial work, several authors published analytical papers in which they attempted to calculate the flow field caused by the interaction of the viscous boundary layer with the inviscid flow behind the shock wave. These papers attacked the problem in two ways: the first method, used by Shen (1952), Li & Nagamatsu (1953, 1955) and Pai (1953), treated the whole flow region between the shock wave and the plate by the boundary-layer equations; and the second method, adopted by Bertram (1952) and Lees (1952, 1954*a*, *b*), followed the suggestion by Becker of dividing the region between shock wave and the wall into inviscid and viscous regions. Bogdonoff & Hammitt (1956) pointed out that there were some basic inconsistencies in the first method which did not exist in the second. Both approaches predicted about the same pressure distributions over flat plates.

Experimental studies of the flow over flat plates, made by Bogdonoff & Hammitt (1956) in the helium hypersonic wind tunnel at Princeton University at Mach numbers between 11 and 15, showed that the pressures on the surface were considerably higher than those predicted by the various analytical methods previously mentioned. In later experimental work (Hammitt, Vas & Bogdonoff

1956; Hammitt & Bogdonoff 1956), it was found that the leading-edge thickness t had an important influence on the surface pressures and that for the higher Reynolds numbers based on t the results depended only on x/t, where x is the distance along the plate from the leading edge. This result led to the conclusion that the pressures on the plate were caused by the inviscid flow field behind the finite leading edge and were independent of the viscous effects of the boundary layer growth. This inviscid part of the flow field seems to be important for very thin leading edges. Since such an effect was not included in the theories for infinitely thin leading edges, the results are not applicable when the leading-edge Reynolds number is greater than 100 for distances from the leading edge up to $10{,}000x/t$.

Other experimental work by Kendall (1957), carried out in air tunnels at Mach numbers of the order of 6, does not show this large dependence on leading-edge thickness, and the experimental pressure distributions agree with the viscous theories fairly well. The indications are that the inviscid effect of the leading edge decreases more rapidly with Mach number than the viscous effect. Hence, the inviscid part of the leading-edge problem may be unimportant at lower Mach numbers, but may predominate at higher Mach numbers.

In the present report, experimental pressure distributions near the leading edge of flat plates are presented for a wide range of leading-edge Reynolds numbers. An analytical treatment is then presented to account for the Reynolds number dependence of these surface pressures.

2. Experimental studies

A detailed description of the Princeton helium hypersonic tunnel has been given previously by Bogdonoff & Hammitt (1954). This tunnel, using helium as the working fluid, is capable of operating at Mach numbers up to 20, and Reynolds numbers between 0·5 and 2·0 million per inch. An axially symmetric conical nozzle with an 0·2 in. throat and a 3·75 in. working section is used. Because the nozzle is not contoured, but conical, there is a continuous Mach number gradient, but no region of uniform Mach number. Tests are conducted in this non-uniform region.

The model used in these experiments is shown in figure 1. It consists of a flat plate with a square leading edge. Pressure orifices are distributed along the surface, being concentrated near the leading edge and spread out farther back. The leading-edge thickness has been measured using a microscope which enables the thickness to be determined to within $0{\cdot}04 \times 10^{-3}$ in. Leading-edge thicknesses between $0{\cdot}12 \times 10^{-3}$ and $4{\cdot}4 \times 10^{-3}$ in. were tested at several Mach numbers and stagnation pressures.

The pressure distributions on the flat surface are shown in figure 2. In this plot, the distance along the surface is expressed in units of the leading-edge thickness. The surface pressure is expressed as the difference between the measured pressure and the pressure at the same point when the model is absent. In this way, a first-order correction is made for the non-uniform pressure in the test section. This pressure gradient due to varying tunnel Mach number is actually small compared with the pressure gradient measured on the surface, so that this first-order correction should be sufficient. Results are presented for a wide range of leading-edge thicknesses at a Mach number of 11·4, measured at the leading edge of the

model. Data for other Mach numbers and more detailed descriptions of these pressure measurements are given by Vas (1957). Since the data for $M = 11{\cdot}4$ are typical, only this one case will be treated in this paper. The results indicate that for the larger leading-edge Reynolds numbers, the pressure distributions are almost independent of Reynolds number, but are dependent at smaller leading-edge Reynolds numbers.

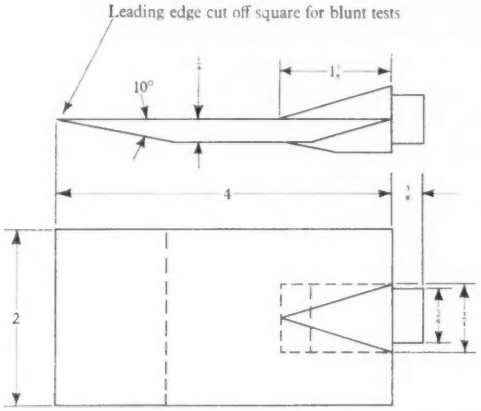

FIGURE 1. Blunted flat plate model used to measure experimental pressure distributions. Dimensions are given in inches.

3. Theory

For a given geometry, the experiments indicate that at high Reynolds numbers the surface pressure distribution is determined by the inviscid flow behind the detached shock wave. At lower Reynolds number, the boundary layer on the body becomes thicker, and modifies the effective body shape, so that the flow field may be described as a flow about the modified body. If this model is correct, the viscous effect can be calculated as the difference between the inviscid flow about the effective body, i.e. the actual body modified by the boundary-layer thickness, and the inviscid flow about the actual body. Through most of the range of Reynolds numbers for which data were presented in figure 2, the viscous effect is a perturbation on the inviscid flow. Therefore a first determination of the viscous effect can be made by calculating the boundary layer in the inviscid flow field and then calculating the modified inviscid flow field about the new effective body shape. A higher order solution may then be determined by using this first-order flow field, and recalculating the boundary layer. As many successive approximations may be made as are required. Because of the difficulty of determining the inviscid flow field behind the detached shock wave, the inviscid solution obtained from the experimental results will be used. This method of solution is essentially the same as was used by Lees & Probstein (1952), except they assumed the inviscid flow field about the body to be uniform and the same as that ahead of the body.

It is interesting to note that, with this method, there are no inherent difficulties at the leading edge. The previous solutions, which assumed an infinitely sharp

leading edge, always introduced a singularity at this point. By recognizing that the leading edge of any real model is always blunt, the present method eliminates this difficulty. The boundary layer grows from the stagnant point solution and no singularity is involved. As the leading edge becomes sharper and the mean free path of the gas molecules becomes of the order of the leading-edge thickness, the flow in this region cannot be treated as a continuum. The model is still correct, but different equations are required to describe the flow.

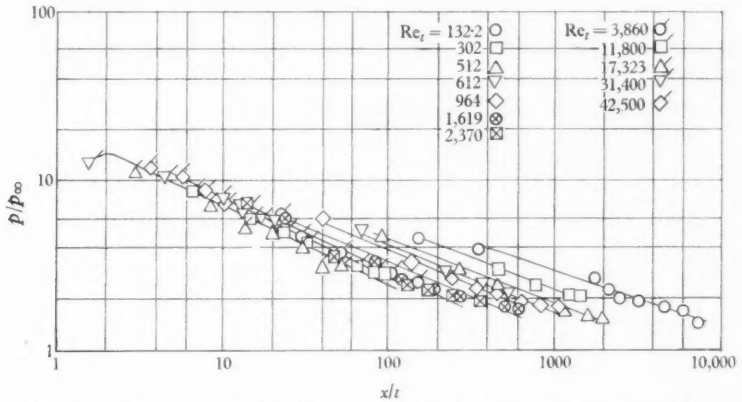

FIGURE 2. Pressure distributions measured in helium on flat plate model for various Re_t; $M = 11{\cdot}1$.

Boundary-layer solution

The zero-order inviscid pressure distribution is taken from the experimental results for the highest Reynolds number. The growth of the boundary layer may be calculated in this flow field by the use of momentum integral techniques. If there were no mass in the boundary layer, the entropy along the outside edge of the boundary layer would always be equal to the value behind the normal shock wave. However, since some flow enters the layer, the entropy at the edge of the boundary layer is continually changing. Far downstream from the leading edge, the entropy will approach the free-stream value, since all of the flow passing through the strong shock wave will be contained in the boundary layer.

The usual equations for the boundary layer are

$$\rho u\frac{\partial u}{\partial x}+\rho v\frac{\partial u}{\partial y}=-\frac{\partial p}{\partial x}+\frac{\partial}{\partial y}\left(\mu\frac{\partial u}{\partial y}\right), \tag{1}$$

$$\frac{\partial(\rho u)}{\partial x}+\frac{\partial(\rho v)}{\partial y}=0, \tag{2}$$

where u, v are the velocity components parallel to x, y, p is pressure, ρ is density and μ is viscosity,

If the equation of motion (1) is integrated in the y-direction (i.e. perpendicular to the plate) between 0 and δ and the continuity equation (2) is used to express the value of v at $y = \delta$, the momentum integral equation is found to be

$$\frac{\partial u_1}{\partial x}\int_0^\delta \rho u\,dy-\frac{d}{dx}\int_0^\delta \rho u(u-u_1)\,dy=\int_0^\delta -\frac{dp_1}{dx}\,dy-\mu_w\left(\frac{\partial u}{\partial y}\right)_{y=0}. \tag{3}$$

In isentropic flow, the pressure can be expressed in terms of the velocity by means of the Bernoulli relation

$$\frac{dp_1}{dx} = -\rho_1 u_1 \frac{du_1}{dx}.$$

When the boundary layer is growing into a region of rotational flow, the entropy changes for each stream line, so the Bernoulli equation cannot be used. In general, for the case of the boundary layer growing in the shock layer behind the highly curved hypersonic shock wave, the relation between pressure and velocity must include the entropy term. In the following development, u_1 and p_1 will be left as independent parameters and will only be related when the entropy on the outside of the boundary layer can be determined.

Let T denote temperature. If the transformation

$$S = \int_0^y \frac{T_1}{T} dy, \quad \delta_S = \int_0^\delta \frac{T_1}{T} dy, \quad \tau = \frac{S}{\delta_S},$$

is introduced, equation (3) reduces to the form

$$-\frac{d}{dx}\rho_1 u_1^2 \delta_S \int_0^1 \left(\frac{u}{u_1} - \frac{u^2}{u_1^2}\right) d\tau + \frac{du_1}{dx}\left[\delta_S \rho_1 u_1 \int_0^1 \frac{u}{u_1} d\tau\right] + \delta_S \frac{dp_1}{dx} \int_0^1 \frac{T}{T_1} d\tau = -\mu_w \frac{u_1 T_1}{T_w \delta_S}\left[\frac{d(u/u_1)}{d\tau}\right]_{\tau=0}. \tag{4}$$

If the viscosity is assumed to follow the law

$$\frac{\mu}{\mu_\infty} = \frac{1}{C}\frac{T}{T_\infty}, \quad \text{where} \quad C = \frac{T_w}{T_\infty}\Big/\frac{\mu_w}{\mu_\infty},$$

and the following quantities are defined

$$F_1 = \int_0^1 \frac{u}{u_1}\left(1 - \frac{u}{u_1}\right) d\tau, \quad F_3 = \left[\frac{\partial}{\partial \tau}\left(\frac{u}{u_1}\right)\right]_{\tau=0},$$

$$F_2 = \int_0^1 \frac{u}{u_1} d\tau, \qquad F_4 = \int_0^1 \frac{T}{T_1} d\tau,$$

then

$$\tfrac{1}{2}F_1 \frac{d(\delta S)^2}{dx} + \left[\frac{dF_1}{dx} + F_1 \frac{d(\log \rho_1 u_1^2)}{dx} - F_2 \frac{d(\log u_1)}{dx} - \frac{F_4}{\rho_1 u_1^2}\frac{dp_1}{dx}\right]\delta_S^2 = F_3 \frac{C\mu_\infty}{\rho \mu_1}\frac{T_1}{T_\infty}. \tag{5}$$

Define $\lambda = (\mathrm{Re}_t/C)(\delta_S/t)^2$ and $\zeta = x/t$, where t, the leading-edge thickness, is the characteristic dimension of the problem. Substitution of these quantities in equation (5) gives

$$\lambda' + 2\lambda\left[\frac{F_1'}{F_1} + \frac{\rho_1'}{\rho_1} + \frac{u_1'}{u_1}\left(2 - \frac{F_2}{F_1}\right) - \frac{F_4}{\gamma F_1 M_1^2 p_1} p_1'\right] = 2\frac{F_3}{F_1}\frac{T_1}{T_\infty}\frac{\rho_\infty u_\infty}{\rho_1 \mu_1}, \tag{6}$$

where the primes denote differentiation with respect to ζ. If a power-series representation for the velocity profile is assumed, this equation can be solved in a manner similar to that used by Morduchow & Clarke (1952).

A sixth degree polynomial will be assumed of the form

$$u/u_1 = a_0 + a_1\tau + a_2\tau^2 + a_3\tau^3 + a_4\tau^4 + a_5\tau^5 + a_l\tau^l. \tag{7}$$

The boundary conditions at the inner and outer edges of the boundary layer, expressed in the (x, S)-plane are

$$\tau = 0, \quad \frac{u}{u_1} = 0, \qquad \tau = 1, \quad \frac{u}{u_1} = 1;$$

$$\mu_\infty C \frac{T_1}{T_\infty}\frac{T_1}{T_0}\frac{\partial^2(u/u_1)}{\partial\tau^2} = \frac{1}{u_1}\frac{dp_1}{dx}\delta_S^2, \quad \frac{\partial(u/u_1)}{d\tau} = \frac{\partial^2(u/u_1)}{d\tau^2} = \frac{\partial^3(u/u_1)}{d\tau^3} = 0,$$

$$\partial^3\left(\frac{u}{u_1}\right)\Big/\partial\tau^3 = 0. \tag{8}$$

The second condition at $y = 0$ follows from the original equation of motion (1), and the third condition comes from differentiating equation (1) with respect to y, and adding the condition of zero heat transfer at the wall.

By using the boundary conditions (8), all of the coefficients of equation (7) may be evaluated in terms of one coefficient. If this is done, equation (7) may be written as

$$u/u_1 = 2(1 - \tfrac{1}{5}a_2)\tau + a_2\tau^2 - (5 + 2a_2)\tau^4 + 2(3 + a_2)\tau^5 - (2 + \tfrac{3}{5}a_2)\tau^6, \tag{9}$$

where

$$a_2 = \frac{\lambda}{2}\left(\frac{T_\infty}{T_1}\right)^2 \frac{T_0}{T_\infty}\frac{u_\infty}{u_1}\frac{1}{\gamma M_\infty^2}\frac{d(p_1/p_\infty)}{d\zeta}.$$

The various integrals used in defining the F's may now be evaluated:

$$F_1 = 0{\cdot}1093 + 0{\cdot}00211a_2 - 0{\cdot}000622a_2^2;$$
$$F_2 = 0{\cdot}7143 - 0{\cdot}01905a_2; \qquad F_4 = 1 + \tfrac{1}{2}(\gamma - 1)KM_1^2;$$
$$F_3 = 2 - 0{\cdot}400a_2; \qquad K = 0{\cdot}3950 + 0{\cdot}02116a_2 - 0{\cdot}000622a_2^2.$$

In these equations, a_2, the profile shape parameter, is a function of ζ. In the expressions for F_1, F_2 and F_4, the terms involving a_2 are small, so for boundary layers where a_2 is relatively constant, an average value of a_2 can be used in evaluating these quantities. Equation (6) can then be written

$$\lambda' + 2\lambda\left[\frac{\rho_1'}{\rho} - \frac{u_1'}{u_1}\left(2 - \frac{F_1}{F_2}\right) - \frac{1}{\gamma F_1 M_1^2}\frac{p_1'}{p_1}\left(F_4 - 0{\cdot}2\frac{T_0}{T_1}\right)\right] = \frac{4}{F_1}\frac{u_\infty}{u_1}\frac{\rho_\infty}{\rho_1}\frac{T_1}{T_\infty}. \tag{10}$$

Equation (10) is now a linear differential equation of the first order which may be integrated. In terms of the quantity $G = p_{0_1}/p_{0_\infty}$, which is a measure of the stagnation pressure at the edge of the boundary layer, equation (10) gives

$$\lambda = \frac{4}{F_1}\left[\int_0^\zeta \left(\frac{1}{G}\left(\frac{u_1}{u_\infty}\right)^a \left(\frac{T_1}{T_\infty}\right)^b G^c e^{-d}\right) d\zeta\right] \div \left[\left(\frac{u_1}{u_\infty}\right)^{a+1}\left(\frac{T_1}{T_\infty}\right)^{b-1+1/(\gamma-1)} G^c e^{-d}\right],$$

where

$$a = 3 + \frac{2}{F_1}(0{\cdot}08571 + 0{\cdot}01905a_2), \quad b = \frac{\gamma}{\gamma - 1} - \frac{K - \frac{1}{5}}{F_1},$$

$$c = 2 - \frac{\gamma - 1}{\gamma F_1}(K - \tfrac{1}{5}), \qquad d = \int_0^G \frac{1}{\gamma F_1 M_1^2}\frac{dG}{G}.$$

This equation can be used now to calculate the growth of the boundary layer along an adiabatic wall once p_1, U_1, T_1, M_1 and G are known as a function of ζ.

Inviscid solution

In order to find the inviscid solution, it is necessary to be able to solve the problem of flow behind a detached shock wave. While this problem has received considerable attention, an adequate solution is not available. We are most interested in the flow well downstream from the leading edge, a case treated by Lees & Kubota (1956) and Chang & Pallone (1956). While these studies give results in general agreement with experimental observations, they were found not to be sufficiently accurate, and it was necessary to use empirical results to provide the required information. The pressure field behind the leading edge is affected by expansion waves from the corner which are reflected back into the body either from the sonic line, the entropy discontinuities, or the shock wave, as shown in figure 3. This pressure field can be determined from the experiments with relatively thick leading edges and used as a first approximation for the field at lower Re_l. Data are available for Re_l up to 60×10^3.

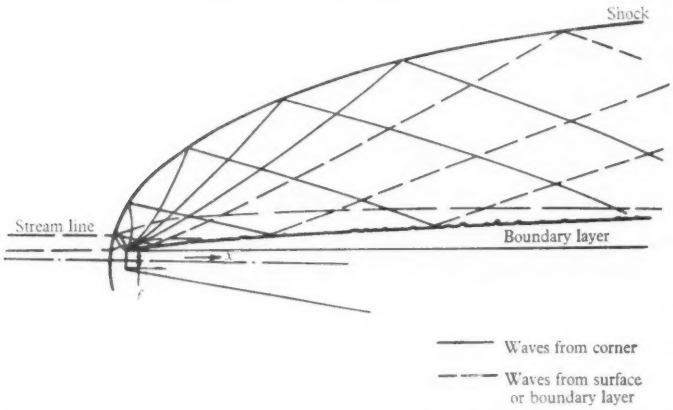

FIGURE 3. Theoretical model illustrating the effect of boundary-layer growth on flow field.

The change in pressure distribution on the plate caused by the boundary layer may be calculated by considering the change in pressure produced by a body of slightly altered contour. If this change is small compared with the value for the unaltered shape, a linearized approximation can be used. For a first approximation, it will be assumed that the boundary condition to be imposed on the inviscid flow is that, on the surface of the plate, the flow deflexion angle is equal to the slope of the effective body shape. The isentropic pressure-angle relation will be used. If this is written in the form of a series,

$$\frac{\Delta p}{p_{\mathrm{in}}} = \frac{\gamma M_1^2}{(M_1^2-1)^{\frac{1}{2}}}\,\theta + \frac{\gamma(\gamma+1)\,M_1^6 - \gamma M_1^2(M_1^2-1)}{4(M_1^2-1)^2}\,\theta^2, \tag{12}$$

only the first term need be used when θ is small. The assumption that $M_1 \gg 1$ is not correct over some parts of the body, even for $M_\infty \gg 1$, so the hypersonic approximation to this relation should not be used.

The question of how an effective body contour can be found from the boundary-layer calculation must be considered. The displacement thickness is essentially a concept which satisfies the continuity relations. When waves reflect from a solid boundary with a boundary layer, the mechanism is not the same as for reflexion from a solid boundary without a boundary layer located at a distance of the displacement thickness from the actual boundary. Since no exact solution to this problem is available, and the disturbances are small, the assumption that the displacement thickness contour represents an effective body contour can be used as first approximation.

4. Calculation

Detailed calculations of the effect of the Reynolds number on the pressure distribution on a blunted flat plate have been made at $M = 11{\cdot}4$ for $\gamma = \frac{5}{3}$, since experimental results were available for this case. The pressure distribution and

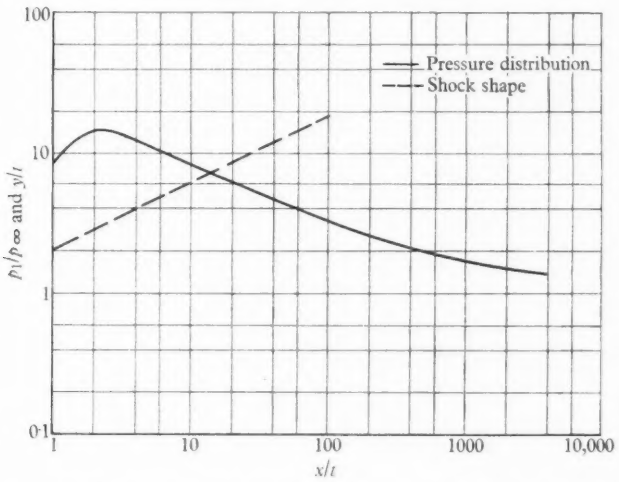

FIGURE 4. Inviscid pressure distribution and shock shape based on experiments at high Re_t; $M = 11{\cdot}4$.

shock shape shown in figure 4 are taken from the experimental results for the high Reynolds number case. The first step in the analysis is to calculate the growth of the boundary layer in this pressure field. For the initial calculation, the entropy on the outside of the boundary layer will be assumed to be that behind a normal shock. With the assumption for the P_1 against x/t relation given in figure 4, λ can be evaluated as a function of x/t by equation (11). Also δ^*/δ_S is a function of the shape of the boundary-layer profile and can be found by integrating the velocity-density distribution:

$$\frac{\delta^*}{\delta_S} = \frac{2}{7} + \frac{\frac{1}{2}(\gamma-1)\,M_\infty^2(u_1/u_\infty)^2}{1+\frac{1}{2}(\gamma-1)\,M_\infty^2\,(1-u_1^2/u_\infty^2)}\,(0{\cdot}3950 + 0{\cdot}02116a_2 - 0{\cdot}000622a_2^2) + \tfrac{2}{105}\,a_2. \tag{13}$$

Therefore, from the definition of λ,

$$\frac{\delta^*}{t}(\mathrm{Re}_t)^{\frac{1}{2}} = \frac{\delta^*}{\delta_S}(\lambda C)^{\frac{1}{2}}, \tag{14}$$

where λ and δ^*/δ_S are both functions of x/t. This relation is shown as a function of x/t in figure 5. The pressure distribution caused by the effective viscous distortion of the body can be found by setting the slope of the displacement thickness curve equal to θ in the first term of equation (12). If this is done, there follows

$$\frac{\Delta p}{p_{\mathrm{in}}} = \frac{\gamma M_1^2}{(M_1^2-1)^{\frac{1}{2}}}\frac{d\delta^*}{dx} = \frac{\gamma M_1^2}{(M_1^2-1)^{\frac{1}{2}}}\frac{Z}{(\mathrm{Re}_t)^{\frac{1}{2}}}, \quad Z = \frac{d}{d(x/t)}\left[\frac{\delta^*}{\delta_S}(\lambda C)^{\frac{1}{2}}\right], \tag{15}$$

where Z is a function only of x/t. The quantity $\Delta p(\mathrm{Re}_t)^{\frac{1}{2}}/p_{\mathrm{in}}$ is shown plotted as a function of x/t in figure 6.

The static pressure on the flat plate can be written

$$\frac{p}{p_\infty} = \frac{p_{\mathrm{in}}}{p_\infty}\left(1+\frac{\Delta p}{p_{\mathrm{in}}}\right).$$

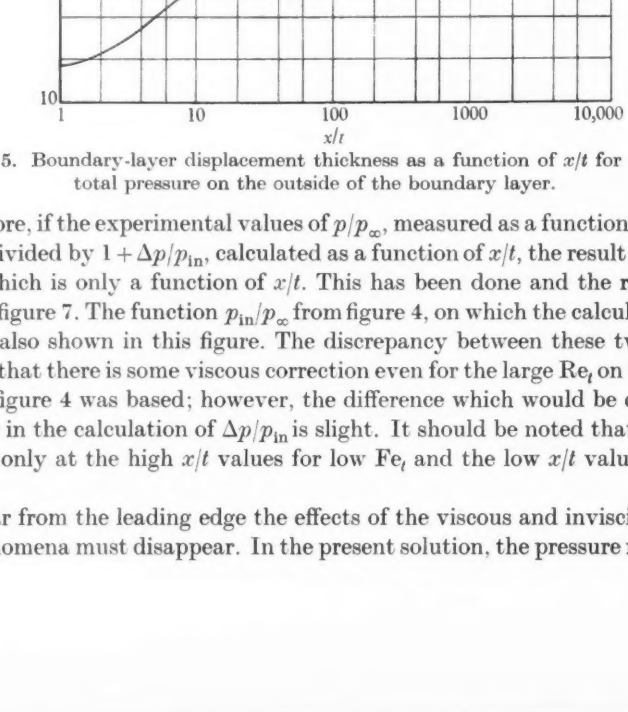

FIGURE 5. Boundary-layer displacement thickness as a function of x/t for constant total pressure on the outside of the boundary layer.

Therefore, if the experimental values of p/p_∞, measured as a function of x/t and Re_t, are divided by $1+\Delta p/p_{\mathrm{in}}$, calculated as a function of x/t, the result should be p_{in}/p_∞, which is only a function of x/t. This has been done and the results are shown in figure 7. The function p_{in}/p_∞ from figure 4, on which the calculation was based, is also shown in this figure. The discrepancy between these two curves indicates that there is some viscous correction even for the large Re_t on which the curve of figure 4 was based; however, the difference which would be caused by this error in the calculation of $\Delta p/p_{\mathrm{in}}$ is slight. It should be noted that data are available only at the high x/t values for low Fe_t and the low x/t values are for high Re_t.

Very far from the leading edge the effects of the viscous and inviscid leading edge phenomena must disappear. In the present solution, the pressure returns to

free stream value but the Mach number and entropy at the edge of the layer do not. This result is incorrect especially at high x/t. The entropy can be found for any Re_t by considering the mass in the boundary layer and tracing the stream line back to the point where it crossed the shock wave. The entropy at the outside of the boundary layer will be a function of both x/t and Re_t, so a new calculation

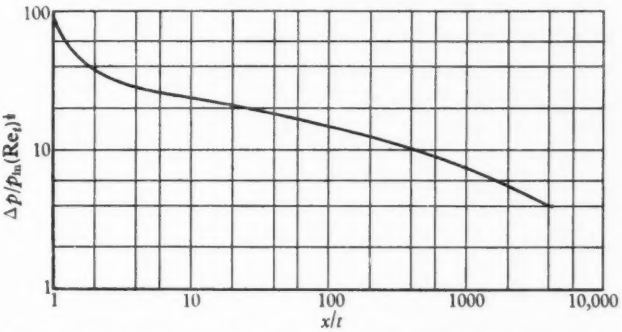

FIGURE 6. Pressure increment caused by boundary-layer displacement thickness as a function of x/t for constant total pressure on the outside of the boundary layer

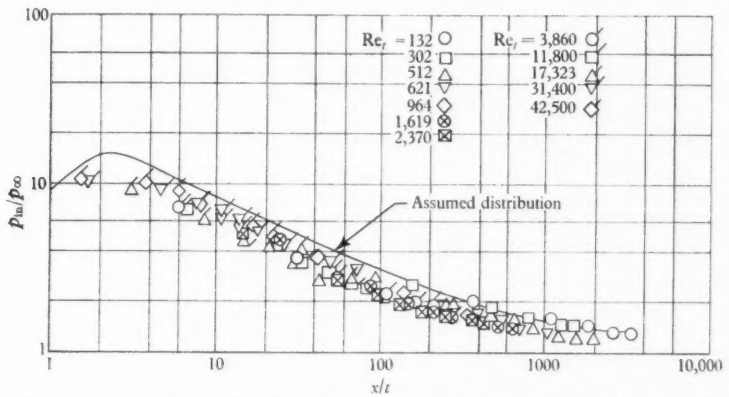

FIGURE 7. Inviscid pressure distribution as a function of x/t calculated by dividing the measured pressure distributions by the calculated viscous correction for constant total head on the outside of the boundary layer.

must be made for each value of Re_t. Such calculations have been made for $\mathrm{Re}_t = 132$ and 2370. The shock shape given in figure 4 is used for these calculations. As has been previously pointed out, the shock shape in the region of the leading edge is practically independent of Re_t. Once $G(x/t, \mathrm{Re}_t)$ is established, equation (11) may be evaluated and a new λ determined. It should be noted that the change in G will also change the value of u_1, T, δ^* and $\Delta p/p_1$. A new curve of p_{in}/p_{∞} may then be plotted, based on the consideration of variable G along the edge of the boundary layer. This result is shown in figure 8. The points for low Re_t are changes from the constant G results, and correlate better with the points at higher Re_t. Since the experimental results at the same x/t and over the full

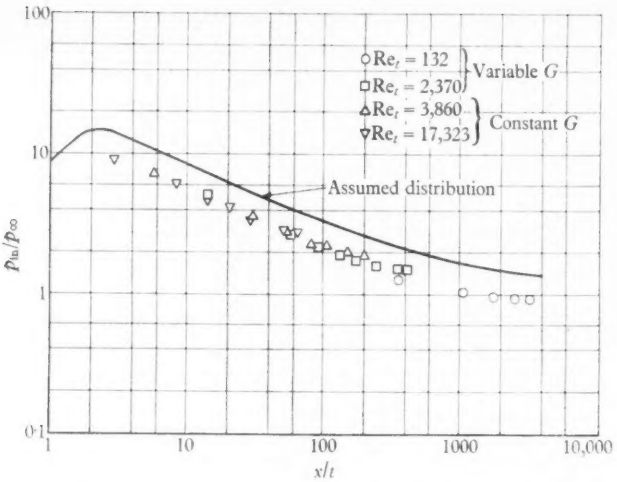

FIGURE 8. Inviscid pressure distribution as a function of x/t, calculated by dividing the measured pressure distributions by the calculated viscous correction for the corrected values of total head on the outside of the boundary layer.

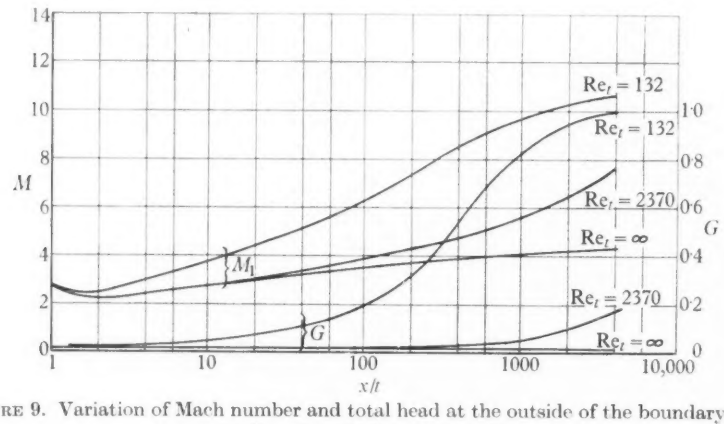

FIGURE 9. Variation of Mach number and total head at the outside of the boundary layer as a function of x/t at various Re_t.

Re_t range are not available, it is hard to make a good comparison. The value of G and M_1 for the various Re_t are shown in figure 9. G and M_1 do approach the free stream values at high x/t and low Re_t as expected. If more accurate results are required, these may be obtained by using the values of pressure and entropy found by the first calculation, to recalculate the whole system.

Correlation with previous work

Lees & Probstein (1952) investigated the viscous part of this problem without recognizing the important inviscid effect of the leading edge. Since the inviscid effect becomes unimportant at high x/t and low Re_t, their work should be a special

case of the present solution. For $G = 1$ and $p_{in}/p_\infty = 1$, the present solution gives

$$\delta^*/x = 1{\cdot}21(\gamma - 1)\, M_\infty^2\, (C/\mathrm{Re}_x)^{\frac{1}{2}}$$

for the growth of the boundary layer. Lees & Probstein obtained a result similar in all respects to this except that the numerical coefficient 1·21 is replaced by 1·197. This slight difference is caused by the different techniques used in solving the boundary-layer equations. The experiments reported by Kendall (1957) agree with the present theory if $p_{in}/p_\infty = 1$ and $G = 1$. These assumptions are probably correct for the case of low M and Re_t, since the x/t parameter is not necessary to correlate the results of this experiment. The present theory provides a means of correlating the results of Kendall (1957) made in a hot-air tunnel at a Mach number of about 6 and those obtained in the Princeton helium tunnel at Mach numbers between 11 and 15.

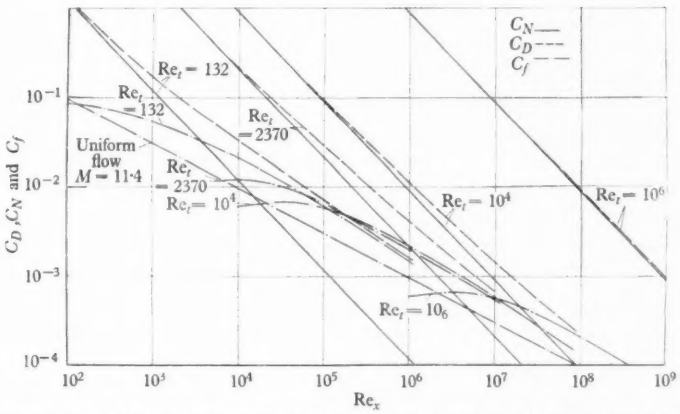

FIGURE 10. Friction drag, nose drag, and total drag for a blunted flat plate at various Re_t; $M = 11{\cdot}4$.

Skin friction and Drag

Since the present solution is for the adiabatic case, no direct information of heat transfer can be obtained, but the friction and drag forces may be calculated. The average skin friction parameter has been calculated on the basis of the boundary layer solutions found in this analysis. The results are presented in figure 10 as a function of Re_t and Re_x. The results for $\mathrm{Re}_t = 132$ and $\mathrm{Re}_t = 2370$ are for the solution which takes into account the variation of G with x/t. The curves for $\mathrm{Re}_t = 10^4$ and 10^6 are for the solution with constant G, since G shows very little variation at these Reynolds numbers over the x/t range of this figure. It is interesting to note that the curves for the various Re_t form an envelope and give fairly uniform values as a function of Re_x over most of the range. The values of C_f calculated by conventional boundary-layer theory (Van Driest 1952), leaving out the change of inviscid flow conditions caused by both the leading edge and the boundary layer, are also shown. The present results give skin friction values of the order of twice the results of conventional theory.

In addition to the friction drag, there is the pressure drag on the nose of the plate. Since the details of the nose affect the flow about the whole body, it is not

reasonable to consider just the skin friction term. The pressure drag is also presented in figure 10. For the low Re_t case ($\mathrm{Re}_t = 132$), the nose drag is smaller than the skin friction drag for $\mathrm{Re}_x > 4 \times 10^3$. For high Re_t, the nose drag predominates up to Re_x of the order of 10^7. The drag coefficients are only for one side of the plate and the pressure drag on one half the blunt nose. The full drag would be twice these values for a symmetrical body. The total drags are also shown on this figure as the sum of the pressure and friction drags.

5. Discussion

These calculations show that by including the effect of the finite thickness of the leading edge, it is possible to derive a theory which accounts for the observed Reynolds number effects found for hypersonic flow about flat plates. Even down to very thin leading edges, the flat plate does not approach the infinitely thin flat plate. The flow conditions are shown to depend on the distance from the leading edge in terms of leading-edge thickness and the Reynolds number.

Some previous theoretical work had treated a strong interaction region where the pressure changes caused by the viscous forces are much larger than the inviscid pressures. If the effects of finite leading-edge thickness are considered, there need be no such region. The present method can be used over the entire body. The inclusion of the stagnation point flow, which must occur in any real case, allows a boundary layer with a finite initial rate of growth which need not cause large pressure changes. The strong interaction region only occurs at low values of Re_t where the growth of the boundary layer is rapid. An understanding of this flow picture eliminates many of the difficulties in treating the nose region which were encountered in the previous work.

The present analysis is a rough calculation designed to show the effects of the various significant parameters. Unfortunately, it was necessary to use numerical techniques to solve the boundary layer equations; however, an analytic solution cannot be expected until it is possible to solve the inviscid blunt-nosed problem so that the viscous solution need not be based on empirical results. The results presented are for the restricted case of $M = 11{\cdot}4$ and $\gamma = \frac{5}{3}$. These values were chosen to match the available data. Calculations over the full range of Mach and Reynolds numbers have not been attempted. This technique can be used to calculate the viscous effect for any case in which the inviscid solution is known and the viscous correction can be considered a perturbation on the inviscid solution. The method can be applied to any two-dimensional plane or axially symmetric body once the basic inviscid pressure distribution is known. For plane two-dimensional bodies, the only change would be in the basic inviscid pressure distribution. For axially symmetric bodies, the boundary-layer solution would be modified to include the effect of the change of radius.

6. Conclusions

1. The Reynolds number effects on the pressure distribution and flow parameters about a body in hypersonic flow can be predicted by conventional boundary-layer theory once the inviscid flow is known.

2. There is no conceptual difficulty in analysing the flow near the leading edge if the real case of a finite leading edge is considered.

3. The skin friction on the surface of a flat plate is of the order of twice the skin friction calculated by conventional flat plate boundary-layer theory. The skin friction is relatively independent of Re_l, but the total drag increases rapidly with Re_l.

The present study is part of a programme of theoretical and experimental research on hypersonic flow being conducted by the Gas Dynamics Laboratory, James Forrestal Research Center, Princeton University, Wright Air Development Center of the United States Air Force, under Contract No. AF 33(616)–2547, with Fred L. Daum as project engineer.

REFERENCES

BECKER, J. V. 1950 Results in recent hypersonic and unsteady flow research at the Langley Aeronautical Laboratory. *J. Appl. Phys.* **21**, 622.

BERTRAM, M. H. 1952 An approximate method of determining the displacement effects and viscous drag of laminar boundary layers in two-dimensional hypersonic flow. *Nat. Adv. Comm. Aero., Wash., Tech. Note*, no. 2773.

BERTRAM, M. H. 1954 Viscous and leading edge thickness effects on the pressures on the surface of a flat plate in hypersonic flows. *J. Aero. Sci.* **21**, 430.

BOGDONOFF, S. M. & HAMMITT, A. G. 1954 The Princeton helium hypersonic tunnel and preliminary results above $M = 11$. *Princeton University Aero. Eng. Rep.* no. 260. (Also published as *WADC TR* 54–124.)

BOGDONOFF, S. M. & HAMMITT, A. G. 1956 Fluid dynamic effects at speeds from $M = 11$ to 15. *J. Aero. Sci.* **23**, 108.

CHANG, H. K. & PALLONE, A. J. 1956 Inviscid leading edge effect in hypersonic flow. *J. Aero. Sci.* **23**, 700.

HAMMITT, A. G. & BOGDONOFF, S. M. 1956 Hypersonic studies of the leading edge effect on the flow over a flat plate. *J. Amer. Rocket Soc.* **26**, 241.

HAMMITT, A. G., VAS, I. E. & BOGDONOFF, S. M. 1956 Leading edge effects on the flow over a flat plate at hypersonic speeds. *Princeton University Aero. Eng. Rep.* no. 326. (Also published as *WADC TN* 55–537.)

KENDALL, J. M. 1957 An experimental investigation of leading edge shock wave boundary layer interaction at $M = 5{\cdot}8$. *J. Aero. Sci.* **24**, 47.

KUO, Y. H. 1953 On the flow of an incompressible viscous fluid past a flat plate at moderate Reynolds numbers. *J. Math. Phys.* **32**, 83.

LEES, L. 1952 On the boundary layer equations in hypersonic flow and their approximate solutions. *Princeton University Aero. Eng. Rep.* no. 212.

LEES, L. 1954*a* Hypersonic viscous flow over an inclined wedge. *J. Aero. Sci.* **20**, 794.

LEES, L. 1954*b* Hypersonic influence of the leading edge shock wave on the laminar boundary-layer at hypersonic speeds, *GALCIT TR*, no. 1.

LEES, L. & KUBOTA, T. 1956 Inviscid hypersonic flow over blunt-nosed slender bodies. *J. Aero. Sci.* **123**, 195.

LEES, L. & PROBSTEIN, R. F. 1952 Hypersonic viscous flow over a flat plate. *Princeton University Aero. Eng. Rep.* no. 195.

LI, TING-YI & NAGAMATSU, H. 1953 Shock wave effects on the laminar skin friction of an insulated flat plate at hypersonic speeds. *J. Aero. Sci.* **20**, 345.

LI, TING-YI & NAGAMATSU, H. 1955 Hypersonic viscous flow on a non-insulated flat plate. *GALCIT Report*, no. 25.

Morduchow, M. & Clarke, Joseph H. 1952 Method for calculation of compressible laminar boundary-layer characteristics in axial pressure gradient with zero heat transfer. *Nat. Adv. Comm. Aero., Wash., Tech. Note*, no. 2784.

Pai, Shih-I 1953 On strong interaction for the hypersonic boundary layer on inclined wedge. *J. Aero. Sci.* **20**, 796.

Shen, S. F. 1952 An estimate of viscosity effect in hypersonic flow over an insulated wedge. *J. Math. Phys.* **31**, 192.

Van Driest, E. F. 1952 Investigation of laminar boundary layer in compressible fluids using the Croco method. *Nat. Adv. Comm. Aero., Wash., Tech. Note*, no. 2597.

Vas, I. E. 1957 An experimental investigation of the pressure on a thin flat plate at hypersonic speeds. *Princeton University Aero. Eng. Rep.* no. 377. (Also published as *WADC TN* 57-104.)

Theory of thin airfoils in fluids of high electrical conductivity

By W. R. SEARS AND E. L. RESLER
College of Engineering, Cornell University, Ithaca, N.Y.

(Received 21 July 1958)

Steady, plane flow of incompressible fluid past thin cylindrical obstacles is treated with two different orientations of the undisturbed, uniform magnetic field; namely, parallel and perpendicular, respectively, to the undisturbed, uniform stream. In the first case, the flow of an infinitely conducting fluid is shown to be irrotational and current-free except for surface currents at the walls of the obstacles. With large but finite conductivity the surface currents are replaced by thin boundary layers of large current density.

In the second case, for infinite conductivity the flow field is made up of an irrotational current-free part and a system of waves involving currents and vorticity extending out from the body. For large, finite conductivity these waves attenuate exponentially with distance from the body.

In both cases the forces on sinusoidal walls and on airfoils are calculated. In the second case positive drag occurs.

Introduction

In this paper we study the steady flow past thin cylindrical bodies of an incompressible fluid of high electrical conductivity. In particular, the approximation of infinite conductivity will be adopted for the most part. Although this approximation is not believed to be appropriate for most problems in the field called 'magneto-aerodynamics' (see, Resler & Sears 1958), it should be appropriate in other situations which involve greater 'magnetic Reynolds numbers'. Such situations may include flows involving high gas temperatures, or flows of liquid metals. Our results will also be of some interest in illustrating phenomena that occur when the fields induced by the motion are large, as contrasted with the typical aeronautical cases where these induced fields are often negligible.

We are concerned solely with the domain where the fluid may be considered a continuum and where the flow of electricity may be described by Ohm's Law. Other simplifications are made in writing the pertinent equations of motion in the next section.

The basic equations

Steady flow of an inviscid fluid of constant density ρ and conductivity σ is described by the following equations:

continuity, $$\operatorname{div} \mathbf{q} = 0; \tag{1}$$

momentum,
$$\mathbf{q}.\nabla\mathbf{q}+\frac{1}{\rho}\nabla p=\frac{1}{\rho}\mathbf{j}\times\mathbf{H}; \tag{2}$$

Ohm's Law,
$$\mathbf{j}=\sigma(\mathbf{E}+\mathbf{q}\times\mathbf{H}); \tag{3}$$

and Maxwell's equations,
$$4\pi\mathbf{j}=\operatorname{curl}\mathbf{H}; \tag{4}$$
$$\operatorname{curl}\mathbf{E}=0; \tag{5}$$
$$\operatorname{div}\mathbf{H}=0; \tag{6}$$

where $\mathbf{q}$ denotes the fluid velocity, p the pressure, $\mathbf{j}$ the current density, $\mathbf{H}$ the magnetic field vector, and $\mathbf{E}$ the electric field vector. We are employing electromagnetic units, so that the permeability of empty space is 1, and we assume that the fluid has the same permeability. In equation (3) we neglect the current component that arises from the flow of charged fluid particles, because this term can be shown to be small, compared to the terms retained, in the type of flow considered here. In equation (4) we neglect 'displacement currents' for the same reason.

By substitution for $\mathbf{j}$ from equation (4) into equation (2), the momentum equation becomes

$$\mathbf{q}.\nabla\mathbf{q}+\frac{1}{\rho}\nabla p=\frac{1}{4\pi\rho}\{\mathbf{H}.\nabla\mathbf{H}-\tfrac{1}{2}\nabla H^2\}. \tag{7}$$

Similarly, both $\mathbf{j}$ and $\mathbf{E}$ can be eliminated from Ohm's Law by means of equations (4) and (5). The result, after some straight-forward vector calculus and use of equations (1), (5) and (6), is

$$-\operatorname{curl}(\mathbf{q}\times\mathbf{H})=\mathbf{q}.\nabla\mathbf{H}-\mathbf{H}.\nabla\mathbf{q}=\frac{1}{4\pi\sigma}\nabla^2\mathbf{H}. \tag{8}$$

The problem is now reduced to the simultaneous solution for given boundary conditions of equations (7) and (8) for $\mathbf{q}$, $\mathbf{H}$ and p, subject to the conditions $\operatorname{div}\mathbf{q}=0=\operatorname{div}\mathbf{H}$.

Small-perturbation flow: Case I

Consider now the case of plane, steady flow in which the stream velocity and the magnetic field are uniform and parallel except for small disturbances; i.e. we suppose

$$\mathbf{q}=(U+u,v,0), \quad \text{where} \quad u,v\ll U, \tag{9}$$

and
$$\mathbf{H}=(H_0+h_x,h_y,0), \quad \text{where} \quad h_x,h_y\ll H_0 \tag{10}$$

We assume now that the ratios of perturbations to free-stream values are of the same order for both the velocity field and the magnetic field, and this will be shown later to be correct, at least for fluids of high conductivity.

To first order, then, the equation of momentum, equation (7), becomes

$$U\frac{\partial\mathbf{v}}{\partial x}+\frac{1}{\rho}\nabla p=\frac{1}{4\pi\rho}\left(H_0\frac{\partial\mathbf{h}}{\partial x}-H_0\nabla h_x\right), \tag{11}$$

where $\mathbf{v}$ denotes the vector (u,v) and $\mathbf{h}$ the vector (h_x,h_y). The x-component equation in equation (11) can be integrated immediately, yielding

$$\rho Uu+p=p_\infty, \tag{12}$$

where p_∞ denotes the undisturbed static pressure.

The y-component equation, upon substitution of $-\rho U(\partial u/\partial y)$ for $\partial p/\partial y$, becomes

$$\Omega = \frac{H_0}{4\pi\rho U}\xi, \tag{13}$$

where Ω and ξ are respectively the curls of the vectors $\mathbf{q}$ and $\mathbf{H}$; i.e.

$$\Omega \equiv \frac{\partial v}{\partial x} - \frac{\partial u}{\partial y}, \tag{14}$$

$$\xi \equiv \frac{\partial h_y}{\partial x} - \frac{\partial h_x}{\partial y} = 4\pi j_z, \tag{15}$$

where j_z is the z-component of current density.

Similarly, equation (8) becomes

$$U\frac{\partial \mathbf{h}}{\partial x} - H_0\frac{\partial \mathbf{v}}{\partial x} = \frac{1}{4\pi\sigma}\nabla^2\mathbf{h}. \tag{16}$$

Infinite conductivity

For fluids of very large electrical conductivity, neglect the right-hand side of equation (16). This equation is then integrable and becomes

$$\frac{\mathbf{h}}{H_0} - \frac{\mathbf{v}}{U} = \text{function of } y = 0, \tag{17}$$

where it is assumed that the function of y is evaluated at large y where the stream and magnetic field are undisturbed.

This relation states that the velocity and magnetic fields are distorted in exactly the same way; the streamlines and magnetic lines of force are always parallel. This is, of course, a result of the infinite-conductivity approximation. It is not, in fact, restricted to the small-perturbation case, as will now be shown. For $\sigma \to \infty$, equation (8) becomes

$$\text{curl}\,(\mathbf{q}\times\mathbf{H}) = 0. \tag{18}$$

But in plane flow, since $\mathbf{q}\times\mathbf{H}$ has only a z-component, equation (18) requires that

$$\mathbf{q}\times\mathbf{H} = \text{constant} \tag{19}$$

Thus if this vector product vanishes anywhere, as it does in the undisturbed part of the flow in the present problem, it must vanish everywhere, and the streamlines and magnetic lines must be parallel to one another.

Returning now to the small-perturbation case, we see, in view of equation (17), that the vorticity Ω is proportional to the current density, so that equation (13) becomes

$$\Omega = \frac{H_0^2}{4\pi\rho U^2}\Omega. \tag{20}$$

Thus, except for the particular case where the stream speed U is equal to the 'Alfvén velocity' $\mathbf{H}_0/\sqrt{(4\pi\rho)}$, we conclude that the flow is irrotational and that the current-density j_z is zero to first order. In the special case the disturbance

produced by the body is propagated in the form of an Alfvén wave, relative to the undisturbed stream, at just the speed of the body. Hence, the body moves in a 'cavity' of its own shape, and exerts no force on the fluid.

At all other stream speeds the flow field about the body is just the same as in a non-conducting fluid, and is determined by the boundary conditions and the required cyclic constants (circulations). We therefore carry over to this field all the familiar solutions of plane, small-perturbation, irrotational, incompressible flow, such as are provided by thin-airfoil theory.

There are, however, important modifications to the force on the body surface, since there are, in general, *surface currents* at such an interface. These are sheets of infinite current density, which allow the solution formed above (equation (17)) to exist and the required boundary conditions at the body surface to be satisfied. We shall illustrate this effect by means of three examples.

(1) *Infinite sinusoidal wall (insulator)*

Let the contour of an insulating wall be defined by $y = \epsilon \cos \lambda x$ where $\epsilon \ll \lambda^{-1}$. For brevity we can adopt the familiar complex notation, real parts being implied everywhere, and write $y = \epsilon e^{i\lambda x}$. The first-order solution for the flow problem is well known:

$$v = iU\epsilon\lambda\, e^{i\lambda(x+iy)} = iu. \tag{21}$$

Thus, the perturbation of the magnetic field is given by

$$h_y = iH_0\epsilon\lambda\, e^{i\lambda(x+iy)} = ih_x. \tag{22}$$

The surface current, in the z-direction, is given by equation (4) in the form

$$4\pi J_s = -h_x(x, +0) + h_x(x, -0), \tag{23}$$

where J_s denotes the current per unit length, flowing in the z-direction, and the values assumed at the interface between fluid and wall have been replaced approximately by the values at $y = \pm 0$ in the usual way. We have determined $h_x(x, +0)$ in equation (22).

Within the insulator there can be no currents, so again the magnetic field must be curl-free. The boundary condition at the interface is provided by the requirement of continuous h_y; hence $h_y(x, -0)$ is given by equation (22). The disturbance must vanish as $y \to -\infty$. The solution, for $y < 0$, is

$$h_y = iH_0\epsilon\lambda\, e^{i\lambda(x-iy)} = -ih_x. \tag{24}$$

The surface current, according to equation (23), is therefore given by

$$4\pi J_s = -2H_0\epsilon\lambda\, e^{i\lambda x}. \tag{25}$$

According to equation (12), the pressure distribution throughout the fluid is the same as in the analogous flow of a non-conductor. The force exerted on the wall, however, is given by the difference between the local static pressure and the force, $H_0 J_s$ per unit area, arising from the surface current. Let this net pressure be denoted by $p_n(x)$; then, to first order,

$$\begin{aligned} p_n(x) &= p(x, +0) - H_0 J_s \qquad (26)\\ &= p_\infty - \rho U u(x, +0) + (H_0^2/2\pi)\,\epsilon\lambda\, e^{i\lambda x}\\ &= p_\infty - \rho U^2 \epsilon\lambda\, e^{i\lambda x} + (H_0^2/2\pi)\,\epsilon\lambda\, e^{i\lambda x}\\ &= p_\infty - \rho U^2 \epsilon\lambda\, e^{i\lambda x}\{1 - 2m^{-2}\}. \qquad (27) \end{aligned}$$

where m denotes the ratio of the stream speed U to the Alfvén velocity,

$$m \equiv \frac{U}{H_0/\sqrt{(4\pi\rho)}}.$$

Thus, the amplitude of the net pressure disturbance on the wall is reduced by the magneto-hydrodynamic effect as compared to the usual result. This pressure disturbance vanishes at a flow speed $\sqrt{2}$ times as great as the Alfvén velocity, and is opposite in sign for greater field strengths H_0.

In these results, the singular case mentioned above for a stream flowing at the Alfvén velocity does not appear, of course, since it involves rotational flow and electric-current flow in the fluid in the z-direction. Presumably, it could only be set up by means of carefully controlled initial conditions.

(2) *Lifting airfoil without thickness*

The classical irrotational small-perturbation flow past a body of this category may be represented by a vortex sheet which produces a discontinuous velocity component u and continuous v. According to equation (17), the discontinuity of u is proportional to the discontinuity of h_x at the same location on the airfoil; the latter determines the surface current as in equation (23). Thus the net force distribution (lift loading) on the airfoil is given by

$$l_n(x) = -\rho U\{u(x,-0)-u(x,+0)\}+(H_0/4\pi)\{h_x(x,-0)-h_x(x,+0)\} \tag{28}$$

$$= 2u(x,+0)\{\rho U - H_0^2/(4\pi U)\} = 2\rho U u(x,+0)\{1-m^{-2}\}. \tag{29}$$

The coefficients of lift and moment become, therefore,

$$c_l = c_{l_0}\{1-m^{-2}\} \quad \text{and} \quad c_m = c_{m_0}\{1-m^{-2}\}, \tag{30}$$

where c_{l_0} and c_{m_0} are the analogous coefficients for the same airfoil in a non-conducting fluid.

It is interesting to notice that, in the approximation of infinite conductivity, it is immaterial whether the airfoil itself is a conductor or insulator. In either case the current is the same, being determined solely by the discontinuity of h_x.

The total current flowing in the z-direction is proportional to the total circulation Γ:

$$(J_s)_{\text{total}} = \frac{H_0}{4\pi U}\Gamma. \tag{31}$$

(3) *Symmetrical airfoil with thickness (insulator)*

The flow about a body of this category is represented by a source-sink distribution, which produces discontinuous v and continuous u. The distortion of the magnetic field is such that the lines of force follow the streamlines around the body. Such a field can be constructed by imagining that magnetic sources and sinks are distributed along the axis. There is no net current at the body and the total force on the cylinder is zero.

However, to determine the pressure distribution on the surface one must give up the magnetic-source-sink approximation and consider the magnetic field within the body; again the resulting discontinuity of h_x involves a surface current.

But the magnetic field within the body is extremely simple, for the streamline pattern has been constructed to satisfy the condition of vanishing velocity component normal to the surface. Thus the magnetic field satisfies the same condition: vanishing normal component. But, if the body is an insulator, the magnetic field is harmonically distributed inside, and the field strength is zero. The 'convection' of magnetic lines by the flow therefore involves very large forces at the body surface, for the surface current is of zero-th, rather than first, order; namely, the surface current is, on the upper surface of the body

$$J_s = -\frac{1}{4\pi}(H_0 + h_x)$$

$$= -\frac{H_0}{4\pi}\left(1 + \frac{u}{U}\right). \tag{32}$$

It will be seen that equation (32) predicts a zero-order surface current even for vanishing U. This is, of course, a consequence of the approximations of our theory, since we have essentially required the streamlines to be distorted around the body even at vanishing stream speed. It does seem qualitatively correct that, even at very small stream speeds in a fluid of great conductivity, the magnetic field must be parted by the body and that large forces must result. The force cannot be calculated by our approximate, first-order formula (26), in view of the large perturbation of the magnetic field; it is of order H_0^2.

Since the conclusion $\mathbf{q} \times \mathbf{H} = 0$ is not limited to small-perturbation flow (equation (19)), it seems clear that the vanishing of the interior field is not a consequence of the small-perturbation approximation but only of the assumptions of infinite conductivity and plane, steady flow.

Finite conductivity

If σ is large but finite, the right-hand side of equation (8) is small, and this equation may be attacked by a 'boundary-layer' approximation. We shall postpone a general treatment to a subsequent paper and consider here only the corresponding small-perturbation case, i.e. equation (16), which also takes on a boundary-layer character for large σ, but has the virtue of being linear.

We first operate on equation (16) with the curl and then substitute for Ω by means of equation (13). The result is

$$\nabla^2 \xi - \kappa \frac{\partial \xi}{\partial x} = 0, \tag{33}$$

where

$$\kappa \equiv 4\pi\sigma U(1 - m^{-2}). \tag{34}$$

The usual boundary-layer arguments show that, as $\kappa \to \infty$, the appropriate approximation to equation (33) within a boundary layer of thickness $O(\kappa^{-\frac{1}{2}})$ is

$$\frac{\partial^2 \xi}{\partial y^2} - \kappa \frac{\partial \xi}{\partial x} = 0. \tag{35}$$

More precisely, the approximation applies for large 'magnetic Reynolds numbers' $R_m = UL\sigma$, where L is the characteristic body dimension, and applies in a layer of thickness $O(LR_m^{-\frac{1}{2}})$, provided that m^2 is not close to 1. The analogy with the

familiar viscous boundary layer is quite complete, except, of course, that linearization is usually not appropriate for such layers. At the outside edge of the magnetic boundary layer, equation (33) goes over into $\partial\xi/\partial x = 0$, which represents our irrotational, current-free flow field.

The magnetic boundary layer therefore serves to eliminate surface-current sheets, replacing them by boundary layers of large current density, just as a viscous boundary layer can be thought of as replacing a vortex sheet.

In the magnetic boundary layer the approximate expression for ξ is $-\partial h_x/\partial y$; thus equation (35) can be integrated once to yield

$$\frac{\partial^2 h_x}{\partial y^2} - \kappa \frac{\partial h_x}{\partial x} = F(x), \tag{36}$$

where $F(x)$ is recognized as the value of $-\kappa\,\partial h_x/\partial x$ at the edge of the layer, i.e. in the potential flow.

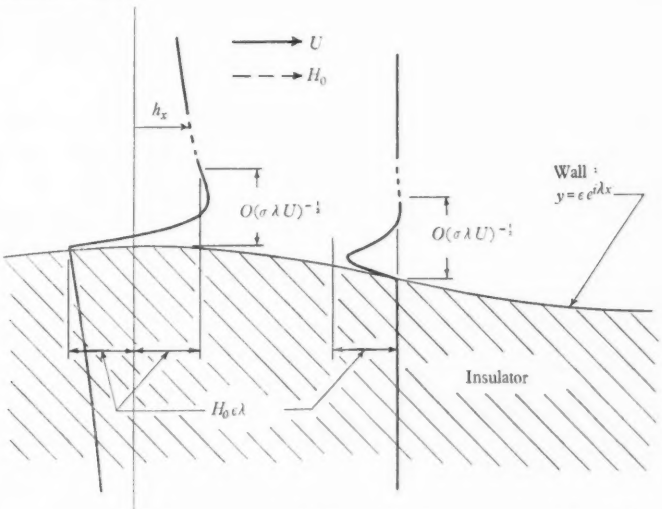

FIGURE 1. Distribution of the magnetic-field perturbation component h_x in the magnetic boundary layer of flow past a sinusoidal insulating wall. The undisturbed magnetic field is parallel to the undisturbed stream.

Let us apply these equations to the case of the infinite wavy wall. The boundary conditions for this problem are consistent with the small-perturbation assumption; namely,

(i) at the wall, from equation (24), $h_x = -H_0\epsilon\lambda\, e^{i\lambda x}$,

(ii) at the outer edge of the magnetic boundary layer, from equation (22),

$$h_x = H_0\epsilon\lambda\, e^{i\lambda x}.$$

The appropriate solution of equation (36) is

$$h_x(x,y) = H_0\epsilon\lambda\, e^{i\lambda x}\left\{1 - 2\exp\left[\sqrt{\frac{\lambda\kappa}{2}}(-i-1)y\right]\right\}. \tag{37}$$

This solution is presented graphically in figure 1 for a case $m < 1$.

Small-perturbation flow: Case II

Consider now the case of plane, steady flow in which the stream velocity and the magnetic field are uniform and perpendicular except for small disturbances; i.e. let

$$\mathbf{q} = (U+u, v, 0), \quad \text{where} \quad u, v \ll U, \tag{38}$$

and

$$\mathbf{H} = (h_x, H_0+h_y, 0), \quad \text{where} \quad h_x, h_y \ll H_0. \tag{39}$$

It will again be assumed that the ratios of perturbation to free-stream values are of the same order for both velocity and magnetic fields.

To first order, the equation of momentum, equation (7), then becomes

$$U\frac{\partial \mathbf{v}}{\partial x}+\frac{1}{\rho}\nabla p = \frac{1}{4\pi\rho}\left\{H_0\frac{\partial \mathbf{h}}{\partial y}-H_0\nabla h_y\right\}. \tag{40}$$

Taking the divergence of both sides of this equation, we obtain

$$\nabla^2\left(p+\frac{H_0}{4\pi}h_y\right) = 0, \tag{41}$$

i.e. the quantity $p+(H_0/4\pi)h_y$ (which might be called the total pressure perturbation including magnetic pressure) is a harmonic function in the x, y-plane.

The form assumed by Ohm's Law, equation (8), in this case is

$$U\frac{\partial \mathbf{h}}{\partial x}-H_0\frac{\partial \mathbf{v}}{\partial y} = \frac{1}{4\pi\sigma}\nabla^2\mathbf{h}. \tag{42}$$

We can obtain interesting forms of equations (40) and (42) by employing the curl operator. Equation (40) becomes

$$U\frac{\partial \Omega}{\partial x} = \frac{H_0}{4\pi\rho}\frac{\partial \xi}{\partial y}, \tag{43}$$

while equation (42) becomes

$$U\frac{\partial \xi}{\partial x}-H_0\frac{\partial \Omega}{\partial y} = \frac{1}{4\pi\sigma}\nabla^2\xi. \tag{44}$$

By cross-differentiation these can be put into the forms

$$\frac{\partial^2\xi}{\partial x^2}-\frac{1}{m^2}\frac{\partial^2\xi}{\partial y^2} = \frac{1}{4\pi\sigma U}\nabla^2\frac{\partial \xi}{\partial x}, \tag{45}$$

and

$$\frac{\partial^2\Omega}{\partial x^2}-\frac{1}{m^2}\frac{\partial^2\Omega}{\partial y^2} = \frac{H_0}{(4\pi U)^2\rho\sigma}\nabla^2\frac{\partial \xi}{\partial y}. \tag{46}$$

Infinite conductivity

Before discussing this case in detail, it may be well to point out that the configuration of the undisturbed flow, having flow velocity and magnetic field at right angles, is a possible one even for fluids of infinite conductivity. To be sure, equation (8) with right-hand side equal to zero is often interpreted as stating that 'magnetic lines of force are convected with the fluid'. However, this is only a convenient interpretation of the fact that the number of lines enclosed by any closed contour is constant if the contour is convected with the fluid (see Cowling

(1957), p. 5, equations (1–13), and Hayes (1949)). In the present case the magnetic field must extend to $x = \pm\infty$; i.e. the magnet must be infinite in length. A possible realization of this configuration might involve a channel which closes on itself within a uniform magnetic field, provided that the radius of the channel were so large as to make the approximation of plane flow tenable.

For $\sigma \to \infty$, the right-hand sides of equations (45) and (46) are negligible and both Ω and ξ satisfy the wave equation. Their general solutions may then be written immediately; they must both be of the form $f(x-my)+g(x+my)$. Let us adopt the notation

$$\left.\begin{aligned}\Omega &= F_1'(x-my)+G_1'(x+my),\\ \xi &= F_2'(x-my)+G_2'(x+my).\end{aligned}\right\} \tag{47}$$

These are equivalent to

$$\left.\begin{aligned}u &= \frac{m}{1+m^2}\{F_1(x-my)-G_1(x+my)\}+\frac{\partial\phi_1}{\partial x},\\ v &= \frac{1}{1+m^2}\{F_1(x-my)+G_1(x+my)\}+\frac{\partial\phi_1}{\partial y},\\ h_x &= \frac{m}{1+m^2}\{F_2(x-my)-G_2(x+my)\}+\frac{\partial\phi_2}{\partial x},\\ h_y &= \frac{1}{1+m^2}\{F_2(x-my)+G_2(x+my)\}+\frac{\partial\phi_2}{\partial y},\end{aligned}\right\} \tag{48}$$

where the condition $\operatorname{div}\mathbf{v} = 0$ has also been satisfied, provided that

$$\nabla^2\phi_1 = 0 = \nabla^2\phi_2.$$

But upon substituting equations (47) into the momentum equations, equation (40), we are able to integrate with respect to x and y, respectively, obtaining

$$Uu + p/\rho = -(H_0/4\pi\rho)\{F_2(x-my)+G_2(x+my)\}+C, \tag{49}$$

and

$$Uu + p/\rho = -(U/m)\{-F_1(x-my)+G_1(x+my)\}+C, \tag{50}$$

where C is a constant. This requires that

$$\left.\begin{aligned}F_2(x-my) &= -\sqrt{(4\pi\rho)}\,F_1(x-my),\\ G_2(x+my) &= \sqrt{(4\pi\rho)}\,G_1(x+my).\end{aligned}\right\} \tag{51}$$

The rotational parts of the velocity and magnetic fields are therefore related in a simple manner. Moreover, the irrotational parts are also related. First, we have equation (42) with right-hand side equal to zero. Substitution of equations (48) and (51) into this equation leads to

$$U\frac{\partial^2\phi_2}{\partial x^2} = H_0\frac{\partial^2\phi_1}{\partial x\,\partial y} \quad\text{and}\quad U\frac{\partial^2\phi_2}{\partial x\,\partial y} = H_0\frac{\partial^2\phi_1}{\partial y^2}, \tag{52}$$

from which

$$U\frac{\partial\phi_2}{\partial x} = H_0\frac{\partial\phi_1}{\partial y}, \tag{53}$$

except for a constant, which must be put equal to zero in view of the undisturbed-flow conditions.

Second, we can make use of equation (19), which applies to this case. For this perturbation case under consideration, it becomes, to first order,

$$H_0u + Uh_y = 0. \tag{54}$$

Upon substitution for u and h_y from equations (48), and in view of equations (51), it follows that

$$U\frac{\partial\phi_2}{\partial y} = -H_0\frac{\partial\phi_1}{\partial x}. \tag{55}$$

In summary, equations (48) involve four unknown functions; $F_1(x-my)$, $G_1(x+my)$, $\phi_1(x,y)$, and $\phi_2(x,y)$ (since F_2 and G_2 are linearly related by (51)); and the last two of these are related by equations (53) and (55). We now illustrate the application of this theory by working out three examples.

(1) *Infinite sinusoidal wall (insulator)*

We again consider the flow over the wall whose contour is given by $y = \epsilon e^{i\lambda x}$. The boundary condition at the wall is, to first order

$$v(x,0) = UY'(x) = iU\lambda\epsilon e^{i\lambda x}. \tag{56}$$

As a second boundary condition we require that no perturbations are propagated toward the wall from the undisturbed stream; i.e. for this flow

$$G_1(x+my) = G_2(x+my) = 0. \tag{57}$$

Since all remaining perturbation quantities will be sinusoidal, we introduce the notation

$$F_1(x-my) = F_0 e^{i\lambda(x-my)}, \tag{58}$$

$$\phi_1(x,y) = f_1 e^{i\lambda(x+iy)} = -i\frac{U}{H_0}\phi_2(x,y), \tag{59}$$

where F_0 and f_1 are constants, and the last equality follows from equations (53) and (55).

No currents flow in the insulator, so that the description of the magnetic field for $y < 0$ is provided by another potential function, say $\phi_3(x,y)$, where, for $y < 0$,

$$h_x = \frac{\partial\phi_3}{\partial x} = i\lambda f_3 e^{i\lambda(x-iy)} = i\frac{\partial\phi_3}{\partial y} = ih_y, \tag{60}$$

where f_3 is a constant.

As before, to satisfy equation (6) we require continuity of the component h_y at the wall-fluid interface. Thus

$$\lambda f_3 = -\frac{\sqrt{(4\pi\rho)}}{1+m^2}F_0 - i\frac{H_0}{U}\lambda f_1, \tag{61}$$

while equation (56) states that

$$\frac{1}{1+m^2}F_0 - \lambda f_1 = iU\lambda\epsilon. \tag{62}$$

In the present problem, moreover, we shall also require the component h_x to be continuous at the solid-fluid interface, because a first-order surface current would produce first-order force components in the tangential direction and there is no mechanism here to resist such force components. Thus,

$$i\lambda f_3 = -\frac{m\sqrt{(4\pi\rho)}}{1+m^2}F_0 - \frac{H_0}{U}\lambda f_1. \tag{63}$$

The simultaneous solution of equations (61), (62) and (63) leads immediately to the results

$$F_0 = -2U\lambda\epsilon\frac{1+m^2}{2i+m+im^2}, \tag{64}$$

and

$$f_1 = U\epsilon\frac{m^2-im}{2i+m+im^2}, \tag{65}$$

from which the wall pressure is found, using equation (50), to be

$$p(x,0) = p_\infty - \rho U^2\lambda\epsilon\frac{m^2-2im-2}{m(m-2i)}e^{i\lambda x}. \tag{66}$$

The function of m that appears in equation (66) is plotted in figure 2 in the form of a vector diagram giving the amplitude and phase of the pressure perturbation.

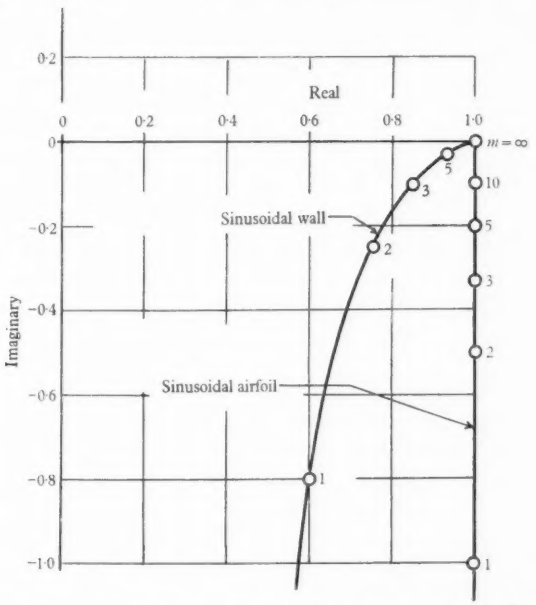

FIGURE 2. Vector diagram showing real and imaginary parts of the functions of m for (*a*) the pressure on a sinusoidal insulating wall as given by equation (66), and (*b*) the pressure (or lift) on a sinusoidal airfoil as given by equation (79). The undisturbed magnetic field is perpendicular to the undisturbed stream.

(2) *Lifting airfoil without thickness (insulator)*

Suppose the boundary condition is

$$v(x,0) = UY'(x) \quad \text{for} \quad -b \leqslant x \leqslant b, \tag{67}$$

so that $y = Y(x)$ gives the airfoil shape. This requires both

$$\frac{1}{1+m^2}F_1(x) + \left(\frac{\partial\phi_1}{\partial y}\right)_{y=+0} = UY',$$

and

$$\frac{1}{1+m^2}G_1(x) + \left(\frac{\partial\phi_1}{\partial y}\right)_{y=-0} = UY'. \tag{68}$$

Once again we require both h_x and h_y to be continuous at the airfoil, for the reasons set forth above. The first of these two conditions, in view of equations (48) and (51), means that

$$\frac{m\sqrt{(4\pi\rho)}}{1+m^2}\{F_1(x)-G_1(x)\} = \left(\frac{\partial\phi_2}{\partial x}\right)_{y=+0} - \left(\frac{\partial\phi_2}{\partial x}\right)_{y=-0} \tag{69}$$

or, with equations (68),

$$m\sqrt{(4\pi\rho)}\left\{\left(\frac{\partial\phi_1}{\partial y}\right)_{y=-0} - \left(\frac{\partial\phi_1}{\partial y}\right)_{y=+0}\right\} = \left(\frac{\partial\phi_2}{\partial x}\right)_{y=+0} - \left(\frac{\partial\phi_2}{\partial x}\right)_{y=-0}. \tag{70}$$

If this equation is compared with equation (53), with due regard for signs, it becomes clear that $\partial\phi_1/\partial y$ and $\partial\phi_2/\partial x$ must be continuous at the airfoil. Thus ϕ_1 may involve a vortex sheet and ϕ_2 a sheet of magnetic sources, at most. In view of this conclusion, we have from the boundary conditions (68) that

$$F_1(x) = G_1(x). \tag{71}$$

At this point it is easy to verify from equation (48) that $u(x, +0) = -u(x, -0)$; but equation (54) states that $u(x, y)$ is proportional to $h_y(x, y)$, which has been made continuous at the airfoil. The conclusion is therefore that

$$u(x, \pm 0) = 0 = h_y(x, 0). \tag{72}$$

We have succeeded in relating explicitly the rotational and irrotational parts of the flow; i.e.

$$\frac{1}{1+m^2}F_2(x) = -\left(\frac{\partial\phi_2}{\partial y}\right)_{y=+0} \tag{73}$$

or

$$F_1(x) = -\frac{1+m^2}{m}\left(\frac{\partial\phi_1}{\partial x}\right)_{y=+0}. \tag{74}$$

The boundary condition (68) can now be expressed in terms of the unknown potential function $\phi_1(x, y)$ alone:

$$\left(\frac{\partial\phi_1}{\partial x}\right)_{y=+0} - m\left(\frac{\partial\phi_1}{\partial y}\right)_{y=0} = -mUY' \tag{75}$$

in the interval $-b \leqslant x \leqslant b$.

Boundary-value problems of this type were treated by Rott & Cheng (1954), and a procedure for constructing their solutions was given. Applied to the present problem, it leads to the result

$$\frac{\partial\phi_1}{\partial x} - i\frac{\partial\phi_1}{\partial y} = i\left\{\left(\frac{z-b}{z+b}\right)^{\beta}\frac{mU}{\pi\sqrt{(1+m^2)}}\int_{-b}^{b}\left(\frac{b+s}{b-s}\right)^{\beta}\frac{Y'(s)\,ds}{s-z}\right\}, \tag{76}$$

where $z = x+iy$ and $\beta = (\frac{1}{2}) - (1/\pi)\tan^{-1}(1/m)$, the $\tan^{-1}$ being in the first quadrant. However, this solution does not seem particularly illuminating in the present studies, and we give instead the solutions for two cases where simpler results are obtained.

(*a*) Suppose, for example, that the airfoil is sinusoidal in shape ($Y = \epsilon e^{i\lambda x}$) and of infinite chord ($b = \infty$). All terms in equation (75) are then sinusoidal, and it is easily ascertained that

$$\phi_1(x, y) = -\frac{mi}{m+i}U\epsilon\, e^{i\lambda(x+iy)} \quad \text{for} \quad y > 0, \tag{77}$$

whence
$$F_1(x) = -\frac{1+m^2}{m+i} U\lambda\epsilon\, e^{i\lambda x} \tag{78}$$

and, from equation (50), the lift loading $l(x)$ is

$$l(x) = 2\rho U^2\lambda\epsilon\left(1-\frac{i}{m}\right)e^{i\lambda x}. \tag{79}$$

The function of m that appears in equation (79) is plotted in figure 2.

(*b*) A family of solutions of equation (75) is given by the so-called Glauert series of thin-airfoil theory (Glauert (1926), p. 88); namely,

$$\left(\frac{\partial\phi_1}{\partial x}\right)_{y=+0} = B_0\frac{1-\cos\theta}{\sin\theta} + \sum_{n=1} B_n \sin n\theta, \tag{80}$$

$$\left(\frac{\partial\phi_1}{\partial y}\right)_{y=0} = -B_0 - \sum_{n=1} B_n \cos n\theta, \tag{81}$$

and their linear combination according to equation (75),

$$-mUY'(x) = B_0\left\{\frac{1-\cos\theta}{\sin\theta}+m\right\} + \sum_{n=1} B_n\{\sin n\theta + m\cos n\theta\}, \tag{82}$$

where $x/b = \cos\theta$.

The profiles of airfoils of this family are found by integration of equation (82). Their lift loading is, from equations (50) and (74),

$$\begin{aligned} l(x) &= -\frac{2}{m}\rho U F_1(x) \\ &= 2\rho\frac{1+m^2}{m^2}U\left\{B_0\frac{1-\cos\theta}{\sin\theta} + \sum_{n=1} B_n\sin n\theta\right\}. \end{aligned} \tag{83}$$

The terms in equation (80) have been selected to satisfy the Kutta–Joukowski condition of finite velocity at the trailing edge, as can easily be checked using equations (48), (71) and (74).

In figure 3 are shown the airfoils of this family obtained by using the terms in B_1 only, for several values of m. These airfoils all produce elliptical lift loading of magnitude proportional to $(1+m^2)/m^2$; i.e. their lift coefficients are

$$c_l = 2\pi\frac{1+m^2}{m^2}\frac{B_1}{U}. \tag{84}$$

It seems clear that this lift, for $m < \infty$, is associated with positive drag.

(3) *Symmetrical airfoil with thickness* (*insulator*)

Within the airfoil we have

$$\operatorname{div}\mathbf{h} = 0 = \operatorname{curl}\mathbf{h}. \tag{85}$$

Again, the boundary values for the inner field are given by the values of h_x and h_y assumed at the airfoil surface; there can be no surface currents for the reasons explained above. Thus the boundary values of h_x and h_y are of first order, and so are $\partial h_x/\partial x$ and $\partial h_y/\partial x$. It follows immediately from equations (85) that $\partial h_y/\partial y$ and

$\partial h_x/\partial y$ are of first order. By integration with respect to y, we have then that the values of both components at the top surface of the airfoil differ from the values at the lower surface by higher-order quantities.

We therefore take both h_x and h_y to be continuous across the singularity sheet that represents the airfoil in the limit, i.e.

$$h_x(x, +0) = h_x(x, -0),$$
$$h_y(x, +0) = h_y(x, -0). \tag{86}$$

In view of equation (54), u must also be continuous across the airfoil.

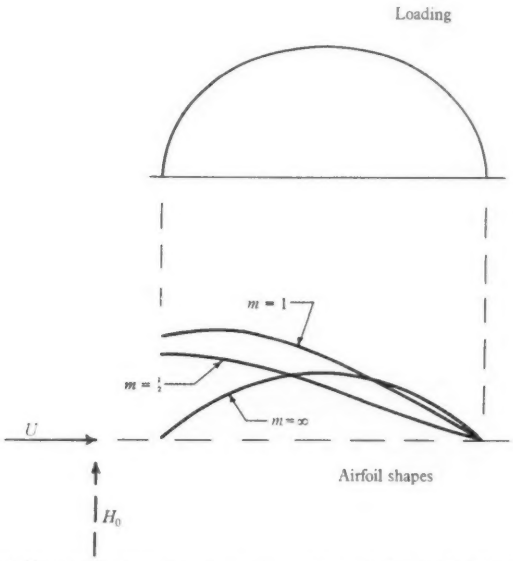

FIGURE 3. Lift loading and corresponding geometries of three airfoils producing elliptic loading for different values of m. The undisturbed magnetic field is perpendicular to the undisturbed stream.

With the aid of equations (48) and (51), it follows that

$$\frac{\sqrt{(4\pi\rho)}}{1+m^2}\{F_1(x)+G_1(x)\} = \left(\frac{\partial\phi_2}{\partial y}\right)_{y=+0} - \left(\frac{\partial\phi_2}{\partial y}\right)_{y=-0} \tag{87}$$

and, using also equation (53),

$$\frac{m\sqrt{(4\pi\rho)}}{1+m^2}\{F_1(x)-G_1(x)\} = \frac{H_0}{U}\left\{\left(\frac{\partial\phi_1}{\partial y}\right)_{y=+0} - \left(\frac{\partial\phi_1}{\partial y}\right)_{y=-0}\right\}. \tag{88}$$

The boundary conditions at the airfoil are

$$v(x, \pm 0) = \pm U Y'(x) \quad \text{for} \quad -b \leqslant x \leqslant b, \tag{89}$$

so that, from equations (48),

$$\left(\frac{\partial\phi_1}{\partial y}\right)_{y=+0} - \left(\frac{\partial\phi_1}{\partial y}\right)_{y=-0} = 2UY'(x) - \frac{1}{1+m^2}\{F_1(x)-G_1(x)\}. \tag{90}$$

By comparison of equations (88) and (90), we have

$$F_1(x) - G_1(x) = 2U\,Y'(x). \tag{91}$$

Now, the continuity of u, in view of equations (48), means that

$$\frac{m}{1+m^2}\{F_1(x) + G_1(x)\} = \left(\frac{\partial \phi_1}{\partial x}\right)_{y=-0} - \left(\frac{\partial \phi_1}{\partial x}\right)_{y=+0}, \tag{92}$$

while the boundary conditions (89) state that

$$-\frac{1}{1+m^2}\{F_1(x) + G_1(x)\} = \left(\frac{\partial \phi_1}{\partial y}\right)_{y=+0} + \left(\frac{\partial \phi_1}{\partial y}\right)_{y=-0}. \tag{93}$$

Suppose that the potential function ϕ_1 involves both a vortex sheet and a source-sink sheet at the airfoil. Then the right-hand side of equation (92) is the vortex-strength distribution, while the right-hand side of equation (93) is twice the corresponding vertical-velocity component, since the source strength does not contribute to either. These quantities are seen to be proportional to one another. But it can be shown (e.g. Rott & Cheng 1954) that the only vortex distributions that satisfy this homogeneous condition are singular at both $x = \pm b$, and this would necessarily lead to infinite loadings there in the present problem. Thus, by means of the Kutta–Joukowski condition at the trailing edge, we conclude that ϕ_1 arises from a source-sink sheet alone.

Then

$$F_1(x) = -G_1(x), \tag{94}$$

and equation (87) states that the magnetic-field singularity at the airfoil is a current sheet only. Combination of equations (88) and (91) yields the following simple formula for the distribution of the fluid sources and the strength of the fictitious current sheet:

$$\frac{H_0}{U}\left(\frac{\partial \phi_1}{\partial y}\right)_{y=+0} = \left(\frac{\partial \phi_2}{\partial x}\right)_{y=+0} = \frac{m\sqrt{(4\pi\rho)}}{1+m^2}F_1(x) = \frac{m\sqrt{(4\pi\rho)}}{1+m^2}U\,Y'(x). \tag{95}$$

The corresponding values of $\partial\phi_1/\partial x$ at the sheet are given by

$$\left(\frac{\partial \phi_1}{\partial x}\right)_{y=0} = \frac{1}{\pi}\,U\,\frac{m^2}{1+m^2}\,P\int_{-b}^{b}\frac{Y'(s)\,ds}{x-s}, \tag{96}$$

where the symbol P means that the Cauchy principal value is to be taken.

The surface pressure can now be calculated from equations (49) or (50):

$$p(x, +0) = p_\infty + \frac{1}{m(1+m^2)}\rho U^2 Y'(x) - \frac{1}{\pi}\rho U^2\,\frac{m^2}{1+m^2}\,P\int_{-b}^{b}\frac{Y'(s)\,ds}{x-s}. \tag{97}$$

The pressure on the lower surface, $p(x, -0)$, differs from p_∞ by an equal amount, and there is no lift.

Examples of pressure distributions calculated from equation (97) are easy to construct. We exhibit here in figure 4 the case of a thin elliptic cylinder. The pressure distribution is plotted for various values of m. The distortion of the distribution from its familiar symmetrical form as m is reduced from infinity obviously implies non-vanishing drag. Its value is

$$D = \frac{2}{m(1+m^2)}\rho U^2\int_{-b}^{b}\{Y'(x)\}^2\,dx. \tag{98}$$

Finite conductivity

For large but finite conductivity, we return to equations (45) and (46) and assume that the right-hand terms are small. The solution can then be carried out by introducing damping into the sinusoidal-wave solutions found in the preceding section, in the same way that viscous damping is introduced in problems of acoustics. This is the same process as Alfvén (1950) used to calculate the damping of propagating magneto-hydrodynamic waves.

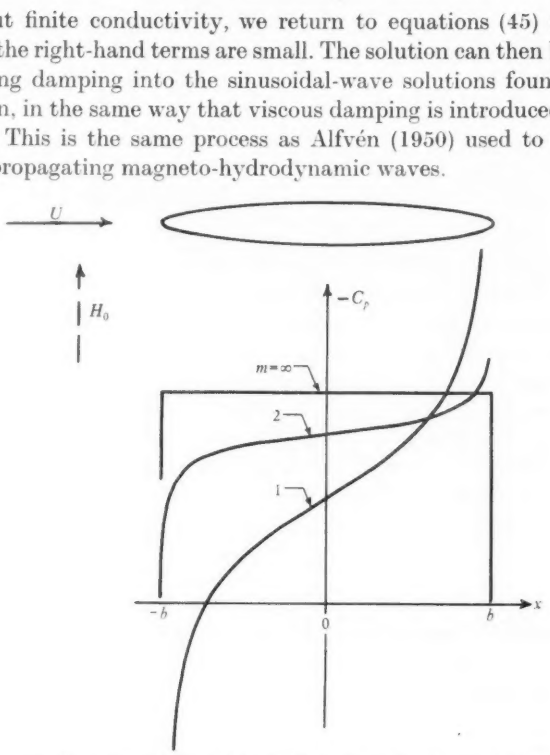

FIGURE 4. Pressure distribution on a thin elliptic cylinder at zero incidence for several values of m. The undisturbed magnetic field is perpendicular to the undisturbed stream.

Thus, for the infinite sinusoidal wall we write, in analogy with equations (47) and (58),

$$\xi = \kappa e^{i\lambda(x-my)} e^{-\mu y}, \tag{99}$$

where κ and μ are constants. Substituting this into equation (45), we have, after neglecting terms of order μ^2 in comparison with terms of order μ,

$$\mu = \frac{(1+m^2)\, m\lambda^2}{8\pi U\sigma - 2m^2\lambda} \approx \frac{(1+m^2)\, m\lambda^2}{8\pi U\sigma}. \tag{100}$$

To help interpret this result, let y_σ denote the value of y at which the waves are damped to $1/e$ times their amplitude at the wall; i.e.

$$y_\sigma = \mu^{-1} = \frac{8\pi U\sigma}{(1+m^2)\, m\lambda^2}. \tag{101}$$

This means that the time to damp to $1/e$, since the waves propagate in the y direction with the Alfvén speed, is

$$\frac{\sqrt{(4\pi\rho)}\, y_\sigma}{H_0} = \frac{2}{\pi}\frac{\sigma l_w^2}{m^2+1}, \tag{102}$$

where l_w denotes the wave length of the wall, $2\pi/\lambda$. The right-hand side of equation (102) is seen to be proportional to a diffusion time, namely, the time required for the magnetic field to diffuse over a distance equal to the minimum spacing between the waves, $l_w/\sqrt{(m^2+1)}$. In this interpretation our result agrees with Alfvén's in the investigation mentioned above [Alfvén (1950), p. 82].

The conclusion reached here is that one effect of small, non-vanishing resistance is damping of the vorticity and current in the waves that emanate from the solid surface. The pressure, including the values of pressure at the solid surface, is also affected; its calculation will be presented in another paper.

By Fourier superposition the solution for sinusoidal waves can be generalized to give the solution for other types of waves, such as are produced by cylinders of various geometries. In every case we find attenuation and diffusion of the waves. These solutions will also be published shortly.

This research was supported jointly by the United States Air Force through the Office of Scientific Research of ARDC and the Mechanics Branch of the Office of Naval Research.

REFERENCES

Alfvén, H. 1950 *Cosmical Electrodynamics.* Oxford University Press.

Cowling, T. G. 1957 *Magnetohydrodynamics.* London: Interscience.

Glauert, H. 1926 *Aerofoil and Airscrew Theory.* Cambridge University Press.

Hayes, W. D. 1949 An alternative proof of the constancy of circulation. *Quart. Appl. Math.* **7**, 235–236.

Resler, E. L., Jr. & Sears, W. R. 1958 The prospects for magneto-aerodynamics. *J. Aero. Sci.* **25**, 235–46.

Rott, N. & Cheng, H. K. 1954 Generalization of the inversion formula of thin airfoil theory. *J. Rat. Mech. Anal.* **3**, 357–82.

The effect of uniform distortion on weak homogeneous turbulence

By J. R. A. PEARSON
Imperial Chemical Industries Ltd., Akers Research Laboratories, Welwyn, Herts

(Received 19 June 1958)

The behaviour of weak homogeneous turbulence subjected to a uniform distortion is studied by means of linearized equations that include the effect of inertial interaction between the mean flow and the turbulent fluctuations and of viscous dissipation. Three particular cases of distortion are investigated in varying degrees of detail; those of uniform rotation, uniform shear, and uniform irrotational distortion. For the first two, the total energy associated with the turbulence is found to decay, but for the third it is found in general to increase without limit. A general solution in terms of the spectrum functions for the restricted case of irrotational distortions is given, particular consideration being paid to the asymptotic limits approached as the distortions (not necessarily the rates of distortion) become large. These show that for an arbitrary initial turbulent spectrum the asymptotic rates of growth are functions of the precise geometrical nature of the distortion, of an integral parameter of the initial spectrum function, of a Reynolds number based on the rate of distortion and the length scale of the initial turbulence, and of the contraction. A particular example, that of initially isotropic turbulence in its final period of decay subjected to an axisymmetric distortion, is worked out in detail and the solution (described in terms of mean turbulent intensities) displayed graphically for several values of the Reynolds number.

1. Introduction

When a weak homogeneous turbulent velocity field is uniformly distorted we may use a suitably linearized form of the Navier–Stokes equations to determine the effect of the distortion on the turbulent field. We suppose that the velocity field is the sum of a steady uniform distortion and of a small turbulent fluctuation. By neglecting quadratic terms in the turbulent velocities, linear equations are obtained. By well-known methods these can be converted into equations for the spectrum functions in wave-number space, and these in turn are, in certain particular cases, simply soluble. These equations preserve in some degree the nature of the full Navier–Stokes equations of motion, in that inertial forces—here the product of the interaction between steady flow and turbulence—pressure forces and viscous forces are all included.

The effect of the interaction terms alone has been considered by Batchelor & Proudman (1954) (B & P hereafter), who suppose the strain to be sudden and

employ a Lagrangian approach in order to evaluate the effect of distortion on any particular small fluid element. A consideration of the simultaneous effects of inertial interaction and viscous dissipation suggests an Eulerian treatment such as has been outlined above. It is found that the results of B & P are obtained more readily by means of the latter treatment, while several other interesting results concerning the asymptotic states achieved after long times of mean strain are derived. The problem has also been discussed by Ribner & Tucker (1952); they survey some of the experimental results that are relevant, sufficiently at least to show that the particular linearization chosen is a suitable approximation to certain wind-tunnel arrangements.

The notation used throughout follows that of Proudman & Reid (1954) (P & R). Mean values or averages, denoted by an overbar, are assumed to be ensemble averages. This avoids any difficulties that might arise if spatial averages were used. The validity of Fourier transformation has been discussed by Batchelor (1953).

2. Dynamical equations

We consider the uniform strain to be caused by a mean motion

$$U_i = C_{ij} x_j, \tag{2.1}$$

where C_{ij} are constants independent of position. For simplicity we shall take them to be independent of time also, though this is not essential; the analysis can be carried out equally well for the case

$$C_{ij} = C_{ij}(t). \tag{2.2}$$

We consider a turbulent velocity field u_i to be superposed on the mean strain U_i such that the velocity becomes the sum

$$v_i = U_i + u_i \tag{2.3}$$

and the pressure p is given by

$$p/\rho = P + \varpi, \tag{2.4}$$

ρ being the uniform density, P the mean component and ϖ the fluctuating component of the reduced pressure. The Navier–Stokes equation and the continuity condition are

$$\frac{\partial v_i}{\partial t} + v_j \frac{\partial v_i}{\partial x_j} = -\frac{1}{\rho}\frac{\partial p}{\partial x_i} + \nu \frac{\partial^2 v_i}{\partial x_j \partial x_j}, \quad \frac{\partial v_i}{\partial x_i} = 0, \tag{2.5}$$

where ν is the kinematic viscosity. By taking mean values we get

$$U_j \frac{\partial U_i}{\partial x_j} + \frac{\partial P}{\partial x_i} - \nu \frac{\partial^2 U_i}{\partial x_j \partial x_j} = 0, \quad \frac{\partial U_i}{\partial x_i} = 0, \tag{2.6}$$

since $\partial U_i/\partial t$, $\overline{u_i}$, $\overline{\varpi}$ are by definition zero; $\partial(\overline{u_i u_j})/\partial x_k$ we take to be zero, because we suppose further that the turbulent field is homogeneous. It can readily be shown that if at any stage the turbulence is homogeneous then it will remain so, and thus the postulate of a homogeneous turbulent field is self-consistent.

The equations for the turbulent components, u_i, become

$$\frac{\partial u_i}{\partial t} = -U_j\frac{\partial u_i}{\partial x_j} - u_j\frac{\partial U_i}{\partial x_j} - u_j\frac{\partial u_i}{\partial x_j} - \frac{\partial \varpi}{\partial x_i} - \nu\frac{\partial^2 u_i}{\partial x_j \partial x_j}, \tag{2.7}$$

$$\frac{\partial u_i}{\partial x_i} = 0. \tag{2.8}$$

Because the turbulence is assumed to be weak, we are justified in neglecting the terms $u_j(\partial u_i/\partial x_j)$ and the equation (2.7) can be linearized to give

$$\frac{\partial u_i}{\partial t} + U_j\frac{\partial u_i}{\partial x_j} + u_j\frac{\partial U_i}{\partial x_j} + \frac{\partial \varpi}{\partial x_i} - \nu\frac{\partial^2 u_i}{\partial x_j \partial x_j} = 0. \tag{2.9}$$

We now define the following velocity product and pressure-velocity product mean values

$$\left.\begin{aligned} R_{ij}(\mathbf{r},t) &= \overline{u_i(\mathbf{x},t)\,u_j(\mathbf{x}+\mathbf{r},t)},\\ P_i(\mathbf{r},t) &= \overline{\varpi(\mathbf{x},t)\,u_i(\mathbf{x}+\mathbf{r},t)},\\ W_{ij}(\mathbf{r},t) &= \overline{\omega_i(\mathbf{x},t)\,\omega_j(\mathbf{x}+\mathbf{r},t)}, \end{aligned}\right\} \tag{2.10}$$

where $\omega_i(\mathbf{x},t)$ represents the vorticity associated with the velocity u_i and is given by

$$\omega_i = \epsilon_{ijk}\frac{\partial u_k}{\partial x_j}. \tag{2.11}$$

The functions on the left-hand side are written as functions of $\mathbf{r}$ and t only, since the original postulate of homogeneity removes the dependence on $\mathbf{x}$. We also define the Fourier transforms of the functions (2.10) as

$$\left.\begin{aligned} \Phi_{ij}(\mathbf{k},t) &= (2\pi)^{-3}\int R_{ij}(\mathbf{r},t)\,e^{-i\mathbf{k}.\mathbf{r}}\,d\mathbf{r},\\ \Pi_i(\mathbf{k},t) &= i(2\pi)^{-3}\int P_i(\mathbf{r},t)\,e^{-i\mathbf{k}.\mathbf{r}}\,d\mathbf{r},\\ \Omega_{ij}(\mathbf{k},t) &= (2\pi)^{-3}\int W_{ij}(\mathbf{r},t)\,e^{-i\mathbf{k}.\mathbf{r}}\,d\mathbf{r}. \end{aligned}\right\} \tag{2.12}$$

The many symmetry properties of the functions (2.10) and (2.12) and the consequences of the continuity equation are all given in P & R and are not repeated here.

In terms of these functions the equation (2.9) leads to the following dynamical equations for $R_{ij}(\mathbf{r},t)$

$$\begin{aligned} \frac{\partial}{\partial t}R_{ij}(\mathbf{r},t) = &-C_{ik}R_{kj}(\mathbf{r},t) - C_{jk}R_{ik}(\mathbf{r},t) - C_{kl}r_l\frac{\partial}{\partial r_k}R_{ij}(\mathbf{r},t)\\ &+\frac{\partial}{\partial r_i}P_j(\mathbf{r},t) + \frac{\partial}{\partial r_j}P_i(\mathbf{r},t) + 2\nu\frac{\partial^2}{\partial r_l \partial r_l}R_{ij}(\mathbf{r},t). \end{aligned} \tag{2.13}$$

We may now take Fourier transforms of the equations (2.13) and eliminate the terms $\Pi_i(\mathbf{k},t)$ by contraction and resubstitution (as in P & R) to obtain the relevant dynamical equations for the spectrum functions

$$\begin{aligned} \frac{\partial \Phi_{ij}(\mathbf{k},t)}{\partial t} = C_{lk}\Big\{&\left(2\frac{k_i k_l}{k^2} - \delta_{il}\right)\Phi_{kj}(\mathbf{k},t) + \left(2\frac{k_j k_l}{k^2} - \delta_{jl}\right)\Phi_{ik}(\mathbf{k},t)\\ &+ k_l\frac{\partial}{\partial k_k}\Phi_{ij}(\mathbf{k},t)\Big\} - 2\nu k^2\Phi_{ij}(\mathbf{k},t). \end{aligned} \tag{2.14}$$

Although well-known methods are available for solving this set of nine first-order simultaneous equations, it is not possible to display the general solution in neat tensorial form for arbitrary C_{ik} and arbitrary initial values of $\Phi_{ij}(\mathbf{k})$. Indeed, in most cases, particular solutions become excessively complex.

One result concerning a general distortion is worth noting. Though the mean strain may be split into a uniform rotation plus a uniform irrotational distortion, the solution of the equations (2.14) (and equivalently for the inviscid case, or sudden strain approximation) is not such that the effects of rotation and irrotational distortion may be completely separated. In their sudden strain approximation, B & P suppose that the effect of rotation may be neglected; an inspection of equations (2.14) shows that this cannot in fact be true.

Three particular cases have been examined in varying degrees of detail, those of uniform rotation, uniform shear and uniform irrotational distortion. The asymptotic form of the solution as $t \to \infty$, when the spectrum is supposed known at some initial instant, provides the most interesting information and this aspect of the solution is the one to which most attention will be given; for this limit tells us whether or not the turbulent field extracts more energy from the mean strain than is dissipated by viscosity. It also tells us how the turbulent field becomes oriented. If the asymptotic solution leads to a continuous increase in turbulent intensity then ultimately the linearization that we have adopted must fail, and inertial interactions within the turbulent field will become important. Indeed, experience shows that these interactions suffice to limit the growth in turbulent intensity. However, if we suppose the initial turbulence to be sufficiently weak, the effect of interactions is only felt after the asymptotic form has been substantially achieved.

These results have some connexion with stability theory: the arbitrary spatially bounded initial disturbance of stability theory is replaced in our case by an initial spectrum of (homogeneous) turbulence. Since in practice the arbitrary initial disturbance of stability theory is usually chosen to be a sinusoidal wave-like motion, the connexion becomes reasonably close. The presence of boundaries (or equivalently, the condition of zero disturbance at infinity) in the former and the absence of boundaries in the latter make the treatments complimentary.

Uniform rotation. This case can be represented by $C_{23} = -C_{32} =$ constant, all other $C_{ij} = 0$. A full solution of the equations (2.14) for this choice of C_{ij} has not been obtained because of their apparent intractability. However, it can readily be shown that the total kinetic energy associated with the turbulent field, $\int \Phi_{ii}(\mathbf{k}, t)\, d\mathbf{k}$, decays in time, in much the same way as it would in the absence of the mean rotation. By taking the inviscid case, we find that the total kinetic energy remains constant. Although these statements are rather crude, they represent all the information that has been obtained; in particular, no information about orientation along or perpendicular to the axis of rotation was derived.

Uniform shear. This case can be represented by $C_{12} =$ constant, all other $C_{ij} = 0$. A complete solution has been obtained, but this is much too complicated to present here. As in the case of uniform rotation the relevant result is that the total energy ultimately decays with time. This result depends, it must be pointed

out, on the asymptotic form of the initial spectrum, $\Phi_{ij}(\mathbf{k}, 0)$, near $k = 0$, which, as Batchelor & Proudman (1956) have shown, must obey the relation

$$\Phi_{ij}(\mathbf{k}, 0) = \frac{C_{lmnp}}{4\pi^2}\left(\delta_{il} - \frac{k_i k_l}{k^2}\right)\left(\delta_{jm} - \frac{k_j k_m}{k^2}\right) k_n k_p + O(k^3 \ln k). \tag{2.15}$$

The precise form of (2.15) makes it very difficult to decide whether any significant orientation is taking place within the decaying system. However, the detailed asymptotic structure of the turbulent field would only be decisively important if the turbulent intensity were increasing, which is not the case. It is perhaps worth noting that the result we have obtained is consistent with the established result that (plane) Couette motion is stable to all small disturbances; this stability is evidently not dependent on the presence of boundaries.

Uniform irrotational distortion. This proves to be the most interesting case of the three and the solution is presented in some detail in the following section. The general solution for a known initial spectrum is found to depend on the precise geometrical form of the distortion. If we define an expansion ratio, c, as the total relative amount of strain that has taken place along the principal axis of maximum rate of expansion, then the asymptotic behaviour of the total kinetic energy associated with the turbulent field can be expressed as a power of c, the index of this power lying between 0 and 1. For distortions in which expansion takes place along two of the principal axes of strain, the index is always unity, but for distortions in which contraction takes place along two of the principal axes of strain, the growth in energy is proportional to the ratio of the two contractions, respectively. Thus for axisymmetric distortion involving expansion along the axis of symmetry the index is zero, and the total energy tends to a constant. The coefficient of proportionality depends on the rate of straining, and involves a rather complicated integral parameter of the initial turbulent spectrum. The special case of isotropic turbulence is treated as an example. This allows the integral parameter to be expressed in a rather simpler form.

3. General solution for irrotational distortion. Asymptotic limit for large distortions

The restricted case of a uniform irrotational distortion will now be considered in detail; the time-dependent solution for an initially known weak turbulent field that is subjected to a uniform mean strain will be developed.

The axes of the co-ordinate system can be chosen to lie along the principal axes of strain such that

$$C_{11} = \frac{1}{T}, \quad C_{22} = -\frac{\alpha}{T}, \quad C_{33} = \frac{\alpha - 1}{T}. \tag{3.1}$$

T represents a characteristic time describing the rate of distortion and α is a geometrical parameter such that $-1 \leqslant \alpha \leqslant \frac{1}{2}$. Let us define an 'expansion ratio' c by the relation

$$C = e^{t/T}, \tag{3.2}$$

whence

$$\frac{\partial}{\partial t} \equiv \frac{c}{T}\frac{\partial}{\partial c}, \tag{3.3}$$

c representing the extension along the principal axis of maximum extension. The equations (2.14) become

$$c\frac{\partial}{\partial c}\Phi_{ij}(\mathbf{k},c)+\lambda^{(l)}\left[\left(\delta_{il}+\frac{2k_ik_l}{k^2}\right)\Phi_{lj}(\mathbf{k},c)+\left(\delta_{jl}-\frac{2k_jk_l}{k^2}\right)\Phi_{li}(k,c)\right.$$
$$\left.-k_l\frac{\partial}{\partial k_l}\Phi_{ij}(\mathbf{k},c)\right]+2\nu Tk^2\Phi_{ij}(\mathbf{k},c)=0, \tag{3.4}$$

where
$$\lambda^{(1)},\lambda^{(2)},\lambda^{(3)}=1,-\alpha,\alpha-1. \tag{3.5}$$

The equivalent equations for the vorticity spectrum functions $\Omega_{ij}(\mathbf{k},c)$ are then

$$c\frac{\partial}{\partial c}\Omega_{ij}(\mathbf{k},c)-(\lambda^{(i)}+\lambda^{(j)})\,\Omega_{ij}(\mathbf{k},c)-\lambda^{(l)}k_l\frac{\partial}{\partial k_l}\Omega_{ij}(\mathbf{k},c)+2\nu Tk^2\Omega_{ij}(\mathbf{k},c)=0, \tag{3.6}$$

where
$$k^2\Phi_{ji}(\mathbf{k},c)=\left(\frac{k^2\delta_{ij}-k_ik_j}{k^2}\right)\Omega_{ll}(\mathbf{k},c)-\Omega_{ij}(\mathbf{k},c). \tag{3.7}$$

To solve (3.6) we observe that the equation

$$\left(c\frac{\partial}{\partial c}-\lambda^{(l)}k_l\frac{\partial}{\partial k_l}\right)F_{ij}(\mathbf{k},c)=0 \tag{3.8}$$

has a solution
$$F_{ij}(\mathbf{k},c)=F_{ij}^{(0)}(\boldsymbol{\chi}), \tag{3.9}$$

where
$$\boldsymbol{\chi}=(ck_1,c^{-\alpha}k_2,c^{\alpha-1}k_3). \tag{3.10}$$

$F_{ij}^{(0)}(\boldsymbol{\chi})$ is an arbitrary function, except when $\alpha=0$. (The case $\alpha=0$ needs special treatment.) Next we observe that the equation (3.6) with $\nu\equiv 0$ has a solution

$$\Omega_{ij}^{(\nu=0)}(\mathbf{k},c)=c^{\lambda^{(i)}+\lambda^{(j)}}\Omega_{ij}^{(\nu=0)(0)}(\boldsymbol{\chi}). \tag{3.11}$$

Finally, we deduce that the full solution of (3.6) is given by

$$\Omega_{ij}(\mathbf{k},c)=c^{\lambda^{(i)}+\lambda^{(j)}}\Omega_{ij}^{(0)}(\boldsymbol{\chi})\,B(\boldsymbol{\chi})/B(\mathbf{k}), \tag{3.12}$$

where
$$B(\mathbf{k})=\exp\left\{-\nu T\left(k_1^2-\frac{1}{\alpha}k_2^2-\frac{1}{1-\alpha}k_3^2\right)\right\}. \tag{3.13}$$

The function $\Omega_{ij}^{(0)}(\boldsymbol{\chi})$ can be obtained since $\Omega_{ij}(\mathbf{k},c)$ is known at the initial instant, $c=1$. The form for $\Phi_{ij}(\mathbf{k},c)$ follows from relation (3.7). The intermediate solution (3.11) is just the one obtained by B & P.

For a general initial vorticity spectrum function, given by $\Omega_{ij}^{(0)}(\boldsymbol{\chi})$, the three mean square turbulent intensities, given by

$$\overline{u_1^2}=\iiint\Phi_{11}(\mathbf{k},c)\,d\mathbf{k},$$
$$\overline{u_2^2}=\iiint\Phi_{22}(\mathbf{k},c)\,d\mathbf{k}$$

and
$$\overline{u_3^2}=\iiint\Phi_{33}(\mathbf{k},c)\,d\mathbf{k},$$

can in principle be evaluated for all values of c thus providing a measure both of the absolute growth or decay of the turbulent intensity and of its relative orientation.

The form of the solution for the asymptotic limit $c \to \infty$ will now be considered, since this may be taken to indicate the long-term effect of the straining motion on the turbulence. It also allows the integrals to be simplified sufficiently for certain general results to be derived.

It proves convenient to discuss the following distortions separately:

(A) $0 < \alpha \leqslant \frac{1}{2}$; two principal axes of contraction.

(B) $\alpha = 0$; 'constant area' deformation.

(C) $-1 \leqslant \alpha < 0$; two principal axes of expansion.

The calculations involved in arriving at the asymptotic limits given below are not included in detail since they are very largely straightforward. However, reference will be made to those points in the calculation at which particular properties—derived from the continuity condition or the equations of motion—of the initial spectrum function are employed.

(A) $0 < \alpha < \frac{1}{2}$. (The case $\alpha = \frac{1}{2}$ is similar but requires slightly more elaborate treatment.)

$$\begin{aligned}\operatorname*{Lt}_{c\to\infty} \overline{u_1^2} &= \operatorname*{Lt}_{c\to\infty} \iiint \Phi_{11}(\mathbf{k}, c)\, d\mathbf{k} \\ &= -\int_{-\infty}^{\infty}\int_{-\infty}^{\infty}\int_{-\infty}^{\infty} \frac{l_1^2}{\{(l_1^2/c^2)+l_2^2+l_3^2\}} \frac{\Omega_{11}^{(0)}(l_1, c^{-\alpha}l_2, c^{\alpha-1}l_3)}{c} \\ &\qquad \times \exp\left\{-\nu T\left(l_1^2+\frac{l_2^2}{\alpha}+\frac{l_3^2}{1-\alpha}\right)\right\} dl_1\, dl_2\, dl_3 + \text{smaller terms},\end{aligned}$$

from (3.12), (3.13) and (3.7), where $\mathbf{l}$ is a variable of integration related linearly to $\mathbf{k}$.

Before we can further simplify this expression we must make use of the result that

$$\Omega_{11}^{(0)}(l_1, 0, 0) \equiv 0. \tag{3.14}$$

[See Batchelor (1953), p. 28.] If we suppose that the function $\Omega_{11}^{(0)}(l_1, c^{-\alpha}l_2, c^{1-\alpha}l_3)$ can be expanded in the form*

$$\Omega_{11}^{(0)}(l_1, c^{-\alpha}l_2, c^{1-\alpha}l_3) = \tfrac{1}{2}c^{-2\alpha}l_2^2 \frac{\partial^2\Omega_{11}^{(0)}}{\partial k_2^2}(l_1, 0, 0) + \tfrac{1}{2}c^{2\alpha-2}l_3^2 \frac{\partial^2\Omega_{11}^{(0)}}{\partial k_3^2}(l_1, 0, 0) + \text{smaller terms}, \tag{3.15}$$

the lower order terms not being present because of (3.14) or because of the conditions of symmetry that must be satisfied by the spectrum function, then we may write

$$\begin{aligned}\overline{u_1^2} &\to -\iiint_{-\infty}^{\infty} \frac{c^{-1-2\alpha}l_1^2 l_2^2}{2\{(l_1^2/c^2)+l_2^2+l_3^2\}^2} \frac{\partial^2\Omega_{11}^{(0)}}{\partial k_2^2}(l_1, 0, 0) \exp\left\{-\nu T\left(l_1^2+\frac{l_2^2}{\alpha}+\frac{l_3^2}{1-\alpha}\right)\right\} dl_1\, dl_2\, dl_3 \\ &\qquad + O(c^{-1-2\alpha}\ln c) \\ &\to -\frac{\pi}{4}\iint_{-\infty}^{\infty} c^{-1-2\alpha} \frac{l_1^2 l_2^2}{\{(l_1^2/c^2)+l_2^2\}^{\frac{3}{2}}} \frac{\partial^2\Omega_{11}^{(0)}}{\partial k_2^2} \exp\left\{-\nu T\left(l_1^2+\frac{l_2^2}{\alpha}\right)\right\} dl_1\, dl_2 + O(c^{-1-2\alpha}\ln c) \\ &\to O(c^{-1-2\alpha}\ln c).\end{aligned} \tag{3.16}$$

* This form is certainly valid near the origin in l-space—where difficulties might otherwise be expected—using Batchelor & Proudman (1956), equation (5.31).

† $\dfrac{\partial^2\Omega_{11}^{(0)}}{\partial k_2^2}(l_1, 0, 0)$ denotes $\dfrac{\partial^2\Omega_{11}^{(0)}(\mathbf{k})}{\partial k_2^2}$ evaluated at $(l_1, 0, 0)$.

In a similar fashion we find that

$$\overline{u_2^2} \to \iiint_{-\infty}^{\infty} \frac{c^{-1-2\alpha}}{2} \frac{(l_1^2+c^2l_3^2)\,l_2^2}{\{(l_1^2/c^2)+l_2^2+l_3^2\}^2} \frac{\partial^2\Omega_{11}^{(0)}}{\partial k_2^2}(l_1,0,0) \times \exp\left\{-\nu T\left(l_1^2+\frac{l_2^2}{\alpha}+\frac{l_3^2}{1-\alpha}\right)\right\} dl_1\,dl_2\,dl_3 + \text{smaller terms}$$

$$\to \frac{\pi\alpha}{4\nu T} c^{1-2\alpha} \int_{-\infty}^{\infty} \frac{\partial^2\Omega_{11}^{(0)}}{\partial k_2^2}(l_1,0,0)\, e^{-\nu T l_1^2} dl_1 + \text{smaller terms}, \tag{3.17}$$

and that

$$\overline{u_3^2} \to \iiint_{-\infty}^{\infty} \frac{c^{-1-2\alpha}}{2} \frac{(l_1^2+c^2l_2^2)\,l_2^2}{\{(l_1^2/c^2)+l_2^2+l_3^2\}^2} \frac{\partial^2\Omega_{11}^{(0)}}{\partial k_2^2}(l_1,0,0) \times \exp\left\{-\nu T\left(l_1^2+\frac{l_2^2}{\alpha}+\frac{l_3^2}{1-\alpha}\right)\right\} dl_1\,dl_2\,dl_3$$

$$\to \frac{\pi\alpha}{4\nu T} c^{1-2\alpha} \int_{-\infty}^{\infty} \frac{\partial^2\Omega_{11}^{(0)}}{\partial k_2^2}(l_1,0,0)\, e^{-\nu T l_1^2} dl_1 + \text{smaller terms}. \tag{3.18}$$

We see then that the total kinetic energy behaves as $c^{1-2\alpha}$—which may be written $c^{1-\alpha}/c^{\alpha}$, that is, as the ratio of the larger contraction to the smaller contraction—and that it becomes wholly oriented axisymmetrically in the plane perpendicular to the principal axis of expansion. The asymptotic limits (3.17) and (3.18) for $\overline{u_2^2}$ and $\overline{u_3^2}$ have been expressed in terms of an integral parameter

$$\int_{-\infty}^{\infty} \frac{\partial^2\Omega_{11}^{(0)}}{\partial k_2^2}(l_1,0,0)\, e^{-\nu T l_1^2} dl_1$$

which may be assumed known if the initial turbulence is completely specified.

The case $\alpha = \frac{1}{2}$ leads to the corresponding results

$$\overline{u_1^2} \to O(c^{-2}\ln c), \tag{3.16'}$$

$$\overline{u_2^2}, \overline{u_3^2} \to \frac{\pi}{4\nu T} \int_0^{\infty} \frac{\partial^2\Omega_{11}^{(0)}}{\partial k_2^2}(l_1,0,0)\, e^{-\nu T l_1^2} dl_1 \tag{3.17'–3.18'}$$

which is a constant, since

$$\frac{\partial^2\Omega_{11}^{(0)}}{\partial k_2^2}(l_1,0,\mathbf{0}) \equiv \frac{\partial^2\Omega_{11}^{(0)}}{\partial k_3^2}(l_1,0,0).$$

(B) $\alpha = 0$.

We find that

$$\overline{u_1^2} \to O(c^{-1}\ln c), \tag{3.19}$$

$$\overline{u_2^2} \to \iiint_{-\infty}^{\infty} \frac{(l_1^2+c^2l_3^2)\,\Omega_{11}^{(0)}(l_1, l_2(2\ln c)^{-\frac{1}{2}}, 0)}{\left(\frac{l_1^2}{c^2}+\frac{l_2^2}{2\ln c}+l_3^2\right)^2} \frac{\exp\{-\nu T(l_1^2+l_2^2+l_3^2)\}}{c(2\ln c)^{\frac{1}{2}}} dl_1\,dl_2\,dl_3$$

$$\to \frac{\pi}{8\nu T}\frac{c}{\ln c} \int_{-\infty}^{\infty} \frac{\partial^2\Omega_{11}^{(0)}}{\partial k_2^2}(l_1,0,0)\, e^{-\nu T l_1^2} dl_1, \tag{3.20}$$

$$\overline{u_3^2} \to \iiint_{-\infty}^{\infty} \frac{(l_1^2+c^2(2\ln c)^{-1}l_2^2)\,\Omega_{11}^{(0)}(l_1, l_2(2\ln c)^{-\frac{1}{2}}, 0)}{\left(\frac{l_1^2}{c^2}+\frac{l_2^2}{2\ln c}+l_3^2\right)^2} \frac{\exp\{-\nu T(l_1^2+l_2^2+l_3^2)\}}{c(2\ln c)^{\frac{1}{2}}} dl_1\,dl_2\,dl_3$$

$$\to \frac{\pi}{8\nu T}\frac{c}{\ln c} \int_{-\infty}^{\infty} \frac{\partial^2\Omega_{11}^{(0)}}{\partial k_2^2}(l_1,0,0)\, e^{-\nu T l_1^2} dl_1. \tag{3.21}$$

The asymptotic limits (3.20) and (3.21) that are $O(c(\ln c)^{-1})$ do not in fact constitute a discontinuity in behaviour of $\overline{u_2^2}$, $\overline{u_3^2}$ at $\alpha = 0$ because of the factor α in (3.17) and (3.18) [and a similar disguised factor in (3.23) and (3.24) below].

(C) $-1 < \alpha < 0$. [The case $\alpha = -1$ is similar, but, like the case $\alpha = \frac{1}{2}$, it requires slightly more elaborate treatment.]

Again using the relations (3.12), (3.13) and (3.7) we obtain the limits

$$\overline{u_1^2} \to \iiint_{-\infty}^{\infty} \frac{(l_2^2 + c^{-2\alpha} l_3^2)\,\Omega_{22}^{(0)}(l_1, l_2, 0) - l_1^2\,\Omega_{11}^{(0)}(l_1, l_2, 0)}{\left(\dfrac{l_1^2}{c^2} + \dfrac{l_2^2}{c^{-2\alpha}} + l_3^2\right)^2} \times \frac{\exp\left\{-\nu T\left(l_1^2 + \dfrac{l_2^2}{-\alpha} + \dfrac{l_3^2}{1-\alpha}\right)\right\}}{c^{1-\alpha}}\, dl_1\, dl_2\, dl_3 = O(c^{-2\alpha-1} \ln c^{1+\alpha}), \quad (3.22)$$

$$\overline{u_2^2} \to \iiint_{-\infty}^{\infty} \frac{l_3^2\,\Omega_{11}^{(0)}(l_1, l_2, 0)}{\left(\dfrac{l_1^2}{c^2} + \dfrac{l_2^2}{c^{-2\alpha}} + l_3^2\right)^2} \exp\left\{-\nu T\left(l_1^2 + \frac{l_2^2}{-\alpha} + \frac{l_3^2}{1-\alpha}\right)\right\} c^{1+\alpha}\, dl_1\, dl_2\, dl_3$$

$$\to \frac{\pi}{2} c \iint_{-\infty}^{\infty} \frac{\Omega_{11}^{(0)}(l_1, l_2, 0)}{|l_2|} \exp\left\{-\nu T\left(l_1^2 + \frac{l_2^2}{-\alpha}\right)\right\} dl_1\, dl_2, \quad (3.23)$$

and an identical asymptotic expression for $\overline{u_3^2}$. The relevant integral parameter that appears in (3.23) is not so simple as the one obtained in (3.17) and (3.18). The convergence of the integral is assured because of the l_2^2 behaviour of $\Omega_{11}^{(0)}$ near $l_2 = 0$ as given by (2.15). We see that the total kinetic energy grows as c and that once again it becomes oriented axisymmetrically in the plane perpendicular to the axis of greatest expansion. For $\alpha \leqslant -\frac{1}{2}$ the mean square component $\overline{u_1^2}$ does increase as $c \to \infty$, whereas for $\alpha > -\frac{1}{2}$, it tends asymptotically to zero.

The case $\alpha = -1$ leads to the solution

$$\left.\begin{aligned}
\overline{u_1^2} &\to \frac{\pi}{2} c \iint_{-\infty}^{\infty} \left[\frac{l_2^2\,\Omega_{22}^{(0)} - l_1^2\,\Omega_{11}^{(0)}}{(l_1^2 + l_2^2)^{\frac{3}{2}}} + \frac{\Omega_{22}^{(0)}}{(l_1^2 + l_2^2)^{\frac{1}{2}}}\right] \exp\{-\nu T(l_1^2 + l_2^2)\}\, dl_1\, dl_2, \\
\overline{u_2^2} &\to \frac{\pi}{2} c \iint_{-\infty}^{\infty} \left[\frac{l_1^2\,\Omega_{11}^{(0)} - l_2^2\,\Omega_{22}^{(0)}}{(l_1^2 + l_2^2)^{\frac{3}{2}}} + \frac{\Omega_{11}^{(0)}}{(l_1^2 + l_2^2)^{\frac{1}{2}}}\right] \exp\{-\nu T(l_1^2 + l_2^2)\}\, dl_1\, dl_2, \\
\overline{u_3^2} &\to \frac{\pi}{2} c \iint_{-\infty}^{\infty} \left[\frac{\Omega_{11}^{(0)} + \Omega_{22}^{(0)}}{(l_1^2 + l_2^2)^{\frac{1}{2}}}\right] \exp\{-\nu T(l_1^2 + l_2^2)\}\, dl_1\, dl_2,
\end{aligned}\right\} \quad (3.24)$$

in which all components grow at the same relative rate. The results (3.16) to (3.24) can be expressed concisely by plotting the asymptotic form for the total kinetic energy, $\overline{u_1^2} + \overline{u_2^2} + \overline{u_3^2}$, expressed as a power of c, the expansion ratio, against the geometrical parameter α. In figure 1 we plot γ against α, where γ is given by the relation:

$$\text{Total kinetic energy} \propto c^{\gamma}.$$

The point $\alpha = 0$ is special in that

$$\text{Total kinetic energy} \propto c(\ln c)^{-1},$$

but as has been explained above this is only an apparent singularity in behaviour.

The results can be further simplified in the case of initially isotropic turbulence, for the tensor spectrum functions can then be expressed in terms of an energy spectrum function $E(k)$, which is such that

$$\Omega_{ij}^{(0)}(\boldsymbol{\chi}) = \frac{E(\chi)}{4\pi\chi^2}(\chi^2\delta_{ij} - \chi_i\chi_j). \tag{3.25}$$

For $0 < \alpha < \frac{1}{2}$

$$\overline{u_2^2}, \overline{u_3^2} \to \frac{\alpha}{4\nu T} c^{1-2\alpha} \int_0^\infty \frac{E(l)}{l^2} e^{-\nu T l^2} dl. \tag{3.26}$$

For $\alpha = \frac{1}{2}$

$$\overline{u_2^2}, \overline{u_3^2} \to \frac{1}{8\nu T} \int_0^\infty \frac{E(l)}{l^2} e^{-\nu T l^2} dl. \tag{3.27}$$

For $\alpha = 0$

$$\overline{u_2^2}, \overline{u_3^2} \to \frac{1}{8\nu T} \frac{c}{\ln c} \int_0^\infty \frac{E(l)}{l^2} e^{-\nu T l^2} dl. \tag{3.28}$$

For $-1 < \alpha < 0$

$$\begin{aligned} \overline{u_2^2}, \overline{u_3^2} &\to \frac{c}{2} \iint_0^\infty \frac{l_2 E[(l_1^2 + l_2^2)^{\frac{1}{2}}]}{l_1^2 + l_2^2} \exp\left\{-\nu T\left(l_1^2 + \frac{l_2^2}{\alpha}\right)\right\} dl_1 dl_2 \\ &= \frac{c}{2} \sqrt{\left\{\frac{-\alpha}{\nu T(1+\alpha)}\right\}} \int_0^\infty \frac{E(l)}{l} e^{-\nu T l^2/\alpha} \int_0^{\sqrt{\left\{\frac{\nu T(1+\alpha)}{-\alpha}\right\}} l} e^{y^2} dy\, dl. \end{aligned} \tag{3.29}$$

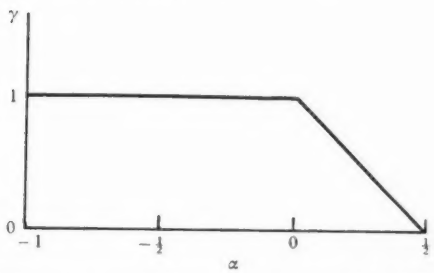

FIGURE 1. Growth of kinetic energy expressed as a power, γ, of the expansion ratio *vs* α.

For $\alpha = -1$

$$\overline{u_1^2}, \overline{u_2^2}, \tfrac{1}{2}\overline{u_3^2} \to \frac{\pi}{8} c \int_0^\infty E(l)\, e^{-\nu T l^2} dl. \tag{3.30}$$

Additional information concerning the orientation that is induced in the turbulence as $c \to \infty$ can be derived by considering the asymptotic form of the vorticity spectrum (3.12). This is such that the dominant term $\Omega_{11}(\mathbf{k}, c)$ is appreciable only when

$$k_1 \to 0 \quad \text{for} \quad \alpha > 0,$$
$$k_1, k_2 \to 0 \quad \text{for} \quad \alpha \leqslant 0.$$

By carrying out the Fourier transformations required to interpret this result in co-ordinate space we find that covariances become, in the limit, independent of separation in the r_1 direction for $\alpha > 0$, and independent of separation in both the r_1 and r_2 directions for $\alpha \leqslant 0$. Thus for $\alpha > 0$ we may say that the turbulence is

truly two-dimensional, since the $\overline{u_1^2}$ component of intensity tends to zero (see (3.16)); for $-\frac{1}{2} < \alpha \leqslant 0$, the turbulence is not only two-dimensional, but covariances are functions of one space variable only, $\overline{u_1^2}$ still tending to zero (see (3.22)); for $-1 < \alpha \leqslant -\frac{1}{2}$ only the ratio $\overline{u_1^2}/\overline{u_2^2}$ tends to zero, and the result is a little weaker; for $\alpha = -1$ the turbulent intensity ceases to be oriented in a plane, though covariances remain functions of one space variable only.

The limiting structure of the velocity spectrum as $c \to \infty$ can also be stated. For the case $\alpha > 0$, we find that the dominant contribution tends to the form

$$\Phi_{ij}(\mathbf{k}, c) \to c^{2-2\alpha}\epsilon_{1im}\epsilon_{1jn}\frac{k_m k_n k_2^2}{(k_2^2+k_3^2)^2}\frac{\partial^2\Omega_{11}^{(0)}}{\partial k_2^2}(ck_1, 0, 0)\exp\left\{-\nu T\left(c^2k_1^2+\frac{k_2^2}{\alpha}+\frac{k_3^2}{1-\alpha}\right)\right\}.$$

Without attempting a rigorous definition, we may say that the spectrum function tends to a universal form where the integral parameter

$$\int_{-\infty}^{\infty}\frac{\partial^2\Omega_{11}^{(0)}}{\partial k_2^2}(k_1, 0, 0)\, e^{-\nu T k_1^2}\, dk_1$$

is all that remains of the initial turbulent distribution.

For the case $\alpha < 0$, the asymptotic structure cannot be so neatly expressed. It is

$$\Phi_{ij}(\mathbf{k}, c) \to c^2\epsilon_{1im}\epsilon_{1jn}\frac{k_m k_n + \delta_{mn}k_1^2}{k^4}\Omega_{11}^{(0)}(ck_1, c^{-\alpha}k_2, 0)$$
$$\times\exp\left\{-\nu T\left(c^2k_1^2+\frac{c^{-2\alpha}k_2^2}{-\alpha}+\frac{k_3^2}{1-\alpha}\right)\right\}.$$

Since this takes its dominant values for k_1, k_2 and k_3 all tending to zero, a highly singular structure is approached. It is universal only in so far as energy is concentrated at zero wave-number.

4. Axisymmetric extension of an initially isotropic turbulent field in its final period of decay

In the previous section, attention has been concentrated on the asymptotic limit that applies as $c \to \infty$. We shall now consider the time-dependent solution for a particular case as an example of the way in which the asymptotic limit is approached. For simplicity we take the initial turbulence to be isotropic, and because our conditions refer specifically to weak turbulent fields we take the turbulence to be in its final period of decay. This may be described by the energy spectrum*

$$E(k) = k^4 e^{-k^2/k_0^2}, \tag{4.1}$$

where

$$\Phi_{ij}(\mathbf{k}, 0) = \frac{E(k)}{4\pi k^4}(k^2\delta_{ij} - k_i k_j), \tag{4.2}$$

and k_0 is a characteristic wave-number.

We choose the case of axisymmetric distortion, for which $\alpha = \frac{1}{2}$, as our straining field. This will lead to a finite asymptotic solution for the total kinetic energy and

* See Batchelor (1953) and the subsequent paper Batchelor & Proudman (1956).

can be compared with the sudden strain solution given by B & P. We shall calculate, as suitable defining characteristics of the turbulent field, the ratios

$$\mu_1 = \frac{\overline{u_1^2(t)}}{\overline{u_1^2(0)}} = \frac{\int \Phi_{11}(\mathbf{k},t)\,d\mathbf{k}}{\int \Phi_{11}(\mathbf{k},0)\,d\mathbf{k}} \tag{4.3}$$

and

$$\mu_2 = \frac{\overline{u_2^2(t)+u_3^2(t)}}{\overline{u_2^2(0)+u_3^2(0)}} = \frac{\int \Phi_{22}(\mathbf{k},t)+\Phi_{33}(\mathbf{k},t)\,d\mathbf{k}}{\int \Phi_{22}(\mathbf{k},0)+\Phi_{33}(\mathbf{k},0)\,d\mathbf{k}}. \tag{4.4}$$

From (3.7), (3.12) and (3.13) we have that

$$\Phi_{11}(\mathbf{k},t) = \frac{(\chi_2^2+\chi_3^2)\,E(\chi)}{4\pi k^4} \exp\left[-\nu T\{(\chi_1^2-k_1^2)-2(\chi_2^2-k_2^2)-2(\chi_3^2-k_3^2)\}\right], \tag{4.5}$$

$$\Phi_{22}(\mathbf{k},t)+\Phi_{33}(\mathbf{k},t) = \left(\frac{c}{\chi^2}+\frac{\chi_1^2}{k^4c^3}\right)\frac{E(\chi)}{4\pi} \times \exp\left[-\nu T\{(\chi_1^2-k_1^2)-2(\chi_2^2-k_2^2)-2(\chi_3^2-k_3^2)\}\right], \tag{4.6}$$

where

$$\chi^2 = \chi_1^2+\chi_2^2+\chi_3^2 \tag{4.7}$$

and

$$(\chi_1,\chi_2,\chi_3) = (ck_1, c^{-\frac{1}{2}}k_2, c^{-\frac{1}{2}}k_3). \tag{4.8}$$

On substituting (4.5) and (4.6) into (4.3) and (4.4) and after slight simplification we find that μ_1 and μ_2 may be written

$$\mu_1 = \frac{3}{4c^2}\int_{-1}^{1} \frac{(1-x^2)\,dx}{\{1-(1-c^{-3})\,x^2\}^2\{[1+2(c-1)\,\tau]+\tau(3-2c-c^{-2})\,x^2\}^{\frac{5}{2}}}, \tag{4.9}$$

$$\mu_2 = \tfrac{3}{8}c\int_{-1}^{1}\left[1+\frac{x^2}{c^6\{1-(1-c^{-3})\,x^2\}^2}\right]\frac{dx}{\{[1+2(c-1)\,\tau]+\tau(3-2c-c^{-2})\,x^2\}^{\frac{5}{2}}}, \tag{4.10}$$

where

$$\tau = \nu T k_0^2. \tag{4.11}$$

τ may be regarded as an inverse Reynolds number where the length scale, k_0^{-1}, is derived from the characteristic length scale of the initial turbulent spectrum, and the time scale, T, is derived from the mean rate of strain. It will be observed that the integrals (4.9) and (4.10) for μ_1 and μ_2 are functions of c and τ only. These integrals have been evaluated exactly and are displayed in graphical form in figures 2–5 for $\tau = 1, 0{\cdot}25, 0{\cdot}1, 0{\cdot}05$, as continuous functions of c. (Using the relation (3.2), these can readily be converted into relations between μ_1 (or μ_2) and time, t.) Also included are the relevant curves for $\mu_1(t)$, $\mu_2(t)$ that would apply in the absence of distortion; interpreted for convenience as $\mu_1'(c)$, $\mu_2'(c)$, these provide a measure of the relative action of viscosity in the absence of mean strain and are calculated from the relation

$$\mu_1' = \mu_2' = \frac{1}{(1+2\nu k_0^2 t)^{\frac{5}{2}}} = \frac{1}{(1+2\tau\ln c)^{\frac{5}{2}}}, \tag{4.12}$$

which is readily derived. The sudden strain approximation of B & P is of course the limiting case that applies when $\tau \to 0$.

We may also derive from (4.9) and (4.10) the asymptotic limits, as $c \to \infty$, $(\tau \neq 0)$,

$$\mu_{1\infty} \to \frac{3}{2(1+\tau)^{\frac{3}{2}}} \frac{\ln c}{c^2}, \tag{4.13}$$

$$\mu_{2\infty} \to \frac{1}{8\tau(1+\tau)^{\frac{3}{2}}}. \tag{4.14}$$

These correspond to the results (3.16′), (3.17′–3.18′) obtained earlier, and of course (4.14) may be obtained directly from the latter result. In general terms we see that $\overline{u_1^2}$ decays more rapidly than it would in the absence of mean strain, while $\overline{u_2^2}+\overline{u_3^2}$ approaches a steady state in which the rate of growth due to straining is exactly balanced by the viscous decay.

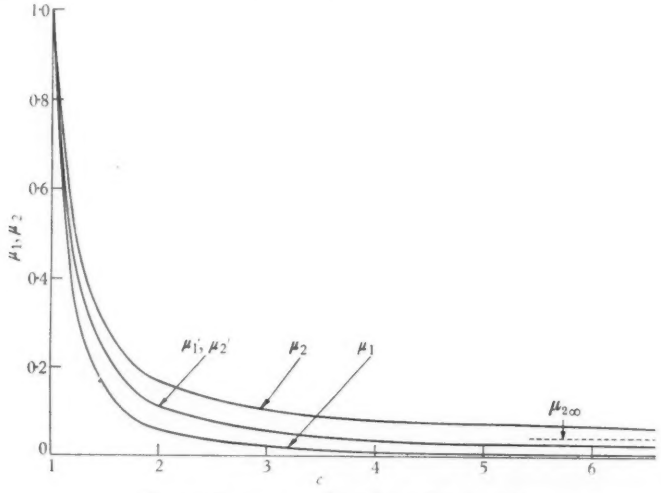

FIGURE 2. μ_1, μ_2 as functions of c; $\tau = 1$.

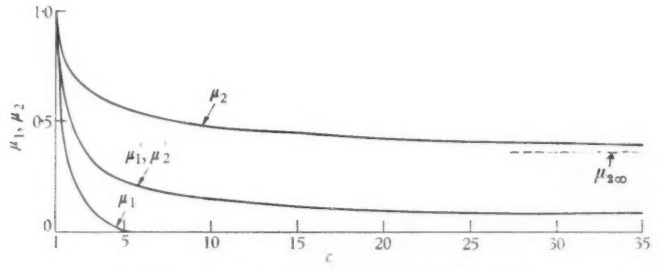

FIGURE 3. μ_1, μ_2 as functions of c; $\tau = 0{\cdot}25$.

5. Discussion

From the linearized treatment of strained turbulence given above and in particular from a consideration of the asymptotic behaviour as $c \to \infty$ (see § 3) it seems clear that in a general irrotational strain a balance cannot be achieved

between interaction and viscous terms alone. The total energy associated with the turbulent components grows indefinitely and, as has been pointed out earlier, must ultimately reach the state at which non-linear turbulent effects are appreciable. This aspect of the problem is treated in some detail by Townsend (1956), Chap. 4, who considers the equilibrium structure attained by the turbulence when it is subjected to just the type of irrotational distortion represented by (3.1). [From an experimental point of view, irrotational distortions are the only

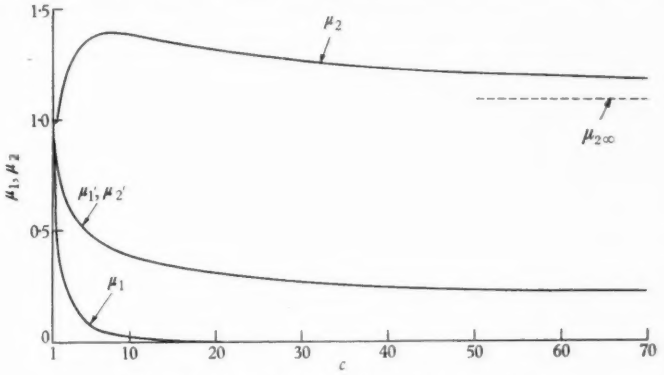

FIGURE 4. μ_1, μ_2 as functions of c; $\tau = 0{\cdot}1$.

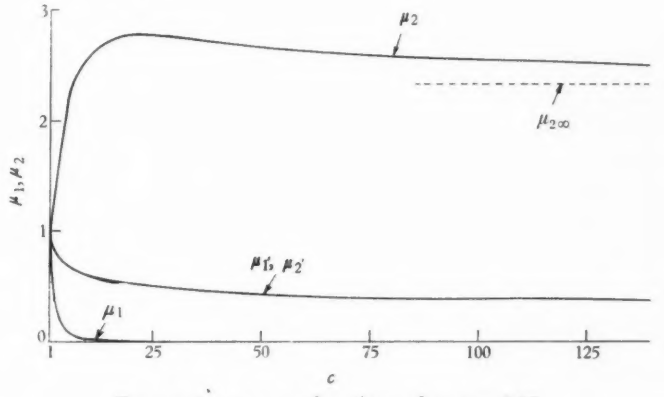

FIGURE 5. μ_1, μ_2 as functions of c; $\tau = 0{\cdot}05$.

type that can be set up instantaneously and so the restriction on generality that has been accepted above for reasons of expediency finds some justification in physical circumstances.] It had been hoped, when this work was started, to include inertial effects in the dynamical treatment, in the manner of P & R, and to use the non-inertial solution obtained in § 3 as a first approximation (from the point of view of structure) to the problem of maintained shear flow turbulence. However, despite the simplifications achieved by considering the turbulence to be two-dimensional, as described at the end of § 3, a dynamical treatment including non-linear terms proved to be virtually intractable.

A more particular application of the linearized solution is suggested by Ribner & Tucker (1952) who summarize certain experimental evidence concerning wind-tunnel turbulence. This refers to the reduction in relative energy of the residual turbulence that persists after screening when the air stream is passed through a rapid contraction. Although the analysis has not been given here it is a relatively simple matter to extend the solution (3.12) to cover the case there C_{ij} is a function of time; it may be supposed that a small element of fluid is subjected as it passes through the contraction to a time varying, but instantaneously uniform, contraction corresponding to the local value for the contraction at its particular station within the wind-tunnel. In this way the behaviour of the low energy turbulent field entering the contraction may be followed through the contraction, account being taken of viscosity as well as of local strain.

However, the calculations involved in an exact analysis would be formidable and the only practicable method would be to employ an approximate solution based on the treatment given in §4 as a crude model. A consideration of the Reynolds number for the turbulence entering the wind-tunnel contraction—based on the integral length scale and the root mean square intensity—for the cases quoted by Ribner & Tucker [11 in the case of McPhail (1944) and 7 in the case of Hall (1938)] shows that the hypothesis of initially weak turbulence is not unreasonable; for the experiments of Batchelor & Townsend (1948) show that the final period of decay is reached at a Reynolds number—based on the dissipation length scale—of about 5. What the results of §3 show is that an axisymmetric contraction is probably the most effective type of contraction for reducing the relative turbulent intensity.

The author wishes to thank Dr I. Proudman both for his suggestion of an Eulerian treatment of uniformly distorted homogeneous turbulence and for his continued encouragement and advice without which this paper, albeit no more than the residue from a more ambitious yet unsuccessful investigation, would never have been prepared. He also wishes to thank Dr G. K. Batchelor for several trenchant comments.

REFERENCES

Batchelor, G. K. 1953 *The Theory of Homogeneous Turbulence*. Cambridge University Press.

Batchelor, G. K. & Proudman, I. 1954 *Quart. J. Mech. Appl. Math.* **7**, 83.

Batchelor, G. K. & Proudman, I. 1956 *Phil. Trans.* A, **248**, 369.

Batchelor, G. K. & Townsend, A. A. 1948 *Proc. Roy. Soc.* A, **194**, 527.

Hall, A. A. 1938 *A.R.C. Tech. Report* no. 1842.

McPhail, D. C. 1944 *R.A.E. Report* no. Aero 1928.

Proudman, I. & Reid, W. H. 1954 *Phil. Trans.* A, **247**, 163.

Ribner, H. S. & Tucker, M. 1952 *N.A.C.A. Tech. Note* 2606.

Townsend, A. A. 1956 *The Structure of Turbulent Shear Flow*. Cambridge University Press.

One-dimensional flow of an ionized gas through a magnetic field

By R. M. PATRICK AND T. R. BROGAN
AVCO Research Laboratory, Everett, Massachusetts

(Received 11 July 1958)

As a primary step towards understanding the flow of a partially ionized gas in a magnetic field, we have studied both theoretically and experimentally the problem in which the gas flow is one-dimensional. This simplification permits a detailed calculation of the flow field and a quantitative comparison of the theory with observations made in a shock tube.

An ionized gas is composed of three species: electrons, ions and neutral particles. To take complete account of all the phenomena occurring when the high-velocity gas interacts with the magnetic field, the motion of all three species must be considered. When this is done, it is found that the electrical conductivity of the gas is a tensor dependent on both the magnitude and geometry of the magnetic field. However, when the collision frequency for the electrons is greater than their cyclotron frequency in a magnetic field, the gas may be treated as a continuum with a scalar conductivity. For such gas states, all of the observed effects for two experimental geometries in which the gas current forms closed loops in the magnetic field can be explained with a simple theory. The interaction produces a flow completely analogous to pipe flow with friction and no heat transfer, where the wall friction force is replaced by the magnetic body force which can choke the flow if the body forces are larger than a certain minimum value.

Using the same experimental geometries, the gas state is then adjusted so that the electrical conductivity is a tensor. Outstanding among the observed effects are ion slip, where the ions and neutrals travel through the field at different velocities, and Hall currents, generated by the drift of the charged particles across magnetic field lines. The observed effects again agree with the predicted values.

Introduction

This paper reports the results of a study of the one-dimensional flow of partially ionized argon through a magnetic field. The ionized argon is produced using the shock-tube technique described by Resler, Lin & Kantrowitz (1952). Argon was, chosen as a working fluid for two reasons. First, its properties at high temperature have been studied extensively in work by Resler *et al.* (1952), Lin, Resler & Kantrowitz (1955), Petschek, Rose, Glick, Kane & Kantrowitz (1955) and Petschek & Byron (1957). Second, the electrical conductivity which can be produced by strong shock waves in a shock tube is large (up to 10^4 mho/m) in comparison with other gases. This latter property permits appreciable inter-

actions between the moving gas and a magnetic field in dimensions appropriate to a shock-tube experiment.

In the experiments reported here, the gas has a component of velocity perpendicular to an externally applied magnetic field. This motion induces an electromotive force which in turn generates currents in the gas. The magnetic fields due to these induced currents are small compared to the applied fields, i.e. the magnetic Reynolds number R_m is much less than unity. Here, $R_m = \mu_0 \sigma v l$, where σ is the electrical conductivity of the gas, v the gas velocity perpendicular to the field, μ_0 the permittivity of free space and l the characteristic length of the interaction.

The energy transfer between the moving gas and the surroundings is negligible for these experiments. This implies that the gas currents form closed loops, with no part of their circuit external to the gas. The experimental geometries will be arranged so that the gas currents flow in a nearly uniform magnetic field and the current density j in the gas is given by $j = \sigma v B$, where B is the strength of the applied magnetic field.

If the Mach number M_1 of a shock wave and the initial pressure p_1 of the gas through which it is propagating are known, all the gas properties behind the shock are determined. Throughout this paper, these two parameters will be used to specify the gas conditions at the entrance to the magnetic field.

The experiments were carried out in two shock-tube geometries which will be called respectively the annular experiment and the end experiment. In the annular experiment, the channel area is constant. For the end experiment the channel area varies linearly in the flow direction, but the magnetic field is more uniform than in the annular experiment, and steady flow persists for a longer time. Also, the end experiment covers a larger range of variation of the experimental parameters than the annular experiment.

The electrical conductivity of a gas is influenced by a magnetic field. The conductivity at low field strength is a scalar quantity. For argon, the limiting conductivity at zero magnetic field was measured by Lin *et al.* (1955). As the magnetic field strength is increased, the conductivity becomes a tensor dependent on both the magnitude and geometry of the applied field. These latter effects have been considered by Schluter (1950, 1951). A measure of the extent to which the magnetic field influences the gas conductivity is given by the magnitude of the parameter $\omega_e \tau_e$, where ω_e is the cyclotron frequency of an electron in a magnetic field with strength B, and τ_e is the average time between collisions for an electron. As $\omega_e \tau_e$ approaches unity, the magnetic field begins to affect the gas conductivity in a significant manner.

For all of the conditions with which this paper is concerned, the flow Mach number of the gas entering the field exceeds unity. Therefore, the most important force exerted by the gas is its dynamic pressure $\frac{1}{2}\rho v^2$, where ρ is the gas density. To influence the motion of the gas in an important way, the force due to the interaction of the gas with the magnetic field must be of the order of the dynamic pressure. The precise conditions needed to produce such a situation are discussed in §II of this paper. To obtain a good estimate of the effects to be expected, we note that the gas current $j = \sigma v B$ interacting with the applied field B produces

a body force $F = \sigma v B^2$. If now the interaction extends over a length l, the pressure difference across the interaction region is $\Delta p = Fl = \sigma v B^2 l$. The extent to which the interaction has disturbed the flow is given by the ratio $\Delta p / \frac{1}{2}\rho v^2$. For an appreciable interaction, we have

$$\frac{\sigma B^2 l}{\rho v} \doteqdot \frac{1}{2}.$$

When the above condition is satisfied in the experiments, the supersonic flow entering the magnetic field is decelerated enough to cause choking and the formation of standing shock waves in the magnetic field.

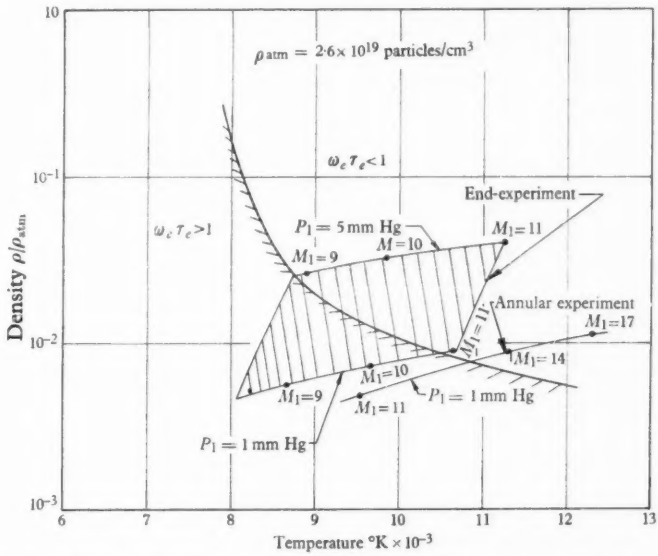

FIGURE 1. The density in atmospheres *vs* the temperature obtained in the experiments at the upstream end of the magnetic field.

Figure 1 shows the gas conditions at the upstream end of the magnetic field for both the experiments to be described in the next section. In the annular experiment, the initial pressure p_1 was held constant at 1 mm of mercury, so that the single line at the lower right corner of the figure gives the initial conditions for this experiment. Several different initial pressures were used for the end experiment. The resulting conditions are represented by the shaded area. On the line running from top left to lower right corners, $\omega_e \tau_e = 1$; the magnetic field B used to calculate ω_e is such that the interaction pressure equals the dynamic pressure of the moving gas with $l = 1$ cm. To the left of this line, the electrical conductivity of the gas is affected to a large extent by the magnetic field; to the right, it is largely unaffected.

In the next section, the experiments, technique and measurements are described. The final section is a development of the theory necessary to explain the experimental results.

I. Description of experiments

1. Annular experiment

The first of two experiments designed to study the flow of an ionized gas in a magnetic field is designated as the annular experiment. An overall sketch of the experimental arrangement is shown in figure 2. The shock tube is divided into two parts; that part to the left of the diaphragm contains argon at room temperature and at a pressure p_1 of 1 mm; that part to the right of the diaphragm (the driver) is filled with a combustible mixture at high pressure. When the mixture is burned, the pressure rises in the driver breaking the diaphragm and sending a strong shock wave to the left through the low-pressure argon. The gas behind this shock is heated, compressed and ionized.

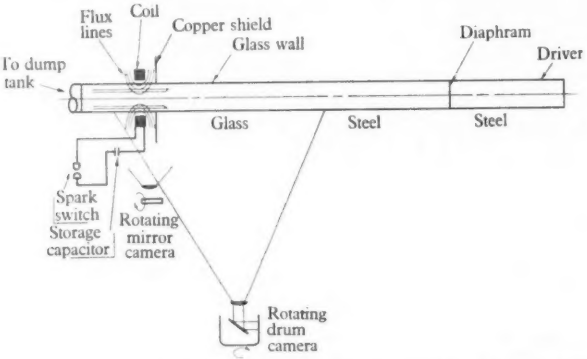

FIGURE 2. Schematic drawing of the shock-magnetic-field experiment.

After propagating through a 10 ft. section of steel tubing 1·5 in. in diameter, the shock enters a Pyrex tube of the same diameter. A slit is placed along the axis of this Pyrex tube, the slit being imaged in a high-speed, air-driven, rotating drum camera. The light emitted by the gas behind the shock is recorded on the film. A sample drum-camera photograph is shown in figure 3 (plate 1). The distance along the tube is the abscissa, while time is the ordinate. The horizontal lines are still pictures of the slit; the illuminated region is the image of the shock traversing the tube. The combination of the camera speed, plus the necessary geometrical factors, permits a precise determination of the shock speed and hence of all the gas properties behind the shock.

After passing through some 4 ft. of Pyrex tube, the shock finally arrives at the test region. Here, a cylindrical non-conducting tube of $1\frac{1}{8}$ in. outside diameter has been placed inside the $1\frac{1}{2}$ in. diameter Pyrex tube, forming an annulus $\frac{3}{16}$ in. thick between the two tubes (figure 4). The upstream edge of the inner tube is machined so that the shock wave enters the annular region without disturbance. The gas inside the inner tube is discarded.

A coil and a copper shield of $\frac{1}{4}$ in. thickness are placed around the annulus (figure 2). The separation between the coil and shield is $\frac{1}{2}$ in. The coil is connected to a 200 μF condenser through an air-spark switch timed to close (by a signal

from a photomultiplier upstream from the annulus) so that the current in the coil is a maximum when the shock reaches the shield. Since the coil, shield and condenser have a resonant frequency of only 1200 c/s, the magnetic field produced by the condenser discharge may be considered to be steady over a test time of some 20 μs.

The copper shield is several skin depths thick at the discharge frequency, so that no magnetic field penetrates through it. The radial component of the magnetic field in the annular region between the coil and shield is thus increased to about double the value it would have without the shield, while the axial field is reduced. The measured radial strength of the magnetic field varies about 20 % over the region of the annulus between the coil and shield. This non-uniformity, plus the presence of an axial field, can be important under some conditions which will be discussed shortly. Magnetic fields with a radial component as large as 6000 G are produced in the annulus between the coil and shield.

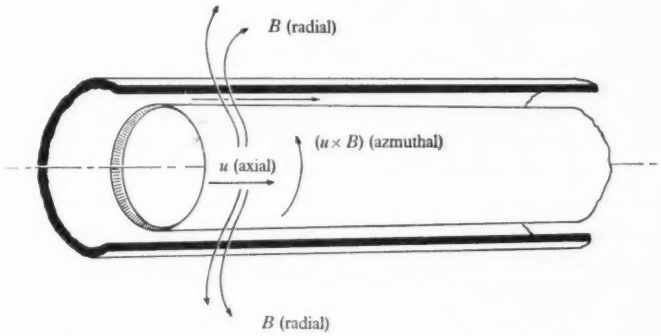

FIGURE 4. Schematic drawing of annular experiment showing co-ordinate system with direction of velocity, applied magnetic field and induced electric field.

As the gas behind the shock enters the magnetic field, the interaction of the gas velocity u with the radial magnetic field B induces an electric current of magnitude uB around the annulus (figure 4), causing a current to flow in the conducting gas. The current density j is equal to σuB, where σ is the gas conductivity. Note that no part of the current path is external to the gas, and that the current loops close in a constant magnetic field. The current j flowing across the magnetic field produces a body force of magnitude σuB^2 in a direction opposite to the gas velocity.

If the argon pressure before passage of the shock is 1 mm of mercury, the ionized gas behind the shock flows through the interaction region for about 20 μs. The time required for a sound wave in the hot gas to traverse the interaction region is about 3 μs, much less than the flow time. Due to this difference between flow time and time for a sound wave to traverse the interaction zone, it is reasonable to assume that steady flow is established through the magnetic field.

We have described previously how a high-speed drum camera is used to determine the shock velocity. A high-speed rotating mirror camera used in the same way produces an enlarged (x, t)-diagram for the gas in the vicinity of the inter-

action zone. Such a photograph for a typical run is shown in figure 5 (plate 2), along with an explanatory diagram. Again, the abscissa is the distance along the shock tube, while the ordinate is time. The hot gas behind the moving shock has an actual flow Mach number of about 2. It enters the interaction zone between the shield and coil from the left. The shock velocity is again given by the slope of the lower boundary of the illuminated region in figure 5. The body force, $\sigma u B^2$, causes the gas to decelerate in the interaction zone. A supersonic flow cannot be continuously decelerated through Mach number 1. Thus, if the magnetic field is sufficiently strong a shock wave will form in the interaction zone as shown in figure 5.

Because of the deceleration in the magnetic field, the shock propagating downstream from the interaction zone will travel at a lower velocity than the initial shock. As a measure of the degree of interaction with the magnetic field the difference in stagnation pressures, $p_{0_1} - p_{0_2}$, behind the initial and transmitted shocks may be compared to the computed pressure loss through the interaction zone. The change in stagnation pressure can be determined directly from the difference between the initial and transmitted shock velocities. The calculation is carried out in § II of this paper. Unfortunately, due to the small aperture of the rotating mirror camera used in this experiment, a visual record of the interaction could be obtained for only a small range of conditions of the gas behind the initial shock ($16 < M_1 < 18$). However, for this small range it was found that the loss in stagnation pressure across the magnetic field, as determined from the rotating mirror camera photographs, agreed with the predicted loss to within 30 %, as will be described in § II.

To study how the strength and geometry of the magnetic field influence the gas conductivity, the current in the gas was measured by a pick-up coil placed around the Pyrex tube forming the annulus. This coil was calibrated by measuring the pick-up due to a known high-frequency electric current in the interaction zone. This calibration current is produced by placing a coil in the interaction zone and exciting it with a signal generator. The gas current was measured over a large range of initial shock Mach numbers at a pressure of 1 mm. It was found that the electrical conductivity of the gas is drastically affected by the magnetic field (but not for those initial conditions for which rotating mirror photography was possible). These measurements will be discussed further in § 2.

2. End experiment

The annular experiment suffers from three disadvantages: first, the non-uniformity of the magnetic field and its strong component in the flow direction; secondly, the relatively short testing time; and thirdly, the limited range of variation of the experimental parameters. These disadvantages offset the inherent simplicity of a constant area flow. Therefore, a second experiment which eliminates these difficulties has been performed.

For the end experiment, a diagram of which is shown in figure 6, the argon shock wave is reflected from the end of the 1½ in. diameter shock tube. Gas from Region 3 (see figure 6) then flows radially outward through the end section; the channel area increases proportional to the radius. Since the gas pressure behind

the reflected shock is several hundred times the pressure before the arrival of the shock, the point indicated by * on figure 6 is a sonic point, as it is the point of minimum channel area. Beyond this point, the flow with no magnetic field is supersonic and the Mach number increases as we go outwards from the tube axis. The gas properties in the stagnation chamber, Region 3, are not affected by the flow beyond the sonic point, so that the radial mass flow is constant regardless of any gas-magnetic field interaction. This flow remains steady for times as long as 100 μs. The radial shock wave which precedes the gas flow eventually reflects back in towards the tube axis, but arrives in the test region too late to be of any consequence.

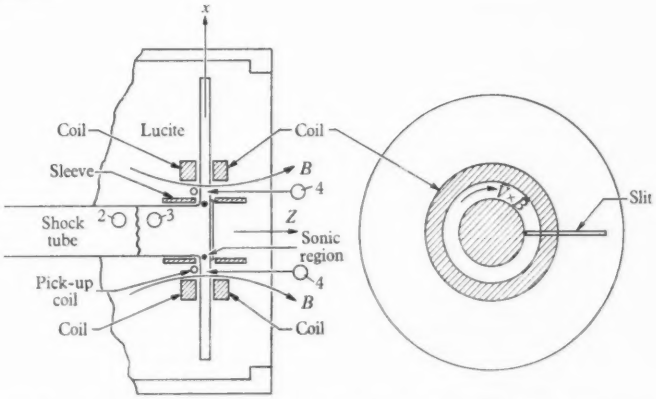

FIGURE 6. Schematic drawing of end experiment showing a side cross-section and end view.

The flow properties at the entrance of the magnetic field, Region 4, are determined by computing the properties of the gas in Regions 2 and 3, following the method outlined by Resler (1952), and matching the flow through the minimum area denoted by * on figure 6. The condition for this match is the continuity equation $\rho_3 u_3 A_3 = \rho^* u^* A^*$, where A^* is the channel area at the sonic point.

The flow conditions in Region 4 without an applied magnetic field were computed by using the conventional methods of one-dimensional isentropic channel flow. These flow calculations were checked by measuring the light emitted from the radial slit (figure 6). In these experiments argon was used as the working gas. The light emitted by highly ionized argon is due mainly to an electron-ion recombination continuum described by Petschek *et al.* (1955). Its intensity distribution in the visible region is given by

$$I_{(\nu)} = K \frac{N_e^2}{T^{\frac{1}{2}}},$$

where K is a constant, ν the frequency, N_e the number density of electrons, T the temperature and $I_{(\nu)}$ is the radiation per cubic centimetre per unit frequency interval. The measured light intensities check the one-dimensional flow calculations within the experimental error of the light intensity measurements (20 %).

When the magnetic field is present in Region 4 (figure 6), the gas flows radially outward through the field produced by the two coils and copper shields. The coil is connected to a 200 μF condenser through an air spark switch which is timed to close so that the current in the coils is a maximum during the experiment. The discharge frequency is 1·1 kc/s, the copper shields are several skin depths thick at this frequency, so that little magnetic field penetrates through the shields. In figure 7, the z-component of the magnetic field is plotted *vs* distance from the shock-tube axis. The radial component of the field is never greater than 4 % of the maximum axial field. The difference between this geometry and that of the annular experiment, where there is a strong field component in the flow direction, is important when the effect of magnetic field on gas conductivity is considered.

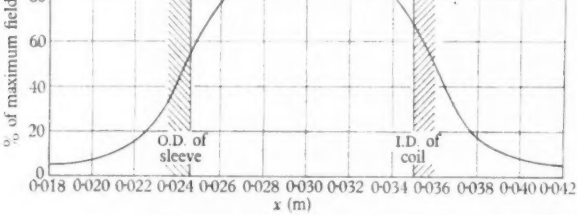

FIGURE 7. The magnetic field distribution in Region 4 as a function of radial distance.

The radial gas velocity v crossing the magnetic field B induces an electric field as shown in figure 6. This field closes in the gas, causing a current of magnitude σuB, and a body force directed towards the axis of the tube. The effect is to decelerate the gas, but this effect is competing with the increasing channel area which tends to accelerate the gas. For strong fields, the gas is decelerated, again producing shock waves in the interaction zone between the coils and shields.

A slit is installed radially outward from the tube axis as shown in figure 6, and the rotating mirror camera is again used to study the interaction of the gas flow with the magnetic field. A typical mirror-camera photograph, along with an explanatory diagram, is shown in figure 8 (plate 3). The exposed region on the left is the interaction zone. The distinct vertical line dividing two regions of different light intensity in this interaction zone is a shock wave produced by the interaction between the flow and field. The radial position of the shock changes during the test time, since the magnetic field varies slightly in a period of 100 μs. However, the field variation is so slow that the flow may be assumed to be steady at any given time. The dark region is the location of the coil. The shock reflecting radially is shown on the right. It is seen that this shock never reaches the interaction zone. Figure 9 (plate 3) is a mirror-camera photograph for the case of a very strong field; in this case, the shock wave is actually reflected by the magnetic field. Steady flow is not possible at these large field strengths.

Due to the high gas density and strong magnetic field obtainable with the end experiment, the gas-field interaction could be studied with the mirror camera over a large range of initial gas conditions (see figure 1). The photographic study could be extended to the region where the gas conductivity is affected by the magnetic field.

The electric current in the gas is measured by a pick-up coil in a manner identical to that in the annular experiment. These gas-current measurements are discussed in §II.

Figure 10 (plate 4) is a photograph of the apparatus for the end experiment. The shock tube is the long pipe entering the picture from the right. The radial flow is established in the large end cap on the tube; this cap also contains the coils and shields. The high-speed, air-driven, rotating-mirror camera is on the extreme right. It has a maximum aperture of f3·5, and a maximum writing speed of 0·5 cm/μs. Various photomultipliers and optical equipment used in the study of the gas properties are also shown.

In the following section, the experimental observations will be compared with a simple theory of one-dimensional gas flow in a magnetic field.

II. Theoretical description of the experimental results

1. Mach-number variation

The equation for the Mach number M_1 as a function of the ratio of heat capacities γ, channel area A, and body forces X is given by Shapiro & Hawthorne (1947) for steady, one-dimensional flow without friction or heat transfer

$$\frac{dM^2}{M^2} = -\frac{2\{1+\frac{1}{2}(\gamma-1)M^2\}}{1-M^2}\frac{dA}{A} + \frac{2\gamma M^2\{1+\frac{1}{2}(\gamma-1)M^2\}dX}{(1-M^2)\rho v^2}, \tag{1}$$

where v is the magnitude of the gas velocity $\mathbf{v}$ and ρ is the gas density. Equation (1) applies to both experimental geometries described in the previous section where the current loops close in the gas. The electric current in the gas can be written

$$\mathbf{j} = \sigma(\mathbf{v}\times\mathbf{B}), \tag{2}$$

where $\mathbf{j}$ is the gas current-density vector, $\mathbf{B}$ the magnetic field and σ the effective gas conductivity.

In this analysis, displacement currents are neglected. Also, the net charge density is assumed to be zero, since at the gas densities used in the experiments the Debye shielding distance is small compared to both the mean free path and the appropriate gyro radius. We may regard equation (2) as defining an effective conductivity σ for currents in the $(\mathbf{v}\times\mathbf{B})$-direction. The effective conductivity depends not only on the temperature and density of the gas for all the experimental conditions, but in some cases depends also upon the magnetic field strength and field geometry.

The component of the magnetic field perpendicular to the gas velocity alone contributes to the current density. The body force per unit volume is $\mathbf{j}\times\mathbf{B}$, and its component X parallel to the flow direction is

$$X = \sigma v B_{\mathrm{perp}}^2,$$

where B_{perp} is the component of B perpendicular to the flow direction.

With the above definition of the effective gas conductivity, one may write the equation for the change in M (equation (1)) as follows:

$$\frac{dM^2}{M^2} = -\frac{2\{1+\frac{1}{2}(\gamma-1)M^2\}}{1-M^2}\left(\frac{dA}{A} - \frac{\gamma M^2 \sigma B^2}{\rho v A}dx\right), \tag{3}$$

where x is the co-ordinate parallel to **v**.

Equation (3) expresses the change in M in terms of the channel area A, and the ratio of magnetohydrodynamic body force to gas momentum, $\sigma B^2 A\,dx/\rho v A$. The analysis will be divided into two parts. The first part deals with the annular experiment where there is no area change and hence $dA = 0$ in (3). The second part deals with the end experiment where the complete equation is integrated to describe the experimental results.

2. Constant area flow (annular experiment)

For the case of constant area, (3) simplifies to

$$dS = \frac{(1-M^2)\,dM^2}{2\gamma M^4\{1+\frac{1}{2}(\gamma-1)M^2\}}, \tag{4}$$

where S is a non-dimensional interaction variable defined by $S = \sigma B^2 x/\rho_0 v_0$ and $\rho_0 v_0$ is the mass flow per unit area. Equation (4) describes the variation of M with distance in the flow direction. M decreases with distance for supersonic flow and increases for subsonic flow. The effect of the interaction is to produce a situation completely analogous to pipe flow with friction and no heat transfer. The state of the gas is described by a Fanno line. If the 'pipe' is long enough, M at the exit will be unity, i.e. the flow chokes.

To find the value $S = S_0$ at which the flow chokes, we integrate (4) from $M = M_0$ to $M = 1$, and assume no shock waves between the limits of integration. The result is

$$S_0 = \frac{1}{2\gamma}\left[\left(\frac{\gamma+1}{2}\right)\log\left\{\frac{2}{\gamma+1}\left(\frac{1}{M_0^2}+\frac{\gamma-1}{2}\right)+\frac{M_0^2-1}{M_0^2}\right\}\right]. \tag{5}$$

Here S_0 is the minimum value of S which will choke the flow with an initial Mach number M_0 (σ is taken to be constant, an approximation accurate to within 20 % for the annular experiment). The function S_0 is plotted against M_0 on figure 11 for $\gamma = 1{\cdot}13$, which is representative of argon under the experimental conditions.

Using the values of electrical conductivity measured by Lin *et al.* (1955), the experimental arrangement gave $S_{\max} = 0{\cdot}5$ ($S_{\max}$ corresponds to $x = l$, the length of the interaction region). The conditions behind strong shock waves in argon are such that the Mach number at the entrance of the field region is approximately equal to 2 for the experimental conditions in the annular experiment (Resler *et al.* 1952). Since $S_{\max} = 0{\cdot}5$, and M upstream is equal to 2, $S_{\max}$ is greater than that value S_0 necessary to cause M at the exit of the field to be equal to unity (figure 11). Therefore, a shock forms in the interaction region which makes the flow subsonic downstream from it. The flow then accelerates to $M = 1$ at the exit of the field. The variation of M in the field region is shown in figure 12.

Furthermore, it is evident by continuity that the gas properties at the exit of the field are independent of the shock position in the field for $S_{\max} \geqslant S_0$, and less than that value of $S_{\max}$ which causes a standing shock at the entrance of the field.

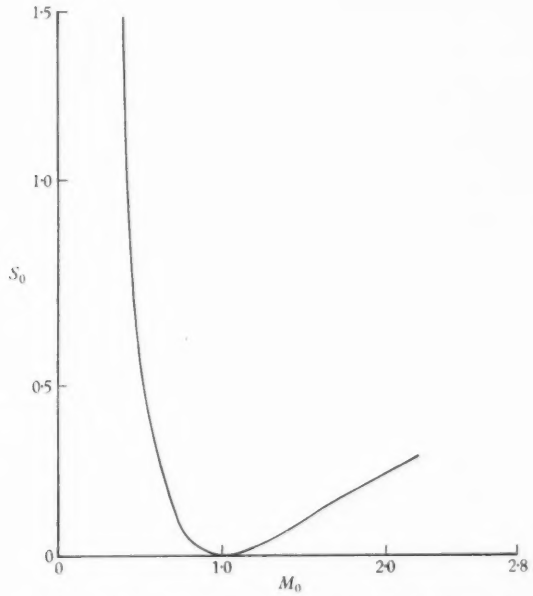

FIGURE 11. Interaction length necessary to change the Mach number M to unity, expressed as a function of the Mach number.

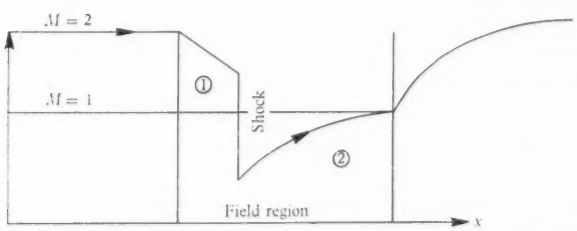

FIGURE 12. Change in Mach number in the field region as a function of distance in the stream direction.

The loss in stagnation pressure p_0 for $S_{\max} \geqslant S_0$ is easily computed using the relationships given by Shapiro & Hawthorne (1947):

$$\frac{dp_0}{p_0} = -\frac{\gamma M^2}{\rho_0 v_0 v} dX = -\gamma M^2 dS. \tag{6}$$

Substituting for dS from (4), we have

$$d(\log p_0) = \frac{(M^2-1)}{M^2\{2+(\gamma-1)M^2\}} dM^2. \tag{7}$$

Since the shock position does not influence the exit conditions, we integrate equation (7) between $M = M_0$ and $M = 1$ to obtain

$$\frac{p_{0_1}}{p_{0_2}} = \frac{1}{M_0}\left[\left(\frac{2}{\gamma+1}\right)\left(1+\frac{\gamma-1}{2}M_0^2\right)\right]^{\frac{1}{2}(\gamma+1)/(\gamma-1)}. \tag{8}$$

The exit conditions, Region 2 of figure 5 (plate 2), are now completely determined.

The gas pressure and velocity must match across the entropy line dividing the gas which has passed through the field, Region 3 in figure 5 (plate 2), from the gas behind the transmitted shock Region 4. Using the theoretical exit properties as initial values for an unsteady expansion downstream of the field region, the gas properties behind the transmitted shock were computed. The match is carried out far enough downstream so that the expansion is essentially complete. The predicted velocity of the transmitted shock was compared to the experimental value measured on the mirror camera photographs described in §I (see figure 5). It was possible over the small range of the experiments to predict the difference between the initial and transmitted shock velocities to within 15 %: in other words, the change in stagnation pressure across the interaction could be predicted to within 30 %.

3. Channel flow with varying area (end experiment)

The particular case of steady, one-dimensional flow considered here is that case where the cross-sectional area A is directly proportional to the co-ordinate x in the flow direction. For this case, equation (3) becomes

$$\frac{dM^2}{M^2} = -\frac{2\{1+\frac{1}{2}(\gamma-1)\}M^2)}{1-M^2}\frac{dx}{x} + \frac{2\gamma M^2\{1+\frac{1}{2}(\gamma-1)M^2\}}{1-M^2}\left[\frac{2\pi\sigma B^2 x}{\rho v A}\right]dx. \tag{9}$$

The flow properties in the magnetic field, Region 4 of figure 6, were computed using this equation. Up to the entrance of Region 4, the flow properties were determined by using only the first term on the right-hand side of (9).

Solutions of (9) were obtained using initial conditions corresponding to several values of M_1 and p_1. A particular set of solutions for $M_1 = 10$ and $p_1 = 5$ mm are presented in figure 13 for various values of the maximum magnetic field strength. The values of $B/B_{\max}$ as a function of x are taken from figure 7. Values of σ were computed for conditions at the entrance to Region 4, i.e. $M = 1{\cdot}1$. Then, in Region 4, σ was taken to be proportional to $T^{\frac{3}{2}}$, where T is the gas temperature (Lin *et al.* 1955). Values of γ were computed from the thermodynamic functions for argon, and these values were then used in the numerical solution of (9). For the calculations, it is assumed that the gas is always in thermodynamic equilibrium.

The upper curves of figure 13 are straightforward solutions of (9) in the supersonic regime. The same initial conditions were used for each value of B, since the first term on the right-hand side of (9) is large compared to the second term at the upstream end of the field region. The lower curves (subsonic regime) were computed by integrating from large values of x to small values, using an initial $M = 0{\cdot}99$. The initial point was determined by computing dM^2/dx from (9) and finding the largest value of x where this quantity is positive. For a given $B_{\max}$,

this point was taken to be the value of x beyond which the magnetic field would not affect the flow, since the magnitude of $B^2(x)$ decreases rapidly with increasing x (figure 7). The vertical lines on figure 13 represent shock waves in the flow obtained by matching the supersonic and subsonic curves for each value of B_{max}.

The physical argument for this procedure is as follows. At the entrance of the field region M is greater than unity (figure 13). Entering the field, the value of M at first increases due to the increasing area. The value of M decreases when the second term on the right-hand side of equation (9) dominates, i.e. the magnetic body forces have a greater effect than the area change. For the conditions of figure

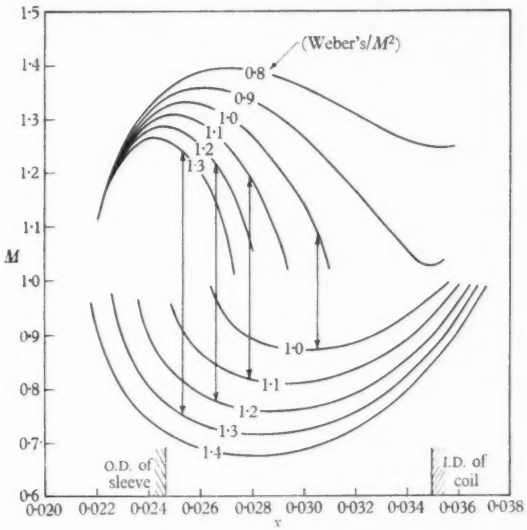

FIGURE 13. The solutions of equation (5) in Region 4, showing the shock waves connecting the supersonic and subsonic regimes.

13, a maximum field strength of 9000 G causes the value of M to decrease almost to unity at the exit of the field. Beyond the field region, M increases. For higher values of B, M decreases more rapidly in the supersonic regime, but cannot decrease continuously through unity as this would correspond to a decrease in entropy. Since the flow downstream from the field region is supersonic, and since the area increases continuously, the minimum value of M at the exit of the field is unity. When the second term in (9) is large ($B_{max} > 9000$ G), this corresponds to M increasing towards unity from a subsonic value in the field. Hence, for sufficiently high values of B_{max}, the flow at the exit of the field will always be such that M is equal to unity if the flow downstream is supersonic. For still larger values of B_{max}, no shock matching condition can be made between the subsonic and supersonic curves in Region 4. An unsteady shock will then be produced which propagates upstream. An example of this situation was shown in figure 9 (plate 3). The flow behind this unsteady shock expands smoothly so as to lead to Mach number unity at the exit of the field.

The shock location was measured from several mirror-camera pictures for experimental conditions that correspond to the theoretical results given in figure 13. These experimental results are plotted in figure 14 along with the computed shock location as a function of B_{max}. For the field strengths involved (of the order of 10^4 G) the electrons in the ionized gas do not make a complete gyro orbit between collisions. The theory using a scalar conductivity, which is

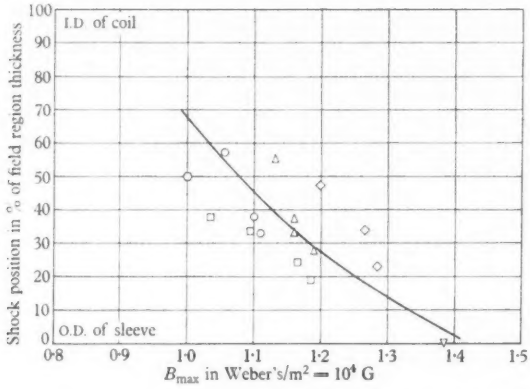

FIGURE 14. The theoretical and experimentally determined shock locations for $M_i = 10$, $p_1 = 5$ mm in the shock tube for various field strengths in Region 4. —, theoretical shock position for $M_i = 10$; $p_i = 5/760$ atm. *Note.* Each type of symbol corresponds to one mirror-camera picture.

a function only of the state of the gas, agrees with the experimental results. Data was taken over the range $9 \leqslant M_1 \leqslant 11$ and $2 \leqslant p_1 \leqslant 10$ mm. These results also agree with the theoretical predictions with errors of the same order as in figure 14.

For conditions with $p_1 < 2$ mm and $M_1 < 11$ (figure 1), the field strengths necessary to cause a shock to form in the field are such that the electrons make a complete gyro orbit between collisions.

4. Non-Scalar Conductivity ($\omega_e \tau_e > 1$)

In the presence of a magnetic field, there are two conditions that cause the effective conductivity σ in equation (2) to be less than the scalar value (Schluter 1950, 1951). The first condition is that the electrons can make a complete gyro orbit between collisions, that is $\omega_e \tau_e > 1$. This gives rise to an electromotive force (the Hall potential) in the $(\mathbf{j} \times \mathbf{B})$-direction which, if a path is provided, may cause an electric current (the Hall current) to flow in this direction. If the conditions are such that the Hall current can flow unimpeded, the conductivity is reduced as follows:

$$\sigma = \frac{\sigma_0}{1 + (\omega_e \tau_e)^2}, \tag{10}$$

where σ_0 is the conductivity in the absence of a magnetic field.

The second condition is the effect of the relative difference between the ion velocity with respect to the magnetic field and the velocity of the neutral particles with respect to that field. This gives rise to a decreased conductivity

$$\sigma = \frac{\sigma_0}{1 + \omega_e \tau_e \omega_I \tau_I}, \tag{11}$$

where ω_I is the appropriate cyclotron frequency for ions, and τ_I is the mean free time for ion-neutral collisions. The above expression assumes that the Hall current is zero. A brief discussion of these two effects is given in the Appendix.

If the magnetic field has a large component along the flow direction, as in the annular experiment, one would expect to find that equation (10) describes the gas conductivity since the electrons will tend to flow along field lines. If, as in the end experiment, the component of the field in the flow direction is small, one would expect that equation (11) would describe the behaviour of the conductivity.

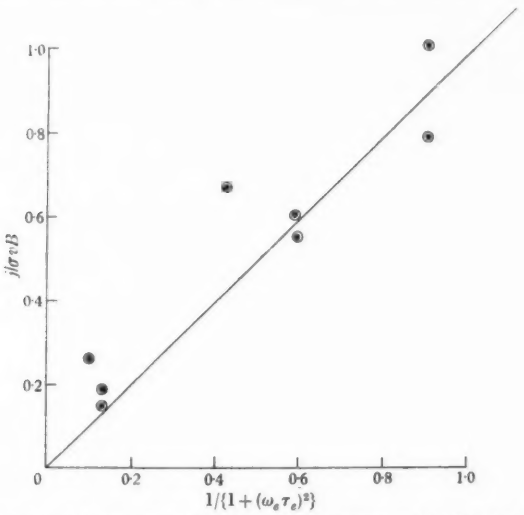

FIGURE 15. The current j measured in the annular geometry divided by σvB, the current if the effective conductivity is scalar, *vs* the factor, $1/\{1+(\omega_e\tau_e)^2\}$.

Annular experiment. The results of the gas-current measurements for the annular experiment are shown in figure 15. The ratios of the measured gas current density j to $\sigma_0 vB$ are plotted *vs* $1/\{1+(\omega_e\tau_e)^2\}$. The variation in $\omega_e\tau_e$ corresponds to a variation in M_1 at $p_1 = 1$ mm. The points are close to the theoretical value predicted by using equation (10) for the gas conductivity. The magnitude of the gas currents indicates that Hall currents can flow along field lines when these lines have an appreciable component parallel to the flow direction.

End experiment. A plot of the shock location as a function of M_1 is given in figure 16 for $p_1 = 1$ mm. The solid curve represents the theoretical shock locations found in the same manner as for figure 13 and with scalar conductivity proportional to $T^{\frac{3}{2}}$. The computed curve and the experiments are for $B_{\max} = 5000$ G.

The dashed curve represents the theoretical shock positions using (11) for σ, which takes ion slip into account. The measured shock locations (circles) indicate that ion slip becomes important under these conditions. The effect of the magnetic field on the gas conductivity was computed using an average for B and an average ion density. This use of average quantities may account for some of the discrepancies between the calculated and measured shock positions. Further, there is an uncertainty in the measured shock position at this low gas density which is equal to approximately 20 % of the field region length.

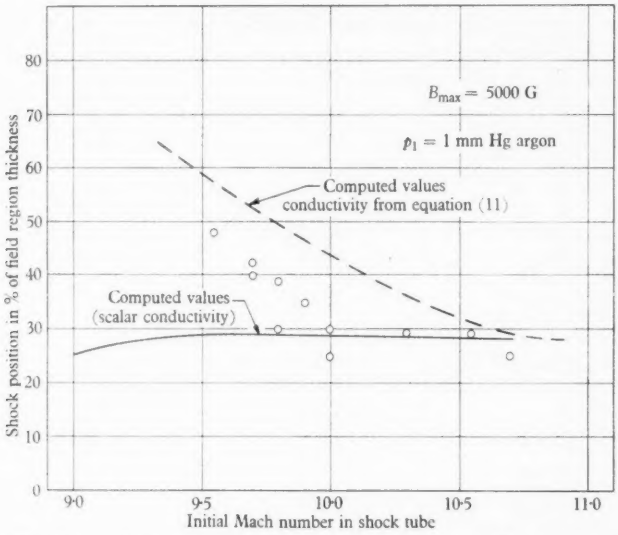

FIGURE 16. The theoretical and experimental shock locations in Region 4 for a constant magnetic field strength, showing one curve which was computed using a scalar conductivity and one which used equation (11) for the conductivity in equation (9).

For conditions such that $\omega_e \tau_e > 1$, the measured gas currents are plotted in figure 17. The three curves in this figure represent the total gas current computed by evaluating the integral

$$I = 2t \int \sigma v B dx \tag{12}$$

through the field region from shield to coil; $2t$ is the channel thickness. For $\sigma = \sigma_0$, the values of σ_0, v and B in the integral were obtained from the data used to compute the shock locations. The other two curves were obtained by using the value of σ given by (10) and (11). From the results plotted in figure 17, it appears that there is no current in the flow direction, i.e. no Hall current, when $M_1 > 9$ at $p = 1$ mm. The measured currents do agree with the values to be expected using (11) for σ. This indicates again that the predominant effect is ion slip, i.e. the difference in velocity between ions and neutral particles.

If no currents can flow in a direction perpendicular to $\mathbf{v} \times \mathbf{B}$, then a potential $\omega_e \tau_e (\mathbf{v}_I \times \mathbf{B})$ will exist in the flow direction, where $\mathbf{v}_I$ is the ion velocity. This was

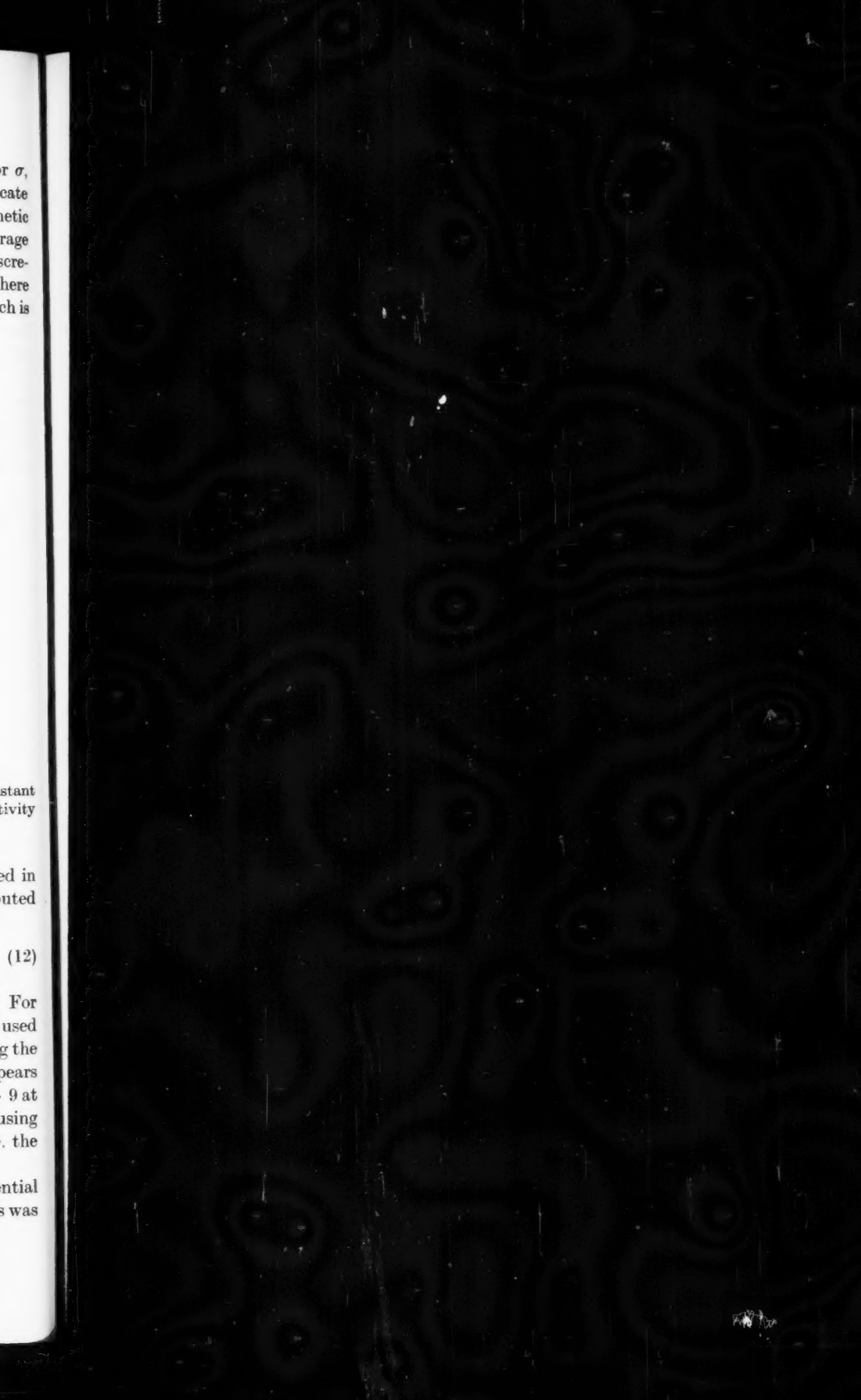

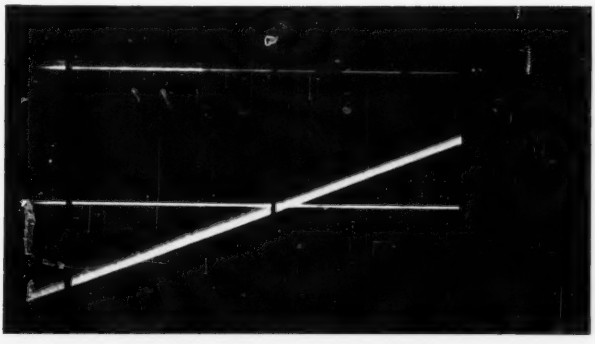

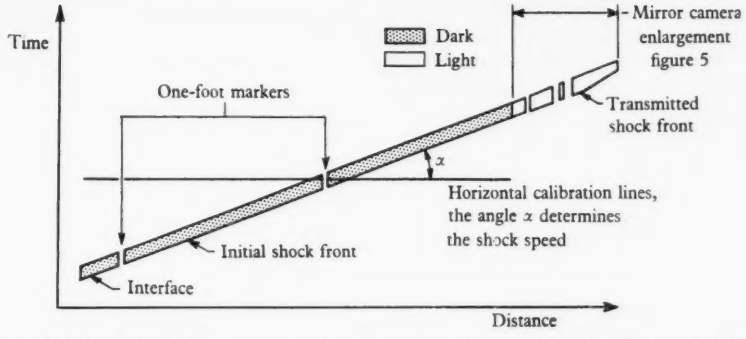

FIGURE 3 (plate 1). Drum-camera photograph showing a time (ordinate) *vs* distance (abscissa) picture of the shock phenomena over 3 ft. of the shock tube with the magnetic field on the right. The horizontal line is a still picture of the slit.

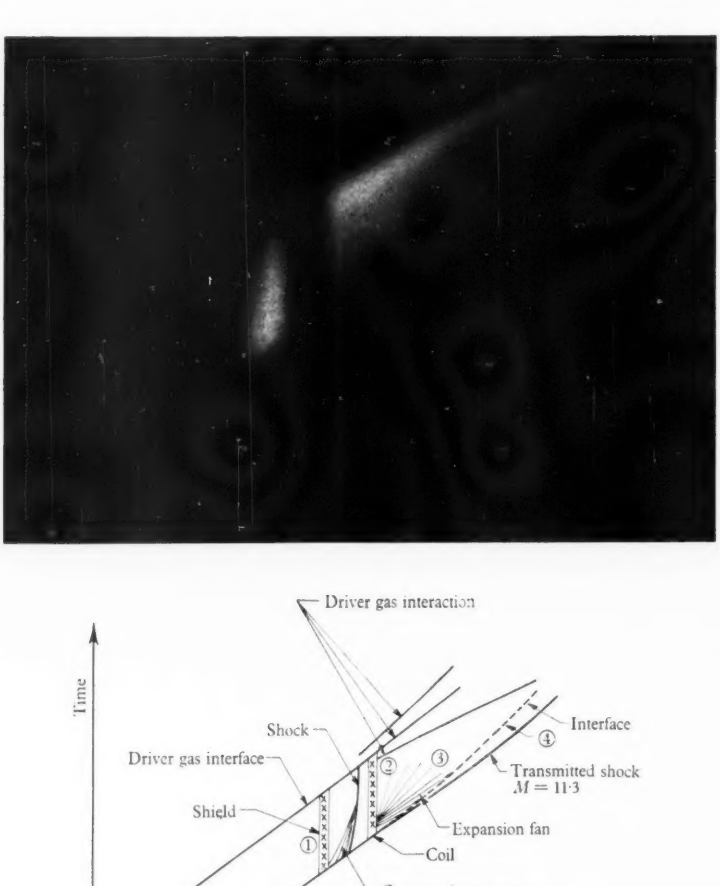

FIGURE 5 (plate 2). Mirror-camera photograph showing a time (ordinate) *vs* distance (abscissa) picture of the shock passing through the magnetic field.

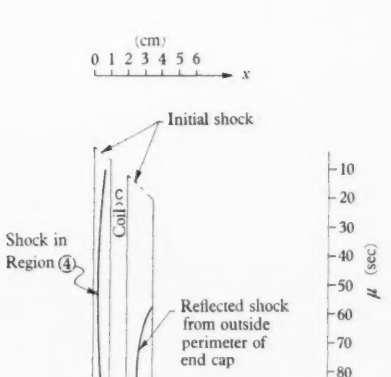

FIGURE 8 (plate 3). A mirror-camera photograph of the light emitted from the slit on the end cap, figure 9 (plate 4), showing the standing shock, and a schematic drawing of the photograph.

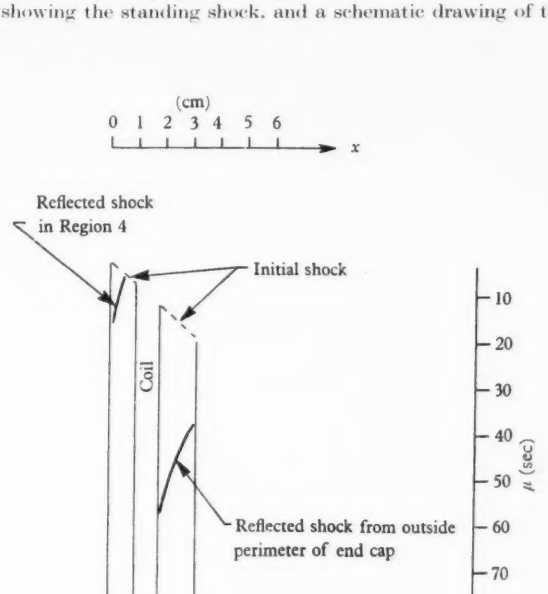

FIGURE 9 (plate 3). A mirror-camera photograph of the end-cap slit showing a reflected shock produced by a magnetic field in Region 4.

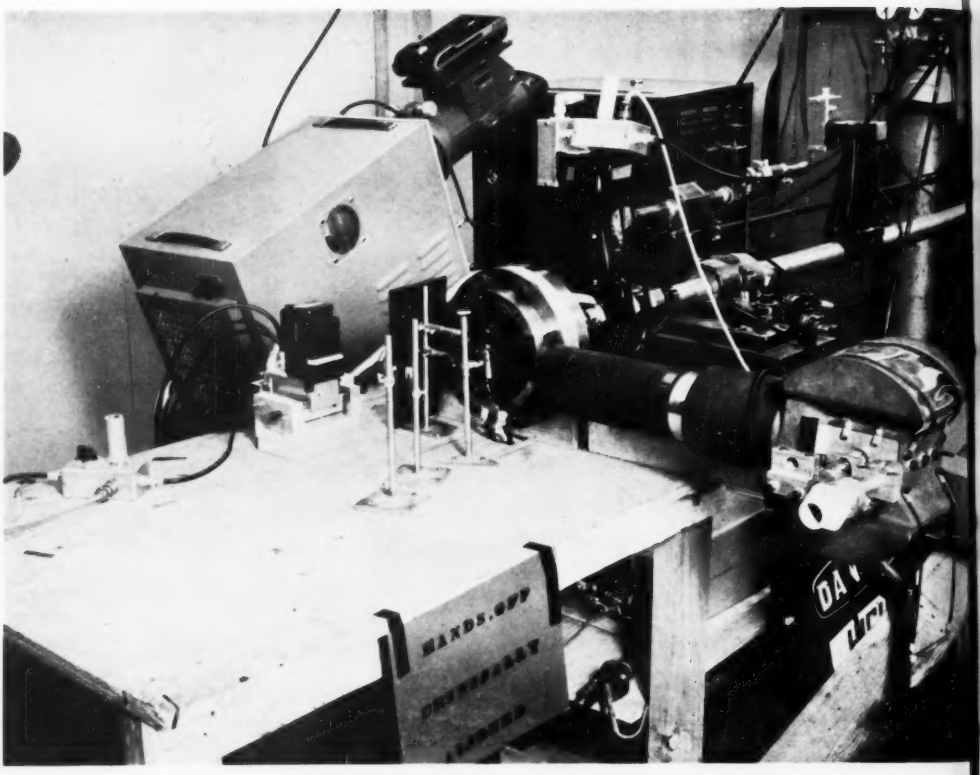

FIGURE 10 (plate 4). An overall photograph of the experimental arrangement, showing the shock tube, end experiment, photomultipliers, mirror camera, and some of the additional instruments.

sh
a
fa
cu

F
w
i

i
d

shown by Schluter (1951). In order to estimate whether or not there could be a current in the flow direction capable of causing the effective conductivity to fall below the value given in equation (11), one must consider the possibility of current loops in the flow direction which close in the boundary layer. This effect

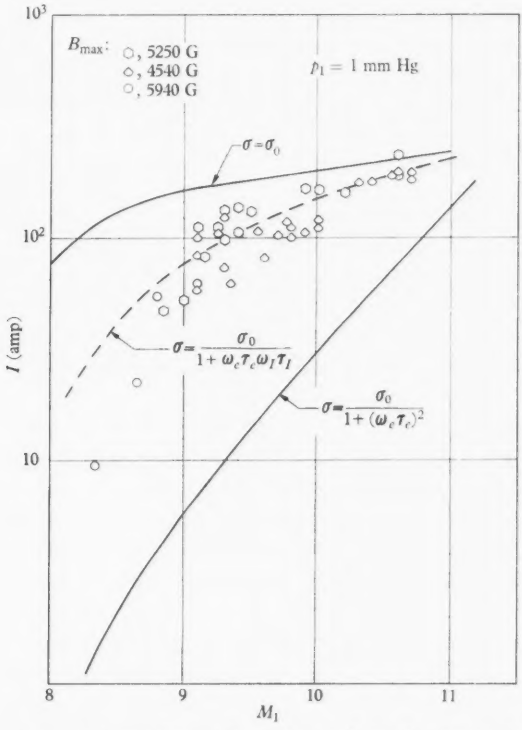

FIGURE 17. The solutions of equation (8) for various values of σ, the conductivity, together with measured values of the gas current I plotted as a function of the initial Mach number in the shock tube, M_i, for $p_1 = 1$ mm and for various values of B_{max}.

is estimated in the Appendix where we show that the current in the $(\mathbf{v}\times\mathbf{B})$-direction, J_y, is given by

$$J_y = \sigma_0 v_I B t \left\{ \frac{1+\dfrac{\sigma_{0B}}{\sigma_0}\dfrac{\delta}{t}\left(\dfrac{1+w_e^2}{1+w_{eB}^2}\right)\dfrac{1}{1+w_e^2}}{1+\dfrac{\sigma_{0B}}{\sigma_0}\dfrac{\delta}{t}\left(\dfrac{1+w_e^2}{1+w_{eB}^2}\right)} \right\}, \tag{13}$$

where $2t$ is the thickness of the inviscid flow region, δ the thickness of the boundary layer, σ_{0B} the boundary-layer conductivity with no magnetic field, $w_e = \omega_e\tau_e$ for the inviscid region, and $w_{eB} = \omega_e\tau_e$ in the boundary layer.

If no effect due to electrons rotating about field lines is present,

$$I = 2t\int \sigma_0 v_I B\, dx.$$

The data on figure 17 indicate that there might be an important effect due to electrons rotating about field lines for values of M_1 below 9. When conditions at the entrance of the field region correspond to values of M_1 between 8 and 9, the maximum displacement thickness for the boundary layer in Region 4 of figure 6 is less than one-tenth the inviscid flow thickness. The maximum possible change in I for a given value of δ would occur if $\sigma_{0B} = \sigma_0$ and $w_{eB} = 0$. With the boundary-layer thickness encountered under the flow conditions of figure 17, this maximum change in I is less than 10 %. Therefore, we conclude that the presence of Hall currents closing in the boundary layer does not explain the low value of I for $M_1 < 9$.

In all of the calculations, we have tacitly assumed that the gas is in thermodynamic equilibrium. The time for the gas to reach equilibrium can be estimated using a method outlined by Petschek & Byron (1957). Applying this method to calculate the time for the gas to reach equilibrium behind the reflected shock, Region 3 of figure 6, we find that in the available test time the gas in Region 3 does not reach equilibrium for $M_1 < 9$. The lack of equilibrium with $M_1 < 9$ probably accounts for the discrepancy between the measured values of I and those predicted by using equation (11) for the conductivity.

Conclusions

From the results of experiments described in this report one may make the following conclusions.

1. One-dimensional iso-energetic, steady flow of a compressible fluid in a magnetic field with no heat transfer or friction may be described by a theory which takes into account the area change of the channel and the magnetic body forces.

2. The effect of a steady magnetic field on one-dimensional iso-energetic gas flow is similar to friction due to viscosity and with sufficient field strengths will produce choking.

3. The maximum effect of a magnetic field is to cause the Mach number at the exit of the field to be equal to unity.

4. In the presence of a magnetic field, the electrical conductivity of a gas is reduced. This reduction is due to (*a*) Hall currents, or (*b*) ion slip.

The authors wish to express their appreciation to A. R. Kantrowitz, H. E. Petschek, R. J. Rosa and Prof. Max Krook for their interest and helpful suggestions. They are also indebted to John Lothrup and Lawrence McInnis for their help in carrying out the experiments.

This work was sponsored by the Ballistic Missile Division, Air Research and Development Command, U.S. Air Force, under Contract AF 04(645)-18.

Appendix

For the experiments described in this paper, one may consider the following special gas conditions. The degree of ionization $\alpha = Ne/NN_A$ is small (approximately 10^{-2} for most experiments), and the electron density is very nearly equal to the ion density (cf. Lin *et al.* 1955). If one neglects terms involving the ratio of

the electron mass m_e to the atom and ion masses, the momentum equation for the electrons leads to the following expression for the current in the gas

$$\mathbf{j} = N_e e(\mathbf{v}_I - \mathbf{v}_e) = \sigma_0\left\{\frac{\text{grad}\, p_e}{N_e e} + \mathbf{E} + \mathbf{v}_e \times \mathbf{B}\right\}, \tag{A 1}$$

where N_e is the number density of electrons, e is the charge on the electron, $\mathbf{v}_I$ is the ion velocity, $\mathbf{v}_e$ is the electron velocity, σ_0 is the gas conductivity in the absence of a magnetic field, p_e is the electron pressure and $\mathbf{E}$ is the electric field. In our experiments, $\mathbf{E}.(\mathbf{v}_I \times \mathbf{B}) = 0$.

The following results, due to Schluter (1950, 1951), give the components j_{par} and j_{perp} of the gas currents, respectively, parallel to and perpendicular to the $(\mathbf{v}_I \times \mathbf{B})$-direction:

$$j_{\text{par}} = \frac{\sigma_0 v_I B}{1 + (\omega_e \tau_e)^2} = \sigma_{\text{par}} v_I B, \tag{A 2}$$

$$j_{\text{perp}} = \frac{\sigma_0 v_I B \omega_e \tau_e}{1 + (\omega_e \tau_e)^2} = \sigma_{\text{perp}} v_I B, \tag{A 3}$$

where

$$\omega_e \tau_e = \frac{Be}{m_e} \frac{m_e}{N_e e^2} \sigma_0.$$

The σ defined in equation (10) is just the σ_{par} of equation (A 2), and gives the effective conductivity in $(\mathbf{v}_I \times \mathbf{B})$-direction if currents are allowed to flow in the stream direction with no external impedance.

For the end geometry experiments described in this paper currents perpendicular to the $(\mathbf{v}_I \times \mathbf{B})$-direction in Region 4 can close only in the boundary layer. If no currents can flow in a direction perpendicular to $\mathbf{v}_I \times \mathbf{B}$, then an electromotive force $\omega_e \tau_e \mathbf{v}_I \times \mathbf{B}$ exists in the flow direction (Schluter 1951). Also, when the degree of ionization Ne/N_A is small compared to unity, there is an additional effect due to a relative velocity between the ions and neutral particles. For the special case outlined in the first paragraph of this Appendix, the velocity of the ions v_I in terms of the neutral particle velocity v_A is

$$v_I = \frac{v_A}{1 + \omega_I \tau_{IA} \omega_e \tau_e}, \tag{A 4}$$

where $\omega_I \tau_{IA}$ is the number of gyro orbits completed by the ions between collisions (Schluter 1951). Since $\mathbf{v}_A \times \mathbf{B}$ is the apparent electric driving force for currents, the effective conductivity in equation (11) will be reduced by the same factor as the electric field in the $(\mathbf{v}_A \times \mathbf{B})$-direction. Hence, $\sigma = \sigma_0/(1 + \omega_I \tau_I \omega_e \tau_e)$ which is equation (11). Finally, the current in the $(\mathbf{v}_A \times \mathbf{B})$-direction is

$$j_{\text{par}} = \left\{\frac{\sigma_{\text{perp}}^2}{\sigma_{\text{par}}} + \sigma_{\text{par}}\right\}\left\{\frac{v_A B}{1 + \omega_I \tau_{IA} \omega_e \tau_e}\right\}. \tag{A 5}$$

If σ_{perp} and σ_{par} are defined as in equations (A 2) and (A 3), the first factor in equation (A 5) equals σ_0.

Equations (A 2) and (A 3) were obtained from an analysis which neglects the variation of collision frequency with velocity. This analysis applies very well to the case where most of the collisions of the electrons are with neutral particles, and

the cross-section for momentum transfer does not change appreciably with the relative velocity between the particles.

For the experiments described in this paper, argon is sufficiently ionized so that electron-ion collisions are the governing factor. The electron-ion collision cross-sections are rapidly varying functions of velocity, and for these conditions the first factor on the right-hand side of equation (A 5) differs from σ_0. Landshoff (1949) has computed the transport properties of a completely ionized gas in the presence of a magnetic field to obtain σ_{par} and σ_{perp} as functions of $\omega_e \tau_e$. These values have been used to compute the theoretical gas current (dashed curve in figure 17).

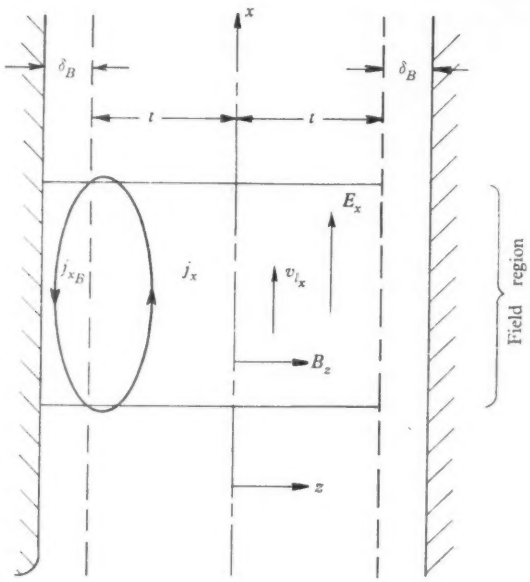

FIGURE 18. Schematic diagram of Region 4 (the y-direction is perpendicular to the plane of the drawing).

In order to estimate the importance of currents in the flow direction for the end geometry described in this paper, consider the following problem as illustrated in figure 18.

In a co-ordinate system where there is no motion of the ions in the x-direction, $E'_y = v_{Ix} B$. One may write the following expressions for the components of the current in the inviscid flow region

$$j_y = 2(\sigma_{\text{perp}} E_x + \sigma_{\text{par}} E'_y) t, \tag{A 6}$$

$$j_x = 2(\sigma_{\text{par}} E_x + \sigma_{\text{perp}} E'_y) t. \tag{A 7}$$

The boundary layer for this calculation is assumed to consist of a layer of gas of thickness δ_B with no motion relative to the wall. Hence, in this layer

$$E'_y = v_{Ix} B_Z = 0,$$

and the current in the x-direction becomes

$$j_{xB} = E_x \delta_B \sigma_{\text{par}_B} = \frac{E_x \delta_B \sigma_{0B}}{1 + w_{eB}^2}, \tag{A 8}$$

where $w_{eB} = \omega_e \tau_e$ in the boundary layer.

One may equate the currents in the x-direction in the inviscid region to the current in the boundary layer. This yields the expression

$$E_x = \frac{E_y' + \sigma_{\text{perp}}}{\sigma_{\text{par}} + \dfrac{\sigma_{0B}\delta_B}{1 + w_{eB}^2}}. \tag{A 9}$$

If this expression is substituted into equation (A 1) we obtain

$$j_y = \sigma_0 E_y' t \left\{ \frac{1 + \dfrac{\sigma_{0B}}{\sigma_0}\dfrac{\delta_B}{t}\left(\dfrac{1+w_e^2}{1+w_{eB}^2}\right)\left(\dfrac{1}{1+w_{eB}^2}\right)}{1 + \dfrac{\sigma_{0B}}{\sigma_0}\dfrac{\delta_B}{t}\left(\dfrac{1+w_e^2}{1+w_{eB}^2}\right)} \right\}. \tag{A 10}$$

Since $E_y' = v_{Ix} B$. this yields the expression for j_y given in equation (13) of this paper.

REFERENCES

Landshoff, R. 1949 *Phys. Rev.* **76**, 904.

Lin, S. C., Resler, E. L. & Kantrowitz, A. R. 1955 *J. Appl. Phys.* **26**, 95.

Petschek, H. E. & Byron, S. 1957 *Ann. Phys.* **1**, 270.

Petschek, H. E., Rose, P. H., Kane, A., Glick, H. S. & Kantrowitz, A. R. 1955 *J. Appl. Phys.* **26**, 83.

Resler, E. L., Lin, S. C. & Kantrowitz, A. R. 1952 *J. Appl. Phys.* **23**, 1390.

Schluter, A. 1950 *Z. Naturf.* **5** A, 72.

Schluter, A. 1951 *Z. Naturf.* **6** A, 73.

Shapiro, A. H. & Hawthorne, W. R. 1947 *J. Appl. Mech.* **14**, 317.

The effect of eddy viscosity on the velocity profile of steady flow in a uniform rough channel

By S. M. A. HAQUE
Department of Mathematics, University of Manchester†

(Received 28 August 1958)

The equation of motion is derived for the steady flow under gravity of a liquid in a uniform channel, including the effects of the friction of the bed and of the eddy viscosity for lateral mixing. The equation is solved to find the distribution of mean velocity across the channel when the cross-section is rectangular, triangular or trapezoidal. Numerical values are also given to indicate the extent to which eddy viscosity may affect the lateral distribution of mean velocity.

1. Introduction

We consider the steady flow of a river or channel with a straight course and having a bed which is uniform in its direction of flow, and which has the same downward slope at all its points. We take the x-axis in the downward direction o flow, and the y-axis horizontal and perpendicular to the direction of flow. Let u denote the mean velocity of the fluid particles lying on the straight line through any point of the bed parallel to the z-axis. The bed will exert a force on the moving fluid, and we shall assume that the force on a cylindrical column of fluid standing on area $dx\,dy$ with generators parallel to the z-axis may be represented by $-f|u|\,u\,dx\,dy$, where f is regarded as the coefficient of friction of the bed. This assumption is usually known in hydraulics as the Chézy formula, and references about it may be found in Stoker (1957, p. 466). The broad argument behind the Chézy formula is that the momentum of the fluid is destroyed when it is brought into contact with the bed by the eddies. The momentum of the column is proportional to u, and we assume that the speed of the eddies is proportional to $|u|$. The rate of destruction of momentum will be proportional to the momentum of the column and to the rate at which it is brought into contact with the bed, and hence can be represented by the term $f|u|\,u\,dx\,dy$, where f is a constant of proportionality.

The mixing process which brings fluid in contact with the bed will also cause lateral mixing. Since the mean velocity of flow will be a function of y, the mixing will give rise to viscous effects, and we assume that the effect is represented by ν, the kinematic coefficient of eddy viscosity. In the two following sections we shall regard ν as a constant, but in later sections we shall make a different assumption which allows for the variation of ν with the variation in depth and mean velocity. The inclination α of the bed to the horizon is assumed to be small, so that $\cos\alpha = 1$ to a sufficient approximation, and we write $\sin\alpha = s$. We shall also make the

† On leave of absence from the University of Dacca, East Pakistan.

assumption that the pressure at any point is approximately the same as the hydrostatic pressure, which is proportional to the depth below the effective surface.

Now consider the motion of a column of fluid standing on area $dx\,dy$. We assume that all points of the column are moving in the x-direction with velocity u, which is the mean velocity of the particles of the column. The forces acting on the column in the x-direction are: (i) $-fu^2\,dx\,dy$ being the frictional force of the bed, (ii) $gsh\,dx\,dy$ due to gravity, and (iii) $\frac{d}{dy}\left(h\nu\frac{du}{dy}dx\right)dy$ due to eddy-viscosity. If the motion is uniform, i.e. if there is no variation with x, the acceleration of the column will be zero, and the component of the force due to pressure will also be zero; therefore the equation of motion will be

$$0 = -fu^2 + gsh + \frac{d}{dy}\left(h\nu\frac{du}{dy}\right). \tag{1}$$

To obtain the Chézy formula, the last term on the right-hand side of (1) is neglected, which gives

$$u^2 = \frac{ghs}{f}. \tag{2}$$

The limitations of formula (2) are that (i) it neglects the boundary conditions at the walls of the channel where the mean velocity is necessarily zero, and that (ii) if dh/dy is discontinuous at any point (e.g. in a triangular channel) du/dy will also be discontinuous, implying an infinite viscous force at that point. These defects arise from the neglect of the last term in (1) in regions where it is important. We shall investigate the results when this term is included.

2. The velocity profile in an infinitely wide rectangular channel with constant eddy viscosity

We consider an infinitely wide rectangular channel, i.e. a channel in which $h = H$, a constant. If eddy viscosity is neglected, the velocity is given by

$$U^2 = \frac{gHs}{f}. \tag{3}$$

We shall seek a solution of equation (1) with constant ν satisfying the boundary conditions $u = 0$ at $y = 0$ and $u = U$, $du/dy = 0$ at $y = \infty$. Substitution of (3) in (1) gives

$$\frac{d^2u}{dy^2} + \frac{f}{H\nu}(U^2 - u^2) = 0, \tag{4}$$

which has the integral

$$\left(\frac{du}{dy}\right)^2 = \frac{2f}{3H\nu}(U-u)(2U^2 - Uu - u^2), \tag{5}$$

the constant of integration being determined from the condition that $du/dy = 0$ when $u = U$.

By the substitution $v = 2U + u$ in (5) it is easy to perform a second integration, and the result can be expressed in the form

$$\frac{u}{3U} = \left\{\frac{\sqrt{3(e^{ky}-1)} + \sqrt{2(e^{ky}+1)}}{\sqrt{3(e^{ky}+1)} + \sqrt{2(e^{ky}-1)}}\right\}^2 - \tfrac{2}{3}, \tag{6}$$

where $k = \sqrt{(2fU/H\nu)}$ and the boundary condition at $y = 0$ has been used to eliminate the constant of integration.

Table 1 gives some values of u/U against ky according to equation (6). From the illustrative values of f and ν that will be considered in § 8, it is seen that k is of the order of the reciprocal of H, so that the effect of eddy-viscosity in reducing the mean velocity is practically confined to a distance equal to a few times the depth.

ky	0	0·2	0·4	0·8	2	4
u/U	0	0·153	0·228	0·502	0·716	0·998

TABLE 1

3. Velocity profile of a rectangular river of finite width with constant eddy viscosity

Let 2η be the breadth of the river. In this case we need a solution of (4) with the initial values $u = 0$ at $y = 0$ and $du/dy = 0$ at $y = \eta$.

Let $u = u_*$ at $y = \eta$; then the first integration of (4) gives

$$\left(\frac{du}{dy}\right)^2 = \frac{2f}{3H\nu}(u_* - u)(3U^2 - u_*^2 - uu_* - u^2).$$

Putting $z = u_* - u$, the above equation reduces to

$$\left(\frac{dz}{dy}\right)^2 = -\frac{2f}{3H\nu}(z-\alpha)(z-\beta)(z-\gamma), \tag{7}$$

where

$$\left.\begin{aligned} \alpha &= \tfrac{3}{2}u_* + (3U^2 - \tfrac{3}{4}u_*^2)^{\frac{1}{2}} \quad (\beta = 0), \\ \gamma &= \tfrac{3}{2}u_* - (3U^2 - \tfrac{3}{4}u_*^2)^{\frac{1}{2}}. \end{aligned}\right\} \tag{8}$$

Equation (7) can be integrated in terms of elliptic functions (e.g. see Milne-Thomson 1950, p. 29); and using the boundary condition that $z = 0$ at $y = \eta$, we get

$$\begin{aligned} \int_\eta^y -\left(\frac{2f}{3H\nu}\right)^{\frac{1}{2}} dy &= \int_0^z \{-(z-\alpha)(z-\beta)(z-\gamma)\}^{-\frac{1}{2}} dz \\ &= \lambda \,\mathrm{dn}^{-1}\left[\left\{\frac{(3U^2 - \tfrac{3}{4}u_*^2)^{\frac{1}{2}} - \tfrac{3}{2}u_*}{z + (3U^2 - \tfrac{3}{4}u_*^2)^{\frac{1}{2}} - \tfrac{3}{2}u_*}\right\}\Big/ m_1\right]. \end{aligned} \tag{9}$$

where

$$\lambda = 2^{\frac{1}{2}}(3U^2 - \tfrac{3}{4}u_*^2)^{-\frac{1}{4}} \tag{10}$$

and

$$m_1 = \frac{(3U^2 - \tfrac{3}{4}u_*^2)^{\frac{1}{2}} + \tfrac{3}{2}u_*}{2(3U^2 - \tfrac{3}{4}u_*^2)^{\frac{1}{2}}}. \tag{11}$$

On simplification (9) yields

$$\left\{\frac{(3U^2 - \tfrac{3}{4}u_*^2)^{\frac{1}{2}} - \tfrac{3}{2}u_*}{(3U^2 - \tfrac{3}{4}u_*^2)^{\frac{1}{2}} - u - \tfrac{1}{2}u_*}\right\}^{\frac{1}{2}} = \mathrm{dn}\left\{\left(\frac{f}{3H\nu}\right)^{\frac{1}{2}}(3U^2 - \tfrac{3}{4}u_*^2)^{\frac{1}{4}}(\eta - y)\Big/ m_1\right\}, \tag{12}$$

from which u_* can be found by use of the condition that $u = 0$ at $y = 0$.

4. Velocity profile in an infinitely wide rectangular channel with eddy viscosity varying linearly with depth and mean velocity

We have so far assumed the kinematic coefficient of eddy viscosity to be constant, but it is perhaps more realistic to assume that eddy viscosity depends on the depth and the mean velocity. The depth of the channel will act as a limiting factor on the size of the eddies, and also we expect more rapidly moving eddies where the mean velocity is greater. The simplest assumption to allow for these facts is to assume that the eddy viscosity varies linearly with depth and mean velocity, and we write

$$\nu = cHu, \tag{13}$$

where H is the uniform depth and c is a dimensionless constant.

Substituting (3) and (13) in (1), we get

$$\frac{d^2u^2}{dy^2} + \frac{2f}{cH^2}(U^2 - u^2) = 0, \tag{14}$$

which is a linear equation with constant coefficients in u^2 and the solution of this equation which satisfies the boundary conditions $u = 0$ at $y = 0$ and $u = U$ at $y = \infty$ is

$$u^2 = U^2\{1 - e^{-(2f/cH^2)^{\frac{1}{2}}y}\}. \tag{15}$$

5. Velocity profile of a rectangular channel of finite width with eddy viscosity varying linearly with depth and mean velocity

We take the breadth to be 2η and seek a solution of (14) with the boundary conditions that $u = 0$ at $y = 0$ and $y = 2\eta$. The solution is

$$u^2 = U^2\left[1 - \frac{\cosh\{(2f/cH^2)^{\frac{1}{2}}(\eta - y)\}}{\cosh\{(2f/cH^2)^{\frac{1}{2}}\eta\}}\right]. \tag{16}$$

The maximum velocity u_* at $y = \eta$ is given by

$$u_*^2 = U^2[1 - \operatorname{sech}\{(2f/cH^2)^{\frac{1}{2}}\eta\}]. \tag{17}$$

6. Velocity profile of a triangular channel with eddy viscosity varying linearly with depth and mean velocity

We have so far assumed the depth to be constant. We now consider a channel whose cross-section has the form of an isosceles triangle of base angle $\tan^{-1}\kappa$. The depth at a distance y from the bank is given by $h = \kappa y$ if $y \leqslant \eta$, and $h = \kappa(2\eta - y)$ if $\eta \leqslant y \leqslant 2\eta$, where 2η is the breadth of the channel. We need consider only the flow in the region $0 \leqslant y \leqslant \eta$, the flow in the other half of the channel being given by symmetry.

Using $\nu = chu$, it is easily seen that the equation of motion (1) reduces in this case to the form

$$y^2\frac{d^2u^2}{dy^2} + 2y\frac{du^2}{dy} - \frac{2f}{\kappa^2 c}u^2 = -\frac{2gs}{\kappa c}y. \tag{18}$$

The solution of this equation satisfying the boundary conditions $u = 0$ at $y = 0$ and $du/dy = 0$ at $y = \eta$ is

$$u^2 = \frac{gs\kappa}{f-\kappa^2 c}\left[y - \frac{\eta}{(\frac{1}{4}+2f/\kappa^2 c)^{\frac{1}{2}}-\frac{1}{2}}\left(\frac{y}{\eta}\right)^{(\frac{1}{4}+2f/\kappa^2 c)^{\frac{1}{2}}-\frac{1}{2}}\right] \tag{19}$$

if $f \neq \kappa^2 c$, and

$$u^2 = \frac{2gs}{3\kappa c}[y(1+\log\eta) - y\log y] \tag{20}$$

if $f = \kappa^2 c$.

7. Velocity profile in a trapezoidal channel with eddy viscosity varying linearly with depth and mean velocity

We have found solutions for a rectangular channel in § 5, and for a triangular channel in § 6. It is possible to combine the equations obtained in these two sections to find solutions for a trapezoidal channel. Assume that in the channel of width 2η, the depth is given by $h = \kappa y$ for $0 \leqslant y \leqslant \eta_1$, $h = H = \kappa\eta_1$ for $\eta_1 \leqslant y \leqslant 2\eta - \eta_1$, and $h = \kappa(2\eta - y)$ for $(2\eta - \eta_1) \leqslant y \leqslant 2\eta$. The equation of motion will be (18) for the regions $0 \leqslant y \leqslant \eta_1$ and $(2\eta - \eta_1) \leqslant y \leqslant 2\eta$, and will be (14) for the region $\eta_1 \leqslant y \leqslant 2\eta - \eta_1$.

We take the general solutions of (18) and (14), and apply the boundary conditions: (i) $u = 0$ at $y = 0$; (ii) u is continuous at $y = \eta_1$; (iii) $du/dy = 0$ at $y = \eta$; (iv) du/dy is continuous at $y = \eta_1$.

Hence, the solution for the region $0 \leqslant y \leqslant \eta$ (the solution for the other half is given by symmetry) is found to be

$$u^2 = \frac{gs\kappa y}{f-\kappa^2 c} + A y^{(\frac{1}{4}+2f/\kappa^2 c)^{\frac{1}{2}}-\frac{1}{2}}, \tag{21}$$

and the solution for $\eta_1 \leqslant y \leqslant \eta$ is

$$u^2 = \frac{gsH}{f} + 2A'\, e^{(2f/cH^2)^{\frac{1}{2}}\eta}\cosh\{(2f/cH^2)^{\frac{1}{2}}(\eta - y)\}, \tag{22}$$

where A and A' are given respectively by

$$\begin{aligned} A\eta_1^{(\frac{1}{4}+2f/\kappa^2 c)^{\frac{1}{2}}-\frac{1}{2}}&[(2f/\kappa^2 c)^{\frac{1}{2}}\sinh\{(2f/cH^2)^{\frac{1}{2}}(\eta-\eta_1)\} \\ &+\{(\tfrac{1}{4}+2f/\kappa^2 c)^{\frac{1}{2}}-\tfrac{1}{2}\}\cosh\{(2f/cH^2)^{\frac{1}{2}}(\eta-\eta_1)\}] \\ &= -gsH/(f-\kappa^2 c)\,[(2f/\kappa^2 c)^{\frac{1}{2}}\sinh\{(2f/cH^2)^{\frac{1}{2}}(\eta-\eta_1)\} + \cosh\{(2f/cH^2)^{\frac{1}{2}}(\eta-\eta_1)\}] \\ &+ gsH/f\,(2f/\kappa^2 c)^{\frac{1}{2}}\sinh\{(2f/cH^2)^{\frac{1}{2}}(\eta-\eta_1)\}, \end{aligned} \tag{23}$$

$$\begin{aligned} 2A'\, e^{(2f/cH^2)^{\frac{1}{2}}\eta}&\left[\cosh\{(2f/cH^2)^{\frac{1}{2}}(\eta-\eta_1)\} + \frac{(2f/\kappa^2 c)^{\frac{1}{2}}}{(\frac{1}{4}+2f/\kappa^2 c)^{\frac{1}{2}}-\frac{1}{2}}\sinh\{(2f/cH^2)^{\frac{1}{2}}(\eta-\eta_1)\}\right] \\ &= -gsH\,\frac{f-\{(\frac{1}{4}+2f/\kappa^2 c)^{\frac{1}{2}}-\frac{1}{2}\}\kappa^2 c}{f(f-\kappa^2 c)\{(\frac{1}{4}+2f/\kappa^2 c)^{\frac{1}{2}}-\frac{1}{2}\}}. \end{aligned} \tag{24}$$

8. Numerical estimation of the effect of eddy viscosity on different velocity profiles

Numerical estimation of the velocity profiles in particular cases is rendered difficult by the fact that reliable values of the coefficient of eddy viscosity are not

available. However, we know (e.g. from Schlichting 1955, p. 406) that in a turbulent flow over a rough surface, the velocity profile is given by

$$\bar{u} = 2{\cdot}5\tau^{\frac{1}{2}}\log z + \text{const.}, \tag{25}$$

where τ is the drag per unit area of the surface and z is the height above the surface.

The value $\bar{\nu}$ of eddy viscosity in the neighbourhood of the surfaces is given by

$$\bar{\nu} = \frac{\tau}{d\bar{u}/dz} = \frac{fu^2z}{2{\cdot}5(fu^2)^{\frac{1}{2}}} = 0{\cdot}4f^{\frac{1}{2}}uz. \tag{26}$$

We assume that the expression (26) for $\bar{\nu}$ holds throughout the fluid, and hence the mean value ν of $\bar{\nu}$ is $0{\cdot}2f^{\frac{1}{2}}uh$. Hence, from the relation $\nu = chu$ used in § 6, we get that

$$c = 0{\cdot}2f^{\frac{1}{2}}. \tag{27}$$

While no strict accuracy is claimed for (27), especially as it assumes the eddy viscosities for vertical and horizontal momentum exchange to be equal, it is presumed that the value of c given by it is at least of the correct order of magnitude.

y/η ...	0·0	0·1	0·2	0·3	0·4	0·5	0·6	0·7	0·8	0·9	1·0
u/U	1·20	1·18	1·15	1·12	1·09	1·06	1·03	0·99	0·95	0·91	0·87
$u/u_{\max}$	0	0·43	0·59	0·71	0·79	0·86	0·92	0·95	0·98	0·99	1·00

TABLE 2

y/η ...	0·0	0·1	0·2	0·3	0·4	0·5	0·6	0·7	0·8	0·9	1·0
u/U	1·04	1·04	1·04	1·04	1·04	1·03	1·02	1·01	0·99	0·96	0·92
$u/u_{\max}$	0	0·36	0·51	0·62	0·71	0·79	0·86	0·92	0·96	0·99	1·00

TABLE 3

The value of f will depend on the nature of the bed and the hydraulic radius of the channel, and it is best determined in terms of Manning's coefficient n which is connected to f by the empirical relationships (see, for example, Rouse 1938, pp. 279 and 280)

$$f = \frac{g}{C^2}, \quad C = \frac{1{\cdot}486R^{\frac{1}{6}}}{n}, \tag{28}$$

where R is the hydraulic radius expressed in feet. For illustrative purposes we shall take $f = 0{\cdot}005$. For a channel of depth of about 20 ft. with a slope of one in a thousand, this coefficient corresponds to a bed of earth, gravel or rubble.

We consider a triangular channel with $f = 0{\cdot}005$ and $s = 0{\cdot}001$. Table 2 gives the results when $\kappa = \frac{1}{3}$, and table 3 gives the results when $\kappa = \frac{1}{6}$. In these tables, U denotes the mean velocity when eddy viscosity is neglected and $u_{\max}$ denotes the mid-stream velocity.

Similar calculations can be made for a trapezoidal channel. With $\kappa = \frac{1}{3}$, $f = 0{\cdot}005$, $s = 0{\cdot}001$, $H = 20$, $\eta = 2\eta_1 = 120$, the results given in table 4 are found.

The results show that the effects of eddy viscosity are important in regions where depth is changing, and in narrow channels. In wide rivers, its effects will be confined to near the walls.

y/η_1 ...	0	0·2	0·4	0·6	0·8	1·0
u/U	1·20	1·16	1·12	1·05	1·01	0·94
$\frac{y-\eta_1}{\eta-\eta_1}$	0	0·2	0·4	0·6	0·8	1·0
u/U	0·94	0·97	0·98	0·99	0·99	0·99

TABLE 4

The author wishes to acknowledge his gratitude to Prof. M. J. Lighthill for his helpful advice during the preparation of this paper, to the Nuffield Foundation for the grant of a Fellowship, and to the University of Dacca for leave of absence.

REFERENCES

MILNE-THOMSON, L. M. 1950 *Jacobian Elliptic Function Tables.* New York: Dover.
ROUSE, H. 1938 *Fluid Mechanics for Hydraulic Engineers.* New York: McGraw Hill.
SCHLICHTING, H. 1955 *Boundary Layer Theory.* London: Pergamon.
STOKER, J. J. 1957 *Water Waves.* New York: Interscience.

On the periodic fundamental solutions of the Stokes equations and their application to viscous flow past a cubic array of spheres

By H. HASIMOTO

Department of Aeronautical Engineering, Faculty of Engineering,
Kyoto University, Japan

(Received 15 June 1958)

Spatially periodic fundamental solutions of the Stokes equations of motion for a viscous fluid past a periodic array of obstacles are obtained by use of Fourier series. It is made clear that the divergence of the lattice sums pointed out by Burgers may be rescued by taking into account the presence of the mean pressure gradient. As an application of these solutions the force acting on any one of the small spheres forming a periodic array is considered. Cases for three special types of cubic lattice are investigated in detail. It is found that the ratios of the values of this force to that given by the Stokes formula for an isolated sphere are larger than 1 and do not differ so much among these three types provided that the volume concentration of the spheres is the same and small. The method is also applied to the two-dimensional flow past a square array of circular cylinders, and the drag on one of the cylinders is found to agree with that calculated by the use of elliptic functions.

1. Introduction

The study of the flow of a viscous fluid past a periodic array of spheres is very important from the theoretical and practical viewpoints. As far as the author is aware, however, many treatments of this problem have been made only by considering some artificial models, even in the case of the slow motion. This may be partly due to the fact that standard methods of constructing the solutions of the Stokes equations, by summing up the induced velocity of the isolated particles, encounter the difficulty of divergence pointed out already by Burgers (1941). Burgers proposed the so-called diffuse field of force to overcome this difficulty. This idea is extended by Brinkman (1947, 1948) and independently by Debye & Bueche (1948), who considered a model consisting of a sphere separated by an infinitely thin shell from a porous medium. Their main concern was in the study of the sedimentation of suspensions and the flow through porous media. The statistical treatment due to Kynch (1954, 1956) using the shielded potential belongs to this category.

Making use of a method analogous to the approximate method due to Wigner & Seitz (1933), Uchida (1949) investigated the flow past a simple cubic lattice of spheres. Although the satisfaction of the periodic condition is not perfect, it may

be regarded as one of the direct attacks on our problem. There is also Kawaguchi's ingenious treatment (1958) of replacing the field by the flow past a sphere in a frictionless circular pipe.

Recently, Tamada & Fujikawa (1957) investigated the two-dimensional flow through an infinite row of parallel circular cylinders on the basis of Oseen's equations and showed that the drag on one of the cylinders tends to the Stokes type in the limit of the small Reynolds numbers. Inspired by their results the author (1958*a*) discussed the flow through a thin screen and obtained an exact solution of the Stokes equation for a periodic series of flat plates set perpendicularly to the uniform flow. Kuwabara (1958) and Miyagi (1958) also treated respectively the flow past a row of parallel flat plates and the flow past a row of circular cylinders on the basis of the Stokes equations. Making use of elliptic functions the author (1958*b*) also determined the two-dimensional flow past a doubly periodic array of circular cylinders.

Taking into account these successful results it is natural for us to suspect that solutions for the case of an array of spheres exist and can be obtained by some kind of direct attack.

In this paper periodic fundamental solutions of the Stokes equations of motion for a viscous incompressible fluid past a periodic array of obstacles are given by use of Fourier series. It is made clear that the divergence pointed out by Burgers may be avoided by taking into account the presence of the mean pressure gradient which is present in our problem. As a simple example, the flow past a cubic lattice of small spheres is examined for three types of lattice (simple, face-centred, body-centred) and the force acting on any one of the spheres is determined as a function of volume concentration. It is found that the ratios of the values of this force to that given by the Stokes formula for an isolated sphere are larger than 1 and do not differ much for these three types so long as the volume concentration of spheres is the same and small. The method is also applied to the two-dimensional flow past a square array of circular cylinders, and the drag on any one of the cylinders is found to agree with that calculated by the author (1958*b*), using elliptic functions.

2. Basic equations and periodic fundamental solutions

Let us consider the steady motion of an incompressible viscous fluid past a periodic array of small obstacles with their centres at

$$\mathbf{r}_n = n_1\mathbf{a}^{(1)} + n_2\mathbf{a}^{(2)} + n_3\mathbf{a}^{(3)} \quad (n_1, n_2, n_3 = 0, \pm 1, \pm 2, \ldots), \tag{2.1}$$

where $\mathbf{a}^{(1)}$, $\mathbf{a}^{(2)}$ and $\mathbf{a}^{(3)}$ are the basic vectors determining the unit cell of the array.

According to the procedure of Lamb (1932) and Burgers (1938) the fundamental solutions of our problem are obtained by solving the following Stokes equation of motion and continuity equation

$$\mu\Delta\mathbf{V} = \operatorname{grad} p + \mathbf{F}\sum_n \delta(\mathbf{r} - \mathbf{r}_n) \quad \left(\Delta = \frac{\partial^2}{\partial x_1^2} + \frac{\partial^2}{\partial x_2^2} + \frac{\partial^2}{\partial x_3^2}\right), \tag{2.2}$$

$$\operatorname{div}\mathbf{V} = 0, \tag{2.3}$$

where $\mathbf{V}$ is the velocity, μ the viscosity, p the pressure, $\mathbf{F}$ the force acting on one of the obstacles, (x_1, x_2, x_3) are the Cartesian co-ordinates of the position vector $\mathbf{r}$, and $\delta(\mathbf{r}-\mathbf{r}_n)$ denotes Dirac's delta function defined by the conditions

$$\int_\tau \delta(\mathbf{r}-\mathbf{r}_n)\,d\mathbf{r} = \begin{cases} 1 & \text{for} \quad \tau \in \mathbf{r}_n \\ 0 & \text{for} \quad \tau \notin \mathbf{r}_n, \end{cases} \tag{2.4}$$

and

$$\delta(\mathbf{r}-\mathbf{r}_n) = 0 \quad \text{for} \quad \mathbf{r} \neq \mathbf{r}_n.$$

Taking into account the periodicity of the flow field we expand $\mathbf{V}$ and $-\operatorname{grad} p$ in Fourier series:

$$\mathbf{V} = \sum_{\mathbf{k}} \mathbf{V}_{\mathbf{k}} e^{-2\pi i(\mathbf{k}.\mathbf{r})}, \tag{2.5}$$

$$-\operatorname{grad} p = \sum_{\mathbf{k}} \mathbf{P}_{\mathbf{k}} e^{-2\pi i(\mathbf{k}.\mathbf{r})}, \tag{2.6}$$

where

$$\mathbf{k} = n_1\mathbf{b}^{(1)} + n_2\mathbf{b}^{(2)} + n_3\mathbf{b}^{(3)} \tag{2.7}$$

are vectors in the reciprocal lattice, which satisfy

$$\mathbf{k}.\mathbf{a}^{(j)} = n_j \quad (j = 1, 2, 3). \tag{2.8}$$

Making use of (2.7) and (2.8) we find the basic vectors $\mathbf{b}^{(1)}$, $\mathbf{b}^{(2)}$ and $\mathbf{b}^{(3)}$ in the reciprocal lattice to be

$$\mathbf{b}^{(1)} = \frac{[\mathbf{a}^{(2)} \times \mathbf{a}^{(3)}]}{\tau_0}, \quad \mathbf{b}^{(2)} = \frac{[\mathbf{a}^{(3)} \times \mathbf{a}^{(1)}]}{\tau_0}, \quad \mathbf{b}^{(3)} = \frac{[\mathbf{a}^{(1)} \times \mathbf{a}^{(2)}]}{\tau_0}, \tag{2.9}$$

where

$$\tau_0 = \mathbf{a}^{(1)}.[\mathbf{a}^{(2)} \times \mathbf{a}^{(3)}] \tag{2.10}$$

stands for the volume of the unit cell in the physical space.

Multiplying (2.2) and (2.3) by $e^{2\pi i(\mathbf{k}.\mathbf{r})}/\tau_0$ and integrating over a unit cell in physical space, we obtain

$$-4\pi^2\mu k^2 \mathbf{V}_{\mathbf{k}} = -\mathbf{P}_{\mathbf{k}} + \frac{\mathbf{F}}{\tau_0} \quad (k^2 = \mathbf{k}.\mathbf{k}), \tag{2.11}$$

$$(\mathbf{k}.\mathbf{V}_{\mathbf{k}}) = 0. \tag{2.12}$$

$\mathbf{P}_{\mathbf{k}}$ satisfies the relation

$$\mathbf{P}_{\mathbf{k}} \times \mathbf{k} = 0, \tag{2.13}$$

which can be proved by taking the curl of (2.6).

We begin by considering the terms for which $\mathbf{k} = 0$. Equation (2.11) yields

$$\mathbf{P}_0 = \frac{\mathbf{F}}{\tau_0}, \tag{2.14}$$

which means that the force acting on an obstacle is balanced by the mean pressure gradient of the fluid. Disregard of this relation would induce paradoxical results e.g. the divergence of $\mathbf{V}_0$ as already shown by Burgers.

Taking the scalar product of (2.11) with $\mathbf{k}$ we obtain, for $\mathbf{k} \neq 0$,

$$(\mathbf{k}.\mathbf{P}_{\mathbf{k}}) = \frac{1}{\tau_0}(\mathbf{k}.\mathbf{F}) = (\mathbf{k}.\mathbf{P}_0) \tag{2.15}$$

or, making use of (2.12) and (2.13),

$$\mathbf{P}_{\mathbf{k}} = \frac{(\mathbf{k}.\mathbf{F})\,\mathbf{k}}{\tau_0 k^2} \quad (\mathbf{k} \neq 0). \tag{2.16}$$

Substitution of (2.16) in (2.11) gives

$$\mathbf{V}_{\mathbf{k}} = \frac{1}{4\pi^2\mu\tau_0}\left[\frac{(\mathbf{k}.\mathbf{F})\,\mathbf{k}}{k^4} - \frac{\mathbf{F}}{k^2}\right] \quad (\mathbf{k} \neq 0). \tag{2.17}$$

Equations (2.5) and (2.6) with (2.14) to (2.17) are the periodic fundamental solutions of the Stokes equations for the flow past a periodic array of obstacles. Their components in Cartesian co-ordinates are given by

$$v_j = v_{0j} - \frac{1}{4\pi\mu}\left(F_j S_1 - \sum_{l=1}^{3} F_l \frac{\partial^2 S_2}{\partial x_l \partial x_j}\right), \tag{2.18}$$

$$-(\operatorname{grad} p)_j = \frac{F_j}{\tau_0} - \frac{1}{4\pi}\sum_{l=1}^{3} F_l \frac{\partial^2 S_1}{\partial x_l \partial x_j}, \tag{2.19}$$

where S_1 and S_2 are given by

$$S_1 = \frac{1}{\pi\tau_0}\sum_{\mathbf{k}\neq 0}' \frac{e^{-2\pi i(\mathbf{k}.\mathbf{r})}}{k^2}, \quad S_2 = -\frac{1}{4\pi^3\tau_0}\sum_{\mathbf{k}\neq 0}' \frac{e^{-2\pi i(\mathbf{k}.\mathbf{r})}}{k^4}. \tag{2.20}$$

and may be proved to be the solutions of the following equations:

$$\Delta S_2 = S_1 \tag{2.21}$$

and

$$\Delta S_1 = -4\pi\left[\sum_{\mathbf{n}} \delta(\mathbf{r} - \mathbf{r}_{\mathbf{n}}) - \frac{1}{\tau_0}\right], \tag{2.22}$$

by use of finite Fourier transforms.

It is important that S_1 is not harmonic even in the domain excluding $\mathbf{r}_{\mathbf{n}}$, because of the presence of the term $4\pi/\tau_0$. This makes clear the reason why the standard method of obtaining S_1 by summing up fundamental solutions of the Laplace equation for isolated particles has encountered difficulties. S_1 is equivalent to the electrostatic potential of a lattice composed of positive unit charges surrounded by the cloud of uniform negative charge which neutralizes them. It is interesting to note that the presence of this uniform charge corresponds to the presence of the mean pressure gradient in our problem (see (2.2)) and rescues the lattice sums from divergence.

3. Evald's technique for evaluating S_1 and S_2

In order to satisfy the boundary condition on the surface of an obstacle, it is necessary to evaluate S_1 and S_2 at small values of $\mathbf{r}$. A technique for this purpose was presented by Evald (1921) in the calculation of the Madelung energy of the ionic crystals in terms of S_1, and is summarized by Born & Misra (1940) in a convenient form.

We start with an integral representation for $1/k^{2m}$:

$$\frac{1}{k^{2m}} = \frac{\pi^m}{\Gamma(m)}\int_0^\infty e^{-\pi k^2\beta}\,\beta^{m-1}\,d\beta. \tag{3.1}$$

Multiplying by $e^{-2\pi i(\mathbf{k}.\mathbf{r})}$ and summing with respect to $\mathbf{k}$, except for $\mathbf{k} = 0$, we have

$$\begin{aligned}\sigma_m = \sum_{\mathbf{k}\neq 0}' \frac{e^{-2\pi i(\mathbf{k}.\mathbf{r})}}{k^{2m}} &= \frac{\pi^m}{\Gamma(m)}\sum_{\mathbf{k}\neq 0}' \int_0^\infty e^{-\pi k^2\beta - 2\pi i(\mathbf{k}.\mathbf{r})}\,\beta^{m-1}\,d\beta \\ &= \frac{\pi^m}{\Gamma(m)}\int_0^\infty \beta^{m-1}\left[\sum_{\mathbf{k}} e^{-\pi k^2\beta - 2\pi i(\mathbf{k}.\mathbf{r})} - 1\right] d\beta.\end{aligned} \tag{3.2}$$

Let us split the integral into two parts, one to be taken from 0 to α, and the other from α to ∞, and then apply Evald's theta transformation formula

$$\sum_{\mathbf{k}} e^{-\pi k^2\beta - 2\pi i(\mathbf{k}.\mathbf{r})} = \frac{\tau_0}{\beta^{\frac{3}{2}-\lambda}} \sum_{\mathbf{n}} e^{-\pi(\mathbf{r}-\mathbf{r_n})^2/\beta} \tag{3.3}$$

to the integral from 0 to α, where α is a moderate constant and

$$\lambda = \begin{cases} 0 & \text{for the three-dimensional case,} \\ \frac{1}{2} & \text{for the two-dimensional case.} \end{cases} \tag{3.4}$$

We get

$$\sigma_m = \frac{\pi^m \alpha^m}{\Gamma(m)} \left[\tau_0 \alpha^{-\frac{3}{2}+\lambda} \sum_{\mathbf{n}} \phi_{-m+\frac{1}{2}-\lambda}\left(\frac{\pi(\mathbf{r}-\mathbf{r_n})^2}{\alpha}\right) - \frac{1}{m} + \sum_{\mathbf{k}\neq 0}{}' e^{-2\pi i(\mathbf{k}.\mathbf{r})} \phi_{m-1}(\pi\alpha\mathbf{k}^2) \right], \tag{3.5}$$

where we have put $\beta = \alpha/\xi$ in the first integral and $\beta = \alpha\xi$ in the second, and $\phi_\nu(x)$ is the incomplete Γ-function

$$\phi_\nu(x) = \int_1^\infty \xi^\nu e^{-x\xi}\, d\xi. \tag{3.6}$$

The function $\phi_\nu(x)$ satisfies the recurrence formulae

$$\phi_\nu' = -\phi_{\nu+1}, \quad x\phi_\nu = e^{-x} + \nu\phi_{\nu-1}, \tag{3.7}$$

and is tabulated in Born & Misra's paper. In particular

$$\phi_0(x) = \frac{e^{-x}}{x}, \quad \phi_{-\frac{1}{2}}(x) = \frac{\sqrt{\pi}}{\sqrt{x}} \operatorname{erfc}(\sqrt{x}), \quad \phi_{-1}(x) = -E_i(-x), \tag{3.8}$$

where

$$\operatorname{erfc}(\xi) = \frac{2}{\sqrt{\pi}} \int_\xi^\infty e^{-\xi^2}\, d\xi \tag{3.9}$$

is the complementary error function and

$$-E_1(-\xi) = \int_\xi^\infty \frac{e^{-\xi}}{\xi}\, d\xi \tag{3.10}$$

denotes the exponential integral.

These functions tend to zero rapidly as $x \to \infty$, and

$$\phi_{-\frac{1}{2}}(x) = \frac{\sqrt{\pi}}{\sqrt{x}} - 2 + \frac{2x}{3} + O(x^2), \quad \phi_{-\frac{3}{2}}(x) = 2 - 2\sqrt{(\pi x)} + 2x + O(x^2), \tag{3.11}$$

$$\phi_{-1}(x) = -\gamma - \log x + x + O(x^2), \quad \phi_{-2}(x) = 1 - x(1 - \gamma - \log x) + O(x^2), \tag{3.12}$$

as $x \to 0$, where $\gamma = 0{\cdot}577215\ldots$ is Euler's constant.

Making use of these expressions we can evaluate the values of S_1 and S_2, etc., which are given in the following sections.

4. The case of a lattice of small spheres

As an application of the fundamental solutions (2.18) and (2.19) we consider the case of periodic array of spheres of equal radius a which is very small compared with the mutual distances of the spheres.

In order to satisfy the remaining boundary conditions on a sphere

$$\mathbf{V} = 0 \quad \text{at} \quad r = \sqrt{(|\mathbf{r}|^2)} = a, \tag{4.1}$$

we have only to know the behaviour of the fundamental solutions as $r \to 0$. Making use of (3.5) and (3.11) we obtain for S_1, S_2 and $\partial^2 S_2/\partial x_j \partial x_l$:

$$S_1 = \frac{\sigma_1}{\pi\tau_0} = \frac{1}{r} - c + O(r^2), \tag{4.2}$$

$$c = \frac{2}{\sqrt{\alpha}} + \frac{\alpha}{\tau_0} - \frac{1}{\sqrt{\alpha}} \sum_{\mathbf{n}\neq 0}{}' \phi_{-\frac{1}{2}}\left(\frac{\pi \mathbf{r}_\mathbf{n}^2}{\alpha}\right) - \frac{\alpha}{\tau_0} \sum_{\mathbf{k}\neq 0}{}' \phi_0(\pi\alpha\mathbf{k}^2). \tag{4.2'}$$

$$S_2 = -\frac{\sigma_2}{4\pi^3\tau_0} = \frac{r}{2} - c_2 + O(r^2), \tag{4.3}$$

$$c_2 = \frac{1}{4\pi}\left[2\sqrt{\alpha} - \frac{\alpha^2}{2\tau_0} + \sqrt{\alpha} \sum_{\mathbf{n}\neq 0}{}' \phi_{-\frac{3}{2}}\left(\frac{\pi \mathbf{r}_\mathbf{n}^2}{\alpha}\right) + \frac{\alpha^2}{\tau_0} \sum_{\mathbf{k}\neq 0}{}' \phi_1(\pi\alpha\mathbf{k}^2)\right] \tag{4.3'}$$

$$\frac{\partial^2 S_2}{\partial x_j \partial x_l} = -\frac{x_j x_l}{2r^3} + \delta_{jl}\left(\frac{1}{2r} - c_{jj}\right) + O(r^2) \quad \left(\delta_{jl} = \begin{cases} 1 & (j = l) \\ 0 & (j \neq l) \end{cases}\right), \tag{4.4}$$

$$c_{jj} = \frac{1}{\sqrt{\alpha}} - \frac{1}{2\sqrt{\alpha}} \sum_{\mathbf{n}\neq 0}{}' \left[\phi_{-\frac{1}{2}}\left(\frac{\pi \mathbf{r}_\mathbf{n}^2}{\alpha}\right) - \frac{2\pi x_{\mathbf{n}j}^2}{\alpha} \phi_{\frac{1}{2}}\left(\frac{\pi \mathbf{r}_\mathbf{n}^2}{\alpha}\right)\right] - \frac{\pi\alpha^2}{\tau_0} \sum_{\mathbf{k}\neq 0}{}' \mathbf{k}_j^2 \phi_1(\pi\alpha\mathbf{k}^2). \tag{4.4'}$$

where $x_{\mathbf{n}j}$ and $\mathbf{k}_j$ denote respectively x_j-component of $\mathbf{r}_\mathbf{n}$ and $\mathbf{k}$.

Burgers has shown that a good approximation to $\mathbf{F}$ can be obtained if we determine $\mathbf{F}$ from the condition that the mean velocity on the sphere vanishes, i.e.

$$\langle \mathbf{V} \rangle = \frac{1}{4\pi a^2} \int_{r=a} \mathbf{V}\, dS = 0. \tag{4.5}$$

Inserting (4.2) to (4.4') into (2.18), neglecting all terms of higher order than (a^2) and using

$$\langle x_j x_l \rangle = \frac{a^2}{3} \delta_{jl}, \tag{4.6}$$

we have

$$4\pi\mu v_{0j} = \left(\frac{2}{3a} - c + c_{jj}\right) F_j + O(a^2), \tag{4.7}$$

i.e.

$$F_j = \frac{6\pi\mu a v_{0j}}{1 - \kappa_j a} + O(a^3), \tag{4.8}$$

where κ_j is a constant determined by the basic vectors $\mathbf{a}_1$, $\mathbf{a}_2$ and $\mathbf{a}_3$:

$$\kappa_j = \tfrac{3}{2}(c - c_{jj}) = \frac{3}{2}\left[\frac{1}{\sqrt{\alpha}} + \frac{\alpha}{\tau_0} - \frac{1}{2\sqrt{\alpha}} \sum_{\mathbf{n}\neq 0}{}' \left(\phi_{-\frac{1}{2}} + \frac{2\pi x_{\mathbf{n}j}^2}{\alpha} \phi_{\frac{1}{2}}\right) - \frac{\alpha}{\tau_0} \sum_{\mathbf{k}\neq 0}{}' (\phi_0 - \pi\alpha\mathbf{k}_j^2 \phi_1)\right]. \tag{4.9}$$

As a typical case we consider the cubic array of spheres. Now, there are three types of cubic lattice:

(1) Simple cubic lattice (S.C.L)

$$\left.\begin{matrix} \mathbf{a}_1 \\ \mathbf{a}_2 \\ \mathbf{a}_3 \end{matrix}\right\} = h \left\{\begin{matrix} (1, 0, 0) \\ (0, 1, 0) \\ (0, 0, 1) \end{matrix}\right\}, \quad \tau_0 = h^3, \qquad \left.\begin{matrix} \mathbf{b}_1 \\ \mathbf{b}_2 \\ \mathbf{b}_3 \end{matrix}\right\} = 1/h \left\{\begin{matrix} (1, 0, 0) \\ (0, 1, 0) \\ (0, 0, 1) \end{matrix}\right\} \tag{4.10}$$

(2) Body-centred cubic lattice (B.C.L)

$$\left.\begin{matrix} \mathbf{a}_1 \\ \mathbf{a}_2 \\ \mathbf{a}_3 \end{matrix}\right\} = \tfrac{1}{2}h \left\{\begin{matrix} (\ 1, & 1, & -1) \\ (-1, & 1, & 1) \\ (\ 1, & -1, & 1) \end{matrix}\right\}, \quad \tau_0 = \tfrac{1}{2}h^3, \qquad \left.\begin{matrix} \mathbf{b}_1 \\ \mathbf{b}_2 \\ \mathbf{b}_3 \end{matrix}\right\} = 1/h \left\{\begin{matrix} (1, 1, 0) \\ (0, 1, 1) \\ (1, 0, 1) \end{matrix}\right\} \tag{4.11}$$

(3) Face-centred cubic lattice (F.C.L)

$$\left.\begin{matrix}\mathbf{a}_1\\ \mathbf{a}_2\\ \mathbf{a}_3\end{matrix}\right\} = \tfrac{1}{2}h \begin{Bmatrix}(1,\,1,\,0)\\ (0,\,1,\,1)\\ (1,\,0,\,1)\end{Bmatrix}, \quad \tau_0 = \tfrac{1}{4}h^3, \qquad \left.\begin{matrix}\mathbf{b}_1\\ \mathbf{b}_2\\ \mathbf{b}_3\end{matrix}\right\} = 1/h \begin{Bmatrix}(\ 1, & 1, & -1)\\ (-1, & 1, & 1)\\ (1, & -1, & 1)\end{Bmatrix} \tag{4.12}$$

According to their symmetry with respect to three co-ordinates axes it is obvious that

$$\left\langle \frac{\partial^2 S_2}{\partial x_1^2} \right\rangle = \left\langle \frac{\partial^2 S_2}{\partial x_2^2} \right\rangle = \left\langle \frac{\partial^2 S_2}{\partial x_3^2} \right\rangle = \tfrac{1}{3}\langle \Delta S_2 \rangle = \tfrac{1}{3}\langle S_1 \rangle \tag{4.13}$$

and

$$c_{11} = c_{22} = c_{33} = \tfrac{1}{3}c. \tag{4.14}$$

Introducing (4.14) into (4.9) we obtain

$$\kappa_1 = \kappa_2 = \kappa_3 = c = -\lim_{r\to 0}\left(S_1 - \frac{1}{r}\right). \tag{4.15}$$

The values of c have been calculated by many authors (e.g. Emersleben 1923) in connexion with the determination of the Madelung constants, and are given in table 1. In this table the values of ca are also given in terms of the volume concentration of spheres:

$$c_\tau = \frac{4\pi}{3}\frac{a^3}{\tau_0}. \tag{4.16}$$

	ch	$ca/\sqrt[3]{c_\tau}$	bh^2
S.C.L	2·8373	1·7601	0·19457
B.C.L	$3{\cdot}639_2$	$1{\cdot}791_8$	$0{\cdot}120_0$
F.C.L	$4{\cdot}584_8$	$1{\cdot}791_7$	$0{\cdot}213_1$

TABLE 1

5. Refinement of the approximation in the case of cubic arrays

In order to refine the rough approximation in the previous section we have only to determine the coefficients of the complementary functions which are derived from S_1 and S_2 by successive differentiation and which are to be added to (2.18).

As one of the most simple cases we consider the case of the cubic array. Let us assume that the mean flow is parallel to the x_1-axis without loss of generality. In this case we can take

$$v_1 = U_0 - \frac{1}{4\pi\mu}\left[\mathbf{G}\left(S_1 - \frac{\partial^2 S_2}{\partial x_1^2}\right) + \mathbf{H}\frac{\partial^2 S_1}{\partial x_1^2}\right], \tag{5.1}$$

$$v_2 = \frac{1}{4\pi\mu}\left[\mathbf{G}\frac{\partial^2 S_2}{\partial x_1 \partial x_2} - \mathbf{H}\frac{\partial^2 S_1}{\partial x_1 \partial x_2}\right], \tag{5.2}$$

$$v_3 = \frac{1}{4\pi\mu}\left[\mathbf{G}\frac{\partial^2 S_2}{\partial x_1 \partial x_3} - \mathbf{H}\frac{\partial^2 S_1}{\partial x_1 \partial x_3}\right], \tag{5.3}$$

$$-(\operatorname{grad} p)_j = \frac{F_j}{\tau_0} - \frac{1}{4\pi}\operatorname{grad}\mathbf{G}\frac{\partial S_1}{\partial x_1}, \tag{5.4}$$

making use of (2.18) and (2.19) and taking into account the symmetry, where **G** and **H** stand for differential operators

$$\mathbf{G} = \sum_{m,n,p=0}^{\infty} A_{mnp} \frac{\partial^{2m+2n+2p}}{\partial x_1^{2m} \partial x_2^{2n} \partial x_3^{2p}}, \quad \mathbf{H} = \sum_{m,n,p=0}^{\infty} B_{mnp} \frac{\partial^{2m+2n+2p}}{\partial x_1^{2m} \partial x_2^{2n} \partial x_3^{2p}}. \tag{5.5}$$

A_{mnp} and B_{mnp} are symmetric with respect to n and p, and some of them can be taken to be zero on account of the relations (2.21) and (2.22).

In particular, U_0, A_{000} and B_{000} are intimately related with the mean velocity U and the force **F** acting on a sphere as follows. The force acting on a sphere is shown to be

$$F_1 = A_{000} = A, \quad F_2 = 0, \quad F_3 = 0, \tag{5.6}$$

by comparison of (5.4) and (2.19). On the other hand, the mean velocity U in the direction of x_1-axis is given by the surface integral

$$U = \frac{1}{h^2} \int_{-\frac{1}{2}h}^{\frac{1}{2}h} \int_{-\frac{1}{2}h}^{\frac{1}{2}h} v_1 dx_2 dx_3, \tag{5.7}$$

taken over a surface which is bounded by a rectangle of area $h \times h$ perpendicular to x_1-axis and is outside every sphere. Making use of the relations

$$S_1 - \frac{\partial^2 S_2}{\partial x_1^2} = \left(\frac{\partial^2}{\partial x_2^2} + \frac{\partial^2}{\partial x_3^2} \right) S_2, \tag{5.8}$$

$$\frac{\partial^2 S_1}{\partial x_1^2} = \frac{4\pi}{\tau_0} - \left(\frac{\partial^2}{\partial x_2^2} + \frac{\partial^2}{\partial x_3^2} \right) S_1, \tag{5.9}$$

for $\mathbf{r} \neq \mathbf{r}_n$, derived from (2.21) and (2.22) and the periodicity of $\mathbf{G}[\partial S_{1,2}/\partial x_j]$ and $\mathbf{H}[\partial S_{1,2}/\partial x_j]$ $(j = 2, 3)$ with respect to x_j, we obtain

$$U = \frac{1}{h^2} \int_{-\frac{1}{2}h}^{\frac{1}{2}h} \int_{-\frac{1}{2}h}^{\frac{1}{2}h} \left(U_0 - B_{000} \frac{1}{\mu \tau_0} \right) dx_2 dx_3 = U_0 - \frac{B}{\mu \tau_0} \quad (B = B_{000}). \tag{5.10}$$

We note that the mean flow is not U_0, but has an additional term which is shown to be of the order of c_τ (see (5.22)). The x_2- and x_3-components of the mean velocity are easily proved to be zero.

Let us proceed to the determination of these constants from the boundary condition (4.1) on a sphere of small radius a.

For this purpose we expand $S_1 - 1/r$ and $S_2 - \frac{1}{2}r$ in spherical harmonics with their common centre at $r = 0$ as follows:

$$S_1 = \frac{1}{r} - c + \frac{2\pi}{3\tau_0} r^2 + \sum_{n=2}^{\infty} \sum_{m=0}^{m \leqq \frac{1}{2}n} a_{nm} Y_{2n}^{4m}(x_1, x_2, x_3) \tag{5.11}$$

$$S_2 = \frac{r}{2} - c_2 - \frac{c}{6} r^2 + \frac{\pi r^4}{30\tau_0} + \sum_{n=2}^{\infty} \sum_{m=0}^{m \leqq \frac{1}{2}n} (b_{nm} + \tilde{a}_{nm} r^2) Y_{2n}^{4m}(x_1, x_2, x_3), \tag{5.12}$$

where use is made of Hobson's theorem (1931, p. 161), together with the cubic symmetry of these functions, and

$$Y_n^m(x_1, x_2, x_3) = r^n P_n^m(\cos\theta) \cos m\phi, \tag{5.13}$$

with

$$x_1 = r\cos\theta, \quad x_2 = r\sin\theta\cos\phi, \quad x_3 = r\sin\theta\sin\phi. \tag{5.14}$$

Also, c and c_2 are given by (4.2′), (4.3′) and table 1, and

$$\left.\begin{matrix} a_{nm} \\ b_{nm} \end{matrix}\right\} = \frac{\epsilon_m \cdot 2^{2n}(2n)!\,(2n-4m)!}{(4n)!\,(2n+4m)!}\left[Y_{2n}^{4m}\left(\frac{\partial}{\partial x_1}, \frac{\partial}{\partial x_2}, \frac{\partial}{\partial x_3}\right) \begin{matrix} S_1 - 1/r \\ S_2 - r/2 \end{matrix} \right]_{r=0}$$

$$(\epsilon_0 = 1, \epsilon_m = 2 \text{ for } m > 0), \quad (5.15)$$

$$\tilde{a}_{nm} = \frac{1}{2(4n+3)} a_{nm}. \quad (5.16)$$

Introducing into (4.1) the expressions (5.1) to (5.3) with (5.6) and (5.10) to (5.12) and equating to zero the coefficients of $P_0, P_2, \ldots$ in v_1 and $P_2' e^{i\phi}, \ldots$ in $v_2 + iv_3$ respectively we obtain the following simultaneous equations

$$\left[\frac{2}{3a} - \frac{2c}{3} + \frac{4\pi}{9\tau_0}\right] F - \frac{8\pi}{3\tau_0} B + \left[\frac{8\pi}{15\tau_0} - 24b + O(a^2)\right] A_{100} + O(a^7) = 4\pi\mu U, \quad (5.17)$$

$$\left[\frac{1}{3a} - \left(\frac{8\pi}{45\tau_0} + 12b\right) a^2 + O(a^4)\right] F + \left[\frac{2}{a^3} + O(a^2)\right] B + \left[\frac{2}{7a^3} + O(a^2)\right] A_{100} + O(a^5) = 0, \quad (5.18)$$

$$\left[\frac{1}{6a} - \left(\frac{4\pi}{45\tau_0} - 4b\right) a^2\right] F + \left[\frac{1}{a^3} + O(a^2)\right] B - \left[\frac{3}{7a^3} + O(a^2)\right] A_{100} + O(a^5) = 0, \quad (5.19)$$

$$\ldots \quad \ldots \quad \ldots$$

$$b \equiv b_{20}.$$

Comparing the main terms in these equations we see at once that, at most,

$$F = O(a), \quad B = O(a^3), \quad A_{mnp} = O(a^{4(m+n+p)+1}), \quad B_{mnp} = O(a^{4(m+n+p)+3}). \quad (5.20)$$

Solving (5.17) to (5.19), we obtain

$$A_{100} = \tfrac{35}{2} b a^5 F + O(a^8), \quad (5.21)$$

$$B = -\frac{1}{6}\left[1 - \left(\frac{8\pi}{15\tau_0} + 21b\right) a^3\right] a^2 F + O(a^8), \quad (5.22)$$

$$F = 6\pi\mu a U/Q, \quad (5.23)$$

where

$$Q = 1 - ca + \frac{4\pi a^3}{3\tau_0} - \left(\frac{16\pi^2}{45\tau_0^2} + 630b^2\right) a^6 + O(a^8) \quad (5.23')$$

and

$$b = b_{20} = -\frac{\pi^3}{15}\left[\alpha^{-\frac{7}{2}} \sum_{\mathbf{n}+0}' (x_{\mathbf{n}1}^4 - 3x_{\mathbf{n}1}^2 x_{\mathbf{n}2}^2)\, \phi_{\frac{7}{2}}\left(\frac{\pi \mathbf{r}_{\mathbf{n}}^2}{\alpha}\right) + \frac{\alpha^2}{\tau_0} \sum_{\mathbf{k}+0}' (\mathbf{k}_1^4 - 3\mathbf{k}_1^2 \mathbf{k}_2^2)\, \phi_1(\pi\alpha \mathbf{k}^2)\right]. \quad (5.24)$$

The numerical values of b are given in table 1. In terms of c_τ equations (5.23′) are rewritten as follows:

$$Q = \left\{\begin{matrix} 1 - 1{\cdot}7601\, \sqrt[3]{c_\tau} + c_\tau - 1{\cdot}5593\, c_\tau^2 + \ldots & \text{(S.C.L.)} \\ 1 - 1{\cdot}791_8\, \sqrt[3]{c_\tau} + c_\tau - 0{\cdot}329_2\, c_\tau^2 + \ldots & \text{(B.C.L.)} \\ 1 - 1{\cdot}791_7\, \sqrt[3]{c_\tau} + c_\tau - 0{\cdot}302_0\, c_\tau^2 + \ldots & \text{(F.C.L.)} \end{matrix}\right\}. \quad (5.25)$$

Making use of (5.25) we can calculate the values of F for three types of cubic lattice, the results being shown in table 2 and figure 1, where $O(c_\tau^\nu)$ stands for the values calculated by retaining the terms of the order of c_τ^ν.

It is found that the values of F are larger than $6\pi\mu aU$, i.e. the value for an isolated sphere, and do not differ much for the three types of cubic lattice, provided that the values of c_τ are the same and small. This conclusion will be applicable also to other types of lattice.

	$\sqrt[3]{c_\tau}$	a/h	$Q:O(\sqrt[3]{c_\tau})$	$Q:O(c_\tau)$	$Q:O(c_\tau^2)$	$Q^{-1}:O(c_\tau^2)$
S.C.L	0	0·00000	1·0000	1·0000	1·0000	1·0000
	0·05	0·03102	0·9120	0·9121	0·9121	1·096
	0·10	0·06204	0·8240	0·8250	0·8250	1·212
	0·20	0·12407	0·6480	0·6560	0·6559	1·525
	0·30	0·18611	0·4720	0·4990	0·4978	2·009
	0·40	0·24814	0·2960	0·3600	0·3536	2·83
	0·50	0·31018	0·1199	0·2449	0·2206	4·5
	0·60	0·37221	—	0·1599	0·0872	12
B.C.L	0	0·00000	1·0000	1·0000	1·0000	1·0000
	0·05	0·02462	0·9104	0·9105	0·9105	1·098
	0·10	0·04924	0·8208	0·8218	0·8218	1·217
	0·20	0·09847	0·6416	0·6496	0·6496	1·539
	0·30	0·14771	0·4625	0·4895	0·4892	2·044
	0·40	0·19695	0·2833	0·3473	0·3459	2·89
	0·50	0·24619	0·1041	0·2291	0·2240	4·47
	0·60	0·29542	—	0·1409	0·1256	8·0
	0·70	0·34466	—	0·0888	0·0500	20
F.C.L	0	0·00000	1·0000	1·0000	1·0000	1·0000
	0·05	0·01954	0·9104	0·9105	0·9105	1·098
	0·10	0·03908	0·8208	0·8218	0·8128	1·217
	0·20	0·07816	0·6417	0·6497	0·6496	1·539
	0·30	0·11724	0·4625	0·4895	0·4893	2·044
	0·40	0·15632	0·2833	0·3473	0·3461	2·89
	0·50	0·19540	0·1042	0·2292	0·2244	4·47
	0·60	0·23448	—	0·1410	0·1269	7·9
	0·70	0·27356	—	0·0888	0·0533	19

TABLE 2

6. Two-dimensional case

The two-dimensional case, i.e. the flow past an array of circular cylinders of radius $r = \sqrt{(x_1^2+x_2^2)} = a$, can be treated in a similar manner.

Putting $\lambda = \frac{1}{2}$ in (3.5), etc., we obtain, for example,

$$S_1 = \frac{\sigma_1}{\pi\tau_0} = \sum_{\mathbf{n}} \phi_{-1}\left(\frac{\pi(\mathbf{r}-\mathbf{r}_{\mathbf{n}})^2}{\alpha}\right) - \frac{\alpha}{\tau_0} + \frac{\alpha}{\tau_0}\sum_{\mathbf{k}\neq 0}{}' e^{-2\pi i(\mathbf{k}.\mathbf{r})}\phi_0(\pi\alpha\mathbf{k}^2) \tag{6.1}$$

$$= -\log(\pi r^2/\alpha) - \bar{c} + O(r^2),$$

$$\bar{c} = \gamma + \frac{\alpha}{\tau_0} - \sum_{\mathbf{n}\neq 0}{}' \phi_{-1}\left(\frac{\pi\mathbf{r}_{\mathbf{n}}^2}{\alpha}\right) - \frac{\alpha}{\tau_0}\sum_{\mathbf{k}\neq 0}{}' \phi_0(\pi\alpha\mathbf{k}^2), \tag{6.1'}$$

$$S_2 = -\frac{\sigma_2}{4\pi^3\tau_0} = -\frac{\alpha}{4\pi}\left[\sum_{\mathbf{n}} \phi_{-2}\left(\frac{\pi(\mathbf{r}-\mathbf{r}_{\mathbf{n}})^2}{\alpha}\right) - \frac{\alpha}{2\tau_0} + \frac{\alpha}{\tau_0}\sum_{\mathbf{k}\neq 0}{}' e^{-2\pi i(\mathbf{k}.\mathbf{r})}\phi_1(\pi\alpha\mathbf{k}^2)\right], \tag{6.2}$$

$$S_1 - \frac{\partial^2 S_2}{\partial x_1^2} = \frac{\partial^2 S_2}{\partial x_2^2} = -\tfrac{1}{2}\log\frac{\pi r^2}{\alpha} - \frac{x_2^2}{r^2} - \frac{\gamma}{2} + \Sigma_2 + O(r^2), \tag{6.3}$$

$$\Sigma_2 = \tfrac{1}{2}\sum_{\mathbf{n}}{}'\left[\phi_{-1}\left(\frac{\pi\mathbf{r}_{\mathbf{n}}^2}{\alpha}\right) - \frac{2\pi x_{\mathbf{n}2}^2}{\alpha}\phi_0\left(\frac{\pi\mathbf{r}_{\mathbf{n}}^2}{\alpha}\right)\right] + \frac{\pi\alpha^2}{\tau_0}\sum_{\mathbf{k}}{}' \mathbf{k}_2^2\phi_1(\pi\alpha\mathbf{k}^2). \tag{6.3'}$$

From these results we can calculate the drag per unit length of a circular cylinder in the array:

$$F_1 \doteqdot \frac{4\pi\mu v_{01}}{\langle S_1 - \partial^2 S_2/\partial x_1^2\rangle} \doteqdot \frac{8\pi\mu v_{01}}{\log(\alpha/\pi a^2) - 1 - \gamma + 2\Sigma_2}. \tag{6.4}$$

In particular, for a square array of period h we get the formula

$$F_1 \doteqdot \frac{4\pi\mu U_1}{\frac{1}{2}\langle S_1\rangle} = \frac{8\pi\mu U_1}{\log(h^2/\pi a^2) - 1 - \gamma + \sum_{\mathbf{n}\neq 0}' [\phi_0(\pi\mathbf{n}^2) + \phi_{-1}(\pi\mathbf{n}^2)]} = \frac{4\pi\mu U_1}{\log(h/a) - 1{\cdot}3105\ldots}, \tag{6.5}$$

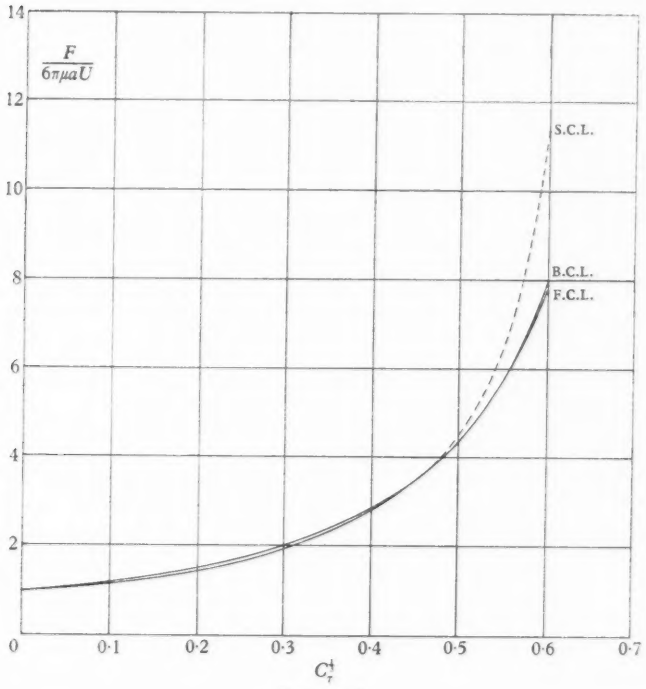

FIGURE 1

where we have put $\alpha = \tau_0 = h^2$ and used the relation

$$\left\langle \frac{\partial^2 S_2}{\partial x_1^2} \right\rangle = \left\langle \frac{\partial^2 S_2}{\partial x_2^2} \right\rangle = \tfrac{1}{2}\langle S_1\rangle \quad (\mathbf{r} \neq \mathbf{r}_\mathbf{n}). \tag{6.6}$$

Recently the author treated the same problem by making use of elliptic functions and obtained a formula corresponding to (6.5) in the form:

$$F_1 = \frac{4\pi\mu U_1}{\log(h/a) - \tilde{c} + (\pi a^2/h^2) + O(a^4/h^4)}, \tag{6.7}$$

where $\tilde{c} = \log\left[2\pi \prod_{n=1}^{\infty} (1 - e^{-2n\pi})^2\right] + \frac{1}{4} - \frac{1}{4}\pi + \frac{1}{2}\pi \sum_{n=1}^{\infty} \frac{1}{\sinh^2 n\pi} = 1{\cdot}3105\ldots.$ (6.8)

It will be seen that the two formulae (6.5) and (6.7) are in perfect agreement with each other to the order here considered.

This problem was suggested by Prof. Ko Tamada. The author wishes to express his cordial thanks to Prof. Tamada, Prof. Isao Imai, and Prof. Susumu Tomotika for their continual encouragement and helpful discussions throughout this work. The author's thanks are also due to the Japan Ministry of Education for a grant in aid for fundamental scientific research.

REFERENCES

Born, M. & Misra, R. D. 1940 *Proc. Camb. Phil. Soc.* **36**, 466.
Brinkman, H. C. 1947 *Appl. Sci. Res., Hague*, **1**, A, 27.
Brinkman, H. C. 1948 *Appl. Sci. Res., Hague*, **1**, A, 81.
Burgers, J. M. 1938 *2nd Report on Viscosity and Plasticity*, ch. III.
Burgers, J. M. 1941 *Proc. K. Akad. Wet. Amst.* **44**, 1045, 1174.
Debye, P. & Bueche, A. M. 1948 *J. Chem. Phys.* **16**, 573.
Emersleben, O. 1923 *Phys. Z.* **36**, 173, 466.
Ewald, P. P. 1921 *Ann. Phys.* **64**, 253.
Hasimoto, H. 1958*a* *J. Phys. Soc. Japan*, **13**, **633**.
Hasimoto, H. 1958*b* *J. Phys. Soc. Japan* (to be published).
Hobson, E. W. 1931 *The Theory of Spherical and Ellipsoidal Harmonics.* Cambridge University Press.
Kawaguchi, M. 1958 *J. Phys. Soc. Japan*, **13**, 209.
Kuwabara, S. 1958 *J. Phys. Soc. Japan* (to be published).
Kynch, G. J. 1954 *Brit. J. Appl. Phys.* **3**, 5.
Kynch, G. J. 1956 *Proc. Roy. Soc.* A, **237**, 90.
Lamb, H. 1932 *Hydrodynamics*, 6th ed. Cambridge University Press.
Miyagi, T. 1958 *J. Phys. Soc. Japan*, **13**, 493.
Tamada, K. & Fujikawa, H. 1957 *Quart. J. Mech. Appl. Math.* **10**, 425.
Uchida, S. 1949 *Rep. Inst. Sci. Technol. Tokyo*, **3**, 97.
Wigner, H. & Seitz, F. 1933 *Phys. Rev.* **43**, 804.

REVIEWS

Collected works of Theodore von Kármán. Vol. I, 1902–13, pp. 530; vol. II, 1914–32, pp. 436; vol. III, 1933–39, pp. 391; vol. IV, 1940–51, pp. 480. London: Butterworths Scientific Publications, 1956. £14. 10*s*. the set.

These four massive volumes contain the one hundred and eleven published papers and lectures of Dr von Kármán during the fifty years 1902–51. While they are an astonishing tribute to the learning, insight, skill and energy of the author, they form only an interim report on his scientific activities, which are still continuing with unabated vigour and enthusiasm.

To review these volumes is as if one attempted to review the *Encyclopaedia Britannica* or passed judgement on the collected works of Leonardo da Vinci. To attempt any critical comment seems impertinent presumption; to relapse into a few phrases of appreciation and gratitude seems miserably inadequate.

Perhaps the most useful task the reviewer can attempt is to provide classified summaries of von Kármán's work, so that the research worker can easily locate the references he may be seeking and quickly envisage the rapid developments in von Kármán's thought. The references in the following brief notes on this great work give the date of publication and the number of the paper in the newly printed volumes.

Compressible flow

The fundamental parameter which discriminates between the different regimes of fluid flow is the Reynolds number $R = Ul/\nu$. The physical significance of this number was pointed out by von Kármán in 1923 (**38**). According to the kinetic theory of gases the kinematic viscosity is given approximately by the formula $\nu = c\lambda$, where c is the mean molecular velocity and λ is the mean free path. Hence

$$R = (U/c)\,(l/\lambda).$$

Now c is of the same order as the acoustic speed, so that U/c is of the same order as the Mach number M; while l/λ measures the size l of a typical dimension of the moving body in terms of the molecular scale. We can distinguish three regimes:

(*a*) the region of Brownian movement for which $U/c \ll 1$, $l/\lambda \sim 1$;

(*b*) the region of hydrodynamic flow for which $U/c \ll 1$, $l/\lambda \gg 1$;

(*c*) the ballistic region for which $U/c \sim 1$, $l/\lambda \gg 1$.

Curiously enough, one of von Kármán's earliest papers (1907, **3**) deals with the 'ballistic regime', and discusses stationary waves in streams of gas in terms of the wave equation

$$(1-M^2)\,f_{xx}+f_{yy}+f_{zz} = 0,$$

where f (a little surprisingly) is not the velocity potential (the existence of which is not assumed), but the logarithm of the density ρ.

His next paper (1908, **4**) discusses the flow of gas and steam flow through a de Laval nozzle, the formation of shock waves and the Schlieren method for the optical examination of the flow. The diagrams (figures 9 and 10) in this paper must

surely be some of the earliest diagrams constructed by aerodynamicists to illustrate the differences between the propagation of acoustic waves in subsonic ($M < 1$) and supersonic conditions ($M > 1$).

In 1932 (**56**) von Kármán published a purely mathematical paper with Norton B. Moore on the wave resistance of supersonic bodies of revolution. This paper has had a great influence on aerodynamic theory, especially as regards the analogy between the von Kármán–Moore formula for wave drag and the classical formula for the induced drag of a lifting line (in **95**). A paper written in 1935 (**67**) gives a fine account of the general theory of the problem of resistance in compressible fluids, including both boundary layer effects and heat transfer.

von Kármán returned to the subject of compressibility effects in gas dynamics in 1941 (**84**), when he gave a general survey of the theory and of the analytical methods of solution (expansion in powers of M, Glauert's transformation, the hodograph method, the Tsien approximation (suggested by von Kármán in 1939)) and discussed the variation of drag and lift in the transonic region and the existence of a critical Mach number. The same themes are developed in a general survey given at the University of Pennsylvania Bicentennial Conference (no date, **85**), and with special reference to supersonic flow in 1947 (**95**). This long and important paper presents von Kármán's 'signal theory', an account of the mechanism of lift and wave drag, a summary of wave-drag calculations, the linearized theory, boundary-layer effects, transonic flow and interaction between boundary layers and shock waves.

The analogy between supersonic gas flow and the 'shooting' or supra-undal flow of water in an open channel was developed and exploited by von Kármán (1938, **72**) in a paper which emphasizes the practical applications of this fruitful comparison, which had been described by Preiswerk (at the suggestion of Ackeret) in the previous year.

von Karman wrote only two papers on transonic flow ($M \sim 1$), but one of these (1947, **96**) has been of outstanding importance as it gave for the first time the similarity law which replaces, for transonic flow, the Glauert rule for incompressible flow and the Ackeret rule for supersonic flow. The other paper (1950, **107**) gives a special, simple and exact solution of the Tricomi equations for transonic flow along an undulating wall.

A region of flow not mentioned in von Kármán's 1923 paper (**38**) is that of free molecule flow ($l \sim \lambda$), but in fact von Kármán had already entered this region in 1913 (**22**), in a paper written in collaboration with H. Bolze and M. Born on the temperature jump at the surface of a body exposed to molecular bombardment.

Incompressible inviscid flow

Although the theory of incompressible flow was not von Kármán's main interest, his contributions to this subject are still of considerable significance. His earliest paper (1918, **29**), written in collaboration with E. Trefftz, generalizes the Joukowski transformation of a circular cylinder into aerofoil sections. The von Kármán–Trefftz transformation

$$(z-A)/(z-B) = [(\zeta-A)/(\zeta-B)]^k$$

reduces to the Joukowski transformation when $k = 2$, and, when k is slightly less than 2, gives a profile with a trailing edge angle of $\delta = 2\pi - k\pi$.

The next paper (1927, **45**) gives a method of calculating the pressure distribution around airship bodies. A piece-wise constant source distribution is assumed along the axis of symmetry and the source strengths are adjusted to give the correct profile at a suitable number of stations. Both longitudinal and transverse motions are considered. Further developments of this work and practical applications are summarized in von Kármán's opening publication from the Daniel Guggenheim Airship Institute (1933, **59**).

A short note (1929, **48**) discusses the effect on the lift of an aerofoil of a discontinuity in the velocity of the wind; and a later note (1942, **86**) gives some comments on Newton's theory of air resistance.

A new presentation of lifting line theory given in 1935 (**66**) starts from the Fourier transform of the potential function and gives an extension to the theory of the lifting surface.

A similar technique is employed in a paper written with H. S. Tsien (1945, **92**), which extends Prandtl's lifting line theory to a wing in a non-uniform flow such as occurs in an open jet wind-tunnel or in a propeller slip stream.

In 1938 (**74**) von Kármán, in collaboration with W. R. Sears, made a most illuminating contribution to the theory of the non-uniform motion of an aerofoil, initiated by H. Wagner in 1925. von Kármán's paper treats specifically the case of a thin aerofoil accelerated from rest, and calculates the lift and pitching moment directly from the formula for the linear and angular momenta of the vortex system. Applications to oscillatory motion and to sharp-edged gusts complete a paper which is notable for its continuous emphasis on the physics of the motion and its remarkable simplifications of the mathematical theory.

The last paper von Kármán wrote on classical hydrodynamics (1949, **104**) gives a special solution of the problem of the closed wake behind a flat plate accelerated along its normal.

In this section we must also include a pioneer paper on the impact of seaplane floats during landing (1929, **50**), written in collaboration with Frank L. Wattendorf. This paper makes a bold application of the concepts of virtual mass and of pressure propagation in a compressible fluid, and has stimulated much research.

Three famous papers (1911, **15**; 1912, **16**; 1912, **17** (with H. Rubach)) must be classified under the heading of incompressible, inviscid flow, although their topic is the mechanism of the production of drag; for they deal with the von Kármán 'vortex street' in a perfect fluid. The pioneer investigation of the first of these papers is superseded and corrected by the results of the second and third. The theory is now well known and provides a convincing picture of the relation between the vortices shed periodically into the wake from a bluff body and the drag experienced by the body in a certain range of the Reynolds numbers. Even now we have no means of completing von Kármán's theory by calculating the frequency with which the vortices are shed.

Aviation

von Kármán's interest in aerodynamics was far from purely theoretical, and he took great interest in the technical problems of aviation and of aeronautical engineering. One of his earliest papers (1908, **5**) describes the advantages of the very 'light-weight' engines which were being manufactured in Paris. The next paper on aeronautics (1914/15, **27**), written in collaboration with E. Trefftz, gives a careful and systematic account of the longitudinal stability and oscillations of an aircraft.

von Kármán was acquainted with the pioneer investigations of F. W. Lanchester and devoted a paper (1921, **33**) to the analytical theory of the 'switch-back model' devised by the latter to represent the dynamic soaring of birds (*Aerodonetics*, London, 1908, p. 277).

von Kármán's practical activities in the field of helicopter design during the years 1916–17, while he was in the Austro-Hungarian Army Air Force, issued later in a long theoretical paper (1921, **34**) on various problems of helicopter flight. A few years later (1924, **41**) he wrote, with Th. Bienen, a long and detailed study of propeller theory.

His other main contributions to research in aviation are a lengthy paper, written with Clark B. Millikan (1934, **62**), on the use of the wind-tunnel in connexion with problems of aircraft design, and an aeronautical conference paper (1947, **97**) on the theory of stability and control at high speeds. The four last-mentioned papers contain so much detailed information that it is difficult to give more adequate summaries.

With his unique experience of the aeronautical world, his profound physical insight and engineering ability, von Kármán was admirably equipped to give magisterial exposition of the development of aviation, and he splendidly fulfilled this task in a number of addresses (1931, **54**; 1932, **58**; 1943, **88**; 1948, **103**).

Fuels and combustion

von Kármán's present interest in problems of fuel and combustion and his recent contributions to this subject are so actual that it is just a little surprising to find him writing a paper with Frank J. Malina in 1940 (**82**) on the characteristics of the ideal solid propellent rocket motor. In 1943 (**89**) and 1944 (**90**) he was active in guiding the preparation of memoranda on long-range rocket projectiles and on jet-propulsion systems. A most remarkably prophetic article published in 1945 (**93**) excitedly foresees the application of nuclear energy to propulsion. An interesting lecture delivered in 1950 (**105**) with G. Gabrielli gives a comparative study of the specific power required for the propulsion of various types of land, sea and air vehicles. Finally, the last paper included in these volumes (1951, **111**), written with G. Millán, lays the foundations of the thermal theory of constant pressure deflagration.

Turbulent and laminar flow

von Kármán's contributions to the theory of turbulent and of laminar boundary layers have exercised a profound influence on the development of this difficult

and important branch of fluid dynamics. Broadly speaking they fall into four sections in chronological order:

(1) the search for 'universal' laws of turbulence, phenomenological in character, and (in fact) rather limited in range;

(2) the construction and use of the 'momentum equation' for boundary layer flow;

(3) 'mixing length' theories, stemming from Prandtl's investigations; and

(4) the theory of 'inner' and 'outer' solutions of the laminar boundary layer equations.

The first paper (1911, **14**) suggests an empirical relation between the coefficient of turbulent viscosity and the coefficient of laminar viscosity in which various fluids are compared with water. The relation has the form

$$(\mu_S/\mu_W)_T = (\mu_S/\mu_W)_L^{2n-1}(\rho_S/\rho_W)^{1-n},$$

where $n = 0{\cdot}6173$, the suffixes S and W refer to the fluid considered and water, while T and L refer to turbulent and laminar conditions.

The famous momentum equation, which has dominated boundary layer theory for so many years, first appears in 1921 (**32**), together with a dimensional argument leading to the 'one-seventh power law' for the velocity distribution in the turbulent boundary layer of cylindrical pipes. The combination of these two concepts to turbulent flow over a flat plate gave a friction coefficient c_f proportional to $R^{-\frac{1}{5}}$, R being the Reynolds number based on the plate length. The same paper also applies the method of the momentum integral to the laminar and turbulent boundary layers on a rotating plate. Similar ideas are developed in an expository article (1922, **36**).

von Kármán's first attempt to construct a statistical theory of turbulence was made in 1924 (**42**) in which the 'probability' $f(\alpha, \beta)$ of the motion described by the stream function $\psi = A\cos(\alpha x + \beta y)$ was estimated by maximizing the integral $\int\int f \log f \, d\alpha \, d\beta$, subject to a condition of energy balance.

'Mixing length' theories first appear in 1928 (**46**) in connexion with drag experiments on long bodies, and a systematic account is given in 1930 (**52** and **53**), together with applications of von Kármán's relation $l \sim U_0'/U_0''$. Further developments are given in (1932, **57**), especially with regard to the 'logarithmic turbulent velocity profile' and the laminar sublayer near the solid boundary; and in (1934, **61**) where the validity of a universal velocity distribution is closely examined, with especial reference to the effect of roughness. A long and valuable historical summary is given in (1934, **64**).

In 1934 (**63**) von Kármán, in collaboration with Clark B. Millikan, developed a new method of obtaining approximate solutions of the laminar boundary layer equations, in which a modification of von Mises's equation was used to obtain a criterion for laminar separation. The inner and outer regions of the boundary layer were treated separately and joined at the inflexion point of the velocity profile. Applications were made to certain 'roof top profiles', and in a subsequent paper by the same authors (1935, **65**) to the problem of the maximum lift of certain airfoils.

The effects of compressibility on boundary-layer theory are studied in 1935 (**67**) and in a paper (1938, **73**) published in collaboration with H. S. Tsien. Finally, in 1939 (**76**) von Kármán gave an important extension of Reynolds's analogy between momentum and heat transfer to the case of a liquid flowing over a solid wall.

The last group of papers in this section deals with statistical theories of turbulence. The first of these (1937, **68**) develops Sir Geoffrey Taylor's early theory (1935) of the correlation function $R(y) = \overline{u_1 u_2}/\overline{u^2} = 1 - \lambda^{-2}y^2 + \ldots$ by obtaining a second relation between $\overline{u^2}$ and $\overline{\lambda^2}$. The next paper (1937, **69**) extends Taylor's general theory of isotropic turbulence by introducing the correlation tensor $R_{ik} = \overline{u_i u_k'}/\overline{u^2}$, discussing the decay of turbulence, and giving a new theory of turbulent shear motion. The Wilbur Wright Memorial Lecture (1937, **70**) gives a splendid account of turbulence and its relevance for the aeronautical engineer. The general mathematical theory is given in a joint paper (1938, **71**) written with L. Howarth, which provides the basic theory of the correlation tensor for isotropic turbulence, and the general theory of the decay of turbulence. Further remarks on this theory are given in (1938, **75**).

Some ten years later (1948, **99**, **101**), von Kármán returned to this subject using the powerful methods of Fourier analysis (Taylor, 1938) for the study of the correlation function and the velocity distribution. Together with C. C. Lin (1951, **108**) he wrote a survey of recent developments in the statistical theory and proposed a simple physical picture of the process of the decay of turbulence. The last paper on turbulence in these volumes is paradoxically entitled 'Introductory Remarks...' (1951, **109**), a title which in fact is most appropriate to the introductory paper at a symposium on cosmical aerodynamics.

Elasticity and strength of materials

Perhaps the greatest volume of von Kármán's research is that devoted to theoretical and experimental elasticity and to problems relating to the strength of materials.

Some of the earliest of these works are articles written for the *Encyklopädie der mathematischen Wissenschaften* on problems of stability in machine construction (1910, **10**), on the physical basis of the theory of stability (1910, **11**), in collaboration with L. Föppl, or for the *Handwörterbuch der Naturwissenschaften* on Elasticity (1913, **23**), Stability (1913, **24**), Equilibrium (1913, **25**), and Hardness (1913, **26**). The first of these articles (**10**) is remarkable for giving (for the first time) the now famous 'von Kármán non-linear equations' for the transverse deflexion of a thin plate loaded by edge thrusts and moments together with transverse loads. These equations appear in vol. I, p. 177 (equation 29).

An early paper (1909, **7**) (written with Alfred Haar) gives a general theory of stress distribution in plastic and granular material and derives the basic equations from a minimum energy principle supplemented by an inequality expressing the conditions for the elastic or plastic regime. A short note (1916, **28**) is devoted to hysteresis in materials. The theory of elastic 'grenzzustände' is taken up again in 1926 (**44**) with special reference to earth pressure. A comparatively recent paper (1950, **106**) discusses in some detail the propagation of plastic deformation in solids.

von Kármán wrote only one paper on technical processes, viz. a study of the theory of rolling processes (1925, **43**).

However, von Kármán's major contribution to the study of elasticity is undoubtedly the magnificent series of papers on problems of buckling and stability, especially of thin plates and tubes.

The earliest of these investigations (1906, **2**, and 1908, **6**) dealt with the classical problem of the buckling of a straight strut and showed that the discrepancy between the Euler theory and experiment disappears if one employs the 'tangent' modulus of elasticity. After a short paper (1909, **8**) on the strength of corrugated fire tubes, von Kármán returned to this topic in his Inaugural Dissertation at Göttingen (1910, **9**) in which he gave a general survey of his research on the buckling of struts. von Kármán's experimental work on the failure of materials under triaxial stress is given in (1911, **12**) and a further study of thin-walled tubes appeared in the same year (**13**).

The theory of deep thin beams was investigated by von Kármán (1923, **37**) using a two-dimensional theory and the theory of T-section beams in 1924 (**40**). A joint paper with K. Friedrichs (1929, **49**) discusses the stressing of aircraft wings.

The next pair of papers is concerned with the post-buckling behaviour of thin metal sheets and shells—a subject of great importance for the aeronautical engineer. Together with Ernest E. Sechler and L. H. Donnell, von Kármán investigated the strength of thin plates under compression assuming the load to be carried by two strips along the edges parallel to the external thrust (1932, **55**). A contribution to a symposium on prob'ems of thin-walled structures (1933, **60**) illustrates some applications of Wagner's tension field theory.

In a paper written with H. S. Tsien (1939, **77**), von Kármán broke new ground by giving a theory of the failure of spherical shells due to 'oil-canning' or 'Durchschlag', i.e. a sudden dimpling of the shell with finite deformation. This topic is considered again in a paper written with Louis G. Dunn and Hsue-Shen Tsien (1940, **80**) which also gives numerous experimental results. Similar ideas were used to account for the buckling of thin cylindrical shells under axial compression in a paper also written with Tsien (1941, **83**).

Finally we must note a few papers on mathematical methods appropriate to problems of elasticity: a brief note of Ritz's method (1953, **21**), a useful survey of the use of series of orthogonal functions in structural problems (1939, **78**), and two elaborate papers (1944, **91** and 1946, **94**), written with N. B. Christensen and Wei-Zang Chien, respectively, on practical methods of computation for the analysis of thin-walled sections with variable twist when loaded in torsion.

Theory of crystals

von Kármán wrote three papers in collaboration with Max Born on the theory of molecular vibrations in crystals. In the first paper (1912, **18**) the theory is applied to optical properties and to the specific heat of crystals with cubic lattices. The next paper (1913, **19**) gives a more elaborate theory of specific heat; and the third paper (1914, **20**) examines the distribution of the characteristic vibrations of a crystal lattice.

'Philosophy' of engineering

von Kármán's general philosophy of engineering as a science and an art can be gathered from a group of some six papers which begin with a biographical notice of Joseph Popper ('Lynkeus') (1918, **30**), and a short article on the significance of Mechanics for the study of the technical physicist (1921, **31**). To this subject he returned again in a lecture given in 1930 (**51**) on Mathematics and Technical Science.

An illuminating and sympathetic comparison of the intellectual approaches to a problem made by engineers and mathematicians is given in a lecture (1940, **79**) and in the first paper published by the Quarterly of Applied Mathematics (1943, **87**).

The Willard Gibbs Lecture (1940, **81**) gives a lengthy, penetrating and stimulating account of the non-linear problems encountered by the engineer in vibration theory, problems of buckling, plasticity, water waves, jets and cavities, viscous boundary layers, and compressible flow: and clearly illustrates the effective use of analytical methods.

Miscellaneous investigations

A number of interesting papers do not fall conveniently under any of the preceding headings and, with some diffidence, are grouped together here. In this group we must include von Kármán's first paper (1902, **1**) on the motion of a heavy rod supported on a hemispherical end by a rough horizontal plate; a paper on thermo-electric equilibrium in solid insulators (1924, **39**); some remarks on the formation of sand ripples (1947, **98**); and a boundary layer theory of the damping of the oscillations of a viscous fluid in a U-tube (1948, **100**).

There is also an important paper (1948, **102**) on a number of problems of aerodynamic engineering, including the air resistance of vehicles, and the stressing of buildings and bridges for wind pressure and vortex shedding.

Certain characteristic features stand out clearly in this rapid survey of von Kármán's scientific work. It is impossible not to be impressed by the extraordinary prescience which he showed in recognizing at once the importance of all the major developments in fluid mechanics and elasticity, even in their earliest stages. Few of his papers 'date'. They all still possess an actuality and freshness which invigorates the reader. It is also characteristic of von Kármán's researches that each one seems to spring naturally and inevitably from some problem of practical engineering. Many of the papers were written in collaboration with younger men, all of whom would readily recognize the good fortune which thus brought them under von Kármán's benign influence.

Probably the best thanks we can give to him for publishing these researches is to point out that they bring the tale only up to 1951 and that it is high time that we had a fifth volume.

G. Temple

EIGHTH CONGRESS
OF THE
INTERNATIONAL ASSOCIATION FOR HYDRAULIC RESEARCH

Montreal, Canada's metropolis and the world's second largest French-speaking city, has been selected to act as host for the eighth congress of the I.A.H.R. Meetings will be held in the Windsor Hotel during the week commencing 24 August 1959. All members, and those interested in the work of the Association, are invited to attend and to contribute to the meeting, both by presentation of papers and participation in the discussion. The two official languages of the congress will be French and English.

The following four subjects have been selected for study in the technical sessions by the General Assembly at the Lisbon Convention in 1957.

A. Hydraulics of gates and valves (including vibration, forces, cavitation, ice).

B. Fundamental hydraulics of ship locks.

C. Density currents (including effects of reservoir sedimentation, hydro-electric intake, fishing industry, etc.).

D. Air entrainment and air vents.

Two seminars for more informal study will be conducted concurrently with the technical sessions on the following subjects.

1. Ice problems in hydraulic structures.

2. Transportation of material in water. (It is intended that this seminar deal primarily with sediments but transport of other material may be included.)

In addition to technical sessions, participants will have the opportunity of touring the St Lawrence Seaway works, some of the major hydro-electric projects in the area, and hydraulic laboratories that have played an important role in these developments. It is to be noted that the St Lawrence Seaway channel—one of the outstanding achievements of modern engineering—will be officially opened in 1959. This route will enable deep-sea shipping to sail up to the heart of the North American continent.

A number of sight-seeing tours will be arranged for the ladies so that they may become acquainted with points of historical and commercial interest in Montreal.

Further particulars regarding the preparation and presentation of papers and participation in the congress may be obtained from Mr Léo Roy, c/o Quebec Hydro-Electric Commission, 107 W. Craig Street, Montreal 1, P.Q., Canada.

JOURNAL OF FLUID MECHANICS

Volume 5, Part 2 February 1959

CONTENTS

The scattering of gravity waves by turbulence
by O. M. PHILLIPS *page* 177

The slow motion of two or more spheres through a viscous fluid
by G. J. KYNCH 193

Temperature fluctuations over a heated horizontal surface
by A. A. TOWNSEND 209

The hypersonic viscous effect on a flat plate with finite leading edge
by ANDREW G. HAMMITT 242

Theory of thin airfoils in fluids of high electrical conductivity
by W. R. SEARS and E. L. RESLER 257

The effect of uniform distortion on weak homogeneous turbulence
by J. R. A. PEARSON 274

One-dimensional flow of an ionized gas through a magnetic field
by R. M. PATRICK and T. R. BROGAN 289

The effect of eddy viscosity on the velocity profile of steady flow in a uniform rough channel
by S. M. A. HAQUE 310

On the periodic fundamental solutions of the Stokes equations and their application to viscous flow past a cubic array of spheres
by H. HASIMOTO 317

REVIEWS

Collected works of Theodore von Kármán 329

Printed in Great Britain at the University Press, Cambridge
(Brooke Crutchley, University Printer)